Proceedings of the 3rd Winter Education Seminar in Rokytnice nad Jizerou 2012

February 1 - 4, 2012

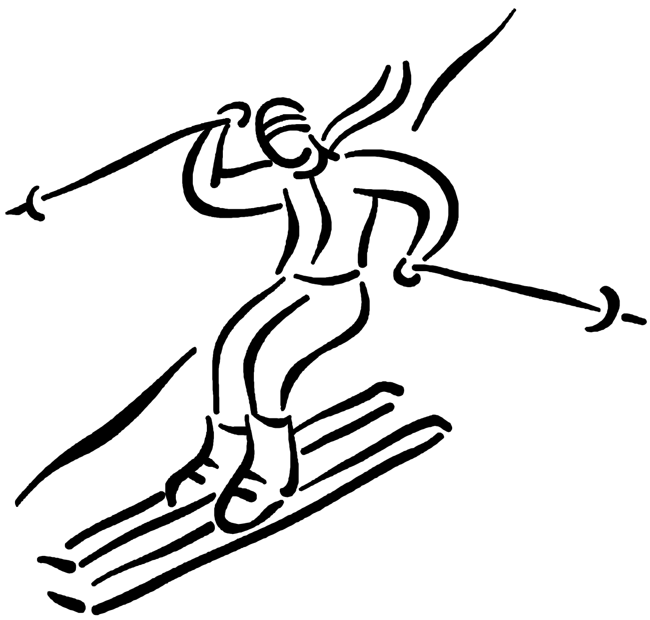

ISBN 978-80-260-3425-4

Published by the FZÚ AV ČR, v. v. i.
Cukrovarnická 10, 162 53, Praha 6, Czech Republic
Editors: Ing. Lenka Hoďáková , Mgr. Zdeněk Remeš, PhD., Ing. Alexander Kromka, PhD., RNDr. Martin Ledinský, PhD.
http://www.fzu.cz/~remes/Rokytnice/workshop.html

ISBN 978-80-260-3425-4

PREFACE

The Proceedings publish the selected talks presented at the 3rd Winter Educational Seminar which took place in **February** Wednesday 1 - Saturday 4, 2012 in the Ski center Horni Domky, Rokytnice nad Jizerou, as a joint activity of two departments of the Institute of Physics AS CR, v. v. i. (FZU), i.e. Department of Thin Films and Nanostructures (26) and the Department of Optical Materials (27). The seminar was organized within the frame of the CABIOM - Carbon-based Biomaterials and Biointerfaces (http://cabiom.fzu.cz/), the Virtual Research Center of the Institute of Physics AS CR, v. v. i.). The aim of the seminar is promoting discussions about the scientific and experimental difficulties young students experience during their PhD. studies face to face to other researchers and thus, to support them during their work and build a natural bridge between young researchers and senior scientists.

The main subject of the given talks was the CVD deposition and material processing as well as characterization of thin films. The discussions were focused on material engineering, CVD technologies, characterization of materials and interfaces, data processing and analysis, and theoretical modeling. The attended researchers and workers referred about the scientific results and they introduced some special methods used in their laboratories, mainly localized at the Institute of Physics of the ASCR, v. v. i.

The number of participants at the 3rd Winter Educational Seminar was as follows: 7 senior scientists from the Institute of Physics of the ASCR, v. v. i., 8 PhD. students and 2 undergraduate students. The seminar was attended this year by external guests coming from the International Laser Centre in Bratislava and from Slovak University of Technology in Bratislava with whom we closely collaborate in the frame of the agreements on international cooperation in research & development in the field of nanocrystalline diamond and diamond-like carbon thin films, fundamental physic of materials, manipulation and characterization of semiconductor surfaces and their nanostructures as well as development of novel analytic techniques.

The 4rd Winter Educational Seminar will take place at the same place in January 30- February 1, 2013, please see http://www.fzu.cz/~remes/Rokytnice/workshop.html for detailed information.

The seminar is open for PhD. students and the undergraduate students working in the Institute of Physics of the Academy of Sciences, v. v. i. as well as for the invited guests. The attendance to the seminar is free of charge for the participants of the seminar under the condition that they will give in English an oral talk about their work or a topic that can be interested for others.

Ing. Lenka Hoďáková, Mgr. Zdeněk Remeš, PhD., Ing. Alexander Kromka, PhD. and RNDr. Martin Ledinský, PhD.
in Prague September 20, 2012

TABLE OF CONTENTS

Preface

Contributed presentations

Dotek atomu p. 05
Antonín Fejfar
Institute of Physics, ASCR, Cukrovarnicka 10, Prague 6, Czech Republic

Silicon solar cell: methods for experimental study and evaluation of materiál parameters in advanced structures p. 23
Jakub Holovský
Institute of Physics, ASCR, Cukrovarnicka 10, Prague 6, Czech Republic

Study of nucleation and growth of diamond thin films p. 39
T. Ižák[1,2*], O. Babchenko [1], M. Varga[1,2], S. Potocky[1], M. Marton[2], M. Vojs [2], M. Domonkos [1,3] and A. Kromka [1]
[1] Institute of Physics AS CR, Cukrovarnicka 10, 16253 Praha 6, Czech Republic
[2] Slovak University of Technology, FEI STU, Ilkovicova 3, 812 19 Bratislava, Slovakia
[3] Faculty of Nuclear Sciences and Physical Engineering, CTU, Břehová 7, 115 19 Praha, Czech Republic

Perspectives in diamond thin film technology p. 50
Alexander Kromka
Institute of Physics, ASCR, Cukrovarnicka 10, Prague 6, Czech Republic

Luminiscenční spektroskopie (Si nanokrystalů) p. 66
Kateřina Kůsová
Institute of Physics, ASCR, Cukrovarnicka 10, Prague 6, Czech Republic

Local photoconductivity mapping of mixed fhase silicon thin films p. 75
M. Ledinský, A. Fejfar, A. Vetushka, J. Stuchlík, B. Rezek and J. Kočka
Institute of Physics, ASCR, Cukrovarnicka 10, Prague 6, Czech Republic

SEM and AFM at FZU ASCR, v.v.i. p. 84
J. Libertínová, Š. Stehlík, B. Rezek
Institute of Physics, ASCR, Cukrovarnicka 10, Prague 6, Czech Republic

Department of Thin Films p. 90
M. Müller
Institute of Physics, ASCR, Cukrovarnicka 10, Prague 6, Czech Republic

Suns V_{OC} metod of IV curve measurement of photovoltaic cells p. 96
V. Pic, P. Pikna
Institute of Physics, ASCR, Cukrovarnicka 10, Prague 6, Czech Republic

Potential for nanotechnology approaches in the production of crystalline and thin film silicon solar cells p. 108
A. Poruba, R. Bařinka, P. Čech, P. Bařinková, J. Hladík, I. Mudroň and J. Řehák
Solartec, s. r. o.

Optical properties of thin NCD films p. 121
Z. Remeš, A. Kromka
Institute of Physics, ASCR, Cukrovarnicka 10, Prague 6, Czech Republic

Stem cells-open opportunities p. 128
N. Romanyuk
Institute of Experimental Medicíně ASCR, v.v.i., Prague

Stabilization Principles of III-V Semiconductor Surfaces p. 140
O. Romanyuk
Institute of Physics, ASCR, Cukrovarnicka 10, Prague 6, Czech Republic

Measurement of the magnetic hysteresi and Backhausen noice at controlable Magnetic conditions p. 157
O. Stupakov
Institute of Physics, ASCR, Na Slovance 2, Prague 8, Czech Republic

Photonic structures and their preparation p. 171
M. Varga[1, 2], L. Ondič[1, 3], K. Hruška[1], J. Potměšil[1], J. Libertínová[1], A. Kromka[1], Z. Remeš[1]
[1]*Institute of Physics of the ASCR,v.v.i., Cukrovarnicka 10, Praha 6, 16253, Czech Republic*
[2]*Institute of Electronics and Photonics, FEI STU, Ilkovičova 3, SK-812 19 Bratislava*
[3]*Faculty of Mathematics and Physics, Charles University, Ke Karlovu 3, 121 16 Prague 2, Czech Republic*

Thermoelectric conversion of heat to electricity – principles, materials, characterization and applications p. 182
J. Hejtmánek, K. Knížek
Institute of Physics, ASCR, Cukrovarnicka 10, Prague 6, Czech Republic

Terahertzová spektroskopia p. 193
L. Fekete
Institute of Physics, ASCR, Na Slovance 2, Prague 8, Czech Republic

Dotek atomu

aneb rastrovací hrotové mikroskopy

A. Fejfar
Fyzikální ústav Akademie věd České republiky
Cukrovarnická 10, 162 53 Praha 6

* e-mail: fejfar@fzu.cz

4.2.2012 Fejfar Dotek atomu

1827
Robert
Brown

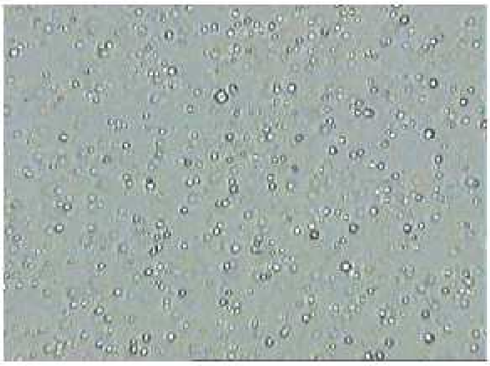

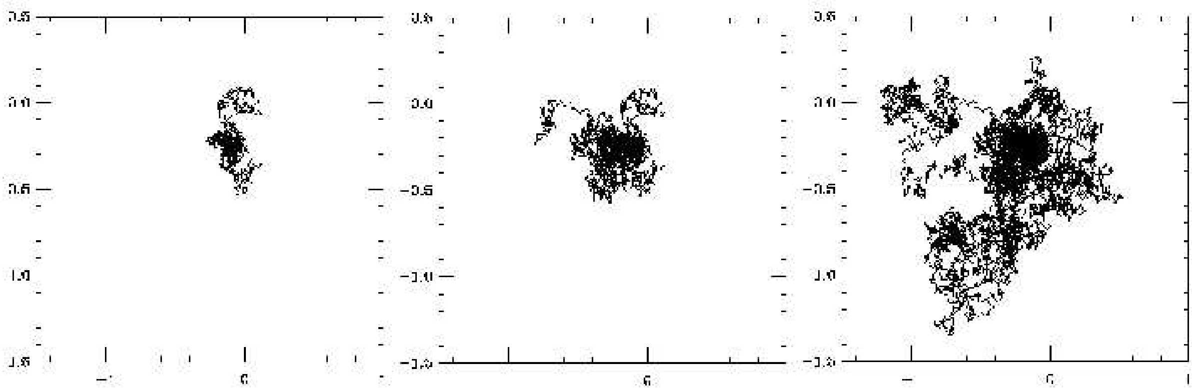

4.2.2012 Fejfar Dotek atomu

A. Einstein

O pohybu malých částic rozptýlených ve stacionární kapalině, vyplývajícím z molekulární kinetické teorie tepla,
Annalen derPhysik
17, 549 - 560

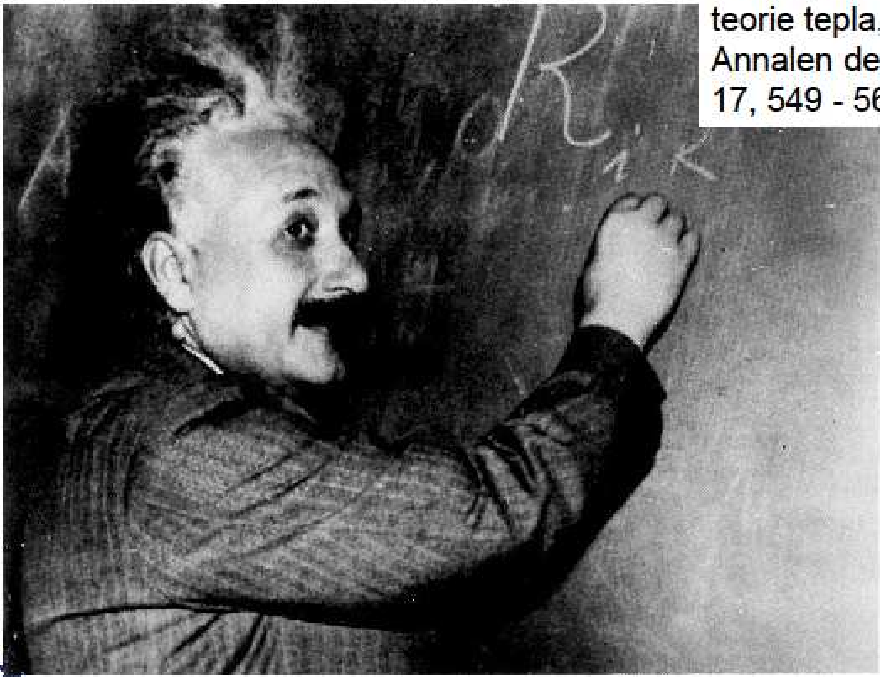

Experimentální důkazy

- Jean Perrin 1909 - The Atoms (NC 1926)
- Max von Laue (1912) - difrakce Roentgenova záření (NC 1914)

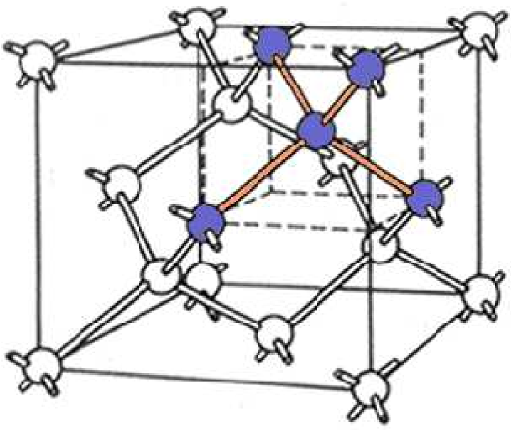

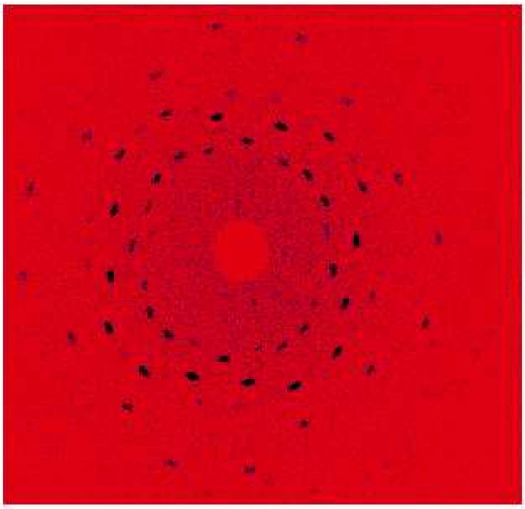

Dnes můžeme atomy vidět přímo:

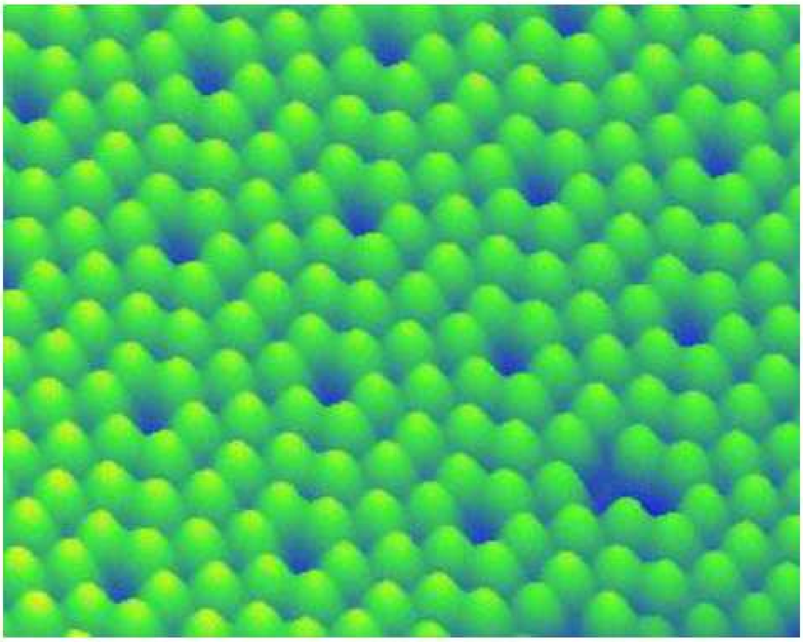

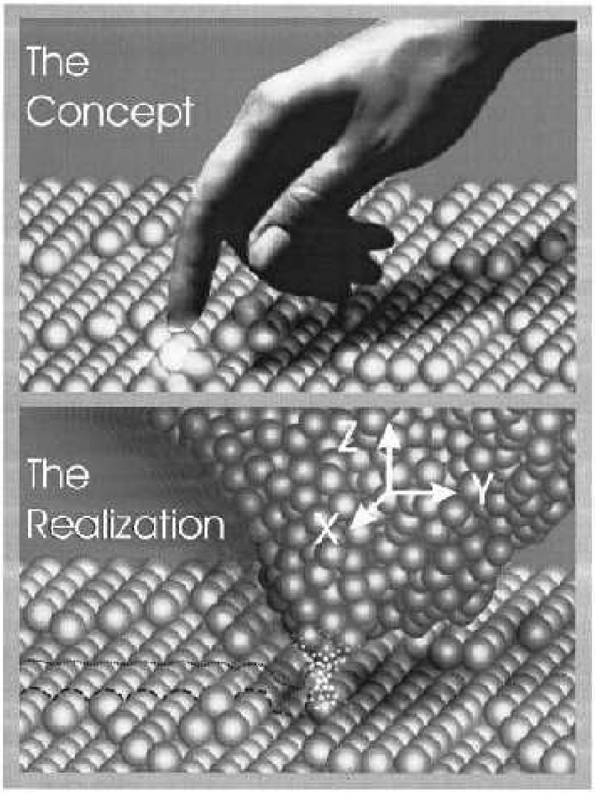

Myšlenka

G. Binnig, H. Rohrer,
Rev. Mod. Phys. 71 (1999) S324.

4.2.2012 Fejfar Dotek atomu

Realizace

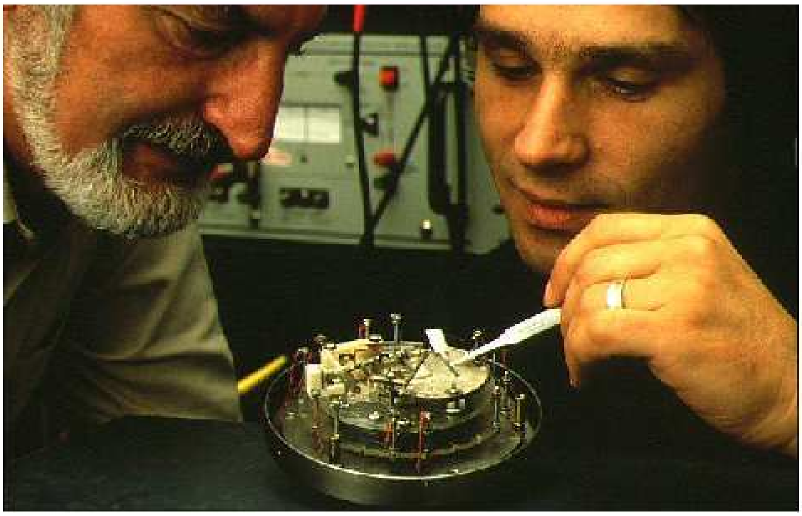

G. Binnig, H. Rohrer (Nobelova cena 1986)

Princip STM

Scanning Tunneling Microscope,
tj. rastrovací tunelovací mikroskop

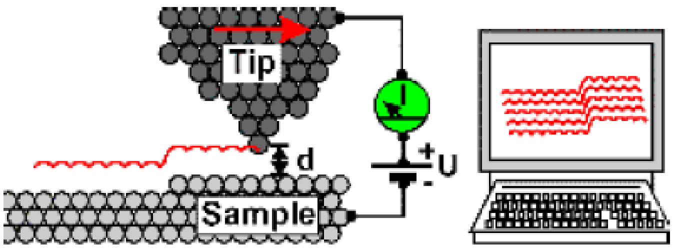

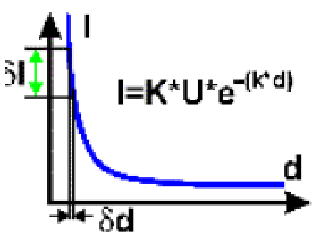

STM

scanning tunneling microscopy

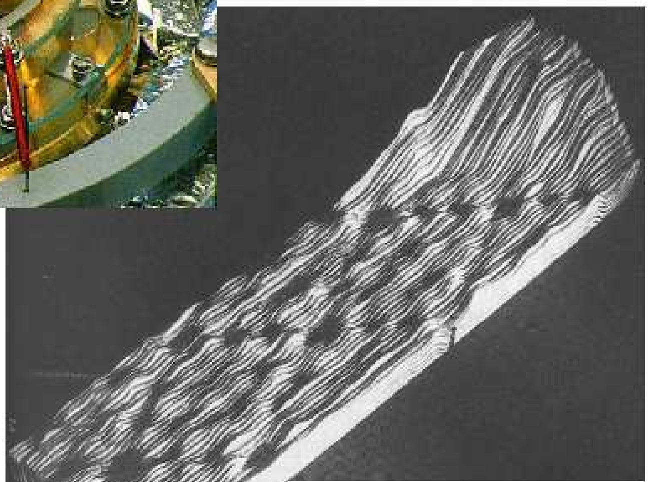

First atomic resolution image of Si(111)-7×7

Atomární schody na povrchu zlata

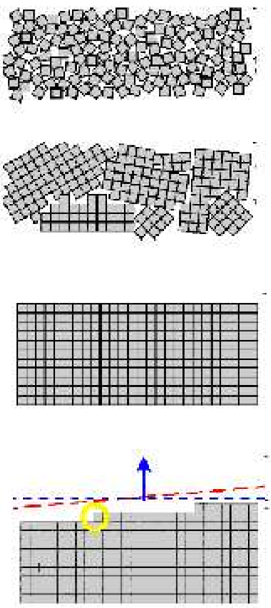

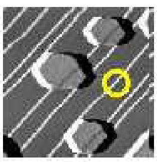

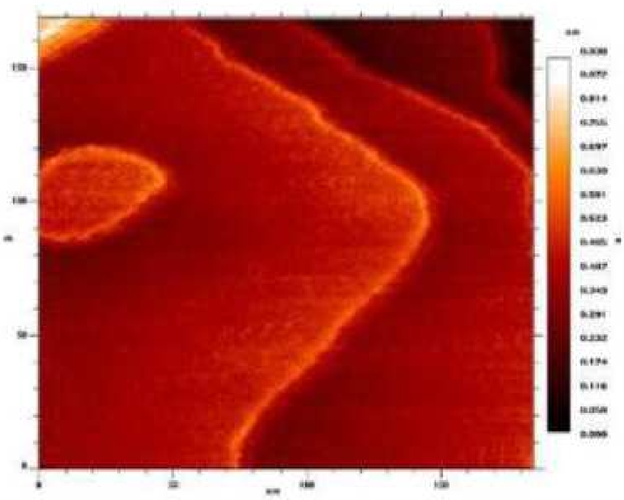

Povrchová rekonstrukce Si(111) 7x7

Atomic Resolution Imaging at 500 fA Tunneling Current

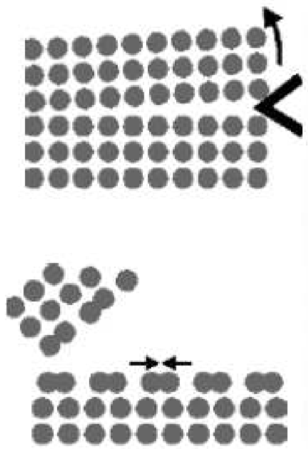

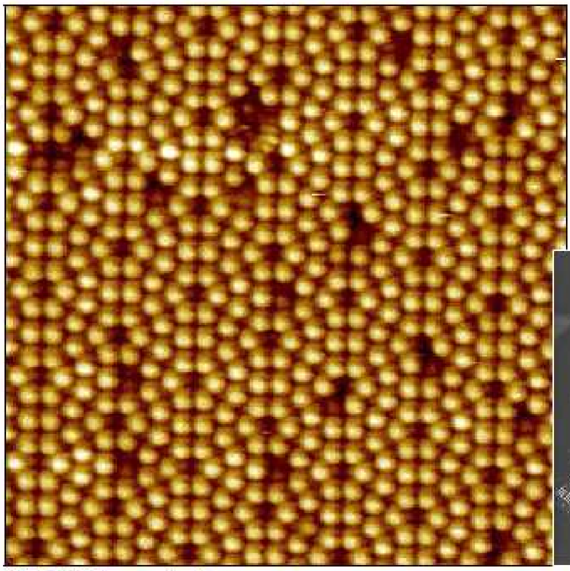

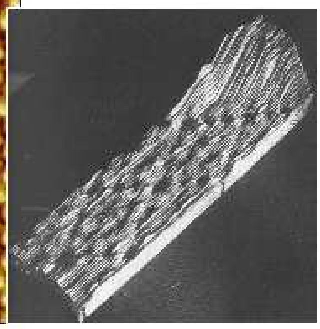

Si[111] 7x7 reconstruction

4.2.2012 Fejfar Dotek atomu

Sondy pro hrotové mikroskopy

Podstatnou roli pro vysoké rozlišení hraje ostrost hrotu –W, PtIr (cca 20 nm)

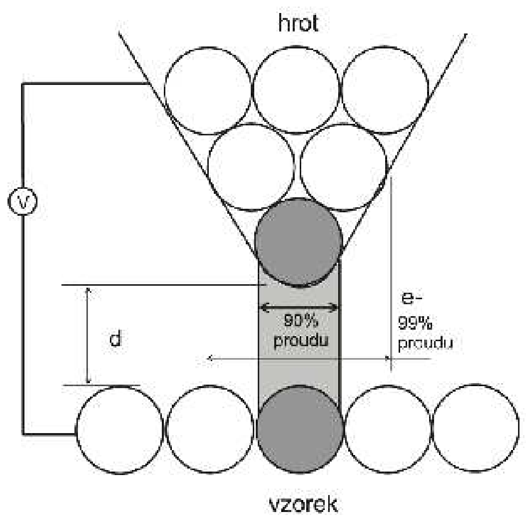

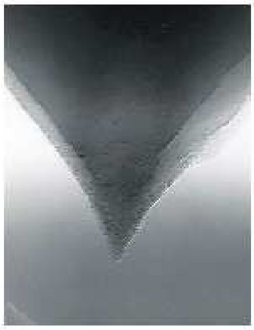

70 nm ------

4.2.2012 Fejfar Dotek atomu

Potřebná přesnost

Hrot - povrch 1 nm = 0,000.001 mm
rozlišení 1 pm = 0,000.000.001 mm

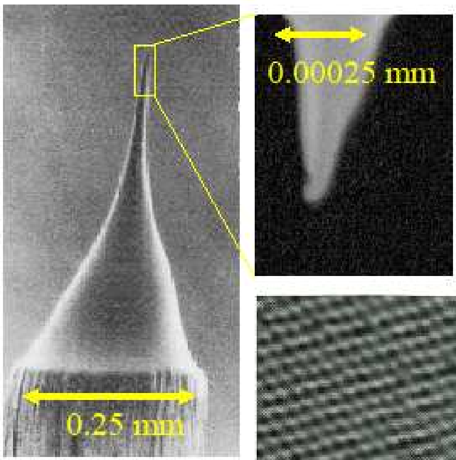

Ag(111)

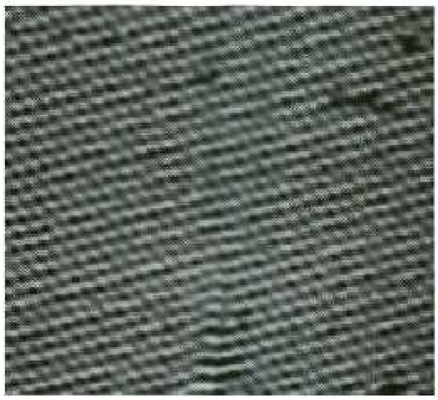

Analogie: stejné výškové rozlišení v našich měřítkách:

Eiffelovka rastrovaná 1 mm nad vozovkou Champs Élysées s přesností 0,001 mm.

Skener

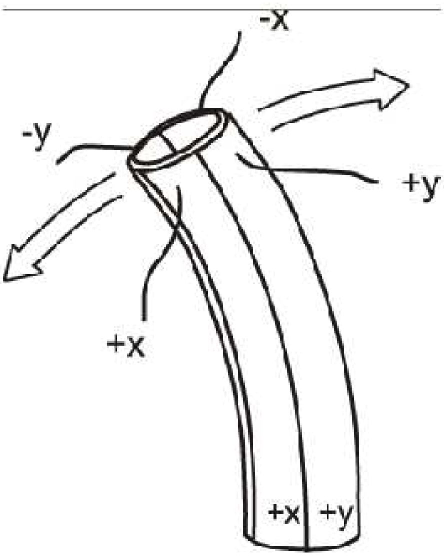

Laboratoř AFM-STM

Omicron system:

- UHV (~10^{-11} mbar)
- LEED
- Auger
- hmotový spektrometr
- iontové dělo
- UHV napařovadlo

Naše dodatky:

- PECVD (RF, VHF)
- STL

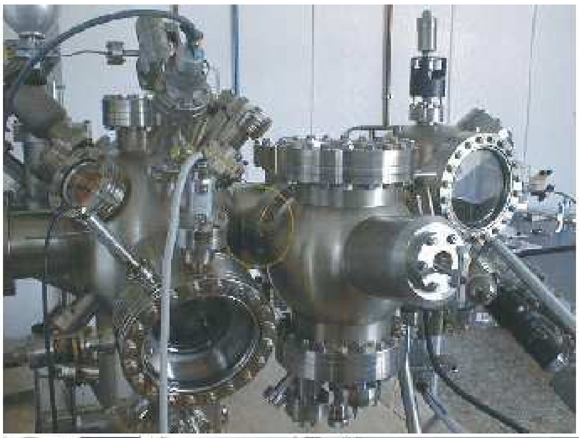

AFM/STM VT-STM

Atomární uspořádání křemíku v krystalu

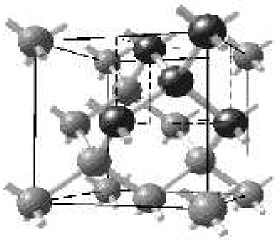

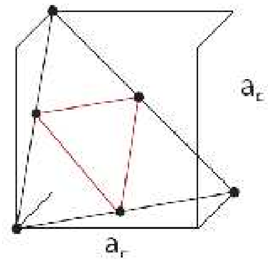

Rovina (111)
v jednotkové buňce

- Silicon has the diamond crystal structure that can be regarded as two interpenetrated f.c.c. lattices displaced by 1/4 [111]
- The cubic lattice constant a_c = 5.43 Å
- The covalent radius of Si is 117 pm (1.17 Å)
- The bond length is 2.34 Å.
- Note that cube diagonal divided by 4: √3.0 (5.43)/4 = 2.35 Å is twice the covalent radius, as it should be.

Povrchová rekonstrukce křemíku

Povrch křemíku

Si(111)

7×7 structuur

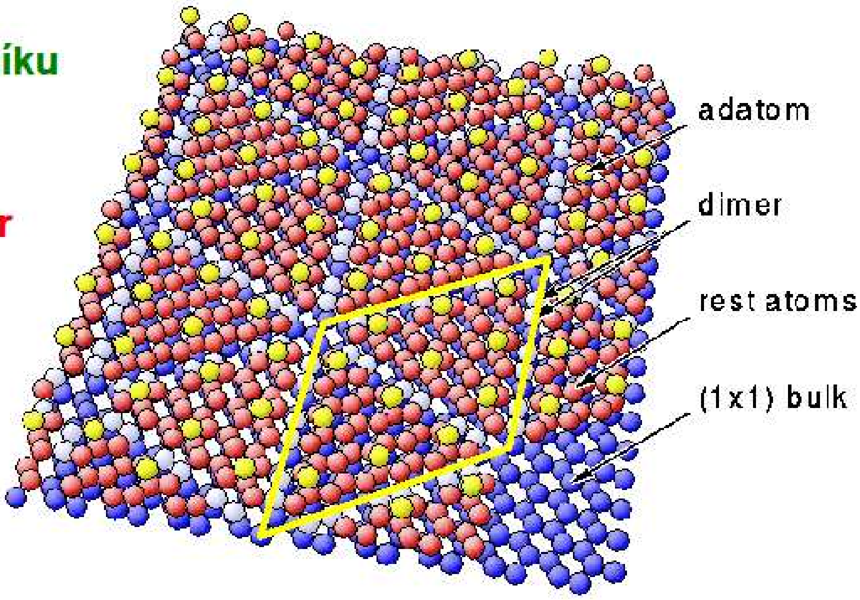

DAS-model (Takayanagi / Tong)

(Bron: FHI)

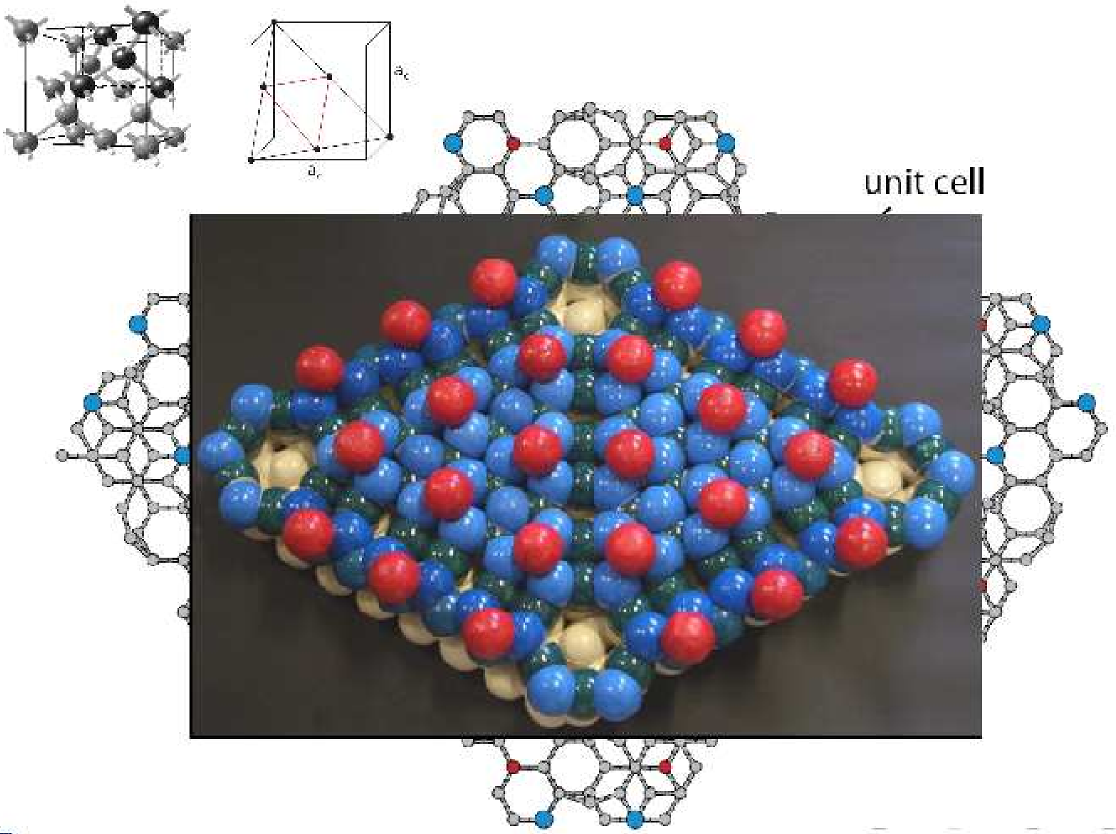

Si(111)-7×7 model

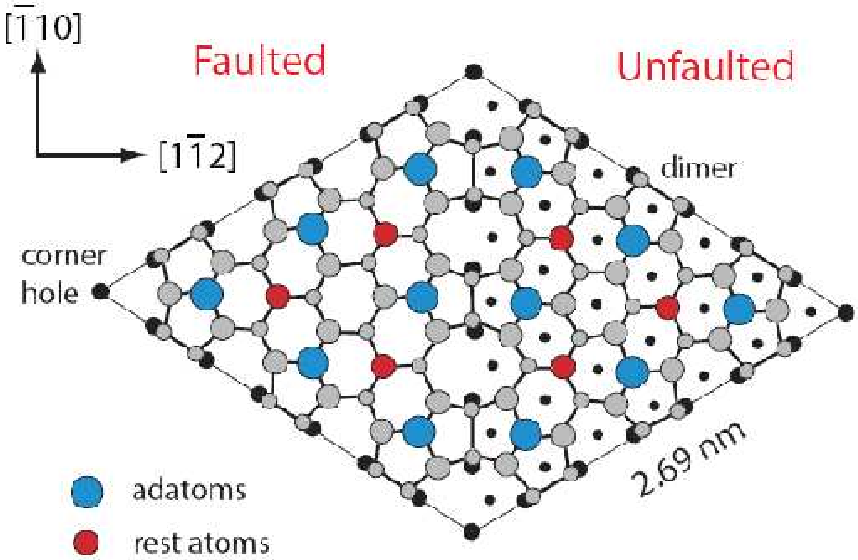

49 db → 19:

- 12 adatoms
- 6 rest atoms
- 1 corner

K. Takayanagi et al., Surf. Sci. (1985)

$(a_c)_{1\times1} = 3.86$ Å

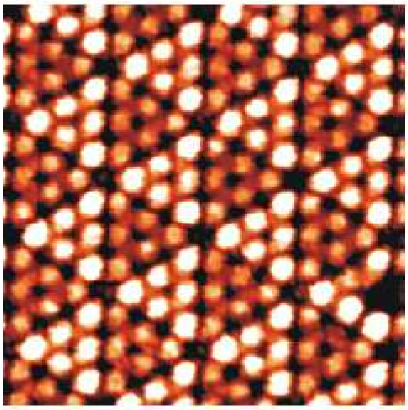

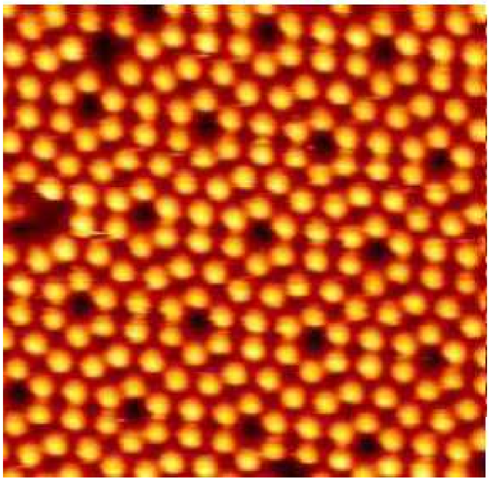

Povrch křemíku (111)-(7 x 7)

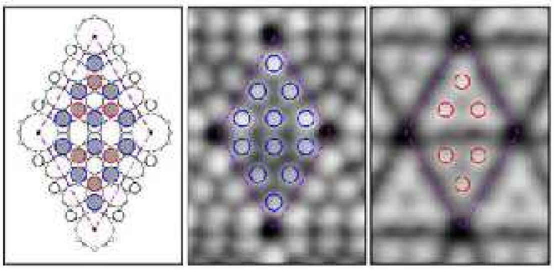

Barvy ?

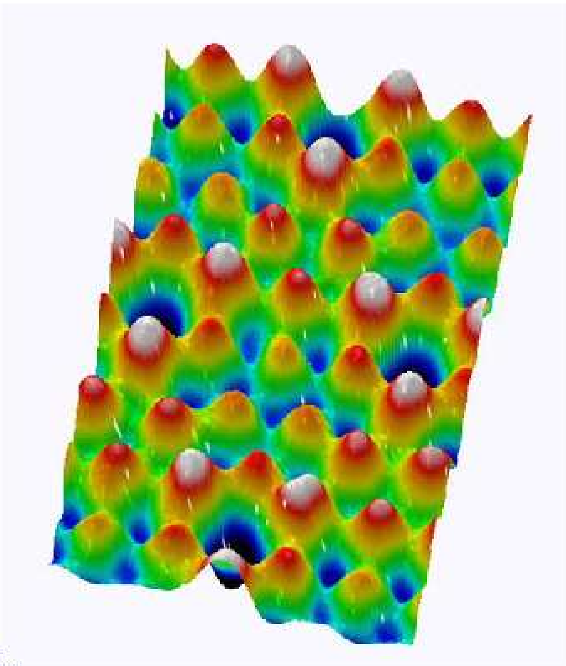

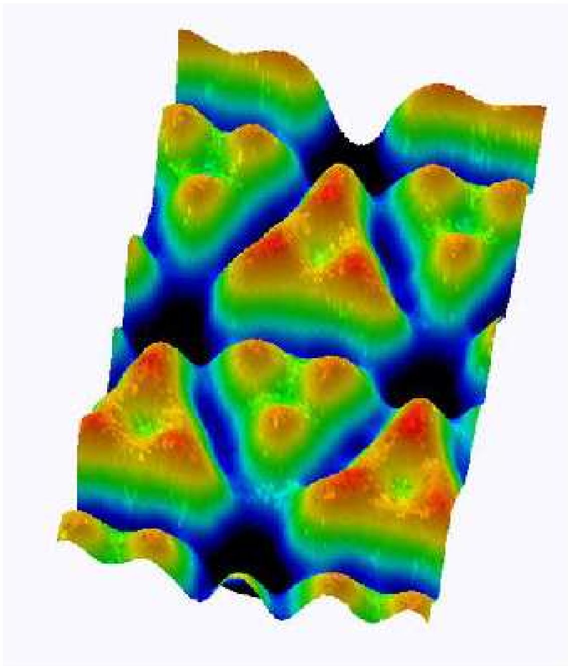

Principip „barevného“ STM

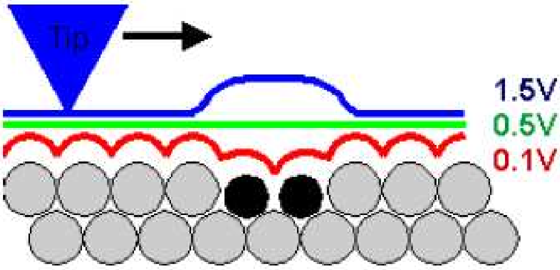

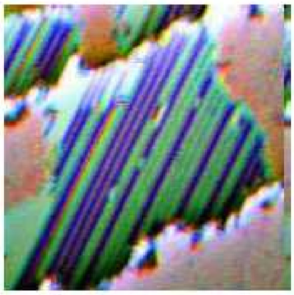

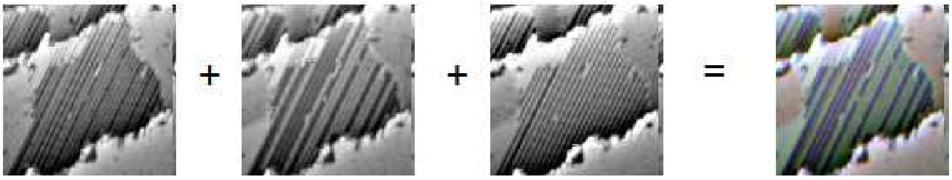

0.3 V 0.5 V 0.8 V

4.2.2012 Fejfar Dotek atomu

STM v barvách

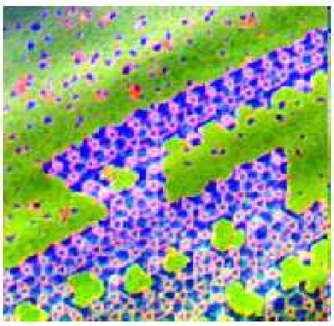

Surface of a 10 monolayer thick island of terbium (Tb) on W(110). The green region is the clean Tb(0001) surface, while the blue-violet region is an adsorbate induced reconstruction of the Tb(0001) surface. The adsorbates, possibly CO, result from impurities from the evaporant, since the degassing (cleaning) process of the Tb evaporation-source had not been finished as this sample was prepared.

120 nm x 120 nm topography
red = 0.3 V
green = 1 V
blue = 1.8 V

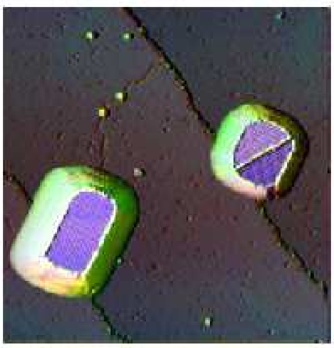

Crystallites or "islands" of GdFe2, prepared by simultanously evaporating Gd and Fe onto the W(110) substrate and annealing at 430°C. The left island is 2.8 nm thick. Among the islands, the substrate is covered with a monolayer of GdFe2. The GdFe2 monolayer exhibits a slightly different color than the GdFe2 of the islands, what means, that the electronic structures are different. The reason is the monolayer being stressed by the underlying W(110) substrate, with a continous stress release to the thicker islands.

75 nm x 75 nm
10% topography+ 90% deviated topography at 0.1 V
Color-information:
three constant current topographical images at:
red = 0.1 V
green = 1 V
blue = 2.1 V

4.2.2012 Fejfar Dotek atomu

STM v barvách

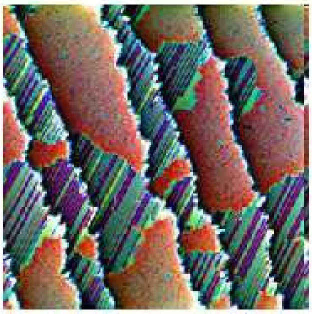

Image size: 125 nm x 125 nm
Tunneling bias: red: 0.3 V, green: 0.8 V, blue: 1.2 V

The rare earth metal terbium (Tb) was evaporated onto a W(110) single crystal as a thin film. The thickness of the film was less than one single atomic layer. At this low coverage the Tb atoms arrange in parallel lines, so- called "superstructures", visible as stripes. Areas with different distances of the monoatomic stripes are visible. Since the electronic structure of the superstructures depend on this stripe distance, each superstructure exhibits a characteristic color in this three color composite.
This is the main *scientific* message of these images:
different colors mean different electronic structure!

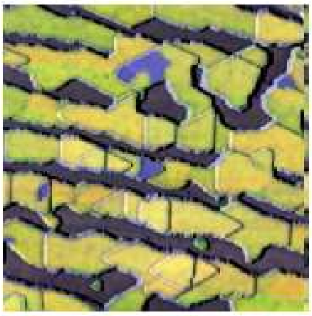

About 4 monolayers of Tb on W(110), annealed at 330°C. At these temper-parameters, the islands mainly grow along the substrate steps. Among the islands, the substrate is covered with a monolayer of Tb. The blue regions are hydrogen being absorbed on top of the surface. Hydrogen is always present in small amounts in the ultra-high vacuum chamber.
140 nm x 140 nm
15% topography+ 85% deviated topography at -0.3 V
current imaging tunneling spectroscopy, obtained after the topography, dI/dU images at:
red = 0.1 V
green = 1 V
blue = 2.1 V

STM v barvách

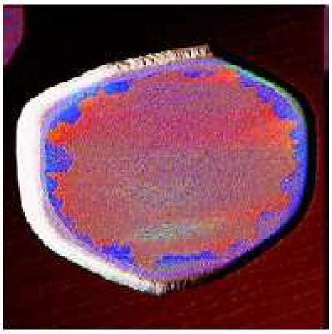

450 nm x 450 nm, Tunneling bias: red: 0.3 V, green: 1 V, blue: 1.8 V

Crystallite or "island" of the rare earth metal Terbium (Tb) grown on a Tungsten (W) single crystal in (110) orientation.
The rare earth metals are extremely sensitive to contamination, for instance from a vacuum that is not good enough or from an insufficient cleaning process of the evaporant.
As this sample was prepared the cleaning process that is carried out by melting and degassing the Tb under high vacuum, was not finished. This results in the formation of diverse adsorbate induced reconstructions. Here they are visible mainly at the rim in blue.

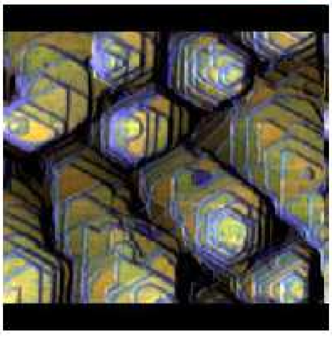

Tb terraces on W(110); during the evaporation process the substrate temperature was lowered from 350 to 300 °C, resulting in the formation of such step pyramid like structures, with each step being only one single atomic layer (0.28 nm) high. Beside hydrogen adsorbtion sites (blue) the terraces exhibit two kind of regions of slightly different color, yellowish and greenish. The difference is due to stacking faults that are present in the Tb(0001) surface.
Image-size: 200 nm x 150 nm
Image: 10% topography+ 90% deviated topography at -0.3 V
Color-information: current imaging tunneling spectroscopy, obtained after the topography, dI/dU images at:
red = 0.1 V
green = 1 V
blue = 2.1 V

STM v barvách

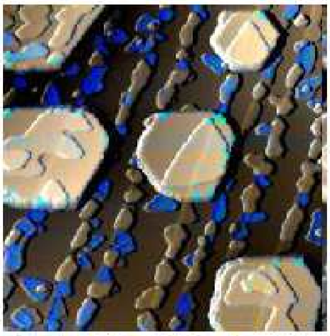

The brown, small and large objects that look like stones are islands of Gadolinium grown on tungsten.
Where the surface appears blue, hydrogen has been adsorbed on it changing the surface electronic structure drastically.

The three color composite process was slightly different for this image than for the other ones: The topographic image was colorized via three current imaging spectroscopical images at different bias voltages.

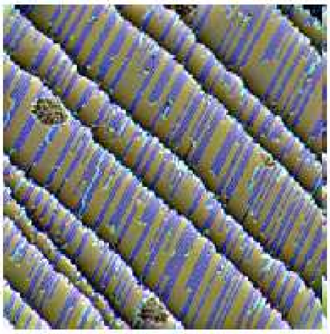

Gadolinium and iron were deposited on the W(110) substrate. They form an alloy, $GdFe_2$, visible as the olive-green areas. A surplus of Gd results in the Gd superstructures, (identical to the Tb superstructures) visible as the blue striped areas.

Povrch GaAs + Si

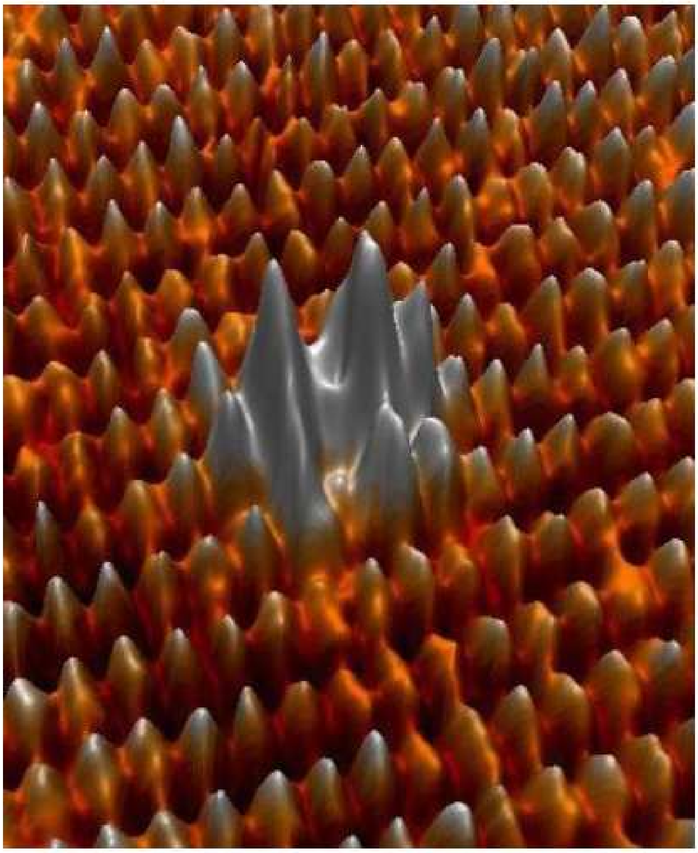

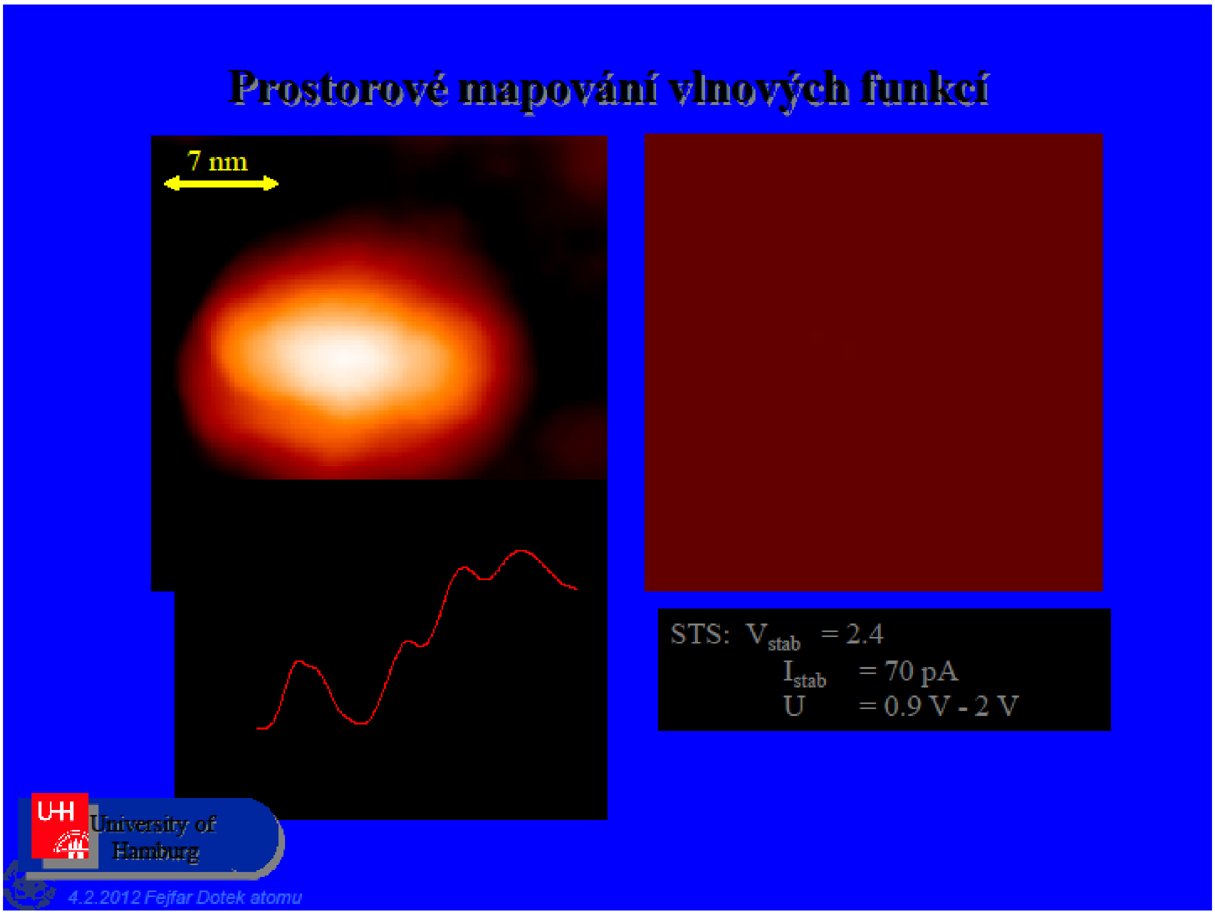
Prostorové mapování vlnových funkcí
7 nm
STS: V_{stab} = 2.4
I_{stab} = 70 pA
U = 0.9 V - 2 V
University of Hamburg
4.2.2012 Fejfar Dotek atomu

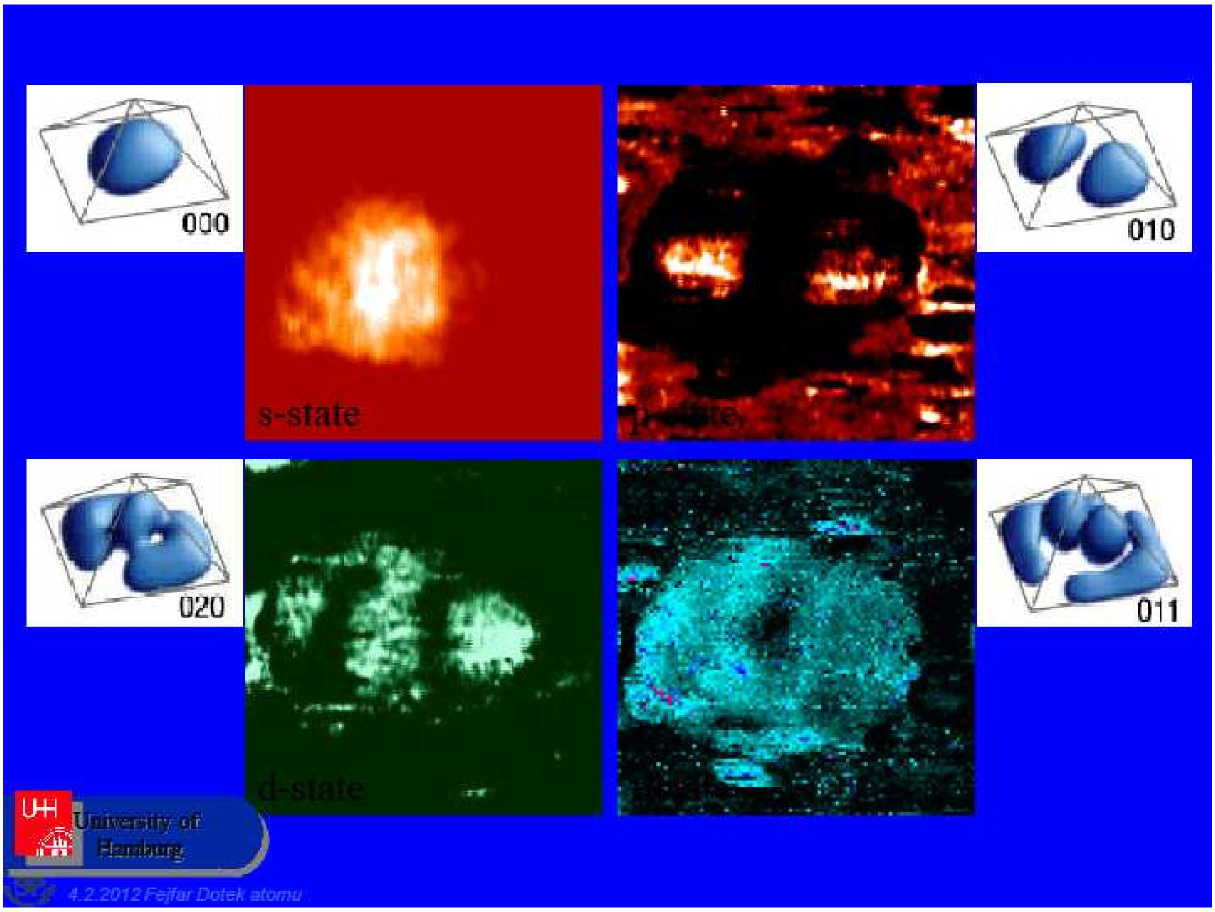
000
s-state
010
020
d-state
011
University of Hamburg
4.2.2012 Fejfar Dotek atomu

Schod na povrchu

zobrazení při konstantním proudu

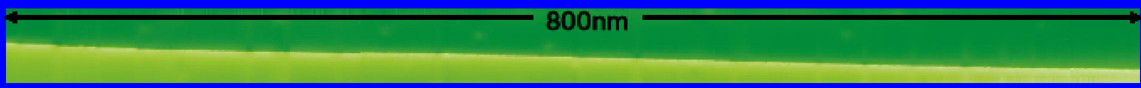

dI/dV zobrazení, V= -100 – 0 mV

v průměru 8 elektronů / bod zobrazení

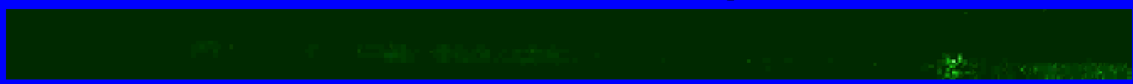

fluktuace

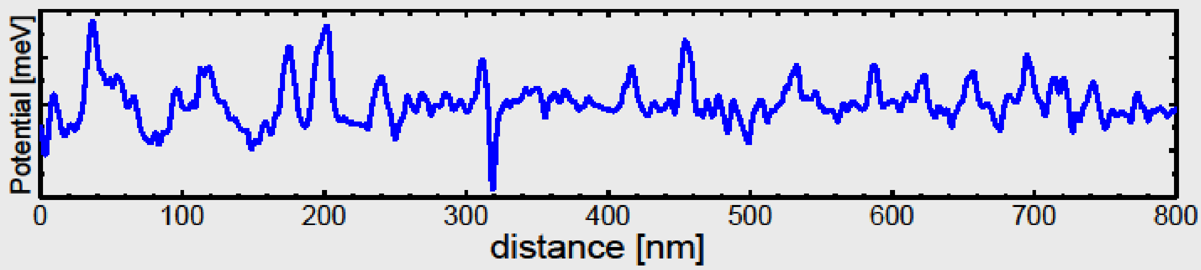

E_0= -76 meV, E_1= -23 meV

Manipulace

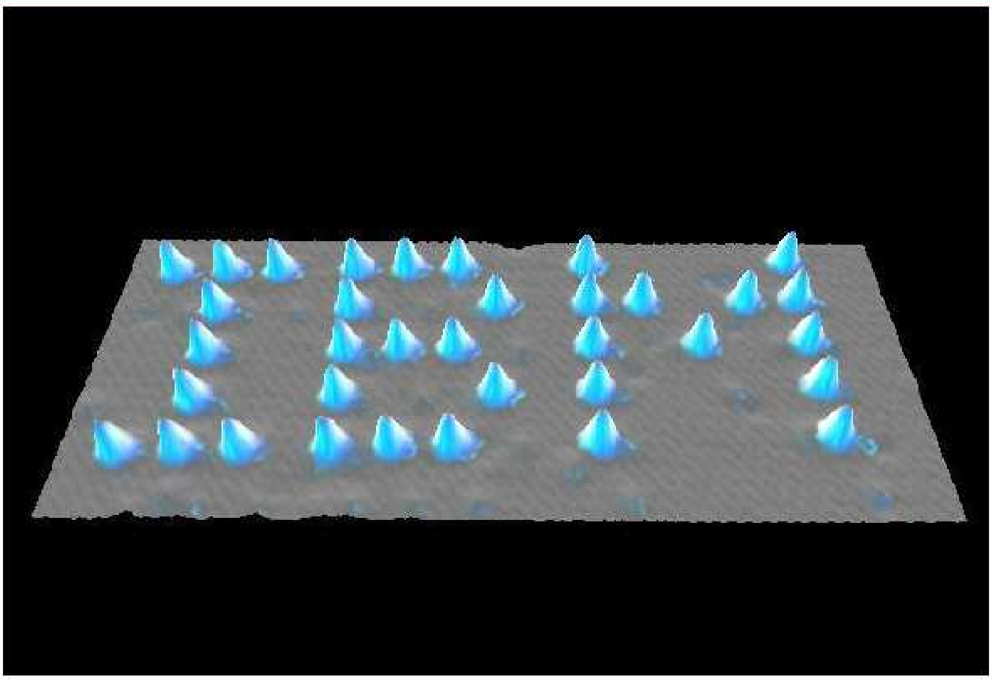

Chemie po krocích

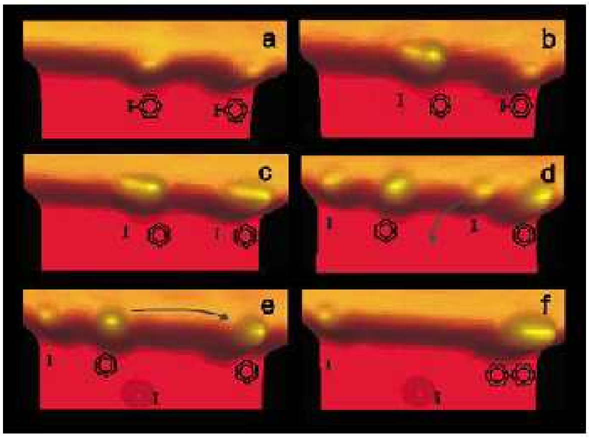

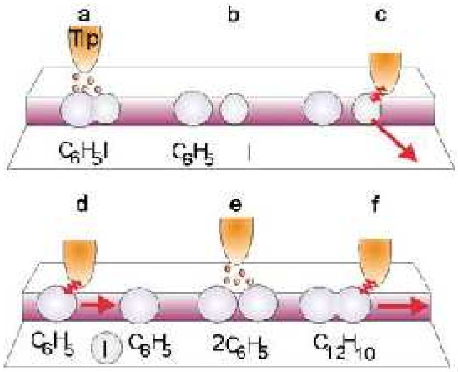

Kvantové ohrady

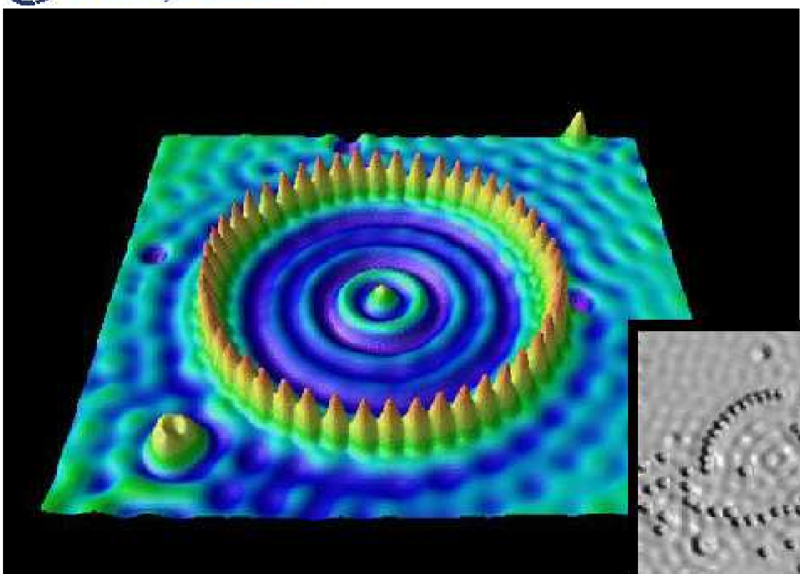

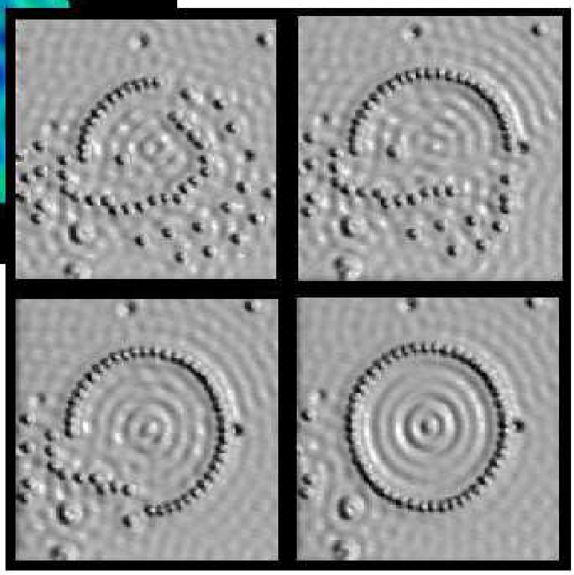

Kvantová fata morgana

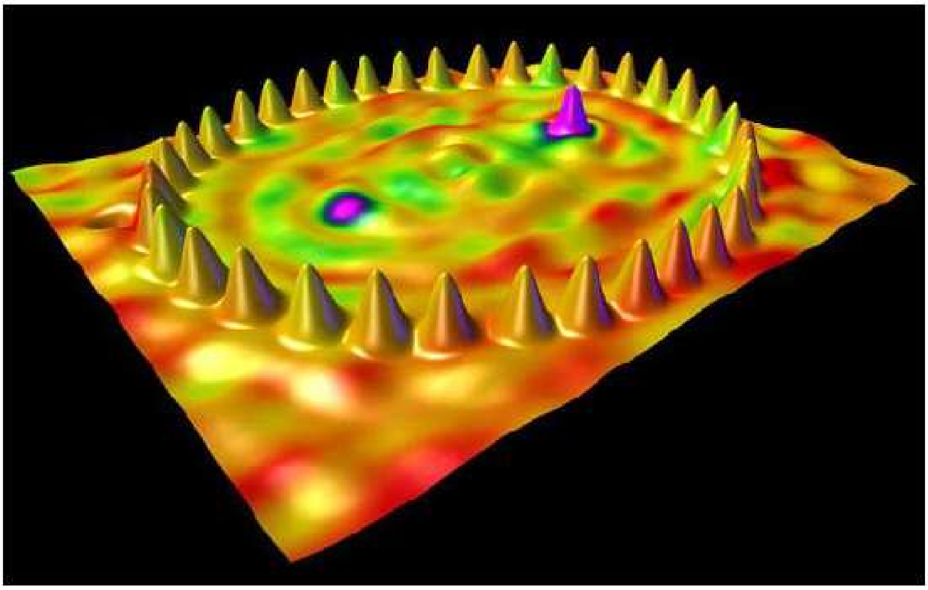

AFM

Atomic
Force
Microscopy

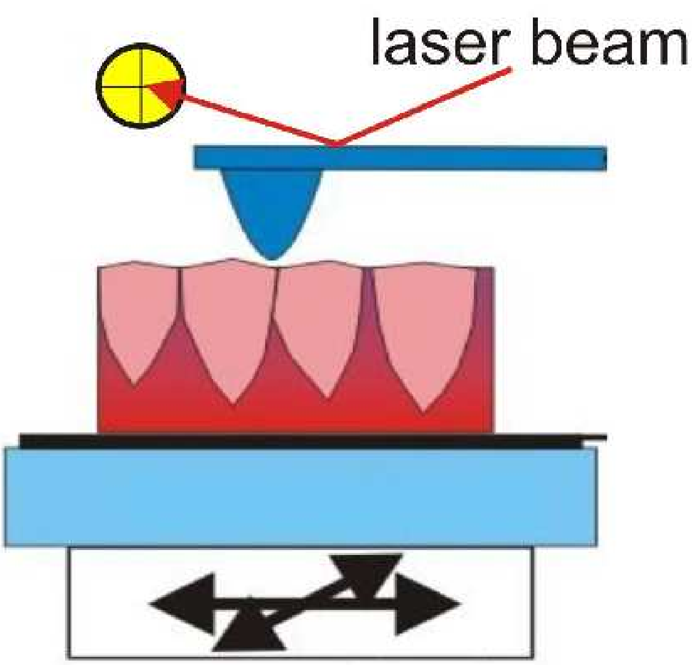

Charles University in Prague
Faculty of Mathematics and Physics

Study programme: Physics
Specialization: Quantum optics and optoelectronics

Mgr. Jakub Holovský

Silicon solar cells: methods for experimental study and evaluation of material parameters in advanced structures

Supervisor: RNDr. Milan Vaněček, CSc.

Institute of Physics,
Academy of Sciences of the Czech Republic, v. v. i.

Outline:

- Motivation
- Introduction
    - Optical simulations
    - Material characterization
    - Dual-junction device characterization
- Conclusion

Motivation:

solar energy: potential of cheap, decentralized, renewable source of energy

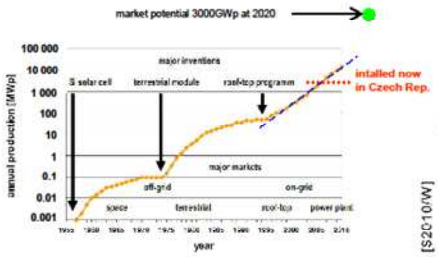

annual growth 45%
(doubles every 2 years)

A. Grubler, Energy Policy 38 (2010) 5174–5188
C. Breyer, Proceedings of 25[th] EUPVSEC 5385-5408

learning rate 20%
(halves every 4 years)

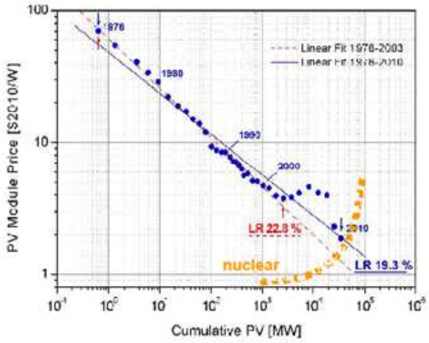

Introduction:

electrical part:

p-i-n solar cell

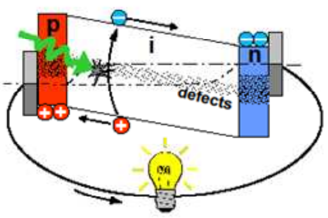

I-V curve

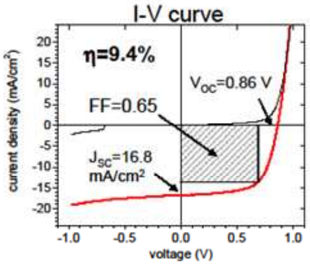

optical part:

flexible thin film
tandem a-Si:H/mc-Si:H
solar cell

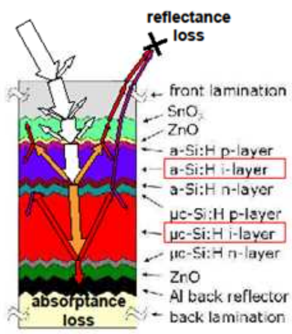

Introduction:

optical + electrical: optical absorption coefficient

$$\alpha_{(\hbar\omega<3eV)} \propto \hbar\omega \cdot \int N_V(E)\ N_C(E+\hbar\omega)\ dE$$

(in dark, limit of T→0)

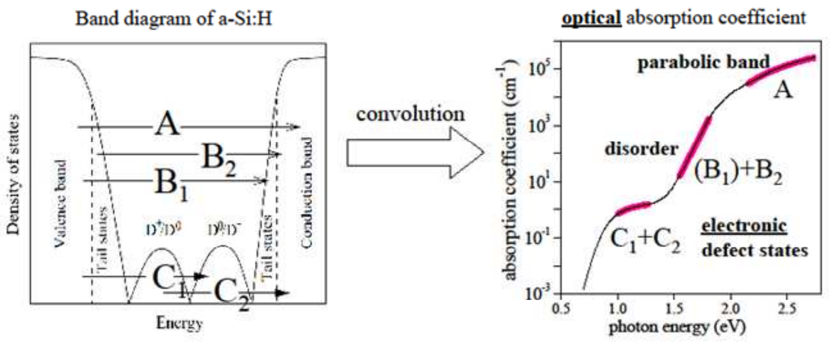

N_D=1.2-2.5·10^{16} · $\alpha_{optical}$(1.2eV)

E. A. Davis, *J. Non-Cryst. Solids*, 1970,

Optical simulations – smooth layer

evaluation of absorption coefficient

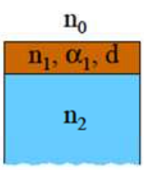

- Fresnel coefficients
- multiple reflections (coherent / incoherent)
- reducing interferences by A/T ratio

$$\frac{A}{T} \cong \frac{e^{\alpha d} - 1 + R_2(1-e^{-\alpha d})}{1-R_2}$$

$$R_2 = \left|\frac{\hat{n}_1 - \hat{n}_2}{\hat{n}_1 + \hat{n}_2}\right|^2$$

approximation

$$\frac{A_{02}}{T_{02}} = \frac{(R_{01}-1)(1-R_{12}-e^{\alpha d}+R_{12}e^{-\alpha d})}{(1-R_{01})(1-R_{12})} + \frac{4\sqrt{R_{10}R_{12}}\ \sin(\delta_1)\sin(\delta_2+2\gamma)}{(1-R_{01})(1-R_{12})}$$

BUT validity of this formula depends on thickness!
→iterative procedure

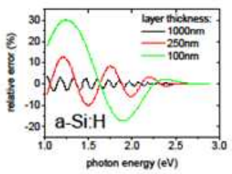

D. Ritter, K. Weiser, Opt. Commun. Vol 57, n.5 1986

Optical simulations – smooth multilayer

simulation of absorptance in multilayer

$\beta = 2\pi N d / \lambda$

- coherent part:

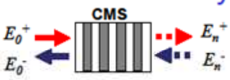

$$\hat{M} = \hat{S}^I_{0,1} \cdot \hat{S}^L_1 \cdot \hat{S}^I_{1,2} \cdot \ldots \cdot \hat{S}^I_{n-1,n}$$

$$r^+_{CMS} = \frac{\hat{M}_{21}}{\hat{M}_{11}} \qquad r^-_{CMS} = -\frac{\hat{M}_{12}}{\hat{M}_{22}}$$

$$t^+_{CMS} = \frac{1}{\hat{M}_{11}} \qquad t^-_{CMS} = \hat{M}_{22} - \frac{\hat{M}_{12}\hat{M}_{21}}{\hat{M}_{11}}$$

$$\begin{pmatrix} E^+_{m-1} \\ E^-_{m-1} \end{pmatrix} = \hat{S}^I_{m-1,m} \cdot \hat{S}^L_m \cdot \ldots \cdot \hat{S}^I_{n-1,n} \cdot \begin{pmatrix} E^+_n \\ E^-_n \end{pmatrix}$$ mutually coherent

absorption in a layer is a balance of intensities: $I = \frac{1}{2}\sqrt{\frac{\varepsilon_0}{\mu_0}}\left[n\left(|E^+|^2 - |E^-|^2\right) + 2k\,\mathrm{Im}(E^{+*}E^-)\right]$

- incoherent part:

$$T_{kl} = |t_{kl}|^2 \frac{n_l}{n_k} \qquad R_{kl} = |r_{kl}|^2$$

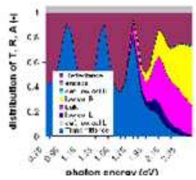

$$\mathrm{M} = S^I_{0,1} \cdot S^L_1 \cdot S^I_{1,2} \cdot \ldots \cdot S^I_{n-1,n}$$

$$R^+ = \frac{\mathrm{M}_{21}}{\mathrm{M}_{11}} \qquad R^- = -\frac{\mathrm{M}_{12}}{\mathrm{M}_{11}}$$

$$\begin{pmatrix} I^+_{M-1} \\ I^-_{M-1} \end{pmatrix} = S^I_{M-1,M} \cdot S^L_M \cdot \ldots \cdot S^I_{N-1,N} \cdot \begin{pmatrix} I^+_N \\ I^-_N \end{pmatrix}$$

$$T^+ = T^- = \frac{1}{\mathrm{M}_{11}}$$

Optical simulations – roughness

Monte-Carlo simulation of absorptance in nanostructured films

fit of total reflectance

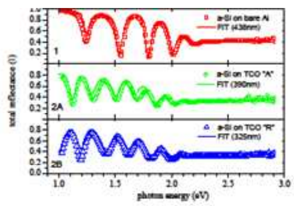

fit of absorptance

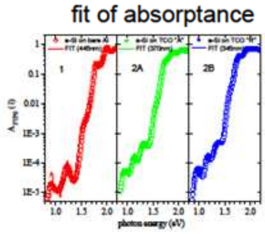

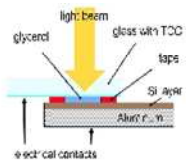

Samples under study: (no.)

- Al foil + a-Si:H (1)
- Al foil „A" + SnO_2 + a-Si:H (2A)
- Al foil „B" + SnO_2 + a-Si:H (2B)
- Corning glass + a-Si:H (0) (measured standardly)

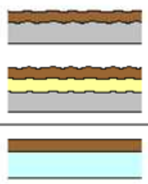

calculated absorption coefficients

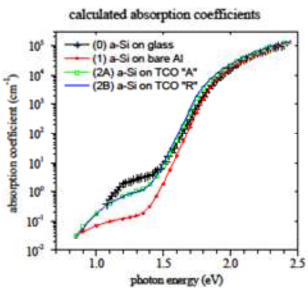

J. Holovský et al., *Physica Status Solidi A*, Vol. 207, p. 578 (2010)

Material characterization

Fourier Transform Photocurrent Spectroscopy (FTPS)

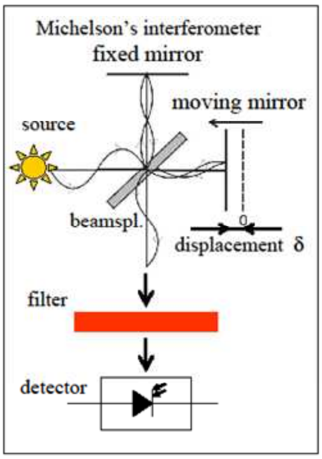

$$J(t) = \mathrm{FT}(\,B(\nu)\cdot F(\nu)\cdot D(\nu)\,)$$

photocurrent — baseline, filter, detector

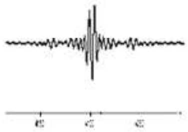

- + Jacquinot → $\Delta\nu \sim (f/\#)^2$ vs. $(f/\#)$ for grating spectrometer
- + Felgett → high speed, <u>constant illumination conditions</u>
- − Felgett → dynamic limit on whole spectrum → <u>filters</u>
- + Nyqist → $\Delta\nu$ = (mirror path length)$^{-1}$
- − Nyqist → λ_{min} = 4 x sampling step of movable mirror
- − <u>high frequency</u>, λ-dependent <u>modulation</u> $f_{modulation} = 2\cdot v\cdot \nu$

A. Poruba et al. , *17th EU-PVSEC*, pp. 2981-2984 (2001)

Complexity of FTPS

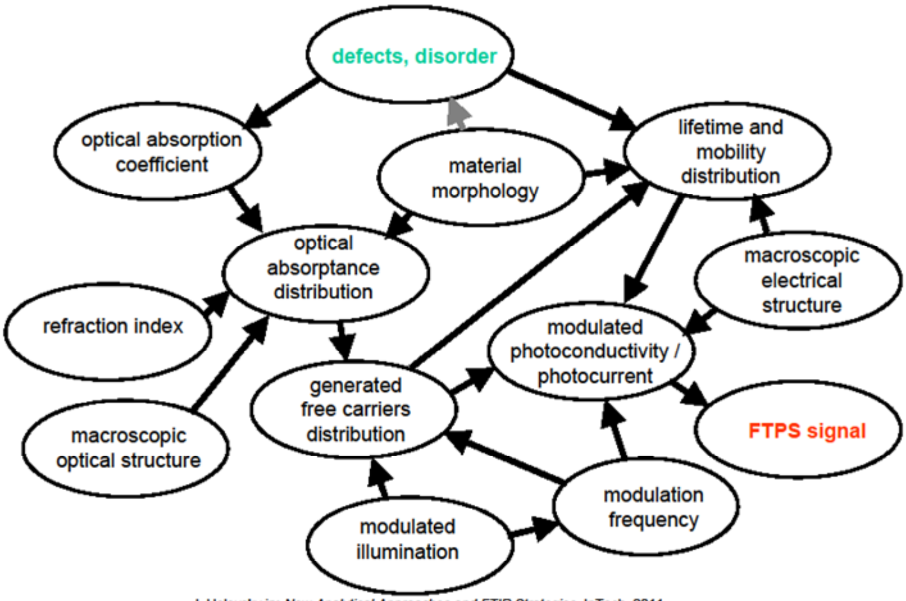

J. Holovsky in: *New Analytical Approaches and FTIR Strategies*, InTech, 2011

Complexity of FTPS

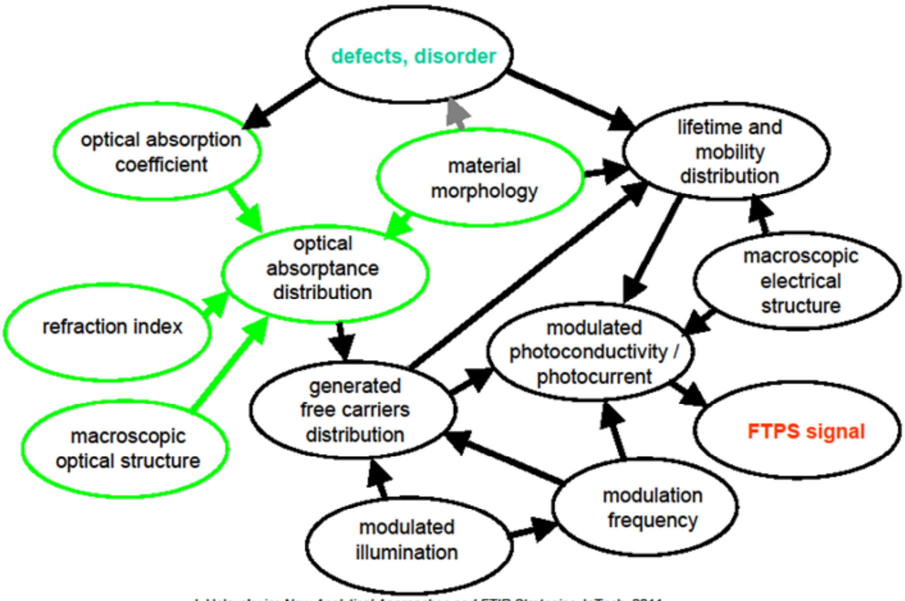

J. Holovsky in: *New Analytical Approaches and FTIR Strategies*, InTech, 2011

FTPS: structure → opt. absorptance

distribution of optical absorptance

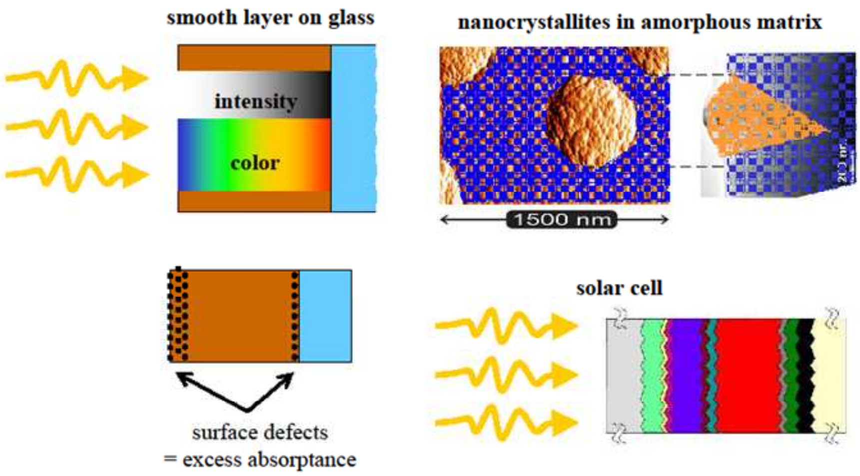

picture: T. Mates, et al., Journal of Physics: Conference Series 61 (2007) 790–794

Complexity of FTPS

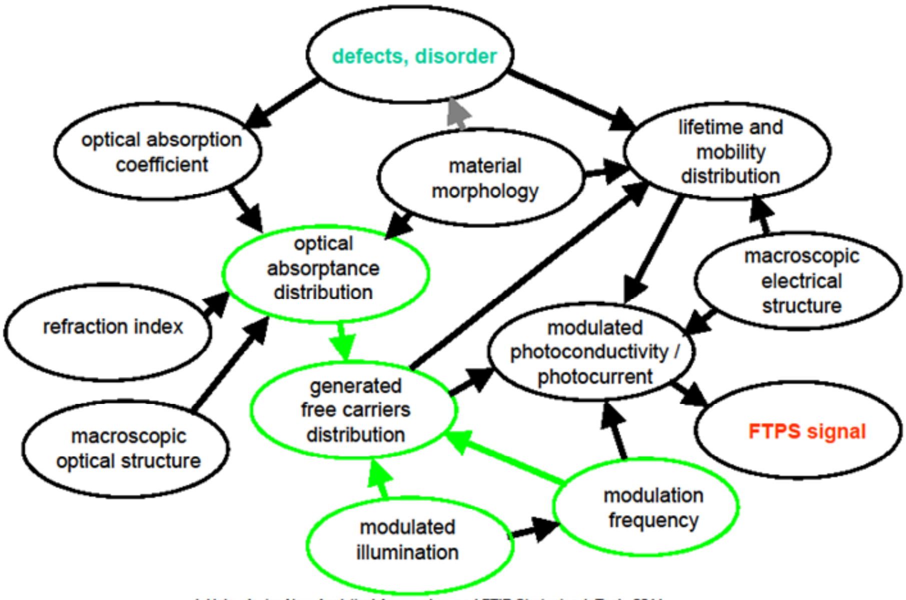

J. Holovsky in: *New Analytical Approaches and FTIR Strategies*, InTech, 2011

FTPS: absorptance → carrier density

optical absorptance and conductive carriers density

$$\varepsilon_2(\hbar\omega < 3eV) \propto \hbar\omega\int N_V(E)\; N_C(E+\hbar\omega)\; dE$$

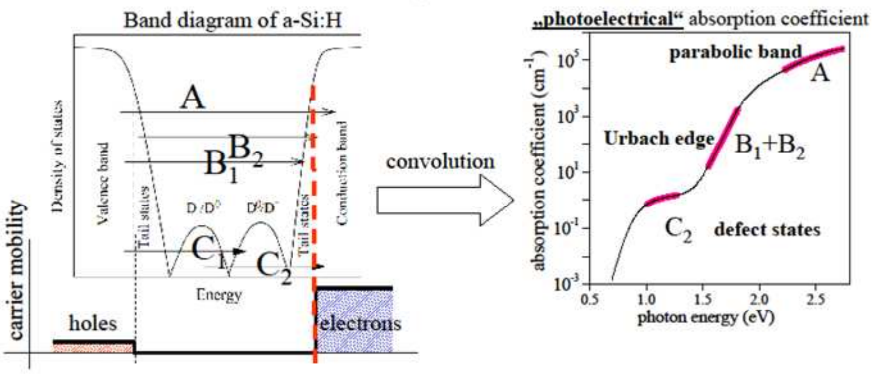

-in „photoelectrical“ absorption coefficient transition C_1 is missing,

-transition B_1 is maintained by thermalization under room temperature

→ we can still calculate with $A_{photoel.}$ as with $A_{optical}$ and $N_{D,\,optical} = 2 \cdot N_{D,\,optoel.}$

FTPS: absorptance → carrier density

frequency dependence of photocarrier density

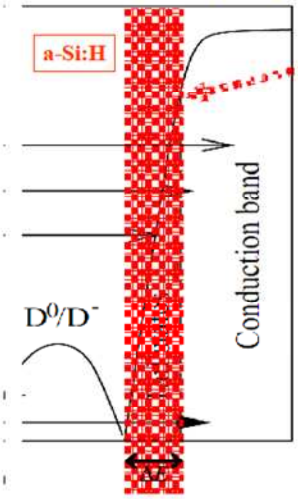

region of thermalization - probability, that electron will be thermally excited above the mobility edge in phase with excitation frequency ω is * :

$$p = \left[1 + \left(\frac{\omega}{f_0}\right)^2 \exp\left(\frac{2\Delta E}{k_B T}\right)\right]^{-1}$$

→ **free carrier generation is generally frequency dependent:**

Modulated Photocurrent Method * showed noticeable effect at frequencies around 1kHz

→ **problem**

* K. Abe, et al. ,Philosophical Magazine B, Vol. 58, No. 2, pp. 171-184 , 1988

FTPS: absorptance → carrier density

frequency dependence of photocarrier density

dual beam phtotocurrent (DBP) and FTPS

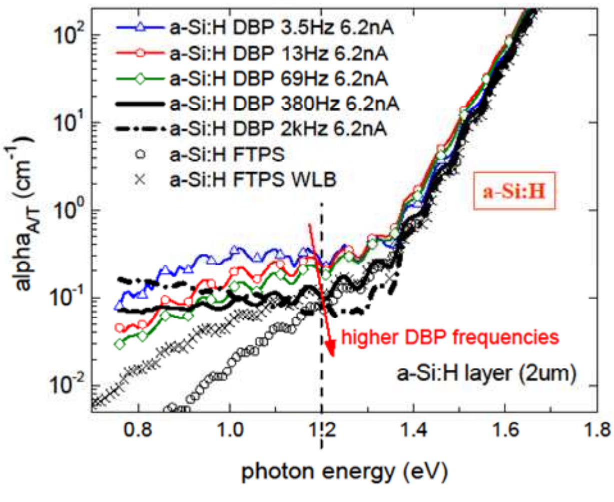

J. Holovský, J. Non-Cryst. Solids 354 (2008) 2167 – 2170

Complexity of FTPS

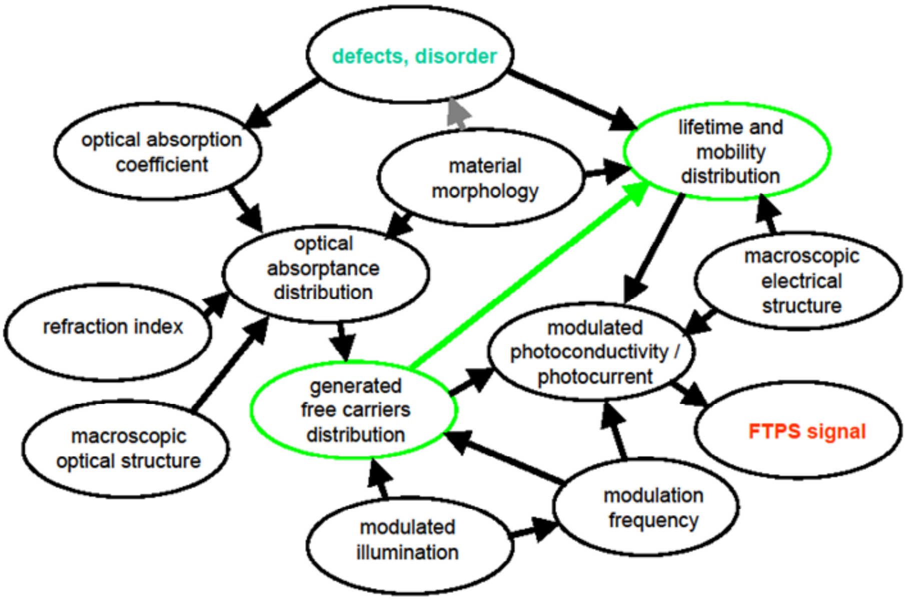

FTPS: carrier density → lifetime

lifetime dependence on illumination

photocurrent density: $j_{ph} = eE \cdot G \cdot \mu \cdot \tau$ (**mobility** — μ, **lifetime** — τ)

BUT! ...the excess carriers change the position of quasi-Fermi levels
→ traps/recombination centers changes → lifetime changes → $\tau = \tau(\Delta N) = \tau(G)$

in classical spectroscopy : $G = G(\lambda)$ → $\tau = \tau(\lambda)$!

→ **a) Dual Beam Photocurrent** : <u>additional $G_{const.}$</u> $>> G(\lambda)$ → $\tau \approx$ const.

problem : <u>no more „in dark“</u> → dependent on $G_{const.}$

→ **b) Constant Photocurrent Method** : change $G(\lambda)$ to keep <u>j_{ph} constant</u> → $\tau \approx$ const.

→ **c) Fourier Transform Phot. Spectr.** : <u>both G and j_{ph} constant</u> → $\tau \approx$ const.

→ „dark“ conditions in FTPS are satisfied only if the <u>IR filter</u> is used

Complexity of FTPS

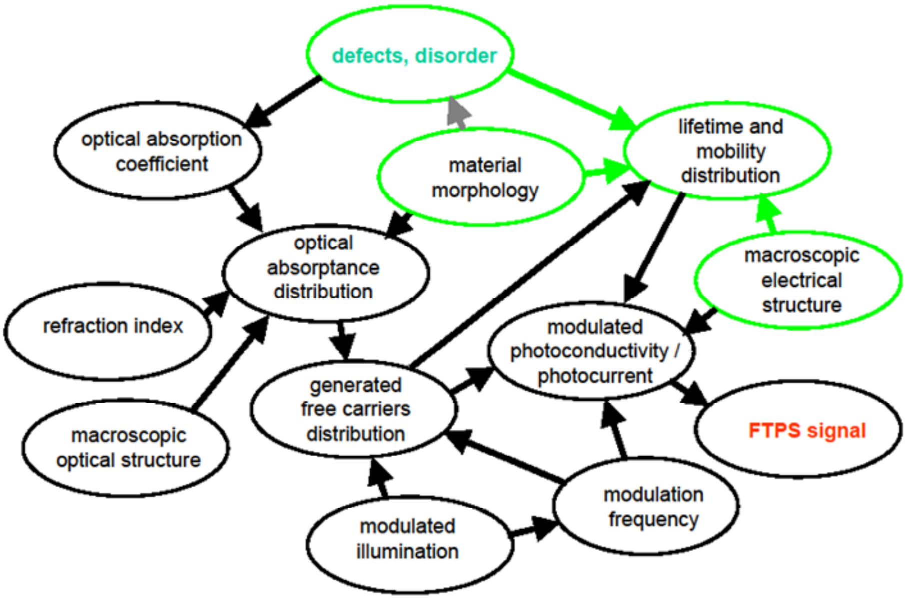

FTPS: structure → mobility lifetime

structural effects influencing mobility lifetime:

a) microstructrual - grains

$\mu\tau$(grains) > $\mu\tau$(amorphous matrix)

nanocrystallites in amorphous matrix

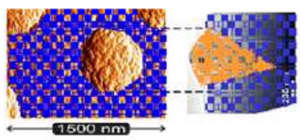

b) surfaces, interfaces

every non passivated interface (surface) represents strongly defective area with strong recombination rate and low lifetime τ

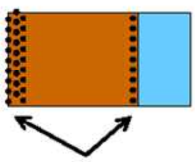

surface defects
= „dead zones“

Complexity of FTPS

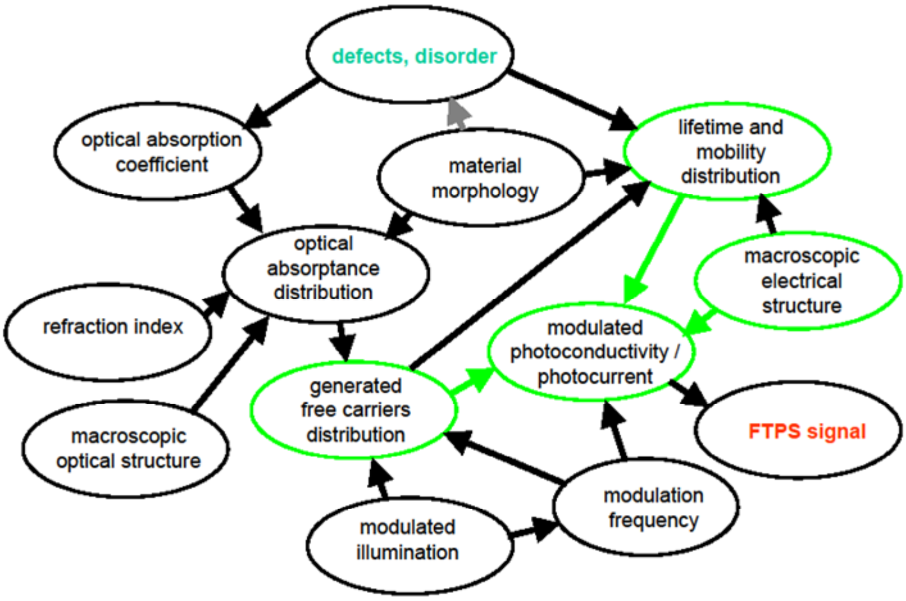

FTPS: distributions → el. current

a) distribution of mobility, lifetime and generation

THIN (<1μm) layer on glass, coplanar contacts:

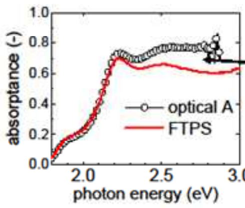

signal loss at high absorption

effect of surface defect states

$$j_{ph} = eE \cdot \int G(\alpha(z)) \cdot \mu\tau(z)\, dz$$

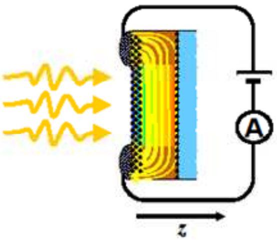

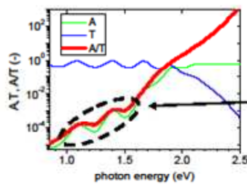

non-vanishing interferences due to surface defects

M. Vaněček, et al. , *J. Appl. Phys.* 78 (1995) 6203-6210

FTPS: distributions → el. current

a) distribution of mobility, lifetime and generation

model representation:

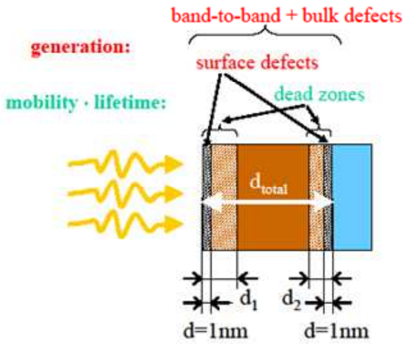

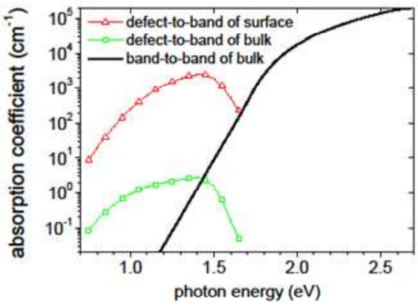

optically simulated as smooth multilayer on substrate - matrix approach

J. Holovský et al., J. Non-Cryst. Solids, 2011, in press

FTPS: distributions → el. current

a) distribution of mobility, lifetime and generation

numerical fit of measured data:

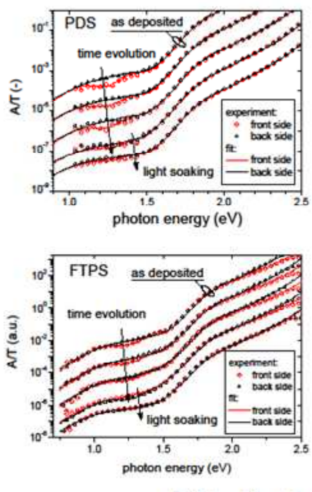

observed time evolution in defect density:

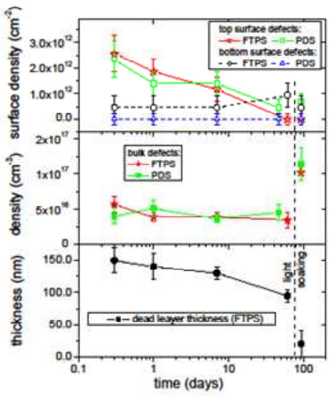

→ all the changes explained only by effct of time evolution of surface states

J. Holovský et al., J. Non-Cryst. Solids, 2011, in press

Complexity of FTPS

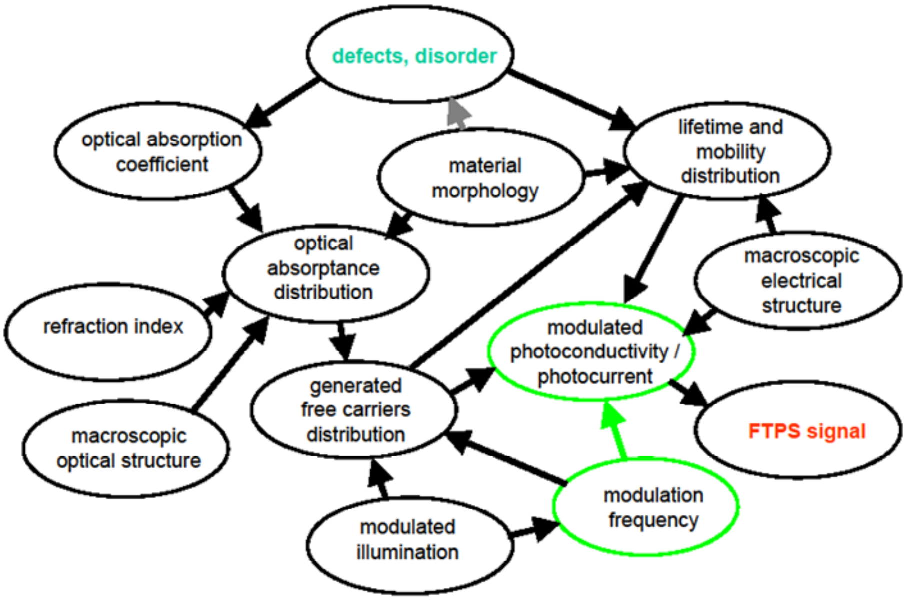

FTPS: distributions → el. current

b) effect of time dependence

continuity equation: $\frac{\partial n}{\partial t} = \frac{1}{e}\nabla \cdot \mathbf{j} + G(t) - R(n)$

time dependent generation → frequency dependence

approximation: $j_{ph} = eE \cdot G \cdot \mu \cdot \tau$

validity:

		amorphous silicon:	crystalline silicon:
slow modulation frequency:	$\partial n / \partial t \cong 0$ $1/\tau >> f = 10^4 Hz$	$\tau = 10^{-6} - 10^{-5} s$ **YES**	$\tau = 10^{-4} - 1s$ **NO**
quasi-homogeneous generation and recombination:	$\nabla n \cong 0$ $\alpha d < 1$	$\alpha(2eV) = 10^4 cm^{-1}$ $d = 1\mu m$ **YES**	$\alpha(2eV) = 3 \cdot 10^3 cm^{-1}$ $d = 100\mu m$ **NO**

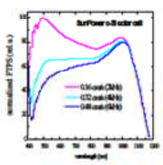

Outline:

- Motivation
- Introduction
  - Optical simulations
  - Material characterization
  - **Dual-junction device characterization**
- Conclusion

Dual-junction device characterization

schematics of tandem solar cell

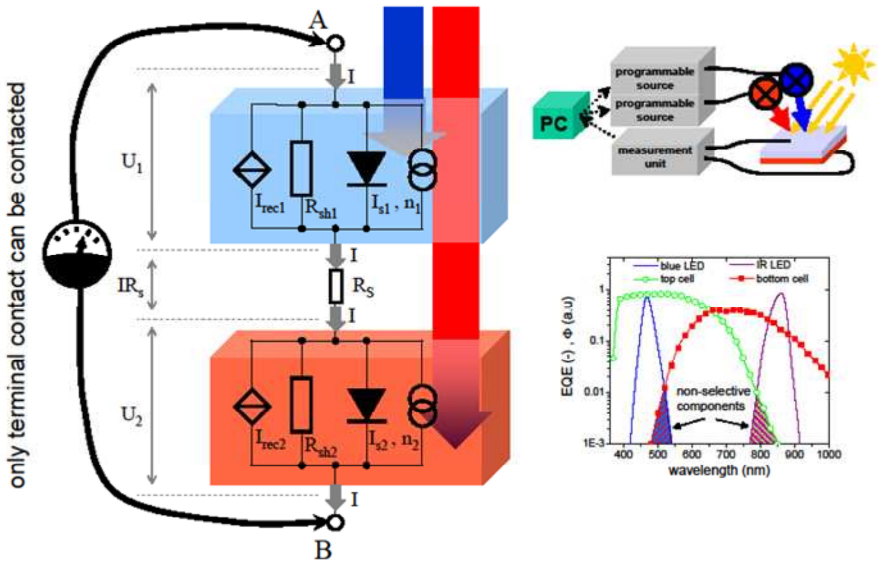

Dual-junction device characterization

measurement of I-V curves of individual sub-cells

selective bias light of variable intensity: $\Phi = J / EQE(\text{bias light})$

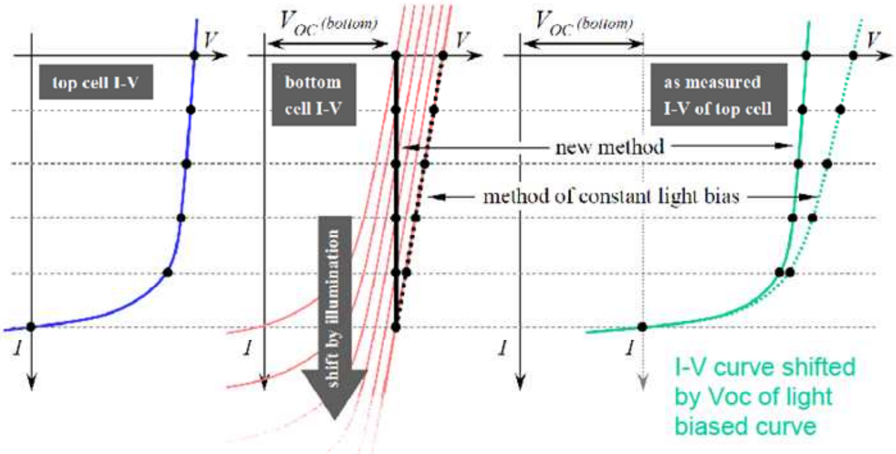

Dual-junction device characterization

measurement of I-V curves of individual sub-cells

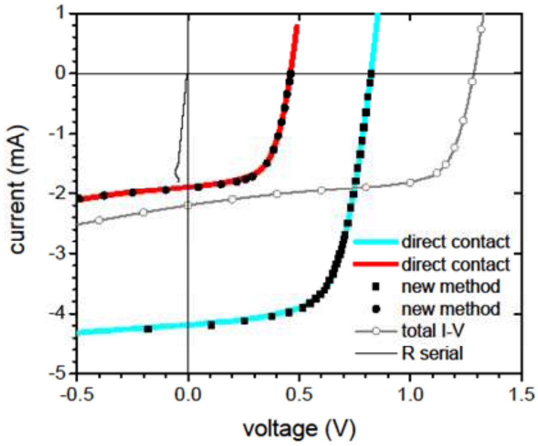

We only have to know individual values of open-circuit voltage (V_{OC}) !

J. Holovský et al., Solar Energy Materials and Solar Cells, 103, p. 128-133 (2012)

Dual-junction device characterization

measurement of V_{OC} of individual sub-cells

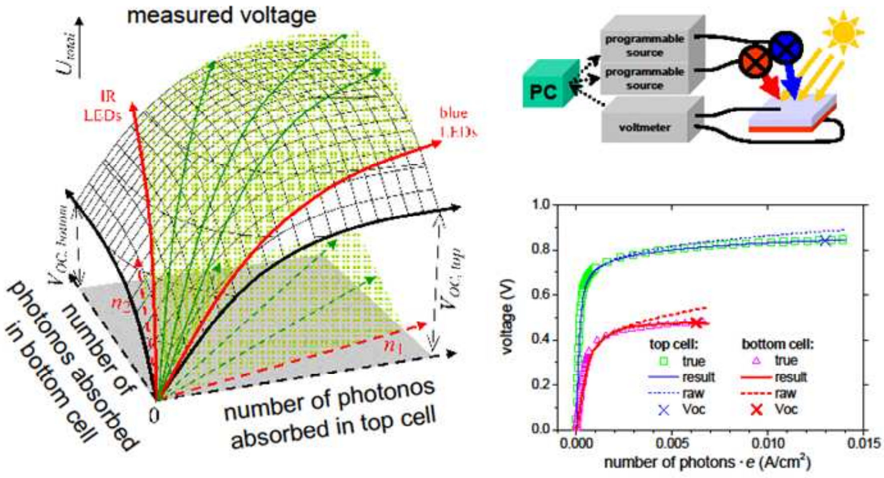

J. Holovský et al., IEEE Journal of Photovoltaics, 2, 164-168, (2012)

Conclusion

Optical simulation
- absorptance / evaluation of absorption coefficient
- smooth / rough, single- / multi-layer
- Monte-Carlo / vector approach

Material characterization
- fundamentals of Fourier transrorm
- fundamentals of material (silicon)
- real structures: surface states, roughness, metal substrates

Characterization of dual-junction solar cells
- electrical and optical representation
- methods to access to individual parameters: FTPS, I-V

Study of nucleation and growth of diamond thin films

T. Ižák[1,2*], O. Babchenko [1], M. Varga[1,2], S. Potocky[1], M. Marton[2], M. Vojs [2], M. Domonkos [1,3] and A. Kromka [1]
[1] Institute of Physics AS CR, Cukrovarnicka 10, 16253 Praha 6, Czech Republic
[2] Slovak University of Technology, FEI STU, Ilkovicova 3, 812 19 Bratislava, Slovakia
[3] Faculty of Nuclear Sciences and Physical Engineering, CTU, Břehová 7, 115 19 Praha, Czech Republic

This study deals with the nucleation and growth of CVD diamond films on Si substrates. In nucleation part two different nucleation methods were studied: (i) the bias enhanced nucleation (BEN) and (ii) ultrasonic seeding. In the case of BEN, (i) the nucleation time and (ii) the influence of bias voltage were studied. For ultrasonic seeding the effect of different solutions of ultradisperzed detonation nanodiamond (UDD) powder with metal particles on the nucleation efficiency and growth process was investigated (i.e. diamond powder, nanosized Ni, microsized Co and Y metal powders). Moreover, the effect of isopropyl alcohol and deionized water on the nucleation efficiency was compared. In the third part, it was focused on the self- and re-nucleation processes in different microwave power deposition systems on non-treated (non-nucleated substrates) in order to achieve more information about nucleation process and plasma properties. The content of CO_2 or CH_4 in the gas mixture and the pressure was varied.

In second main part of this study, the diamond film growth in various chemical vapour deposition (CVD) systems was demonstrated: hot filament CVD (HFCVD), focused microwave plasma CVD (FMWP) and pulsed linear antenna microwave plasma CVD (PLAMWP). The growth process of micro- to nano- crystalline diamond films, as low temperature diamond growth (LTDG) and re-nucleation process was studied (including the influence of Ar and N_2 addition, the effect of increasing CO_2 and CH_4). Systematic study was realized also on the pressure, temperature and gas mixture. The surface morphology of diamond films was analysed by SEM microscopy and their chemical composition (sp^2 vs. sp^3 carbon bonds) by Raman spectroscopy. The surface chemistry was characterized by activation energies.

Acknowledgements
This work was supported by the grant P108/12/G108 (GAČR Excellence Center) and it was carried out in frame of the LNSM infrastructure. We would like to gratefully appreciate to K. Hruska, M. Michalka for SEM measurements and J. Potmesil and O. Rezek for technical support.

Institute of Physics AS CR

3rd Winter Educational Seminar, Rokytnice nad Jizerou
(February Wednesday 1 - Saturday 4, 2012)

Study of nucleation and growth of diamond thin films

T. Ižák[1,2*]***, O. Babchenko***[1]***, M. Varga***[1,2]***, S. Potocky***[1]***, M. Marton***[2]***, M. Vojs***[2]***, M. Domonkos***[1,3] ***and A. Kromka***[1]

[1] Institute of Physics AS CR, Cukrovarnicka 10, CZ-16253 Praha 6, Czech Republic
[2] Slovak University of Technology, FEI STU, Ilkovicova 3, 812 19 Bratislava, Slovakia
[3] Faculty of Nuclear Sciences and Physical Engineering, CTU, Břehová 7, 115 19 Praha, Czech Republic

Rokytnice nad Jizerou, 2012

Introduction to nucleation of diamond films

- **Pre-treatment of the substrate surface** → to enhance the **nucleation density**
  → enhance the formation of **diamond nuclei** on non-diamond substrates
  → nucleation density on **untreated** non-diamond substrates **10^5 cm^{-2}**

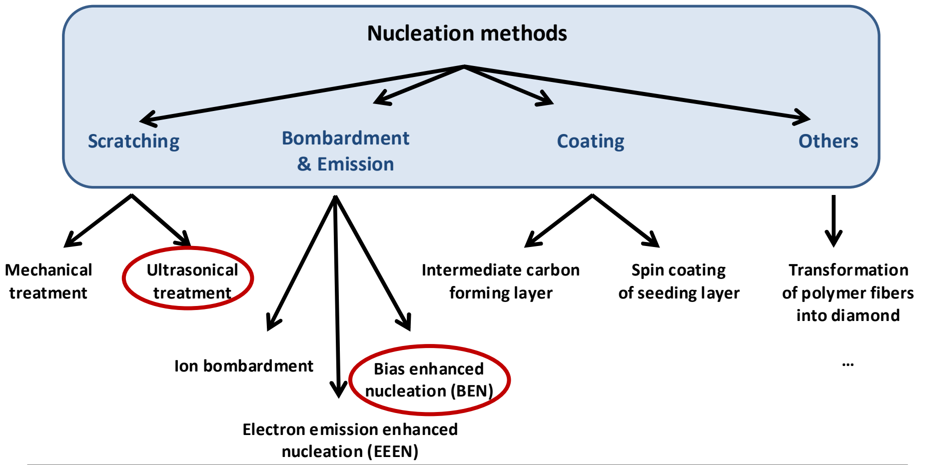

BEN vs. ultrasonic seeding

Bias enhanced nucleation

+ high nucleation density >10^8 cm^{-2}
– only conductive substrates
– 2D geometry
– complicated system (only HFCVD)

Ultrasonic seeding

+ high nucleation density 10^7-$10^{11}$$cm^{-2}$
+ all type of substrate
+ 3D geometry
+ simple, fast method

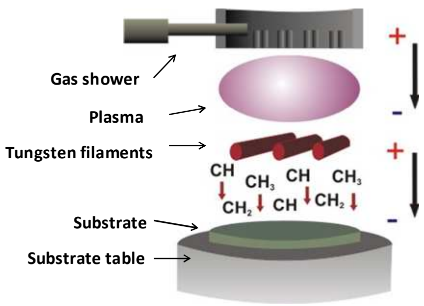

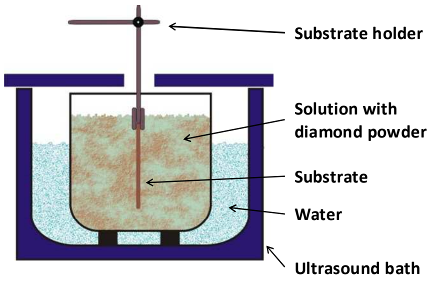

Nucleation – Experimental part

Bias enhanced nucleation

Ultrasonic seeding

Effect of <u>nucleation time</u>

Effect of <u>bias voltage</u>

<u>Influence of solution</u>
- Deionized (DI) water
- Isopropyl alcohol

<u>Influence of mixture</u>
- Diamond powder (DP)
- Combination of DP with Ni, Co, Y

Bias Enhanced Nucleation

Effect of process time (at constant U_b= - 170V)

30 min	60 min	120 min

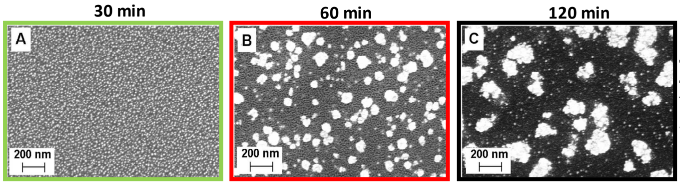

no diamond clusters	~ 10^8 cm^{-2}, 50 ÷ 100 nm	~ 10^7 cm^{-2}, 100 ÷ 130 nm

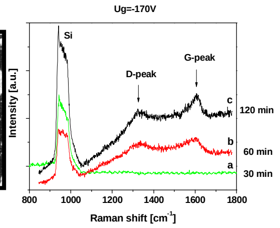

Effect of bias voltage (at constant t = 120 min)

- 120 V	- 170 V	- 220 V

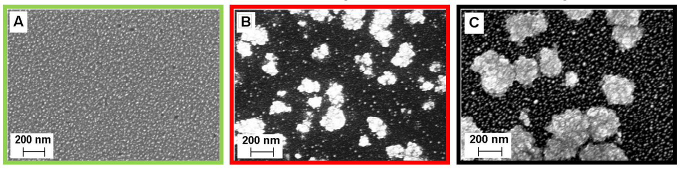

no diamond clusters	~ 10^7 cm^{-2}, 150 ÷ 200 nm	~ 10^7 cm^{-2}, 200 ÷ 400 nm

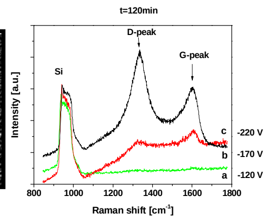

Ultrasonic Seeding

Isopropyl alcohol+DI water nanodiamond (ND) powder	Deionized water ND powder	Deionized water ND powder+Ni	Deionized water ND powder+Co	Deionized water ND powder+Y

After nucleation (i.e. ultrasonic seeding)

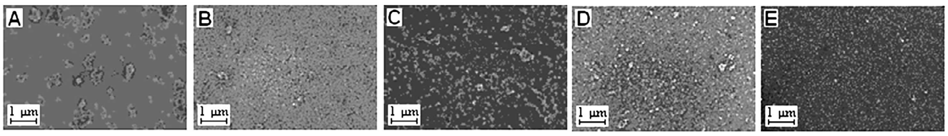

After 10 min growth (i.e. high-lighting the nucleation centers)

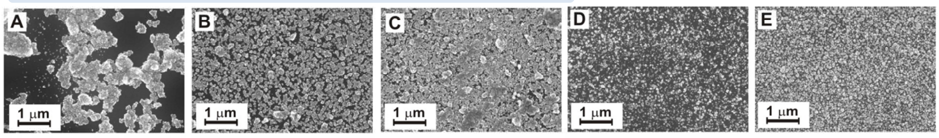

After 1 h growth (i.e. over-grown the layer)

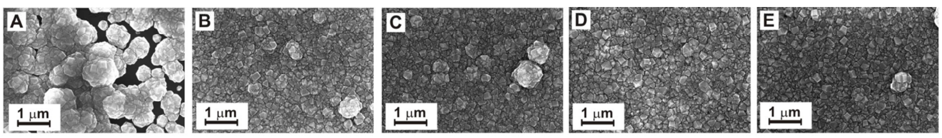

Self- and re-nucleation

Motivation:

- Diamond growth **without any pre-treatment** → useful for soft substrates
- Study of self-nucleation → more information about **growth process & plasma character**
- Nucleation density → as high as possible →

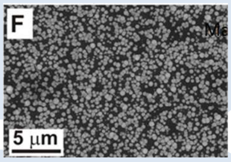

Definitions:

Self-nucleation - nucleation (formation of diamond clusters) on non-treated substrates

Re-nucleation - nucleation during the growth process (secondary nucleation) (important for UNCD growth)

Experiments:

- **Comparison** of PLAMWP & FMWP apparatus
- **Influence** of CO_2, CH_4, pressure, temperature, etc. on self-nucleation

---

- Substrates: Si & SiO_2
- Analysis methods: SEM microscope & Atlas software (statistical distribution)

Self- and re-nucleation – Effect of CO_2

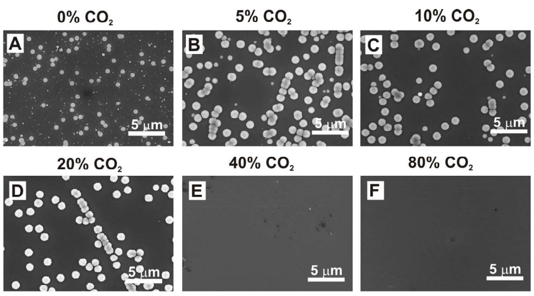

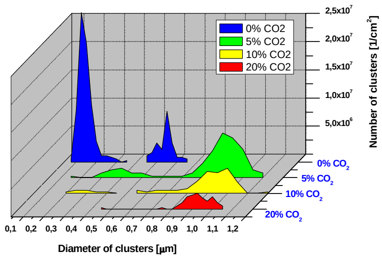

Effect of pressure:

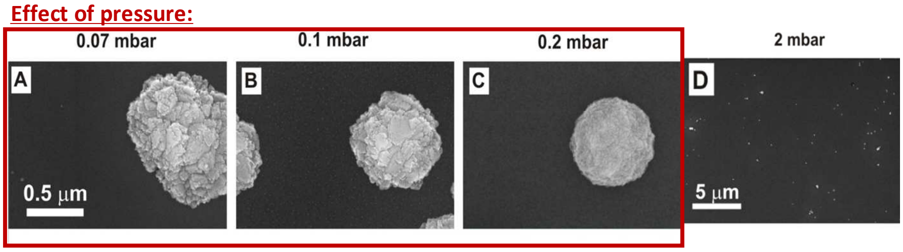

Self- and re-nucleation – Effect of CH_4

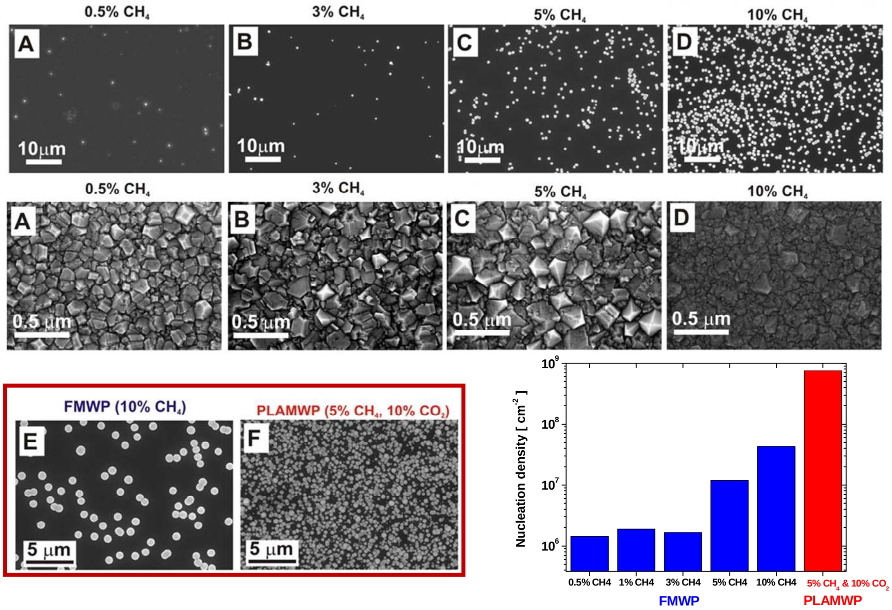

Introduction to diamond growth

- **HPHT** (high pressure – high temperature): 5-10 GPa, 2000°C
- **CVD** (chemical vapor deposition): hot filament, microwave plasma

Principle of CVD

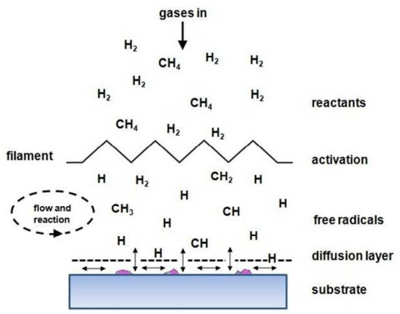

Bachmann triangle

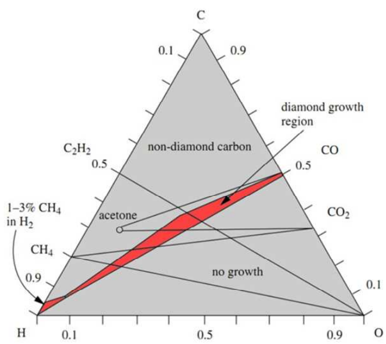

P.W. May, Phil. Trans. R. Soc. Lond. A 358 (2000), 473-495

- **Trend:** low temperature & large area deposition

Deposition systems

HF CVD (Hot Filament CVD)	FMWP (Focused MW Plasma)	PLAMWP (Pulsed Linear Antenna MW Plasma)

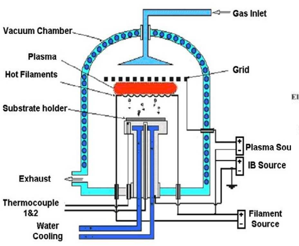

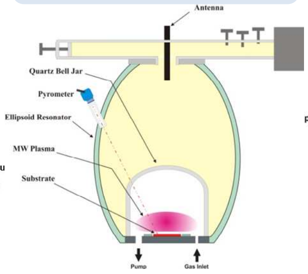

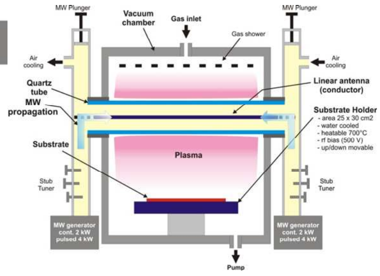

HF CVD

- \+ Double-bias assisted system (BEN nucleation)
- \+ Fast & cheap
- − Low quality (contamination from filaments)
- − Short lifetime of filaments
- − Not advisable to add oxygen (refractory metals burn rapidly)
- − Limited deposition area

FMWP

- \+ Microwave plasma (high quality diamond films)
- \+ Fast deposition
- − Focused plasma (limited deposition area)
- − Hot plasma (deposition temperature > 400 °C)

PLAMWP

- \+ Large area deposition (20 x 30 cm^2)
- \+ Cold plasma (low temperature diamond deposition)
- \+ Wide range of application: (CNT growth, low T plasma treatment…)
- \+ Fully compatible with industry
- − Low growth rate & relatively expensive

Izak T. et al., Study of nucleation and growth of diamond thin films 11

From MCD to NCD

Effect of negative bias voltage (in HFCVD)

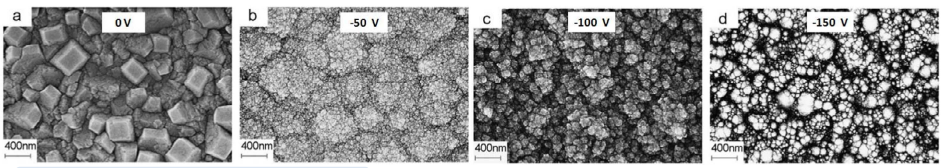

Effect of argon addition (in HFCVD)

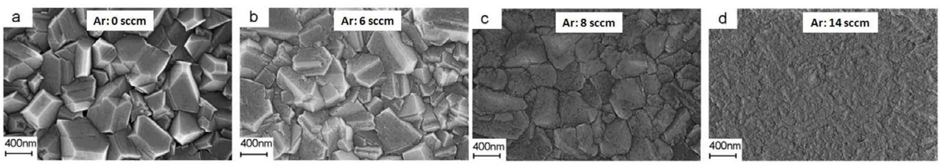

Effect of methane addition (in FMWP)

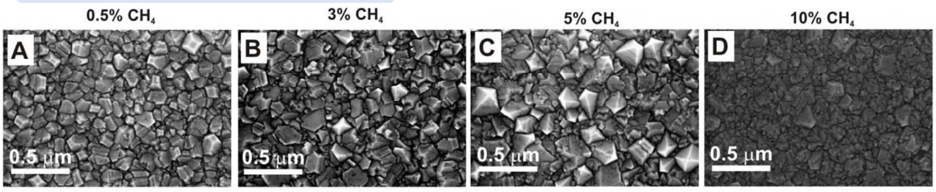

Izak T. et al., Study of nucleation and growth of diamond thin films 12

From MCD to NCD

Effect of methane addition (in FMWP)

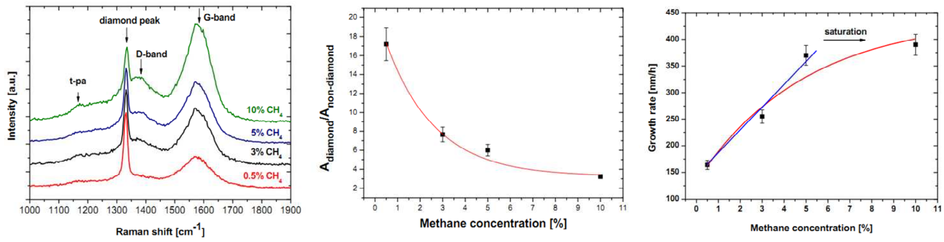

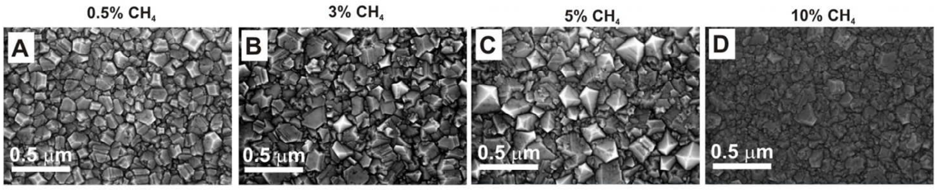

Izak T. et al., Study of nucleation and growth of diamond thin films 13

From MCD to NCD

Effect of CO_2 addition (in PLAMWP)

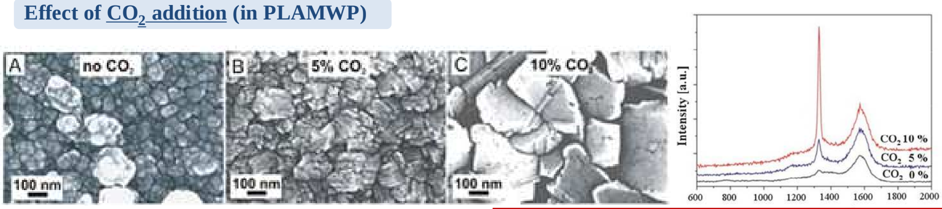

Effect of pressure (in PLAMWP)

0.1 mbar **2 mbar**

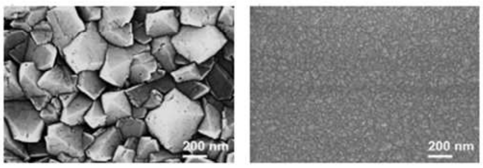

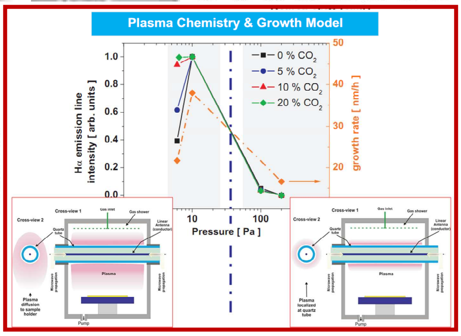

(Kromka et al., 22[nd] Diamond Conference, 4-8 September 2010, Garmisch-Partenkirchen, Germany)

Izak T. et al., Study of nucleation and growth of diamond thin films 14

Low Temperature Diamond Growth

Motivation: Normally high deposition temp. (800–900 °C) ⟶ **limitations** in applications to high melting materials

NCD on AF glass (~750°C)

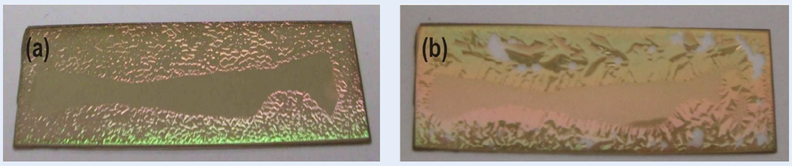

Few hours after deposition | **Few days after deposition**

Solution

Changed growth chemistry

→ **Halogenated precursors** - F_2 and Cl_2 (T_{sub} =370 °C)
→ **Oxygen containing precursors** - CO/H_2, $CO/H_2/O_2$, or CO_2/CH_4 (T_{sub} =130°C)
→ **Argon/nitrogen addition** – mainly UNCD

Developing of new plasma systems

→ using of **linear system** instead of focus plasma *(cold plasma)*

▪ LTDG in Linear-antenna plasma MWCVD

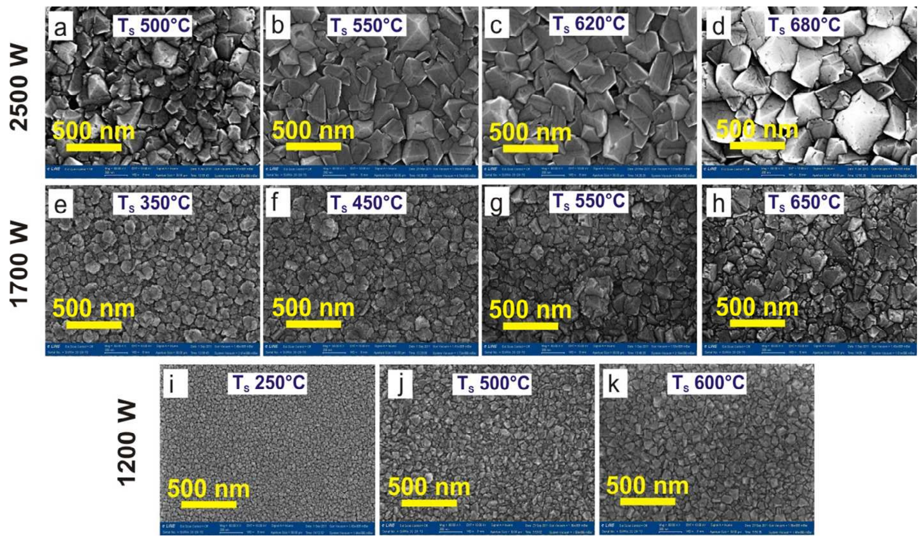

Source: Izak et al., Low temperature diamond growth by linear antenna plasma CVD over large area, physica status solidi (b), 2012 (accepted paper)

▪Raman spectra & Activation energy

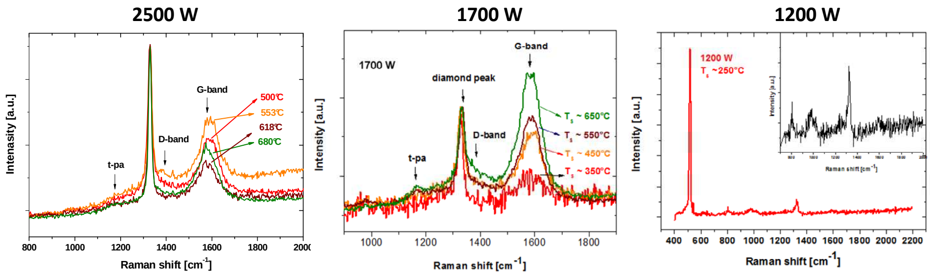

Growth rate vs. $T_{substrate}$

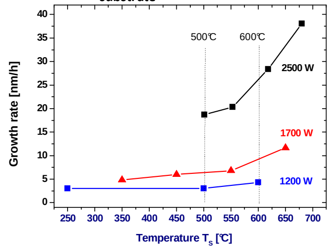

Arrhenius plot

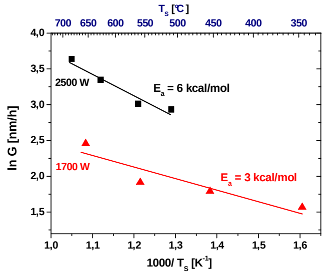

Source: Izak et al., Low temperature diamond growth by linear antenna plasma CVD over large area, physica status solidi (b), 2012 (accepted paper)

Applications of LTDG

Grazing angle reflectance (GAR) spectroscopy under the Brewster's angle

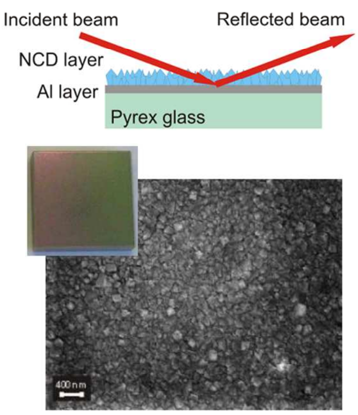

(O. Babchenko et al., Deposition of nanocrystalline diamond films on temperature sensitive substrates for infrared reflectance spectroscopy, phys. stat. sol. (b), submitted)

(H. Kozak et al., Optical characterisation of organosilane-modified nanocrystalline diamond films, Chem. Papers, 2011, 65(1), p. 36-41)

Attenuated total reflectance (ATR) spectroscopy with diamond-coated ATR prism

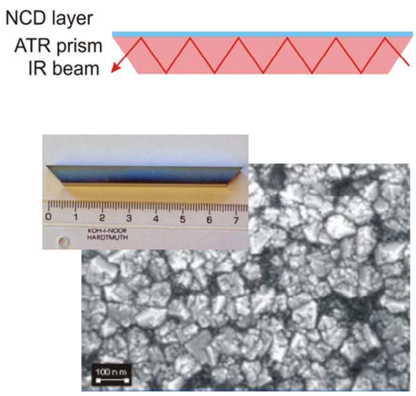

(Z. Remes et al., Using diamond-coated ATR prism for FTIR spectroscopy of functionalized diamond nanoparticles, Diam. Relat. Mater., submitted)

Thank you for your attention!

This work was supported by the grant P08/12/G108 (GAČR Excellence Center) and it was carried out in frame of the LNSM infrastructure. We would like to gratefully appreciate to K. Hruska, M. Michalka for SEM measurements and J. Potmesil and O. Rezek for technical support.

Ing. Tibor Ižák, PhD. , *izak@fzu.cz*

Institute of Physics AS CR, Cukrovarnicka 10, CZ-16253 Praha 6, Czech Republic

Perspectives in Diamond Thin Film Technology

Alexander Kromka et al.
Institute of Physics, Academy of Sciences of the Czech Republic, v.v.i.
Cukrovarnická 10, Praha 6, 162 00, Czech Republic, kromka@fzu.cz

Synthetic diamond thin films are routinely grown over world not only for basic research but also for industrial uses. At the Institute of Physics (IoP), diamond thin films are grown since 2002. The first installed deposition system is base on microwave plasma enhanced chemical vapor deposition (CVD) in hydrogen reach gas mixture (<2% methane diluted in hydrogen). This system is well suitable for fast growth of high quality diamond films up to 5 cm in diameter. The main advance of the system is cavity like resonator which allows running stable CVD process for several days at relatively high pressures (>200 mbar). Later on, in year 2008 was installed the linear antenna microwave plasma CVD system which work at much lower pressures (<10 mbar). The main advantage of this system is deposition over large area and stable plasma for various gas mixtures (i.e. argon reach, high methane content, etc.). Bothe these CVD techniques can be classified as complementary processes which opens nvoel field for basic research. For example, diamond films are first grown by linear antenna microwave plasma CVD process and after then they are hydrogenated in elippsoidal cavity microwave CVD system. Similarly, experiments work well also in opposite direction. Additional advantage of linear antenna microwave plasma CVD process is so called cold plasma due to low pressure. It means that thermal overloading of the substrates from plasma is minimized.
In close cooperation of research groups at IoP, especially Rezek's group and Remes's group, we have optimized the CVD process for low temperature (aluminum, glass) and mechanically soft substrates (thin gold layer, germanium, etc.). In specific cases, novel diamond nucleation and seeding processes have been developed to satisfy need for growth of ultra-thin diamond film over soft substrates. These substrate-treatment process include polymer-based composites and nanofibers. Within the presented lecture, technological steps as nucleation/seeding process, the CVD growth and plasma structuring are reviewed with respect to experimental activities at the IoP-Cukrovarnicka. Join activities are formally under the umbrella of CABIOM centre which is the virtual centre on Carbon-based Biomaterials and Biointefaces (http://cabiom.fzu.cz/). Mission of the center is addressing scientific and technological challenges of interfacing human cells and organic molecules with advanced carbon-based materials for bio-electronic and bio-sensor applications in health care, environment, security, and more. Selected activities running at IoP-Cukrovarnicka are included in the present lecture. Technological progress in the large area growth of diamond films and carbon nanotubes by the modified linear antenna microwave plasma CVD system are pointed out too. A challenging part, diamond overcoated mirrors or ATR prisms, are shown as multifunction optical elements suitable for detection of adsorbed or grafted molecules. Furthermore, combination of pulsed microwave plasma with radiofrequency substrate biasing results in growth of oriented CNTs over large area is mentioned too.
Acknowledgement: This work was supported by the grants IAAX00100902 (GAAV) and P108/12/G108 (GACR Excellence Center). We would like to gratefully appreciate to many researchers from the IoP, to K. Hruska and J. Libertinova for SEM measurements, to O. Rezek and J. Potmesil for technical support and to Z. Polackova for wet chemical treatment. There were also scientific contributions from undergraduate and PhD. students. This work was carried out in frame of the LNSM infrastructure.

Perspectives in Diamond Thin Film Technology (Review on scientific activities at FZU Cukrovarnicka 2008-2011)

Alexander Kromka
http://www.fzu.cz/~kromka/
Rokytnice 2012

Acknowledgment to people

- **Department 27 – core technology**
  - *Technical support:*
    Zdeňka Poláčková, Jiří Potměšil, Ondřej Rezek,
  - *PostDoc:*
    Zdeněk Remeš, Halyna Kozák, Štepán Potocký
  - *PhD students:*
    Marina Davydova, Neda Neykova, Oleg Babchenko, Tibor Ižák
  - *Bc. student:*
    Mária Domenkos
  - *several semester works (5 students)*

CABIOM cabiom.fzu.cz
Carbon-based Biomaterials and Biointerfaces
Virtual Research Center of the Institute of Physics ASCR, v. v. i.

- **Cross-departmenal**
  - ***Bohuslav Rezek** and his group: Egor Ukraintsev, Marie Krátká, Martin Ledinský, Jan Čermák, Lukáš Ondič*
  - *Vlastimil Jurka, Karel Hruška (SEM, EBL)*
  - *Pavel Hubík, Jiří J. Mareš (electrical characterization, Hall meas.)*
  - *J. Zemek (XPS)*
  - *etc.*

2

Acknowledgment to people

Laboratory of carbon technology (Dr. Kromka) http://www.fzu.cz/~kromka

- focus on focus on all purpose diamond and CNT technology
- PhD students (4), postdocs (2), senior scientists (1)

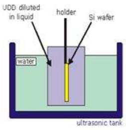

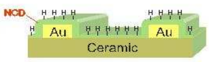

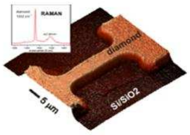

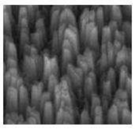

large area CVD reactor

Laboratory of functional nano-interfaces (Dr. Rezek) http://www.fzu.cz/~rezek

- **main (overlapping) directions: 1) opto-electronics, 2) bio-electronics**
- focus on study and control of interfaces and junctions at nanoscale
- merging diamond, silicon, organics
- PhD students (3), postdocs (2), senior scientists (1)

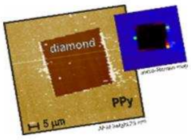

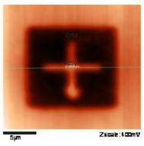
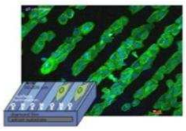
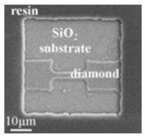

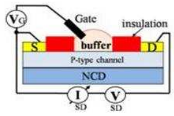

Acknowledgment to people

- **1st Faculty of Medicine, Charles University, Prague**
  - ***Marie Kalbáčová***, *Antonín Brož, Lenka Nosková, Hana Hartmanová*
- **Institute of Physiology ASCR, Prague**
  - ***Lucie Bačáková***, *Lubica Grausová*
- **Charles university**
  - ***Peter Malý***, *Jana Preclíková, Braňo Dzurnák*
- **Czech Technical University**
  - ***Vaclav Prajzler, Pavel Kulha,*** *Pavla Nekvindova*
- **and others: VUT, …**

- **R&D with industry**
  - MPO: Modular SEM microscope (fi. Tescan)
  - TACR: Advanced plasma sources (fi. SVCS)
  - others (Zdenek Remes – fi. Solartec)
  - and others.

4

Funding of Diamond-Related Activities

- CABIOM center
  - http://cabiom.fzu.cz

CABIOM
Carbon-based Biomaterials and Biointerfaces
Virtual Research Center of the Institute of Physics ASCR, v. v. i.

- Funding (national projects within CABIOM team)
  - **IAAX00100902** (GAAV), KAN400100701 (AVČR), LC510 (MŠMT),
  - **P108/12/G108** (2012 - 2018) – Centre of Excellence (GAČR)
  - **P108/12/0996** (BIOSCAF-GAČR), **P108/12/0910** (FaST-DiAS, GAČR)
  - **P108/11/0794** (COLAGEN-GAČR), **P205/12/0908** (Linear plasma, GAČR)
  - **Fellowship J.E. Purkyně** (AVČR)

- Bilateral projects
  - France: CEA Sacley, CNRS Grenoble
  - Sweden: University Uppsala
  - Japan: AIST, UTokyo
  - Taiwan & Russia (nanoparticles)
  - Slovakia

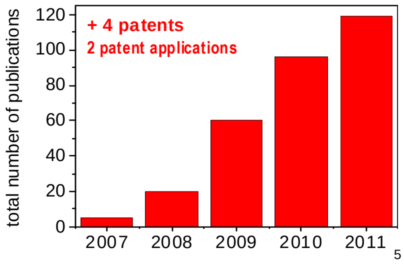

5

Why new materials? – not only NANO/BIO

- Excellent intrinsic properties
  - transmittance, conductivity, toughness/elasticity …
- Long-Time Stability
- Sensitivity & Selectivity
- Stability to Environment
  - mechanical / chemical / thermal / radiation …
- Compatibility to Environment
  - biological!
- Economical Availability
  - large area deposition (=mass production)

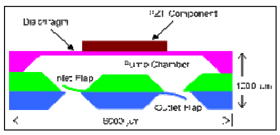

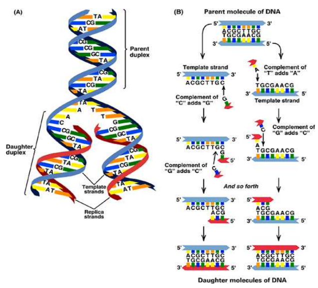

Why Diamond? – defined surface

Property		Diamond	Comment ...
Surface termination	+++++++	- H	hydrophobic, conductive
		- O	hydrophilic, non-conductive
		- NH_2, - F, - Cl ...	welcomed: molecule binding

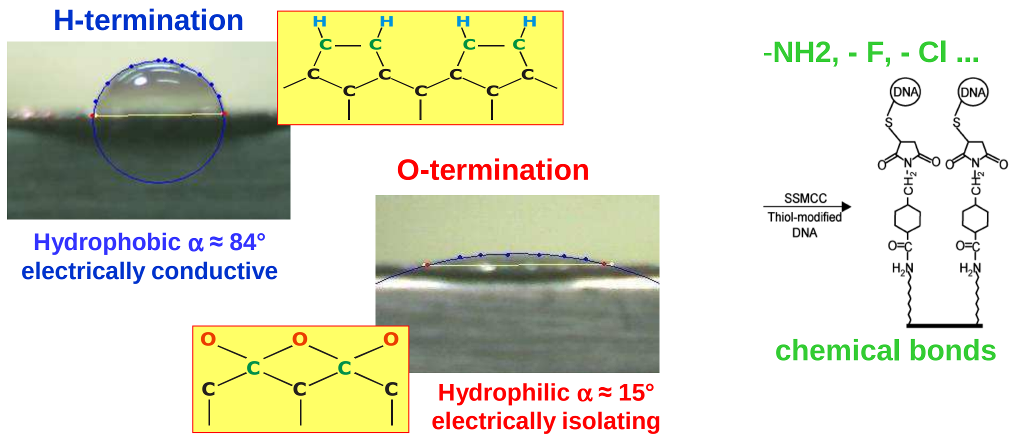

Why Diamond? – extraordinary properties

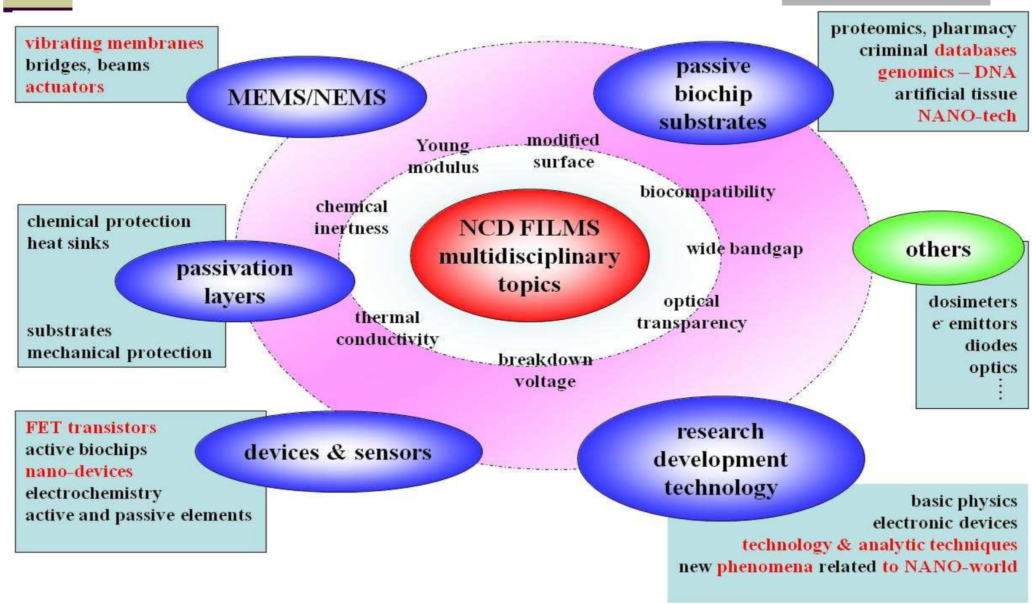

Nucleation and seeding

- bias enhanced nucleation
- ultrasonic seeding
- diamond-polymer composites

BEN

Mortet *et al.*, DRM 14 (2005)
Preclíková et al., Opt. Lett.ers(2010)

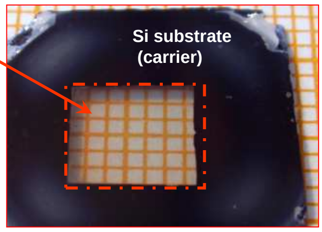

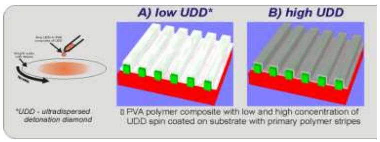

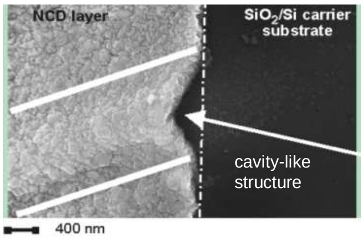

Kromka *et al.*, DRM 14 (2008)
Kromka et al., pss a 246 (2009)

ultrasonic seeding

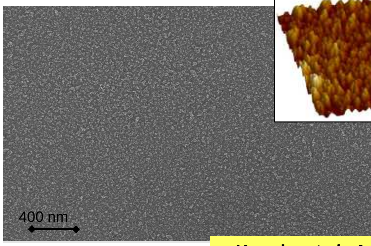

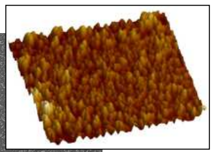

RMS = 5.5 nm
C: 48.5 at.%

Ultra thin films!

Kromka *et al.*, Adv. Eng. Mat. 11 (2009)

Diamond CVD growth

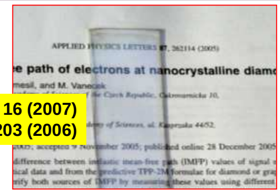

Potocky *et al.*, DRM 16 (2007)
Potocky *et al.*, pss a 203 (2006)

Mortet *et al.*, DRM 13 (2004)

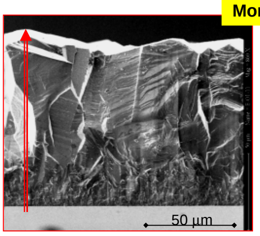

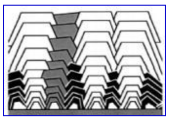

evolutionary selection growth model

- growth at low T_S (400°C)
- growth at high pressure (250 mbar)
- large area deposition (linear antenna)
- selective area deposition (*nanowires*)

Kromka *et al.*, submitted to Vacuum

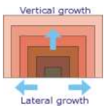

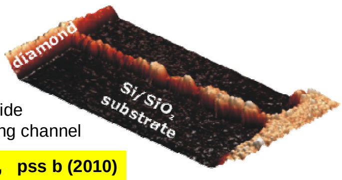

250 nm wide
4.7 µm long channel

Babchenko *et al.*, pss b (2010)
Babchenko *et al.*, send to Vacuum

10

Diamond microwave CVD reactors

- from **methane** (CH_4) employing „chemical vapor deposition“ (CVD) **in microwave plasma** discharge **on arbitrary substrate**

focused plasma reactor

[Kromka et al., CVD 14 (2008) 181]

large area (linear plasma) reactor

[Kromka et al., Vacuum (2010), in press]

Diamond microwave CVD reactors

focused plasma reactor

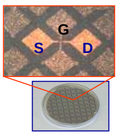

20 – 250 mbar

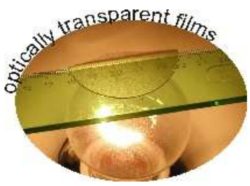

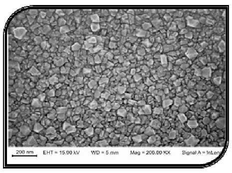

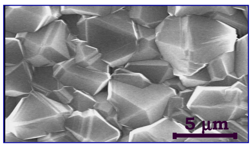

- Slow growth
- Nano-sized grains
- Ultra-thin layers

- Fast growth
- Rough surface
- Thick layers

large area (linear plasma) reactor

0.01 – 10 mbar

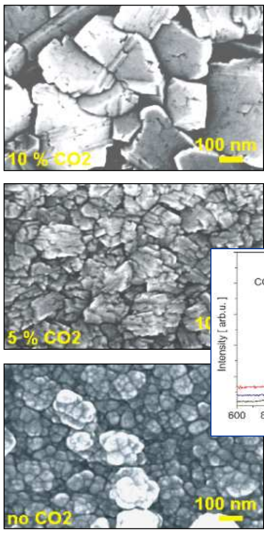

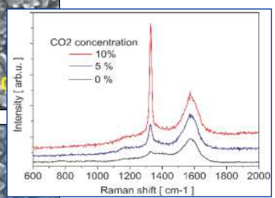

Plasma processing

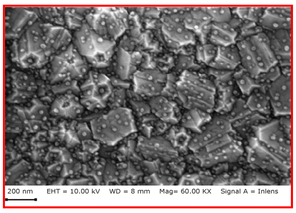

Thermal processing

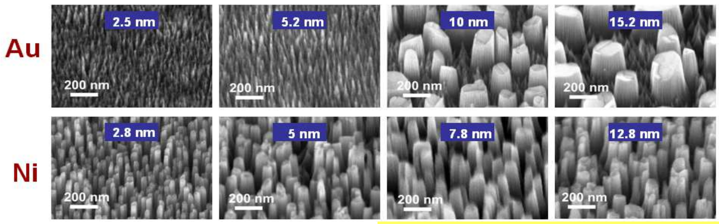

Plasma etching

Babchenko *et al.*, CEJP 7(2009)
Izak *et al.*, send to Vacuum

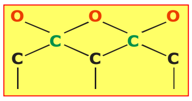

- etching & nanostructuring (nanorods)
- surface treatments (O/H/F …)

Selective oxidation

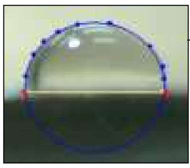

SAOS – 2 cells
2 days cultivation

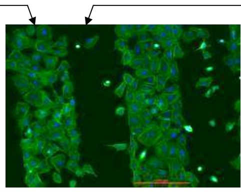

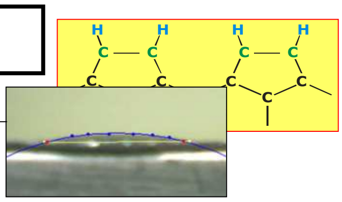

Kalbacova *et al.*, pss b 245 (2008)
Rezek et al., Sensors 9 (2009)
Michalikova *et al.*, Vacuum 84 (2010)

Diamond-related activities at FZU

Nucleation/seeding
- bias enhanced nucleation
- ultrasonic seeding
- diamond-polymer composites

Diamond microwave plasma CVD
- growth at low T_S (400℃)
- growth at high pressure (250 mbar)
- large area deposition (linear antenna)

- selective area deposition (*nanowires*)

Plasma processing
- etching & nanostructuring (nanorods)
- surface treatments (O/H/F …)

Advanced Analytic Techniques
- probe microscopes (AFM/KFM)
- optical techniques (FTIR/PDS)
- microRaman spectroscopy

Inter-disciplinary oriented R&D
- surface & interface phenomena
- surface/bulk defects
- optical phenomena (femto-spectr.)

- molecules at diamond
- cell & tissue engineering

Novel Devices & Demonstrators
- piezorezistors as MEMS
- ISFETs as biosensors
- IDTs as chemical or gas sensors

- passivation layer (Al/graphite/quartz)
- multilayer optical composites (BAR)

- heat spreaders
- Silicon-on-Diamond (SOD)
- waveguides & photonic crystals
- others

14

“Phenomena” at diamond surface

- Osteoblastic cells plated on H/O-diamond micropatterns

Inter-disciplinary oriented R&D
- surface & interface phenomena
- surface/bulk defects
- optical phenomena (femto-spectr.)

- molecules at diamond
- cell & tissue engineering

Rezek et al., Sensors 9 (2009)

green = actin fibers (cytoskeleton)
blue = nuclei

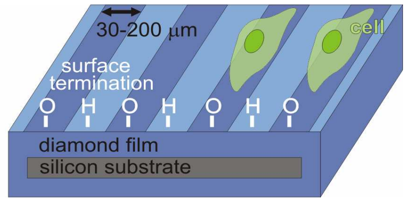

Cells strongly prefer diamond surfaces with O-termination (hydrophilic) compared to H-termination (hydrophobic).

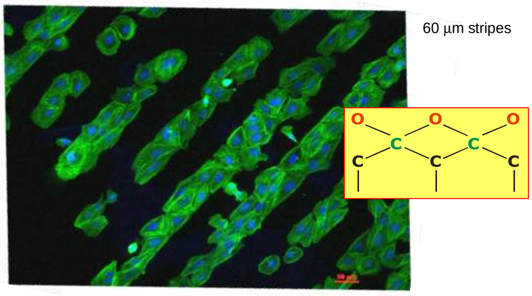

60 μm stripes

➔ preferential arrangement of cells into micro-arrays on O-diamond

15

Phenomena at diamond surface

- model in agreement with general effect of hydrophobic/-philic surfaces on proteins
- cell assembly independent of diamond conductivity (B-doping)

Rezek et al., DRM 18 (2009)
Rezek et al., Sensors 9 (2009)

AFM in solution

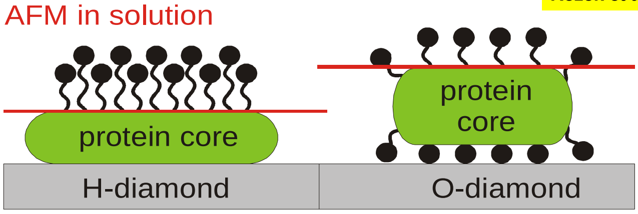

hydrophobic hydrophilic

➔ proteins in different conformation due to different wetting properties, those can be locally tailored by diamond surface atoms

Details on AFM measurements: *Dr. Egor Ukraintsev*

16

Phenomena at diamond surface

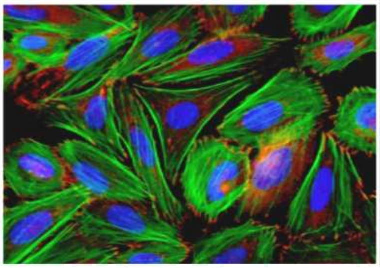

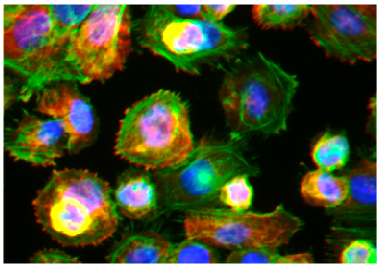

osteoblasts (SAOS-2), cultured for **48 h**

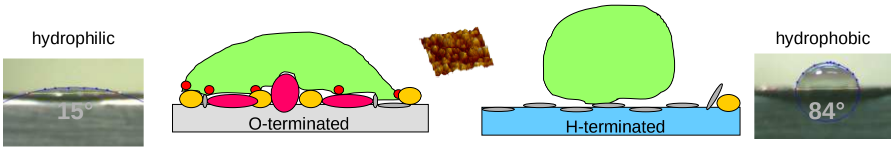

➔ human cell growth strongly influenced by diamond surface atoms

Kalbacova et al., pss b 244 (2007)

17

Phenomena at diamond grains – Prof. Maly

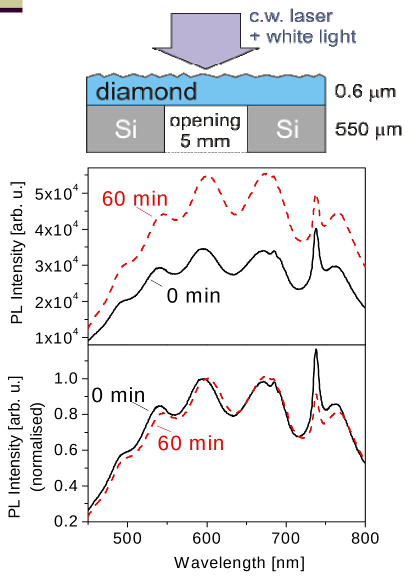

Inter-disciplinary oriented R&D
- surface & interface phenomena
- surface/bulk defects
- **optical phenomena (femto-spectr.)**

- molecules at diamond
- cell & tissue engineering

Effect of laser irradiation on PL of NCD membrane excited by femtosecond laser pulses (**405 nm, 80 fs, 82 MHz, mean power density 6000 W.cm^{-2}**).
Vacuum pressure 7 Pa, room temperature.
Black solid curve – unexposed sample, red dashed curve – sample irradiated by the excitation laser for 60 min.

Preclikova et al., Optics Lett. 35 (2010)
Dzurnak et al., DRM 18 (2009)

Shift in interferences => change in thickness or in ***refractive index***

18

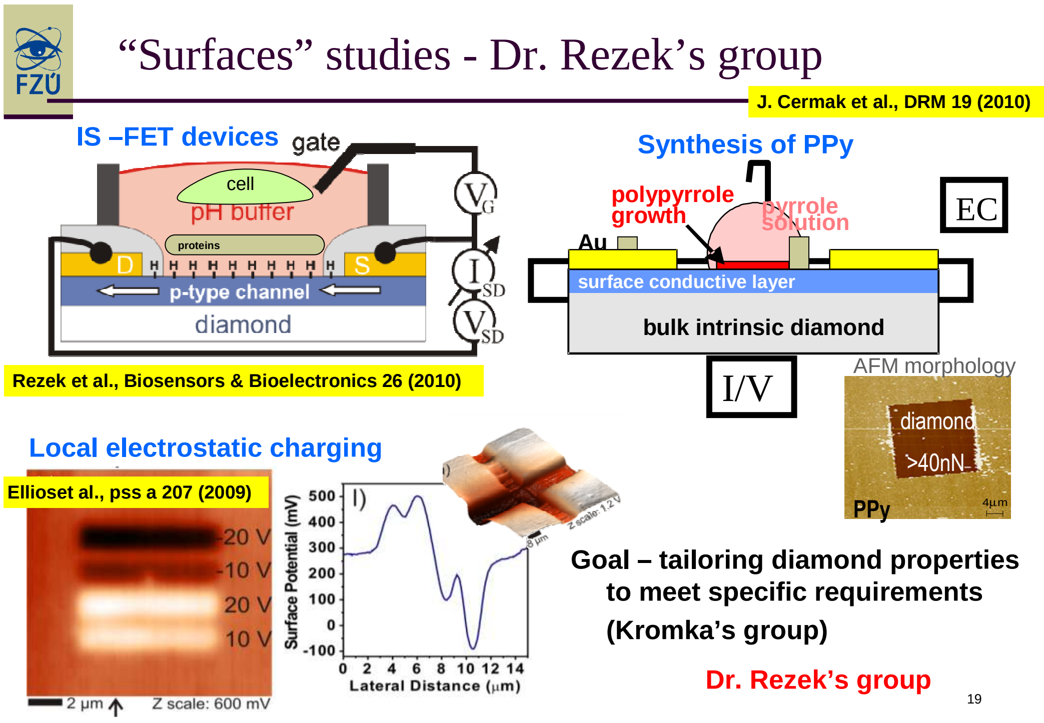

“Surfaces” studies - Dr. Rezek’s group
J. Cermak et al., DRM 19 (2010)
IS –FET devices
gate
cell
pH buffer
proteins
D
S
p-type channel
diamond
V_G
I_{SD}
V_{SD}
Rezek et al., Biosensors & Bioelectronics 26 (2010)
Synthesis of PPy
polypyrrole growth
pyrrole solution
EC
Au
surface conductive layer
bulk intrinsic diamond
I/V
AFM morphology
diamond
>40nN
PPy
Local electrostatic charging
Ellioset al., pss a 207 (2009)
-20 V
-10 V
20 V
10 V
2 µm
Z scale: 600 mV
Surface Potential (mV)
Lateral Distance (µm)
Goal – tailoring diamond properties to meet specific requirements (Kromka’s group)
Dr. Rezek’s group
19

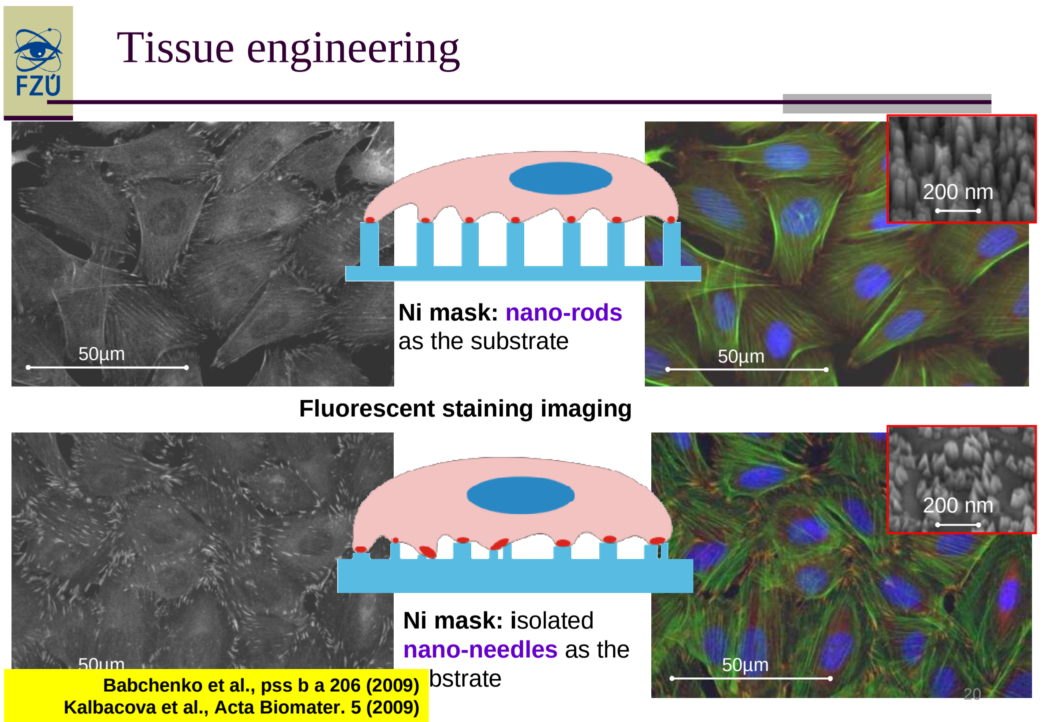

Tissue engineering
50µm
200 nm
Ni mask: nano-rods as the substrate
Fluorescent staining imaging
Ni mask: isolated nano-needles as the substrate
Babchenko et al., pss b a 206 (2009)
Kalbacova et al., Acta Biomater. 5 (2009)
20

Tissue engineering

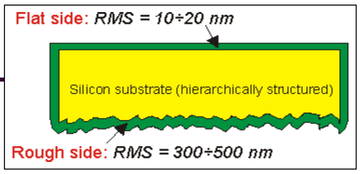

- **growth on FLAT or ROUGH surface**

(defined NANO-topography over MICRO-flatness)

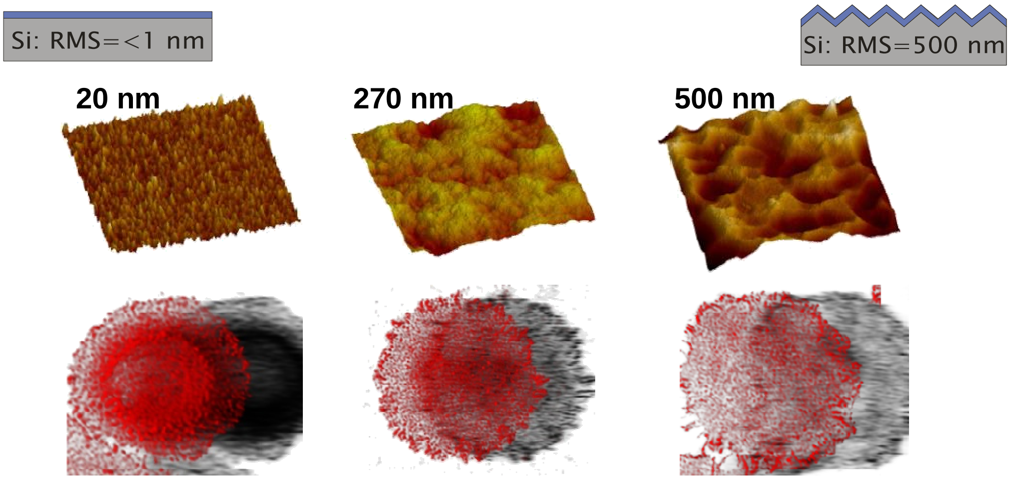

Fluorescent images of vinculin (red) present in SAOS-2 cells cultivated for 1 h

Tissue engineering

48 h after seeding

NANO on NANO

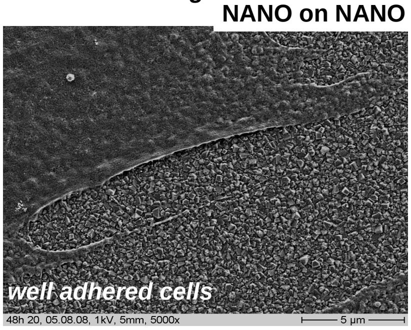

NANO on MICRO

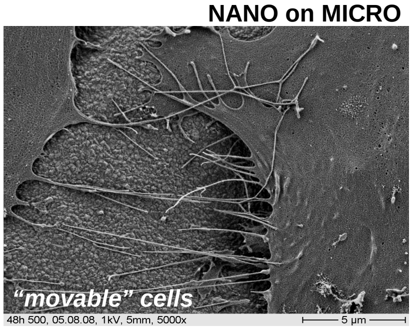

What about order of proteins?

many extensions and in all directions (filopodia/ lamellipodia on the surface and protuberances and "nanotubes" on the top of the cell)

Kromka et al., Adv. Eng. Mater. 11 (2009)
Kalbacova et al., Acta Biomater. 5 (2009)

Novel Diamond Devices

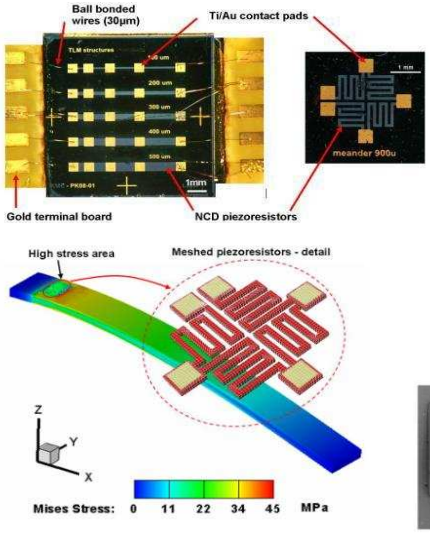

Novel Devices & Demonstrators

- piezorezistors as MEMS
- ISFETs as biosensors
- IDTs as chemical or gas sensors

- passivation layer (Al/graphite/quartz)
- multilayer optical composites (BAR)

- heat spreaders
- Silicon-on-Diamond (SOD)
- waveguides & photonic crystals
- others

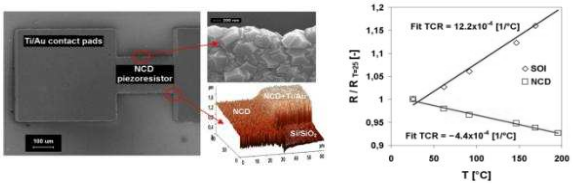

Kulha et al., Vacuum 84 (2010)
Kulha et al., JVC (2010)

23

Novel Diamond Devices - FETs

Solution-gated field-effect transistors

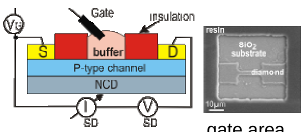

gating through liquid

gate area 927 µm²

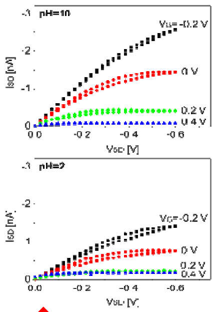

sensitivity to pH

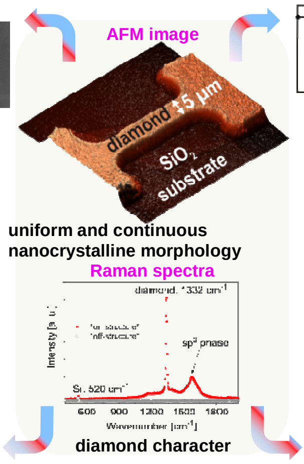

Solid-state field-effect transistors

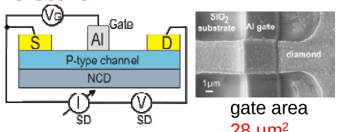

gating through Al

gate area 28 µm²

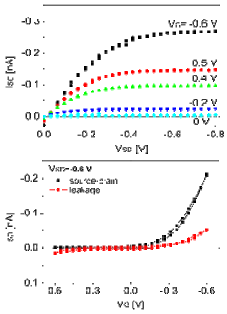

Kozak et al., Sensor Letters 8 (2010)

Clear transistors characteristics in SG- and SS-FETs !

24

Novel Diamond Devices – chemical sensor

embeded-metal electrodes in sensor device

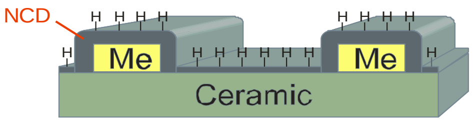

- *Sensor realized on NCD*
- *Low surface conductivity*

Advanced:

-surface area & sensor size

-others (simplicity…)

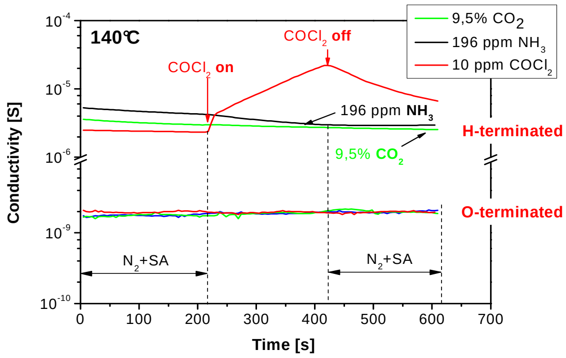

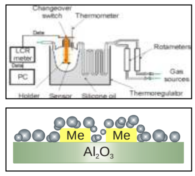

Largest ΔSC for Phosgene !

Why?

Davydova et al., pss a 206 (2009)
Kromka et al., DRM 19 (2010)

Novel Diamond Devices – chemical sensor

Presence of phosgene

a) phosgene dissolves in water

$COCl_2 + H_2O \rightarrow CO_2 + 2\,HCl$

b) **CO_2** becomes an acid when it is mixed with H_2O

$CO_2 + 2\,H_2O \rightarrow H_2CO_3 + H_2O \rightarrow H_3O^+ + HCO_3^-$

c) **HCl** is a strong acid and dissociates completely in H_2O

$HCl + 2\,H_2O \rightarrow H_3O^+ + Cl^-$

In Air

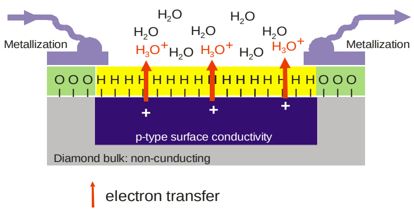

In Air including Phosgene

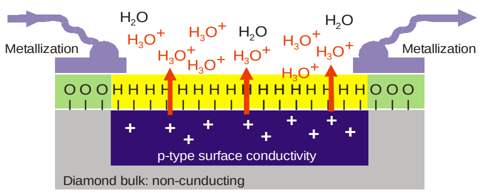

Davydova et al., JVC (2010)
Davydova et al., Vacuum (2012)

26

Novel Diamond Devices – Photonic Crystals

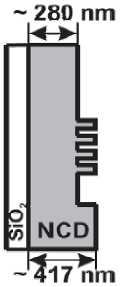

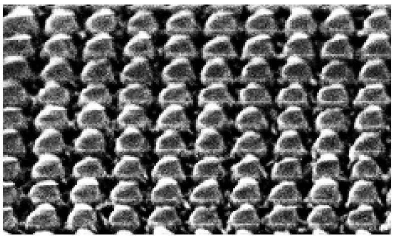

SEM image at angle: 45°: nano-pillars
ϕ=220 nm, gap 100 nm

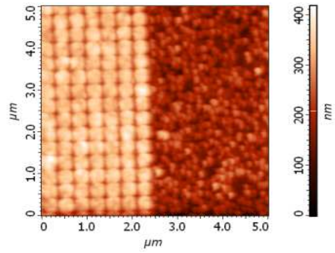

AFM image: nano-pillars height 140 nm

Complex nano-technology:
- CVD growth on quartz
- EBL at nano “scale”
- Plasma etching
- Metal evaporation
- etc.

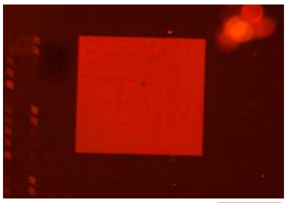

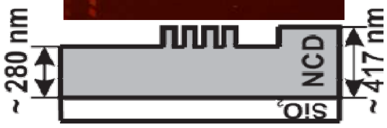

Enhanced photoluminescence: ~10x (green ⇨ red)

Ondic et al., NanoACS (2010)

27

Diamond-related activities at FZU

Nucleation/seeding
- bias enhanced nucleation
- ultrasonic seeding
- diamond-polymer composites

Diamond microwave plasma CVD
- growth at low T_S (400℃)
- growth at high pressure (250 mbar)
- large area deposition (linear antenna)

- selective area deposition (*nanowires*)

Plasma processing
- etching & nanostructuring (nanorods)
- surface treatments (O/H/F …)

Advanced Analytic Techniques
- probe microscopes (AFM/KFM)
- optical techniques (FTIR/PDS)
- microRaman spectroscopy

Inter-disciplinary oriented R&D
- surface & interface phenomena
- surface/bulk defects
- optical phenomena (femto-spectr.)

- molecules at diamond
- cell & tissue engineering

Novel Devices & Demonstrators
- piezorezistors as MEMS
- ISFETs as biosensors
- IDTs as chemical or gas sensors

- passivation layer (Al/graphite/quartz)
- multilayer optical composites (BAR)

- heat spreaders
- Silicon-on-Diamond (SOD)
- waveguides & photonic crystals
- others

Acknowledgement to the “CABIOM” team

Laboratory of Diamond and Carbon Nano-Structures

Your partner in the carbon nano-world

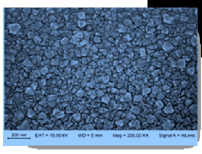

Luminiscenční spektroskopie (Si nanokrystalů)

Kateřina Kůsová
Institute of Physics, Academy of Sciences of the Czech Republic, Prague, Czech Republic

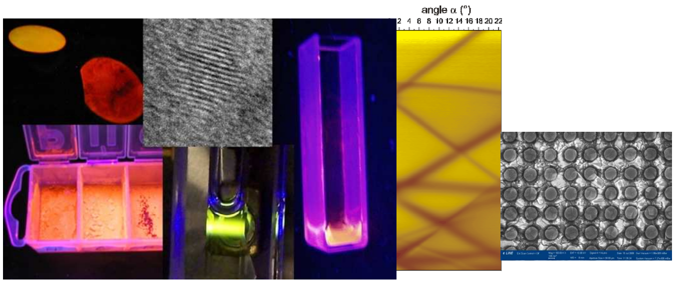

Luminiscence Si nanokrystalů

- laser “na” křemíku: nahrazení (části) elektronických spojů optickými -> Si nanokrystaly

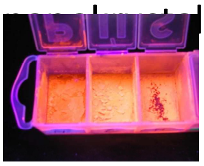

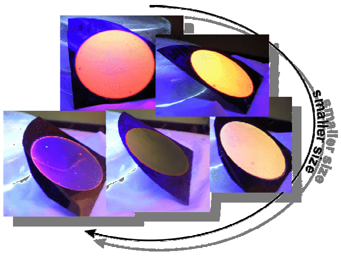

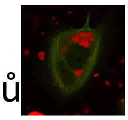

- další možnost použití Si nanokrystalů luminiscenční zobrazování v bioaplikacích

Kateřina Kůsová: Silicon nanocrystals as fast and efficient light emitters 74

Proč laser?

- Light Amplification through Stimulated Emission of Radiation
- stimulovaná emise: populační inverze

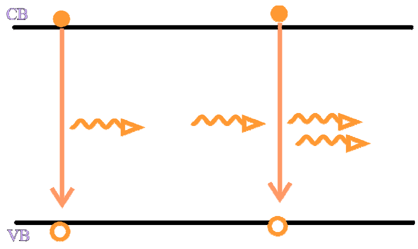

- laserové světlo: „jedna“ vlnová délka, nízká divergence svazku, vysoká koherence

Laser

- aktivní prostředí:
  - silná luminiscence
  - malé ztráty (např. rozptylem)
  - populační inverze

  optický zisk (VSL/SES)
- rezonátor
  - malé ztráty
  - rezonátor pro konkrétní vlnovou délku
  - „vhodné“ vyvázání světla

Luminiscence

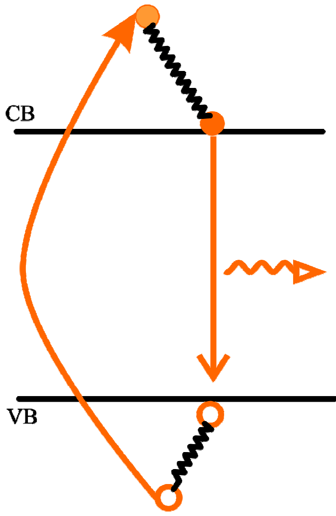

- elektroluminiscence (LED)
- katodoluminiscence (CRT obrazovky)
- chemiluminiscence (světlušky, plankton)
- triboluminiscence, sonoluminiscence,…
- **fotoluminiscence**
  – spektrum
  – doznívání
  – kvantová účinnost

Zářivé přechody

- Fermiho zlaté pravidlo

$$P_{ij} = \frac{2\pi}{\hbar}|\langle\phi_i|\mu|\phi_j\rangle|^2\delta(E_i - E_j + \hbar\omega)$$

Molekuly:
- HOMO + LUMO
- hladiny + pravděpodobnosti přechodu

Krystalické látky:
•valenční a vodivostní pás
•elektrony (díry) jsou rovinné vlny

$$\phi_r(r)\phi_{\mathrm{angl}}(\varphi,\vartheta)$$

Fourierova transformace

reciproký (k) prostor, pásová struktura

nanokrystaly ???

Zářivé a nezářivé přechody

CdSe		Si
1.5 ns	τ_{rad}	500 µs
> 1,000 ns	τ_{Aug}	3 µs

CdSe

Si

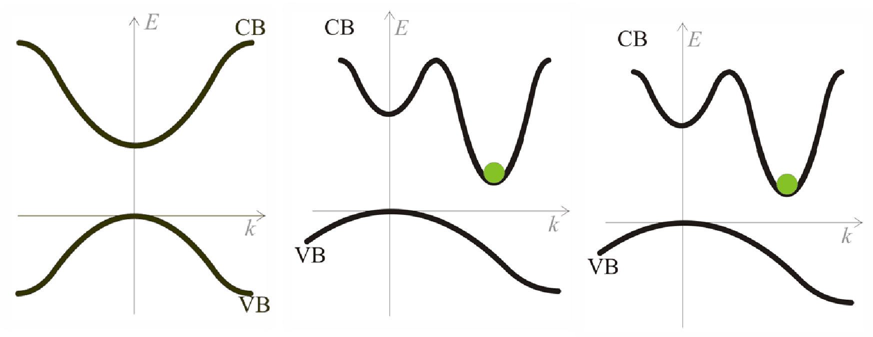

Zářivé a nezářivé přechody

CdSe		Si
1.5 ns	τ_{rad}	500 µs
> 1,000 ns	τ_{Aug}	3 µs
1.498 ns	τ	2.98 µs
1	η^{ideal}	10^{-3}
0.6	η^{real}	10^{-6}

$$\frac{1}{\tau} = \frac{1}{\tau_{rad}} + \frac{1}{\tau_{non\text{-}rad}}$$

$$\eta = \frac{\nu_{rad}}{\nu_{rad} + \nu_{nonrad}} = \frac{\tau}{\tau_{rad}}$$

CdSe

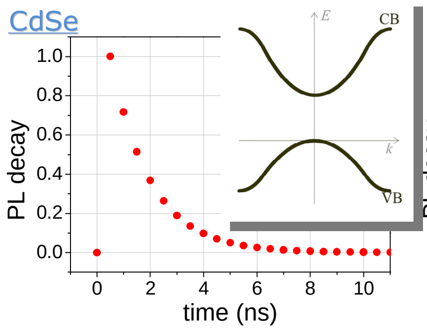

Si

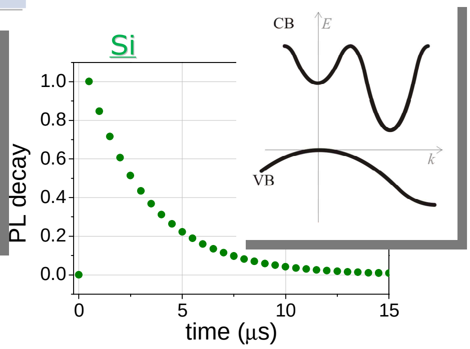

Si nanokrystaly

- ❑luminiscence Si nanokrystalů: 1991
- ❑kvantová účinnost 1-5 % (10 000x víc než v objemovém křemíku)
- ❑potlačení nezářivých … ů

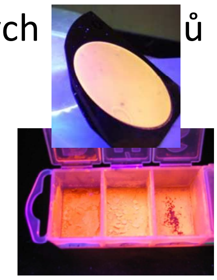

Co jsou nanokrystaly?

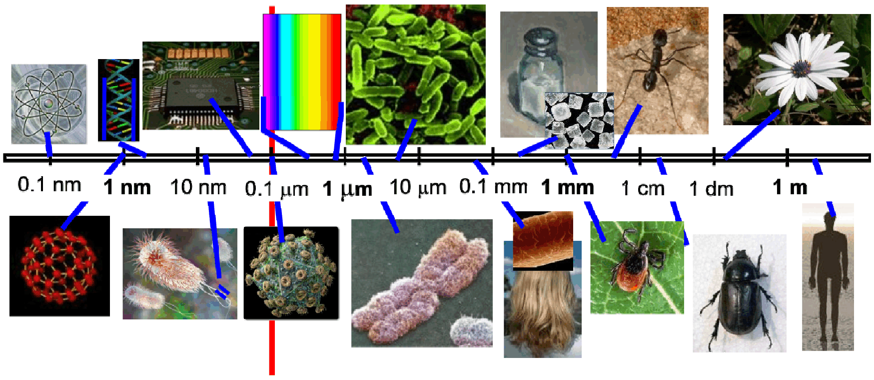

- nanočástice, nanokrystaly, kvantové tečky
- průměr: 2.5–3 nm
  - –600 Si atoms, 6 mřížkových konstant
- Bohrův poloměr excitonu: objemový křemík 5 nm

Kvantové omezení

- kvantové jevy „mění“ chování

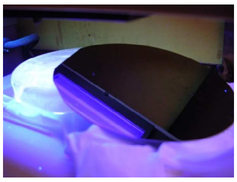

- spektrum (vlnová délka, barva) luminiscence je dána velikostí nanokrystalu

EviDots: www.evidenttech.com

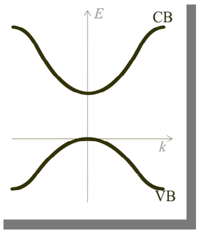

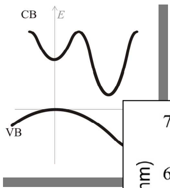

Oxidované Si nanokrystaly

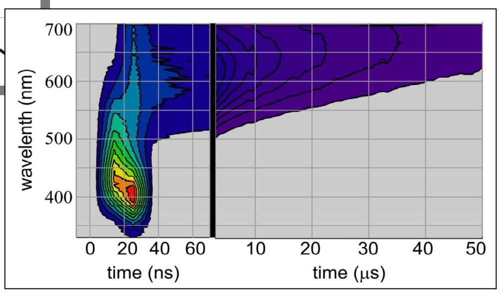

- QY: 2-3%
- zářivá doba života 100 μs

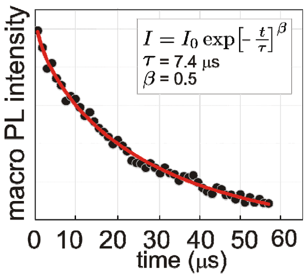

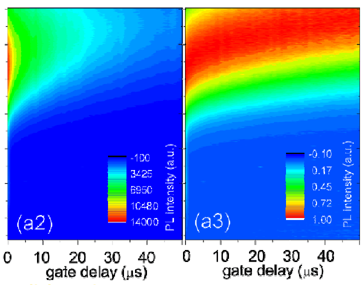

Vliv povrchu

	1x1x1 cm³	**20 nm** průměr	**3 nm** průměr
poměr povrch/objem (m^2/cm^3)	10^{-3}	300	2000

- z oxidovaných nanokrystalů připravujeme nanokrystaly pasivované methylovými skupinami ($-CH_3$)
- forma: koloidní disperze
- výrazná změna luminiscenčních vlastností

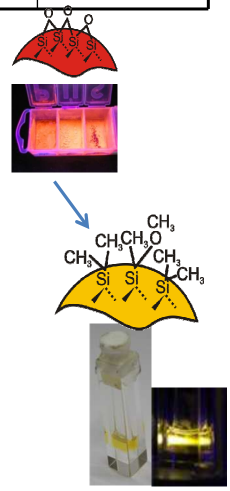

Methylované Si nanokrystaly

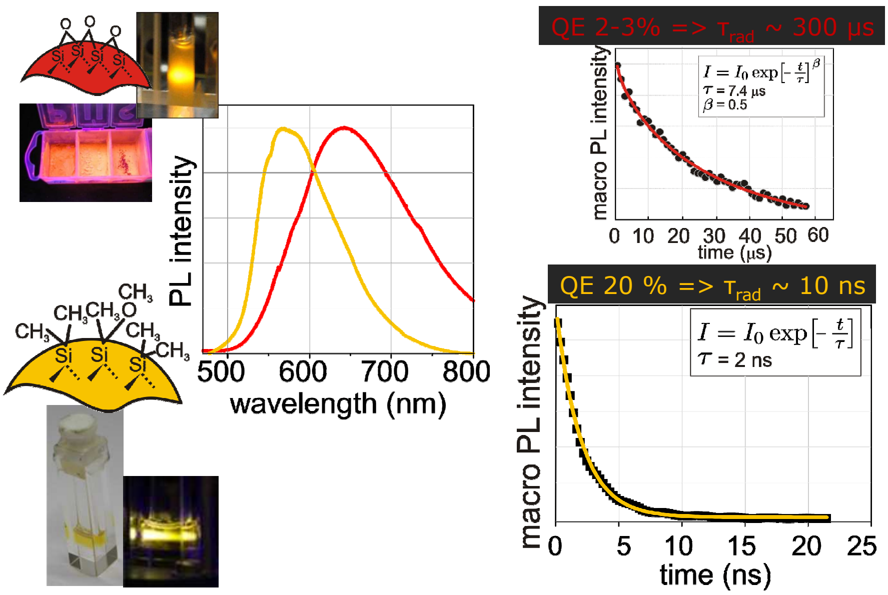

Pásová struktura a optické přechody

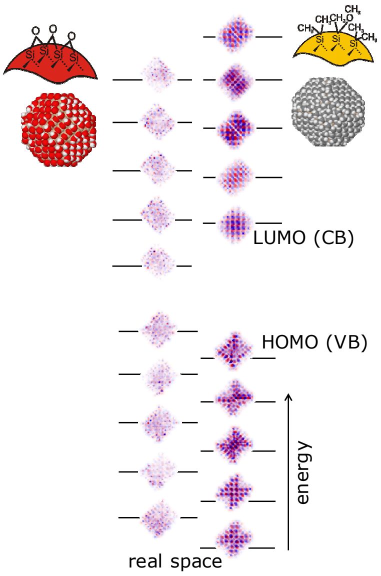

$$\phi_r(r)\phi_{\mathrm{angl}}(\varphi,\vartheta)$$

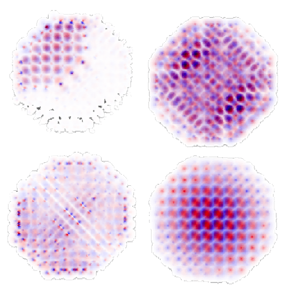

P. Hapala, P. Jelínek

Pásová struktura a optické přechody

- pásová struktura i u nanokrystalů má smysl, ale je nutné brát v úvahu i prostorový překryv
- začíná být „rozmazaná“

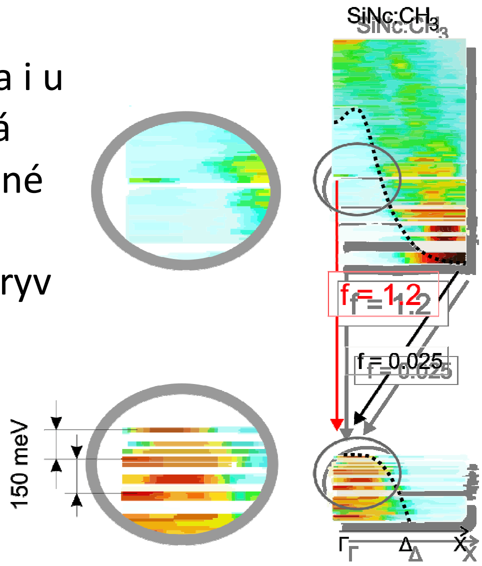

Závěr

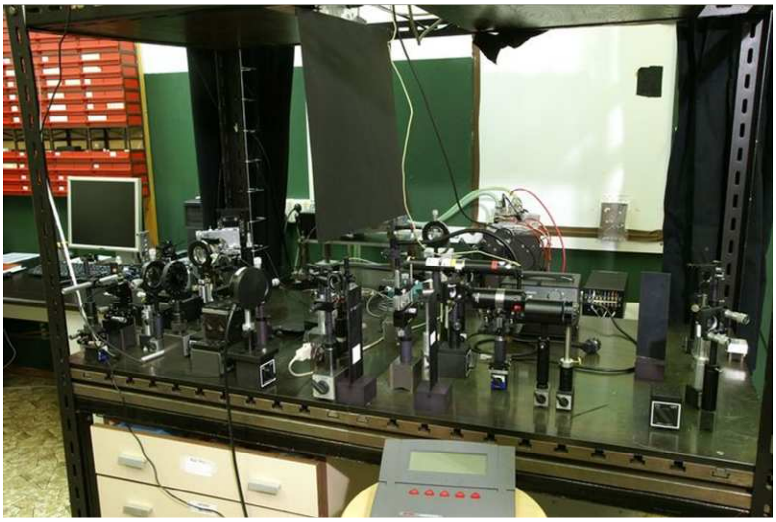

Kateřina Kůsová: Silicon nanocrystals as fast and efficient light emitters 89

Local photo conductivity mapping of mixed phase silicon thin films

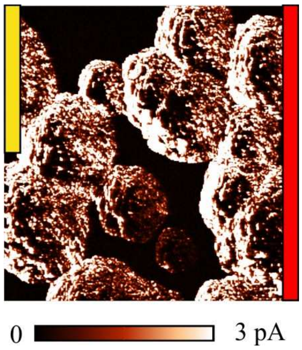

M. Ledinský, A. Fejfar, A. Vetushka, J. Stuchlík, B. Rezek and J. Kočka

Institute of Physics, Academy of Sciences of the Czech Republic, Cukrovarnická 10, Prague 6, Czech Republic

Outline:

1. Local conductivity mapping by AFM
2. Photo response of µc-Si:H at nm scale
3. Local photoconductivity excited by 442 nm laser

1) C-AFM

Conductive AFM in UHV

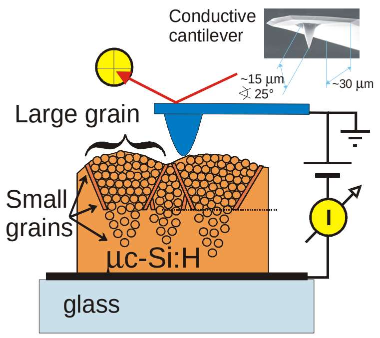

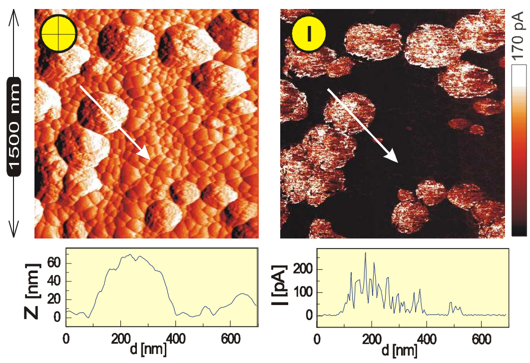

All results were measured
on 2x2 µm at -2 V
on the sample contact

B. Rezek et al.: Appl. Phys. Lett. **74**, 1475-1477 (1999)

Open questions remain -

Photoconductivity

first photo-response results

Measured on PIN diode (on the top µc-Si:H n-type layer)

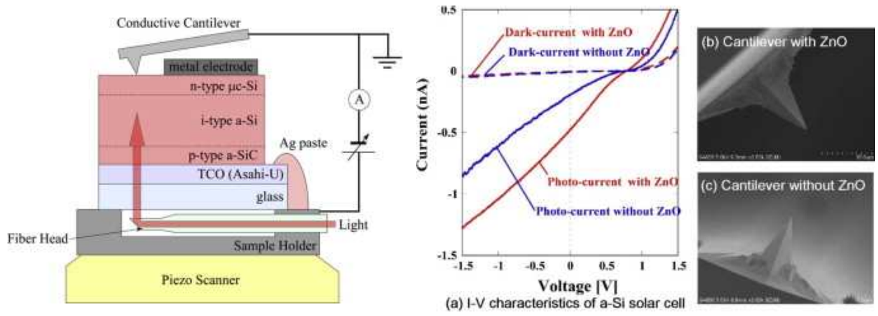

Gifu U.: M. Kawai et al.: Current Applied Physics **10**, S392-S394 (2010)

- excitation from the bottom side is in practice not optimal
- this is not the first photo-conductive AFM measurement on µc-Si:H

standard C-AFM

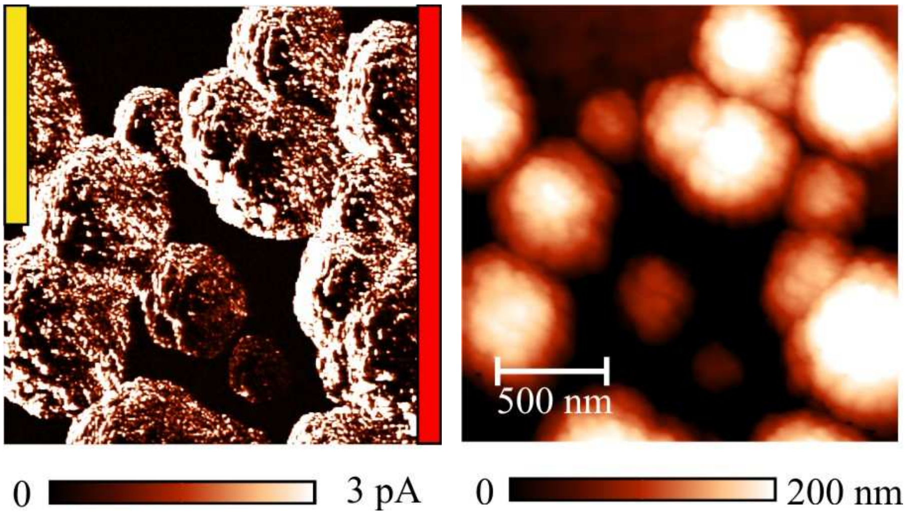

Why there is no photo-response?

C-AFM

1. Cantilever effectively shadows the sample – dark current is measured

2. AFM detection diode illuminates the sample and the white light intensity is negligible in comparison with red AFM diode

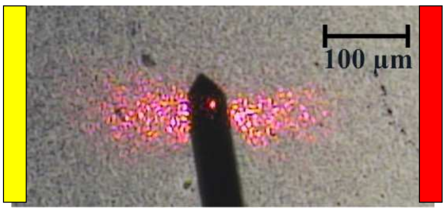

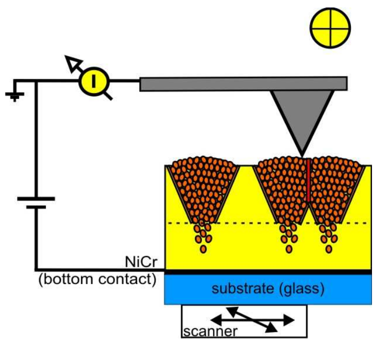

measurement in constant height mode –
the diode may be switched off but **no topography**

C-AFM

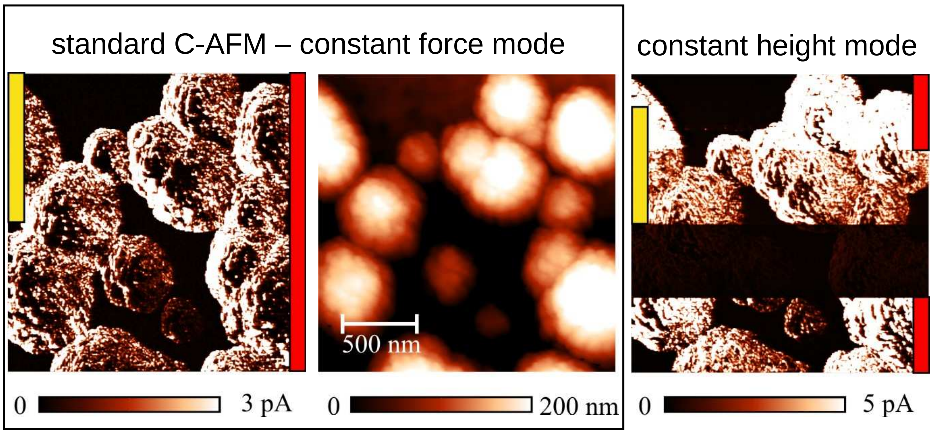

• response on white light and AFM diode illumination
• when the AFM diode is on, there is no response on white light
• all standard C-AFM results = Photoconductive local current maps

Conductive AFM in UHV

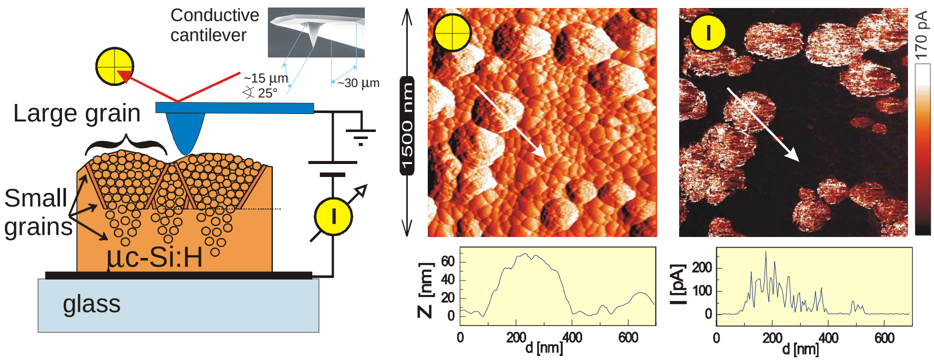

B. Rezek et al.: Appl. Phys. Lett. **74**, 1475-1477 (1999)

2) dark C-AFM

dark C-AFM

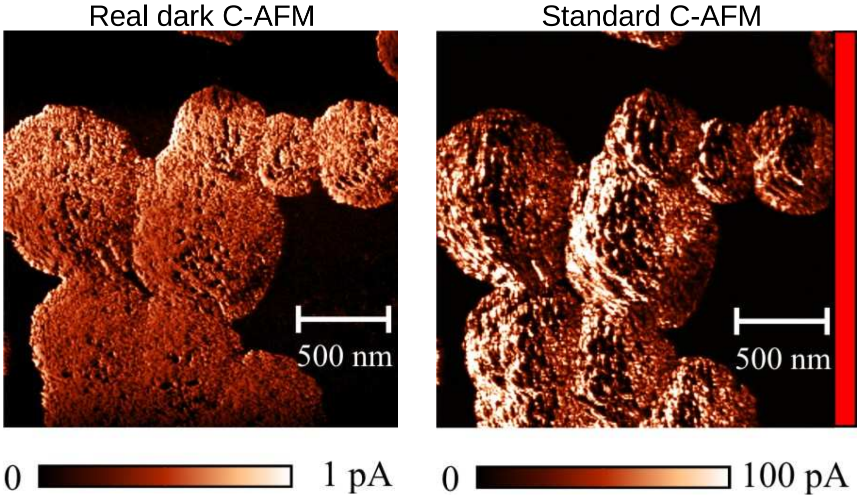

- ~100 x difference in photo/dark currents
- current through the grains in dark is homogenous

dark C-AFM

dark I-V characteristics

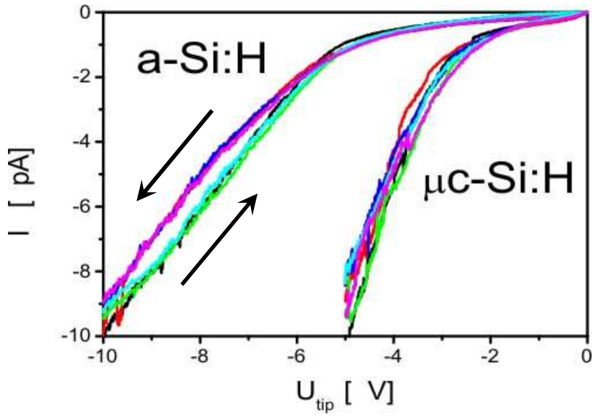

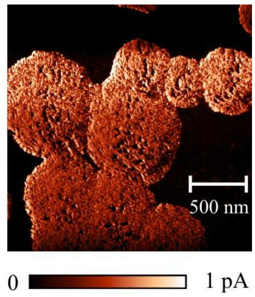

- easier interpretation
- very good repeatability (no current decreasing – typical for photo I-V)
- small hysteresis in a-Si:H (charge trapping)

Well defined dark conditions →
Let's start with photo-current AFM

photo C-AFM

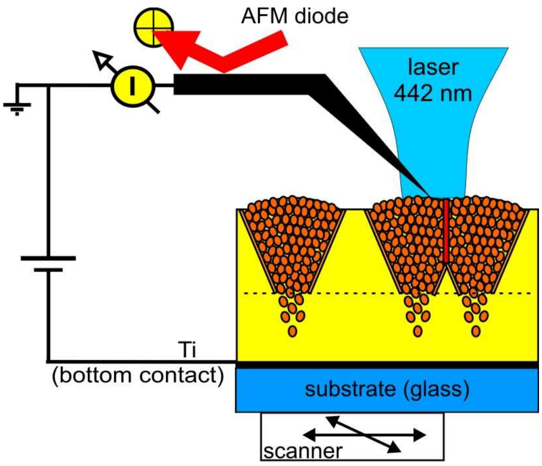

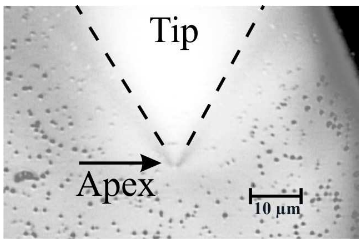

Local light excitation (in z axis ~ 40 nm) and local detection – given by the tip diameter ~ 50 nm.
Excitation volume = 10^5 nm^3

Typical defect density in silicon thin film 10^{17} cm^{-3},
then in excitation volume ~ 10 defects only!!!

photo C-AFM

Nose type cantilever – tip may be blocked at the grain boundary – line artifacts in local current maps and topo

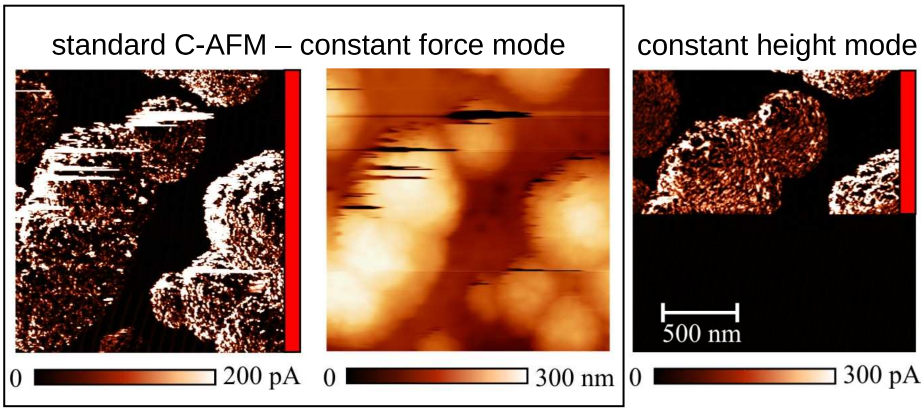

Very good agreement with results measured by standard cantilever.

ICANS 24 Nara M.Ledinský et al. Local dark and photo conductivity mapping of mixed phase silicon thin films by AFM *14/16*

photo C-AFM

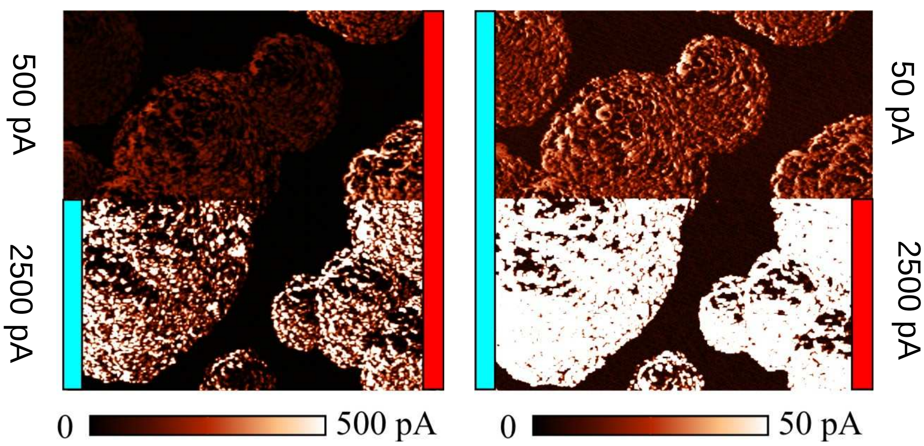

- clear photo-response with AFM diode on
- low photocurrent for illumination by laser only – high absorption
- I(laser+diode)/I(laser) – diffusion length rough estimation – 300 nm

ICANS 24 Nara M.Ledinský et al. Local dark and photo conductivity mapping of mixed phase silicon thin films by AFM *15/16*

Summary

1. Results of standard C-AFM measurement is always local photocurrent map.

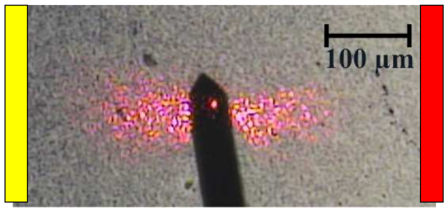

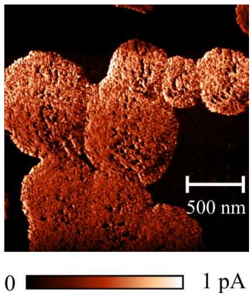

2. Dark currents maps show the same µc-Si:H / a-Si:H contrast. Dark I-V characteristics are well reproducible.

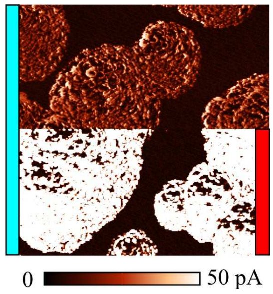

3. Local current is determined by absorption depth for 442nm HeCd laser illumination. Charge carriers diffusion length was estimated to ~ 300 nm.

Current as a function of grain size

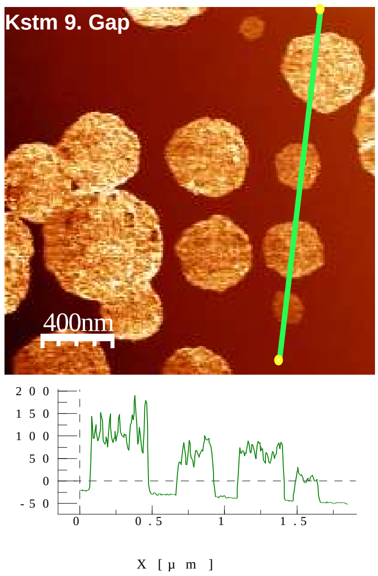

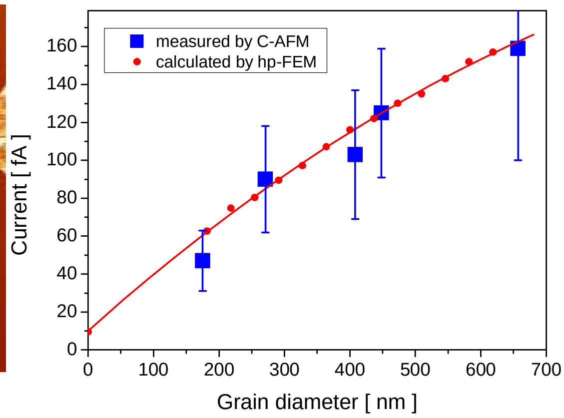

A. Fejfar et al., Phys. Status Solidi (a) **207**, 582-586 (2010).

thickness = 900 nm,
grain apex half angle = 20°
tip radius = 20 nm
Conductivities:
a-Si: 10^{-9} S/cm, µc-Si: 10^{-5} S/cm,
Surface layer: 1nm, $3*10^{-9}$ S/cm

photo C-AFM

Cross-section of local photocurrent maps

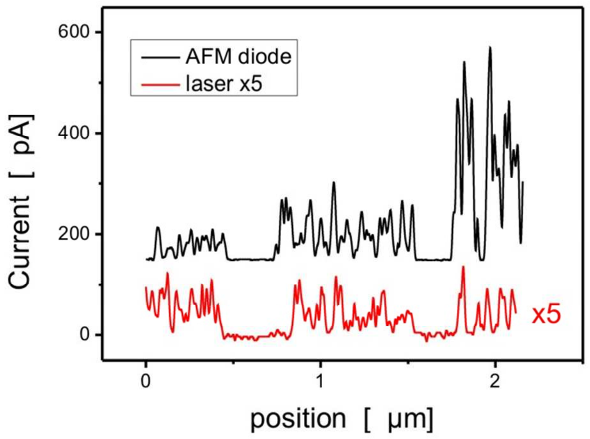

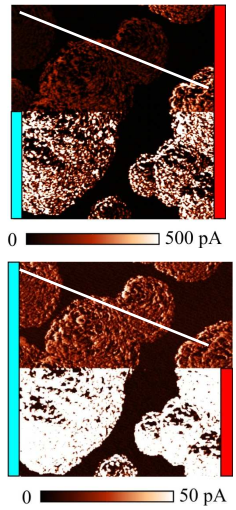

For 442 nm illumination – no change in the current level from grain to grain –
- highly conductive layer on the top of the layer – parallel resistance of all grains

Diffusion length estimation

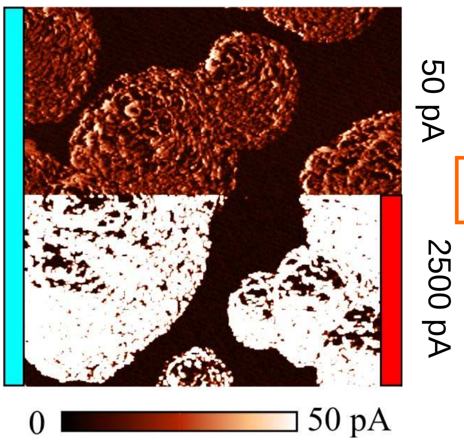

$I_{laser} / I_{(laser+diode)} \sim 1/50$

$$I_{laser} / I_{(laser+diode)} \sim I_{DIFF}/I_0 = I_0 {*} e^{-d/L}/I_0 \sim 1/50 \sim e^{-4}$$

$L = d/4 \sim 300$ nm

SEM and AFM at FZU AVCR, v.v.i.

3rd Winter Educational Seminar

Rokytnice nad Jizerou 2012, February 1 - 4

Jitka Libertínová

Štěpán Stehlík

Bohuslav Rezek

Scanning Electron Microscopy (SEM)

The combination of high magnification, large depth of focus, high resolution, and ease of sample observation makes the SEM one of the most heavily used instruments in research areas today.

Atomic Force Microscopy (AFM)

Scanning Probe Microscopy gives an opportunity to carry out studies of spatial, physical and chemical properties of objects with the typical dimensions of less than a few nanometers. Owing to its multifunctionality, availability and simplicity, AFM has become one of the most prevailing “tools for nanotechnology” nowadays.

The MIRA3 LMH FEG-SEM by TESCAN is a third generation of MIRA series of high resolution scanning electron microscopes equipped with a high brightness Schottky Field Emission gun.

Specification of selected parameters:

Electron Gun	High brightness Schottky Emitter
Resolution (In-Beam SE)	1 nm at 30 kV 2 nm at 3 kV
Resolution (SE-ET)	1.2 nm at 30kV 3 nm at 30kV (W) 2 nm at 30kV (LaB6) 2.5 nm at 3 kV 8 nm at 3kV (W) 5 nm at 30kV (LaB6)
Resolution (BSE)	2.0 nm at 30 kV
Magnification	3.5x to 1,000,000x
Accelerating Voltage	200 V to 30 kV
Probe Current	2 pA to 100 nA
High vacuum mode	< 9 × 10-3 Pa

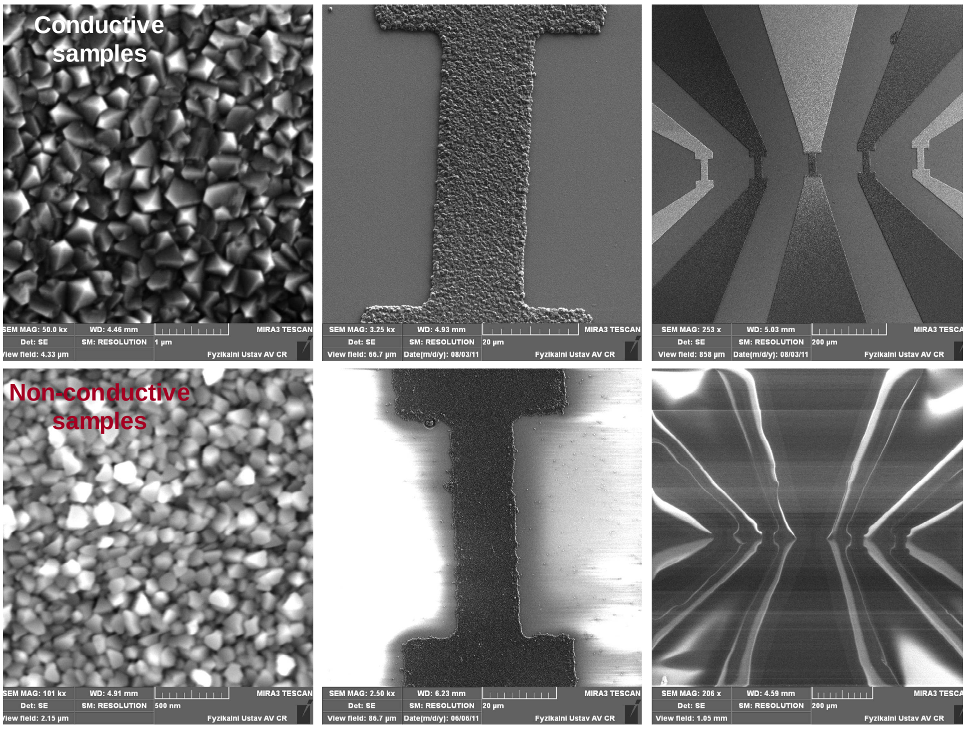

SE **In-Beam SE**

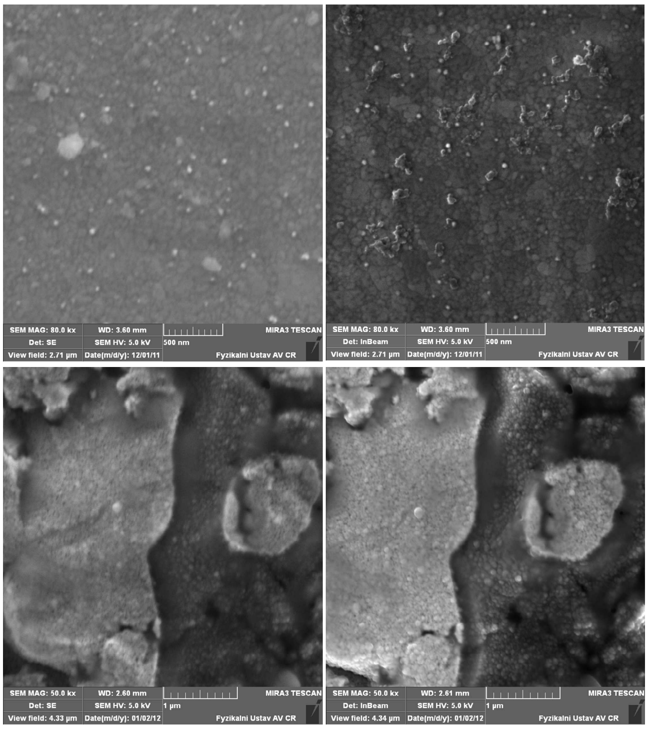

NCD particles on Au

NCD layer on Au and ceramic

SE **BSE**

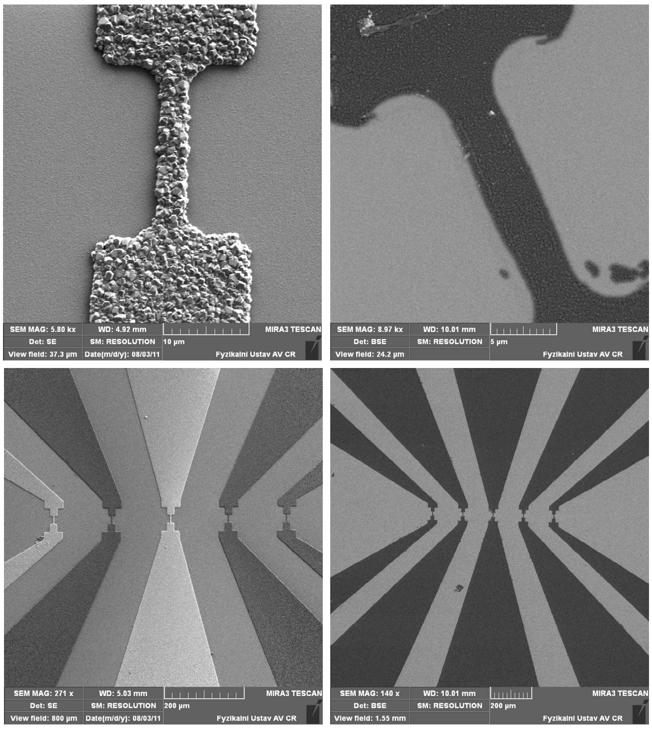

Images courtesy of Marie Krátká

AFM NTEGRA Prima by NT-MDT is a multifunctional device for performing the most typical tasks in the field of Scanning Probe Microscopy.

Air, liquids and controlled environment (low vacuum, nitrogen, controlled humidity, heating stage)

In air & liquid : AFM (contact + semi-contact + non-contact) / Lateral Force Microscopy / Phase Imaging/ Force Modulation/ Adhesion Force Imaging/ Lithography

In air only: STM/ Magnetic Force Microscopy/ Electrostatic Force Microscopy/ Scanning Capacitance Microscopy/ Kelvin Probe Microscopy/ Spreading Resistance Imaging/ Lithography

Scanning by the sample, scanning by the probe and dual-scanning

Scanning by probe	Scanning by sample
100x100x10 um	100x100x10 um
	Less than 1x1x1um

Up to 200x200x20 um (DualScanTMmode)

Low noise

Low thermal drift

Modular concept

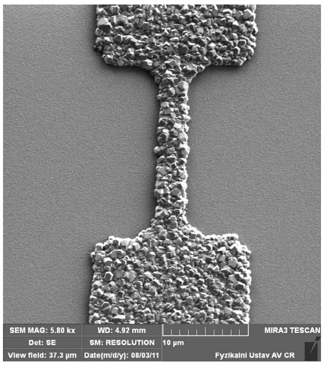

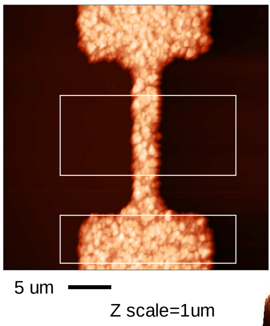

Topography

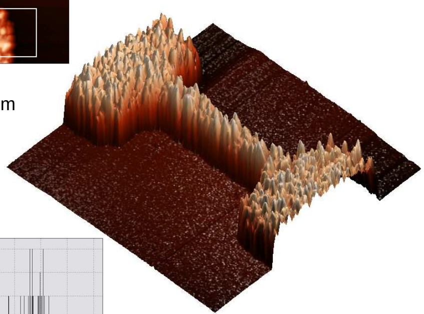

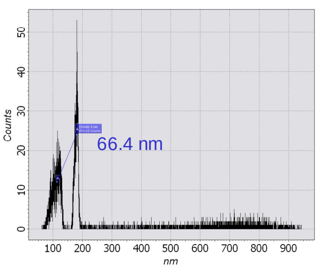

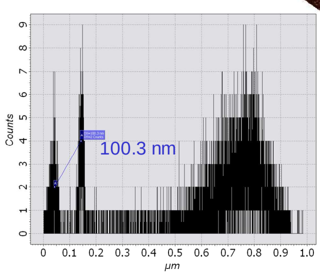

Topography

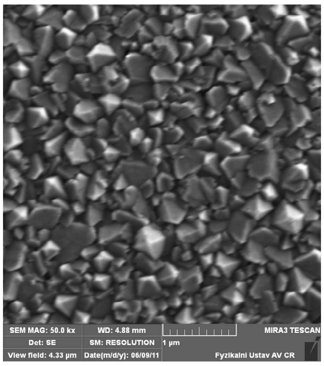

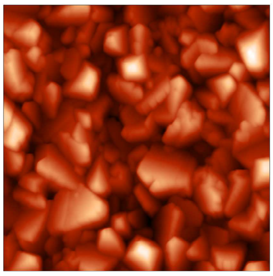

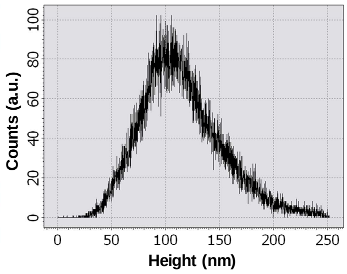

0.5 um ——— Z scale=250nm
Lz = RMS roughness = 39 ± 2 nm
Lx = 96 nm

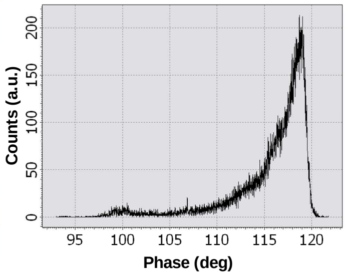

0.5 um ——— Z scale=20deg
RMS phase = 4.3 ± 0.2°

Kelvin Probe Microscopy

UDD-H nanoparticles on Au, Si tip (example)

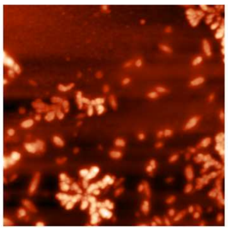

0.5 um ——— Z scale=60nm

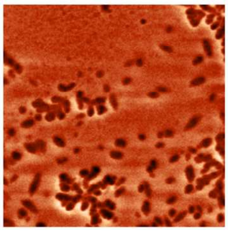

0.5 um ——— Z scale=80mV

Au droplets on H-terminated NCD

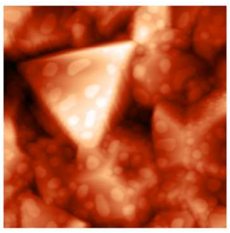

0.5 um ——— Z scale=500nm

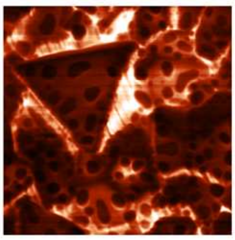

0.5 um ——— Z scale=300mV

Images courtesy of
Štěpán Stehlík

Lithography

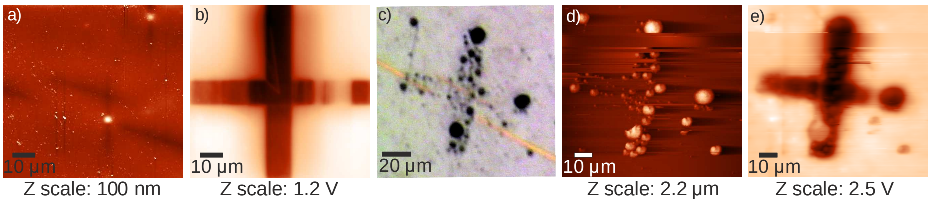

AFM topography on negatively charged areas (a) before and (d) after nanoparticle assembly. (b,e) Corresponding KFM potential maps. (c) Optical microscope image of the charged cross after assembly.

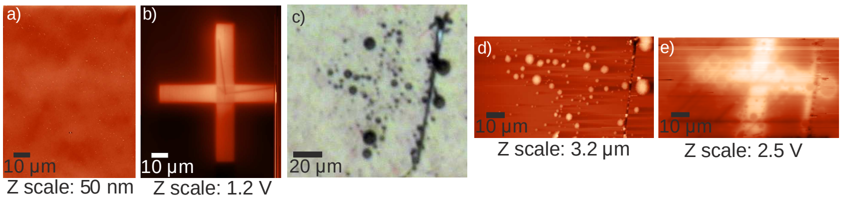

AFM topography on positively charged areas (a) before and (d) after nanoparticle assembly. (b,e) Corresponding KFM potential maps. (c) Optical microscope image of the charged cross after assembly.

Images courtesy of
Elisseos Verveniotis

In liquid (PBS solution)

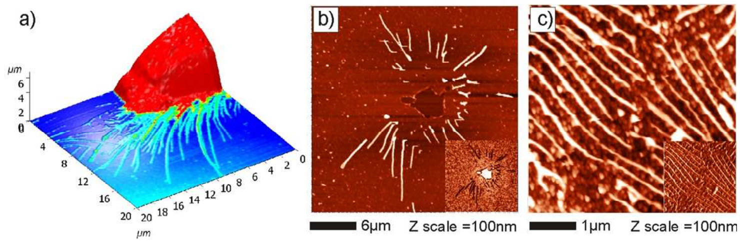

AFM morphologies of human cell on linear-antenna NCD: a) cell with filopodia extensions on H-NCD, b) area after the cell removal on H-NCD, c) detail on the filopodia on O-NCD with higher cell density. The inset images show AFM phase.

Images courtesy of
Egor Ukraintsev

Martin Müller

Department of Thin films

Insitute of Physics
Academy of Sciences of the Czech Republic

Prague, Czech Republic

Příprava podložek

- **Křemík monokrystalický (i, n^+, p^+)**
  - Čištění povrchu křemíku
    - Základní čištění: líh, deionizovaná voda
    - Odstranění povrchové oxidové vrstvy: 30 s v 30% **HF**
- **Corning C7059**
  - Čištění povrchu corningu
    - Základní čištění: aceton, metanol, líh, deionizovaná voda
    - Čištění povrchu od nečistot: 30–60 minut ve směsi 3:1 H_2SO_4 : 30% H_2O_2 při 80–100 °C (=**piranha**)
    - Úprava povrchu na hydrofilní (také odstranění prachových a kovových částic): 30–60 minut ve směsi 5:1:1 H_2O : $\mathbf{NH_4OH}$: 30% $\mathbf{H_2O_2}$ v ultrazvuku

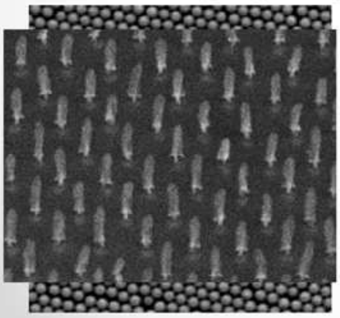

Vakuové napařování

- Příprava kovových kontaktů **Al**, **Ti** a **Au** (**Ag**, **Cr**, **Ni**, ..)
- Litograficky vyrobené kovové planžety -> masky pro napařování kontaktů určitých tvarů
- Vakuum: $p < \mathbf{10^{-3}\,Pa}$
  turbomolekulární turbína + předčerpání
- Zahřívání W lodičky (drátu) průchodem el. proudu, vypařování atomů kovu, přímočarý pohyb atomů kovu od W lodičky, kondenzace na povrchu vzorku
- Tloušťka napařené vrstvy ~ $1/r^2$

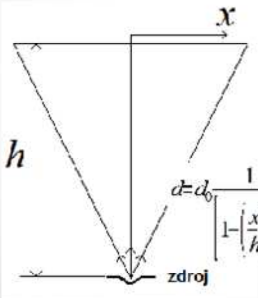

Vakuové naprašování

- Příprava vrstev slitin kovů nebo směsí více látek se stejným stechiometrickým složením jako zdrojového materiálu (**ITO**)
- Příprava tenkých vrstev kovů s vysokou teplotou tání (**Pt**, **Pd**)
- Zbytkové vakuum $p < \mathbf{10^{-3}\,Pa}$, inertní plyn (Ar) -> ~1 Pa
- Ionty argonu jsou v elektrickém poli urychleny směrem k povrchu terče, z něhož vyrážejí atomy, které se následně dostanou na povrch naprašovaného vzorku, kde vytvářejí tenkou vrstvu.
- Reaktivní naprašování – reakce atomů kovu s kyslíkem (Zn ->**ZnO**)
- Vyšší energie atomů kovu (~1–10 eV) než při napařování (~0,1 eV) -> lepší přilnavost atomů k podložce

PECVD Laboratory

- Process chamber: two parallel electrodes, one connected to RF generator, second with substrate holder, substrate temperature **180 – 250 °C**, **f = 13.56 MHz**
- Decomposition of **SiH_4**, **B_2H_6** and **PH_5** in a glow discharge -> chemisorption of Si, B and P on surface of sample
- Plasma: source gas molecules, radicals Si_xH_y, hydrogen radicals, ions,..
- Adsorption of radicals at substrate surface, hydrogen removing, cross linking with neighboring silicon atoms -> film growth

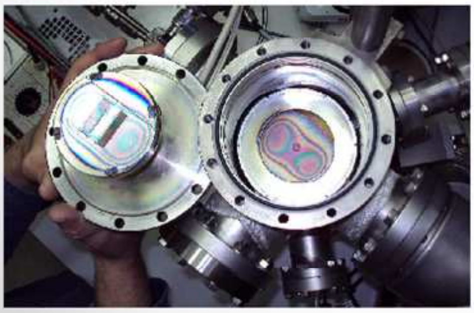

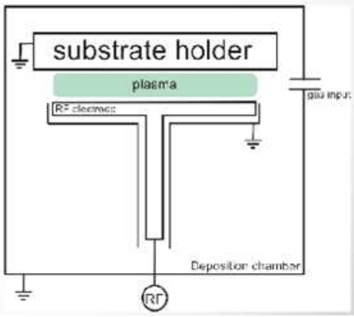

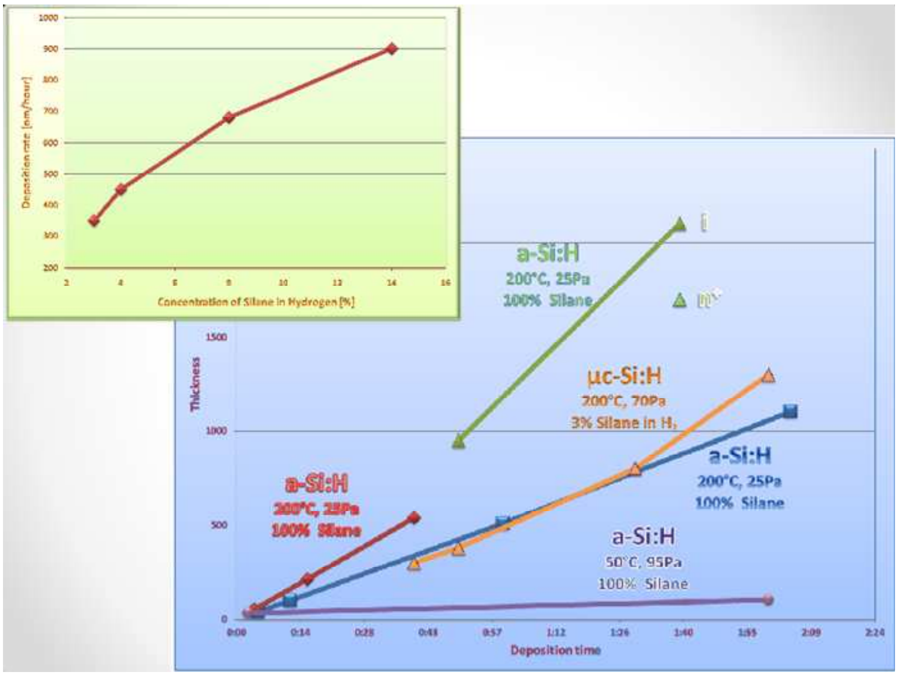

Influence of Gold Catalytic Layer on Growth of Silicon Nanowires

Martin Muller[1], Dat Phuoc Duong[2], The Ha Stuchlikova[1], Jiri Stuchlik[1], Martin Ledinsky[1], Antonin Fejfar [1], Jan Kocka[1], J. Cervenka[1], S. Bakardjieva[1]

[1]Institute of Physics,
Academy of Sciences, Prague, Czech Republic
[2] Institute of Chemical Technology,
Vietnam Academy of Science and Technology, HCM City, Viet Nam

Silicon nanowires by PECDV

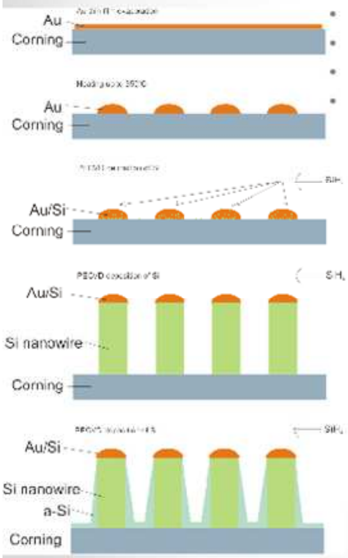

- Cleaning of Corning substrate in *Piranha* H_2SO_4:H_2O_2:H_2O
- Vacum evaporation of 99,99% Au wire from tungsten boat
- Heating in vacuum chamber for 15 min at 350°C
- PECVD of Silicon under conditions for a-Si deposition (VLS growth)
  - pressure of 100 Pa with a dilution 2 sccm silane in 10 sccm hydrogen
  - RF power 0.13 W cm^{-2}, frequency 13.56 MHz.

  - Absorption of Si in metal particles
  - Saturation -> nucleation site for crystallization
  - 1D growth

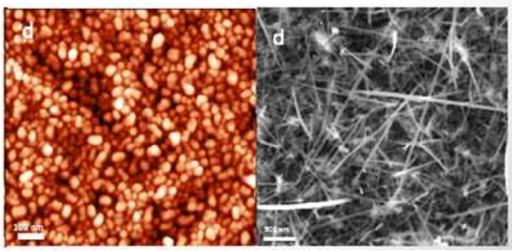

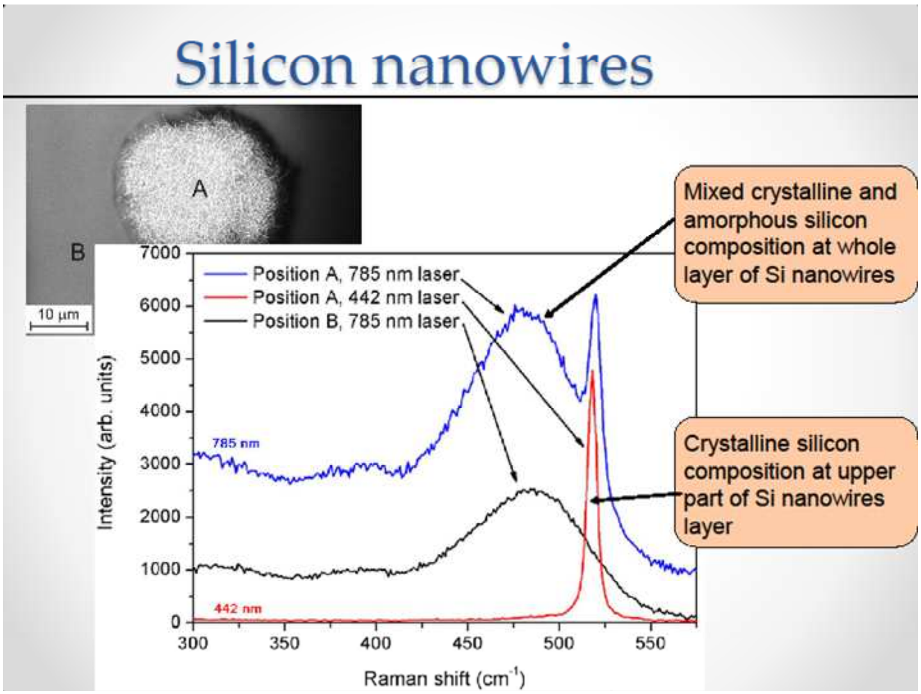
Silicon nanowires
A
B
10 μm
Position A, 785 nm laser
Position A, 442 nm laser
Position B, 785 nm laser
785 nm
442 nm
Intensity (arb. units)
Raman shift (cm⁻¹)
Mixed crystalline and amorphous silicon composition at whole layer of Si nanowires
Crystalline silicon composition at upper part of Si nanowires layer

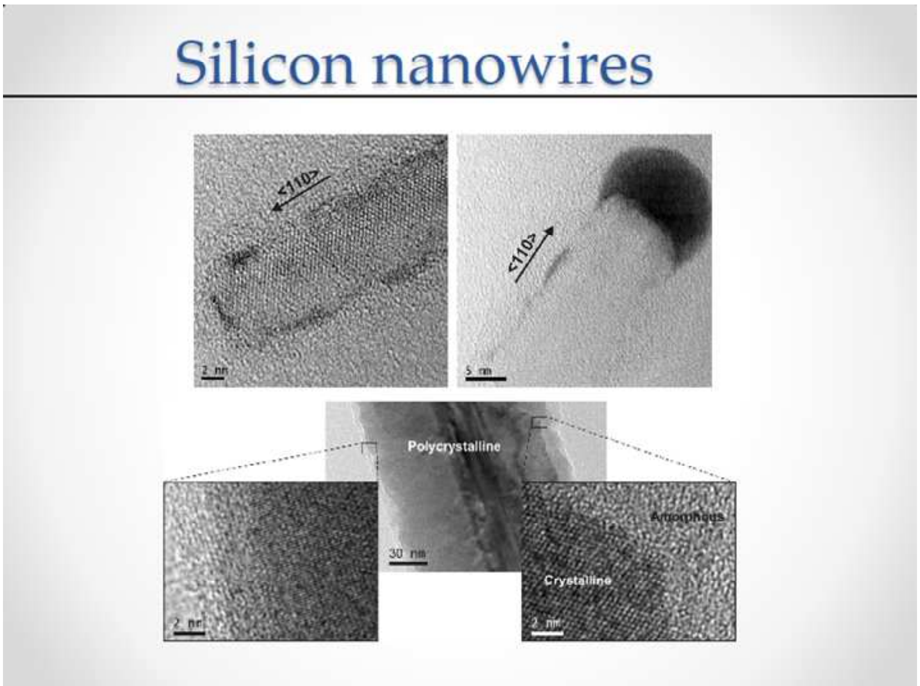
Silicon nanowires
<110>
<110>
2 nm
5 nm
Polycrystalline
30 nm
Amorphous
Crystalline
2 nm
2 nm

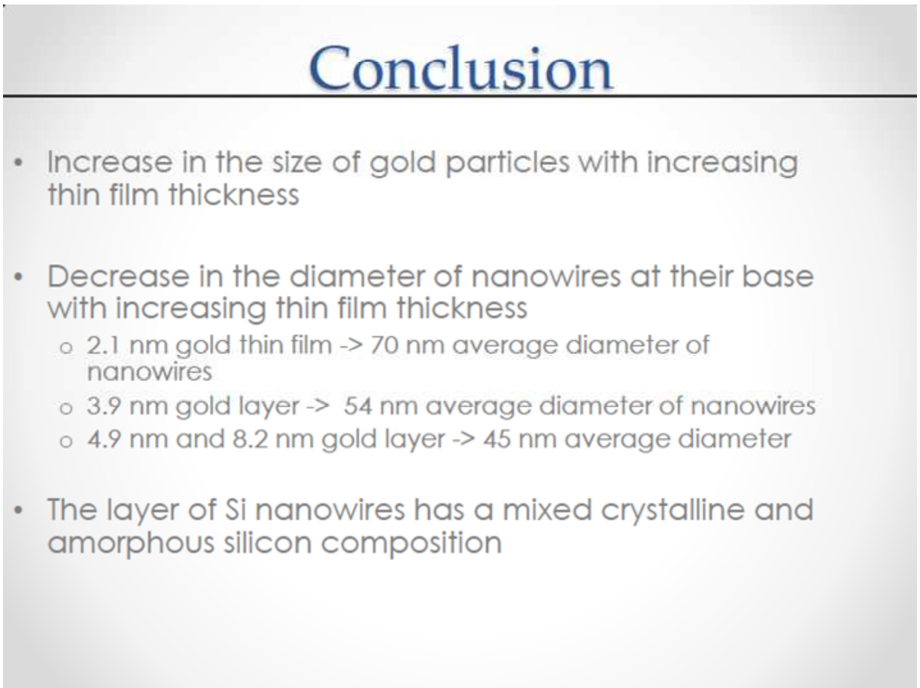
Conclusion
• Increase in the size of gold particles with increasing thin film thickness
• Decrease in the diameter of nanowires at their base with increasing thin film thickness
o 2.1 nm gold thin film -> 70 nm average diameter of nanowires
o 3.9 nm gold layer -> 54 nm average diameter of nanowires
o 4.9 nm and 8.2 nm gold layer -> 45 nm average diameter
• The layer of Si nanowires has a mixed crystalline and amorphous silicon composition

SUNS-V_{OC} METHOD

of IV Curve Measurement
of Photovoltaic Cell

Vlastimil Pic, Petr Pikna 1/2012

IV characteristic measurement

- FV cell sample
- IV characteristic of FV cell
- Current measurement method of IV
- SUNS-Voc method

FV cell sample

Poly-Si thin film solar cell

p+ 100 nm - Anode
p 1500 nm
n+ 100 nm - Cathode
SiN 200 nm
Borosilicate glass substrate
14x14x 3 mm

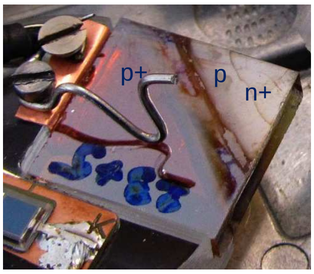

Diode in the Dark

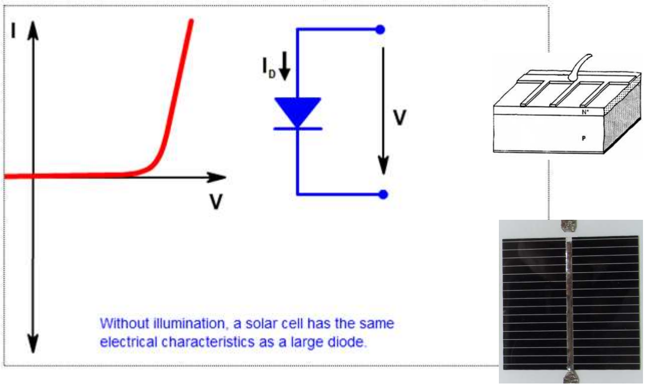

$$I = I_0 \left[\exp\left(\frac{qV}{nkT} \right) - 1 \right]$$

Diode under Illumination

FV cell is a source

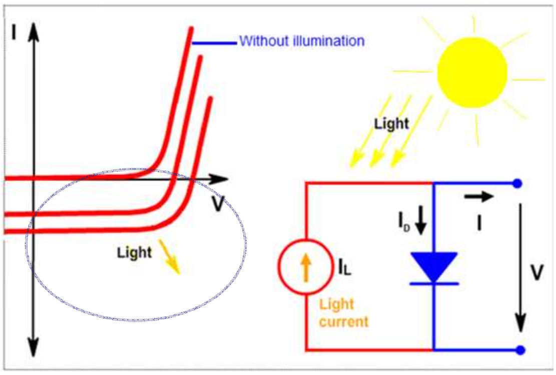

$$I = \left| I_0 \left[\exp\left(\frac{qV}{nkT}\right) - 1 \right] - I_L \right|$$

Diode – Source

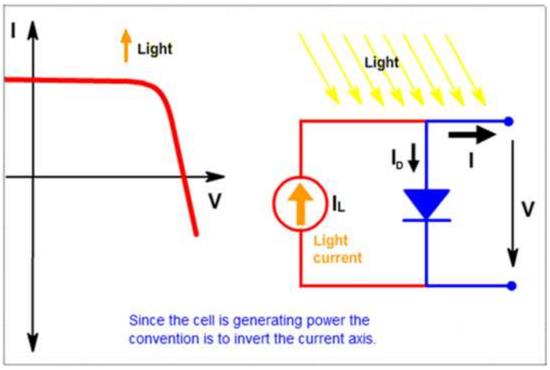

Light Intensity

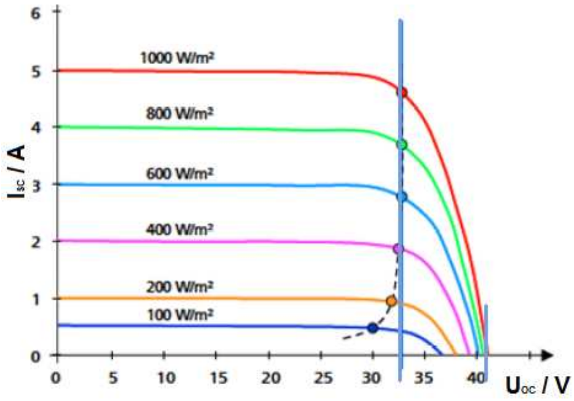

$$I_{PV} = \boldsymbol{R}.P$$

R responsivity, *P* light intensity

Non-linearity less than 1 % over 6-9 decades for Si diode

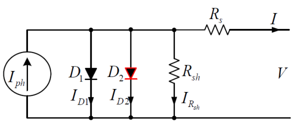

Voltage = f(Light)

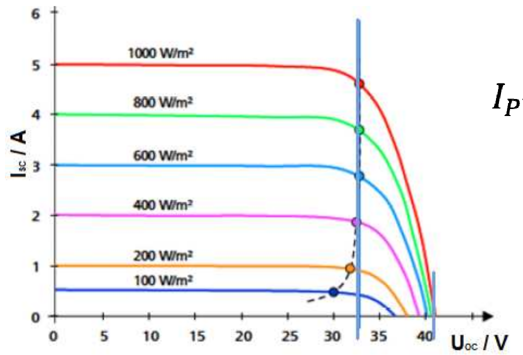

$$I_{PV} = \boldsymbol{R}.P$$

$$I_{PV} >> I_{01} + I_{02} \quad \Longrightarrow \quad V_{OC} \approx \frac{kT}{q} \ln \frac{I_{PV}}{I_{01}}$$

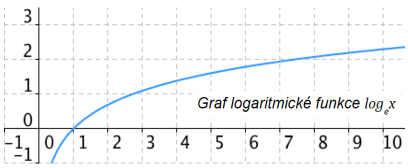

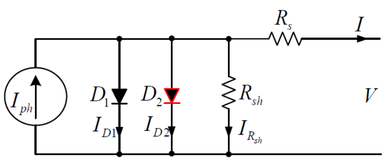

Current-Voltage Method

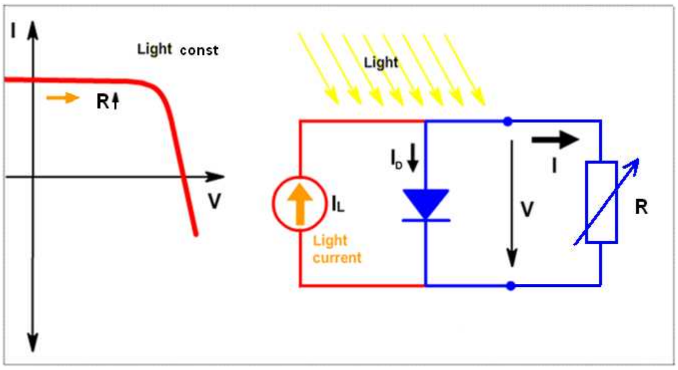

Direct measurement of voltage and current (V and I)

Standard Testing Conditions: 25℃, **1000 W.m^{-2}**, AM = 1.5

1000 W.m^{-2} = 1 SUN

Current-Voltage Method

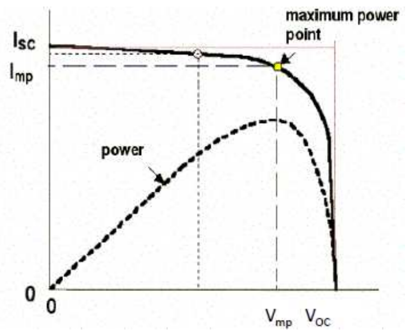

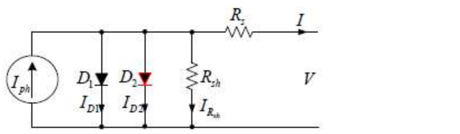

$$I = I_{ph} - I_{01}\left(e^{\frac{V+IR_s}{V_{t1}}} - 1\right) - I_{02}\left(e^{\frac{V+IR_s}{V_{t2}}} - 1\right) - \frac{V+IR_s}{R_{sh}}$$

A_1, A_2 - diode ideality factors, I_{01}, I_{02} - dark saturation currents

R_s - series resistance, R_{sh} - shunt resistance

Direct measurement of voltage and current (V_{OC} and I_{SC})

Max. gained power = $I_{mp}.V_{mp}$

IV Curve by Suns-V_{oc} Method

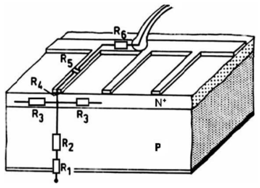

Wafer-based solar cell – **metallized**, common Current IV measurement

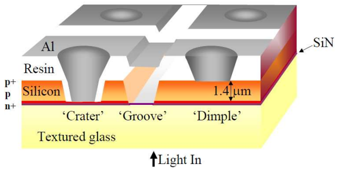

Metallized thin film solar cell (CSG Solar sample)

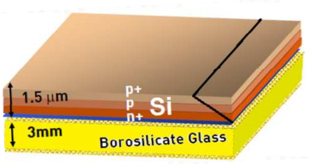

Thin film solar cell (in production)
no metallization →

→ high series resistance of the contact
→ current IV measurement brings error

Suns-V_{oc} Method

Current – Voltage method: Direct measurement of V and I (R↑)
at const test conditions 25℃, **1000 W.m^{-2}**, AM = 1.5

SUNS-V_{oc} method: Direct measurement of V and Light (P↓)
at constant test conditions 25℃, AM = 1.5

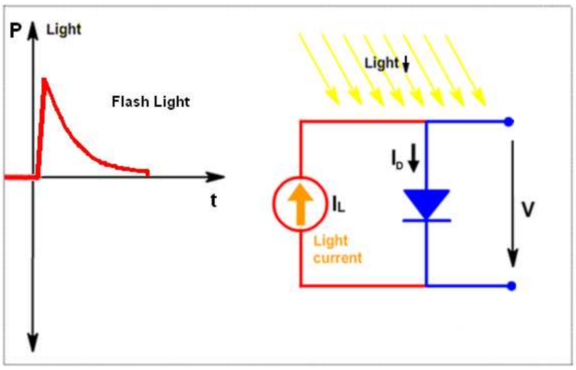

Suns-V_{oc} Method

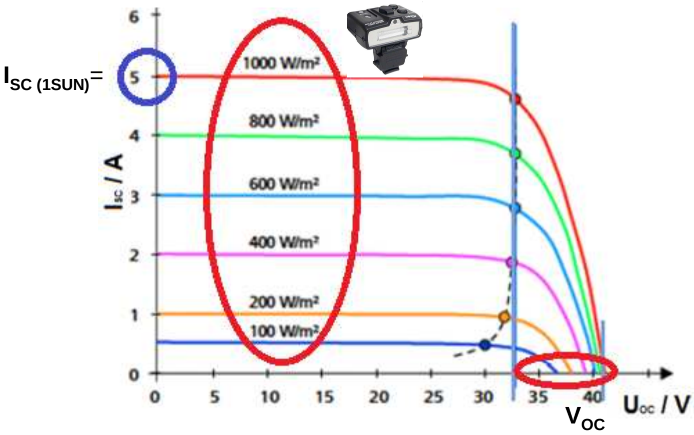

V_{OC} = f(**Light Intensity**)

I_{SC} at 1 SUN (ie. 1000W/m²)

Suns-V_{oc} Method

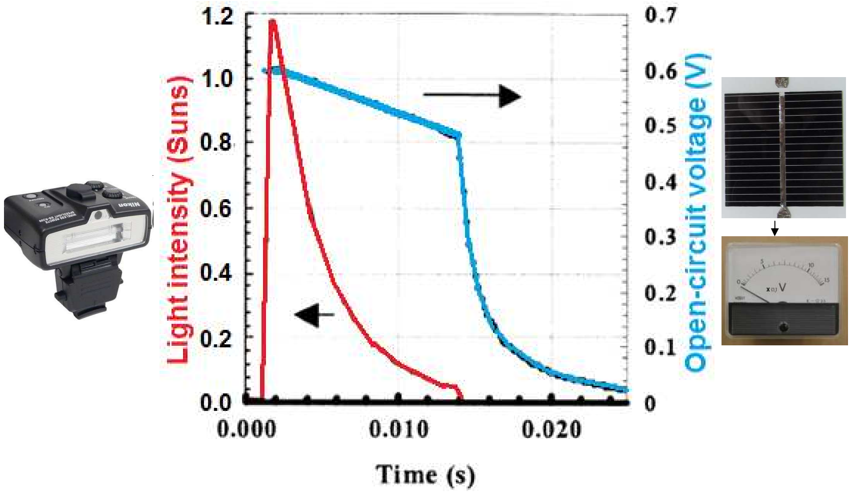

Light intensity decreases gradually → Quasi-steady-state

Suns-V_{oc} Method

$I = I_{sc}$(1 - Light intensity)

I_{sc} .. short circuit current, input parameter measured by other method

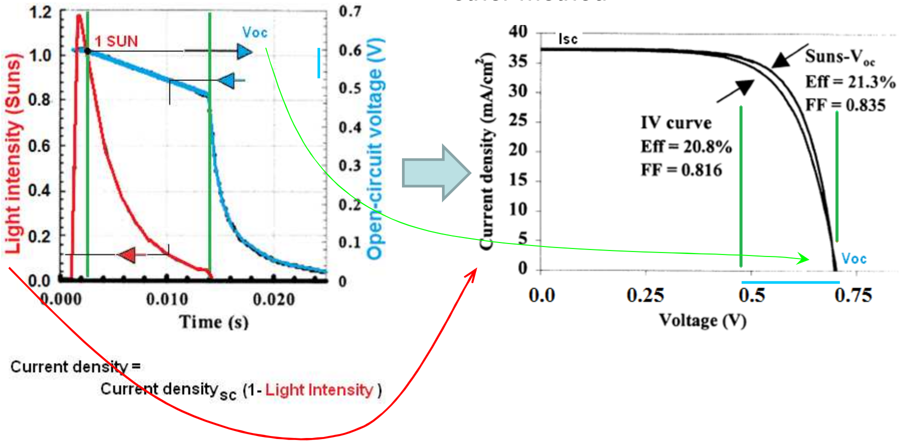

24/10/2012 15

Suns-V_{oc} Method

Searched IV characteristic

I=f(V, P=1000W/m²)

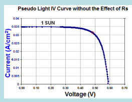

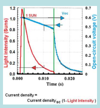

Measured input values

$P=f_1(t)$ (1)

$V=f_2(t)$ -> $t= f_2^{-1}(V)$ (2)

Math equation

I = Isc(1-P) (3)

Only input parameter measured by other method

Substituting (1) and (2) into (3)

$P=f1(f_2^{-1}(V))$

$I = Isc(1-f_1(f_2^{i}(V)))$ -> $I = f_3(V, 1\ SUN)$

Eq.

24/10/2012 16

Suns-V_{oc} Method

MEASURED INPUT

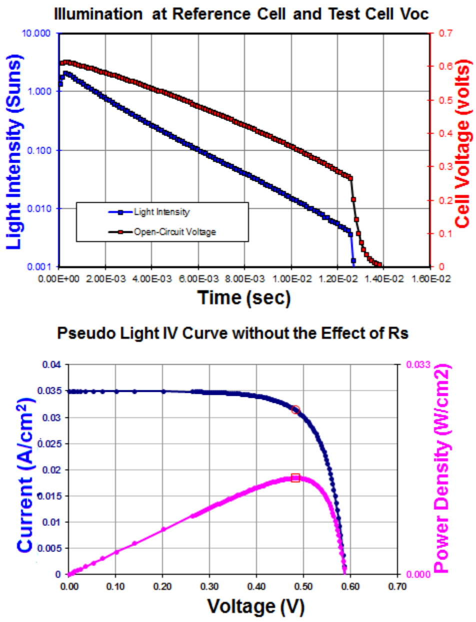

EVALUATED OUTPUT

Comercial Suns-V_{oc} SetUp

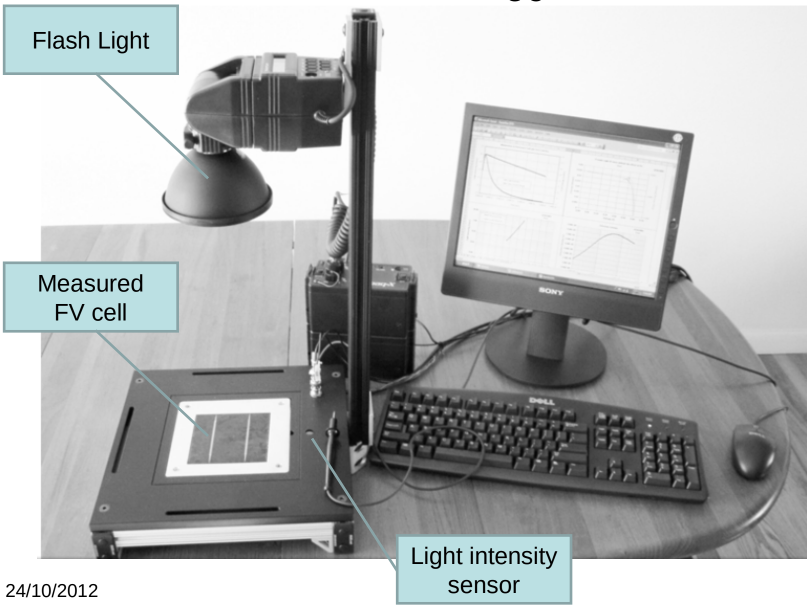

Comercial Suns-V_{oc} SetUp

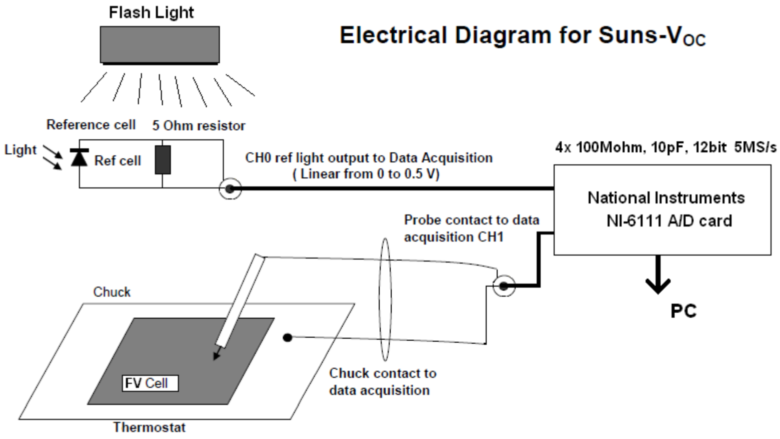

24/10/2012 19

SUNS-Voc Experimental Setup

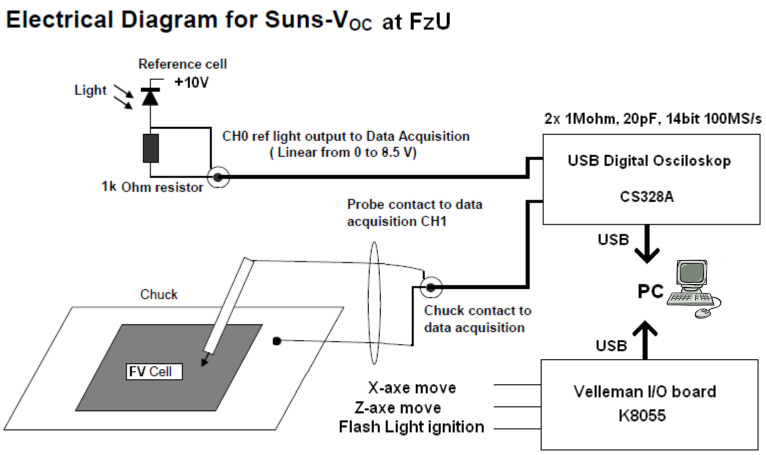

24/10/2012 20

SUNS-Voc Experimental Setup

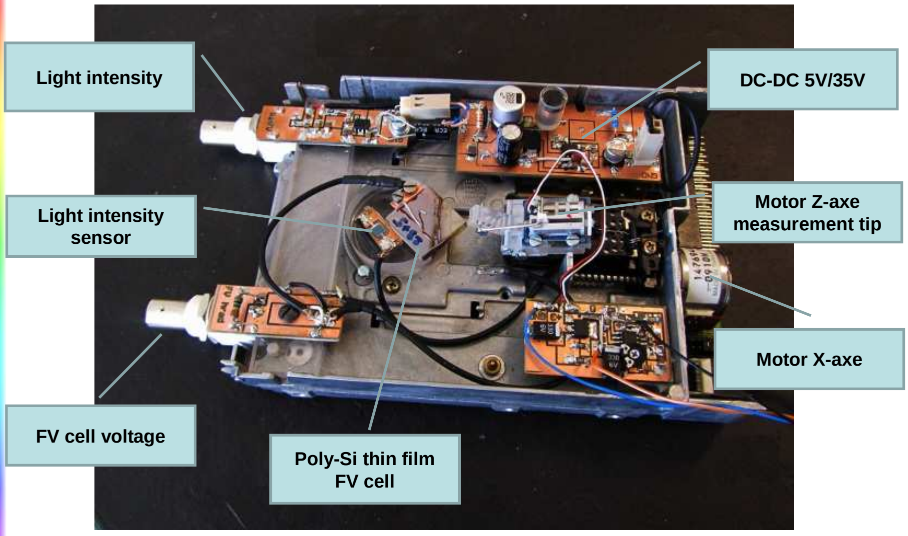

SUNS Voc at FzU - parameters

Reference cell: Light intensity ~0.005 - 7 SUNS (7000 W/

Output: 0-8.5V

Supply: 12V-36V

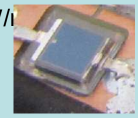

The following can be controlled from Local control board and via PC

Flash light ignition

Measurement tip motion: X-axe 16mm track, 184um step

Z-axe 10mm track, analog control

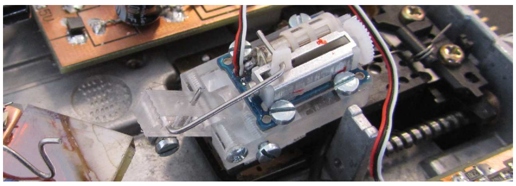

End

24/10/2012 23

Potential for nanotechnology approaches in the production of crystalline and thin film silicon solar cells

Aleš Poruba, Radim Bařinka, Pavel Čech, Pavlína Bařinková, Jiří Hladík, Igor Mudroň and Jaromír Řehák

Solartec, s.r.o., Televizní 2618, 756 61 Rožnov pod Radhoštěm

Increasing the solar cell conversion efficiency together with reducing their production cost are the trends of the last years which are necessary for the near future grid parity of "the energy from the sun". This paper deals mainly with the first part of trends, i.e., with enhanced cell efficiency while keeping the production cost nearly the same or even lower taking into account the potential for the implementation of nanotechnologies in both monocrystalline and thin film silicon devices.

Continuous progress in decreasing the final price of the energy produced from photovoltaic is based on reduction of the production cost of solar cells, keeping the high production yield as well as on enhancing the cell efficiency. Standard c-Si cell production sequence with screen-printed metallization. Usually 5 or 6" mono or multi-crystalline silicon p-type wafers are used as the substrates.

Individual steps can be realized as the batch or in-line processes, where in-line procedures are preferred for the multicrystalline silicon solar cell production. For the final product – photovoltaic (PV) module – solar cells are soldered into the strings (mostly serial interconnection) and are encapsulated into the sandwich structure glass - EVA foil – solar cell – EVA foil – Tedlar foil.

Contrary to "bulk silicon" PV structures thin film Si solar cells (based on either p-i-n single amorphous silicon cell or tandem structure amorphous – microcrystalline solar cells) are grown directly on glass (sometimes "plastic") substrates covered with TCO - Transparent Conductive Oxide (ZnO or SnO2) making the electric contact to the thin p+ silicon layer. After the PE CVD deposition of all individual silicon layers (boron doped, undoped and phosphorus doped) back contact is usually formed as non-transparent by sputtering aluminium or silver (sometimes as the double layer thin TCO + metal). Subdivision of the whole active area into the individual cells and their material interconnection (to increase the generated voltage) is realized using various laser scribing steps before and after PE CVD processes.

Approaches toward industrial cells with >20% efficiency (in Solartec)

Aleš Poruba, Radim Bařinka, Pavel Čech,
Pavlína Bařinková, Jiří Hladík, Igor Mudroň and
Jaromír Řehák

SOLARTEC
Výroba solárních článků a fotovoltaické aplikace

Outline

- Production sequence of standard c-Si solar cells on p-type substrates
- Standard and advanced characterization of wafers and solar cell structures
- Modeling the cell performance by PC1D
- The way how to exceed the cell efficiency of 20%

Standard production steps in c-Si technology

- saw damage etching
- surface texturing
- n-type (P) diffusion
- $(SiO_2+)Si_3N_4$ ARC
- Ag/Al(+Al) print BS
- Ag screenprint FS
- paste sintration
- edge isolation (if not done before)
- measuring and sorting

Alkaline **texturing** (equipment)

- dose process (50-100 Si wafers)
- mixture of NaOH (KOH) + isopropylalcohol
- temperature 70-80°C
- processing time ≈ 30min
- purity of the Si surface plays an important role for homogeneous nucleation of pyramids and their growth

Phosphorus diffusion and ARC deposition

- dose processes (100-400 Si wafers)
- Si wafers on quartz boats (in a quartz tube)
- process time ≈ 60-90min
- clean room

- source of phosphorus - $POCl_3$
- diffusion temperature 820-950°C

- source gasses SiH_2Cl_2 and NH_3 („dry“ pumping system)
- deposition temperature ≈ 800°C

Screenprinting the metallic pastes and sintration (paste co-firing)

Screenprinting semiautomatic machine from Baccini

Infrared belt furnace (6 independent zones)

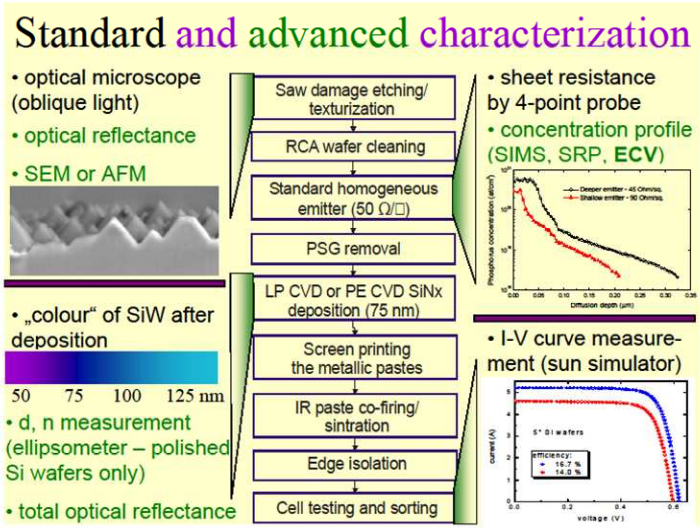

Another types of solar cell characterization

- Dark I-V curve measurement (various temperatures)
- Quantum efficiency (Jsc=f(λ))
- LBIC (Light Beam Induced Current)
- Photoluminiscence
- Electroluminiscence (microplasma)
- Noise diagnostics
- „Suns-Voc“ method (pseudo I-V curve measurement)

Example of LBIC results (405, 830nm)

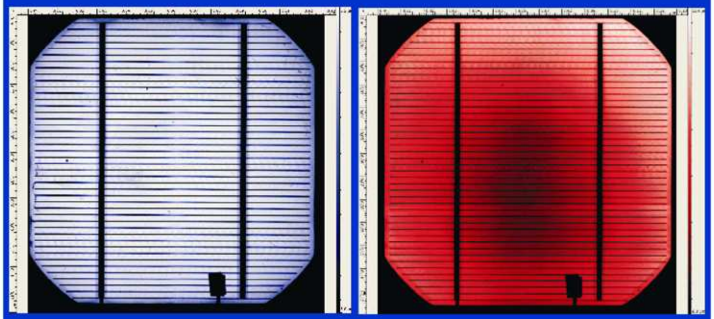

Each characterization method contributes to the detection of “problems”

BUT

they are not able to identify the cause and origin

↓

- necessity of „step by step“ monitoring of some „typical“ parameter
- (minority) carrier lifetime (or carrier diffusion length) is the most important parameters

Diffusion length and carrier lifetime

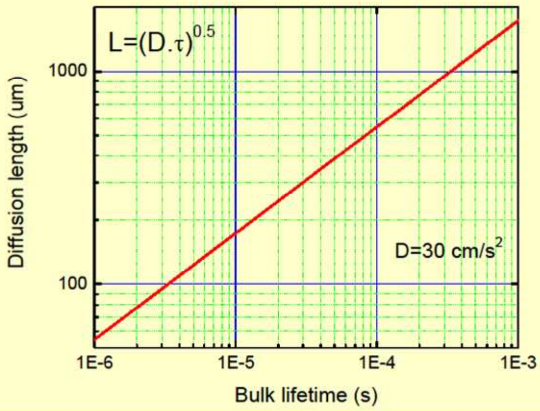

Lifetime measurement by MW PCD and QSSPC

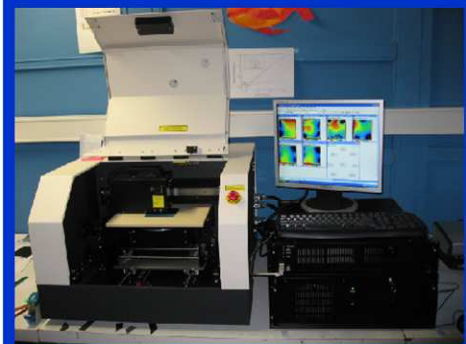

Principle of methods – measurement of carrier concentration decay (in time) after their pulse light generation

Surface recombination as a specific problem for the bulk lifetime measurement

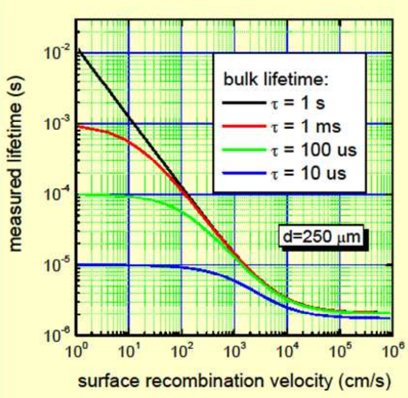

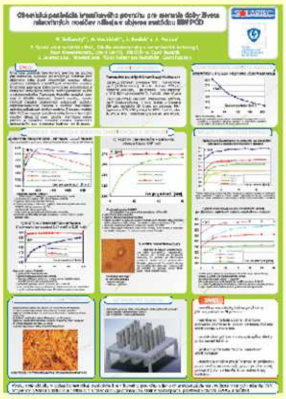

Modelling by PC1D program

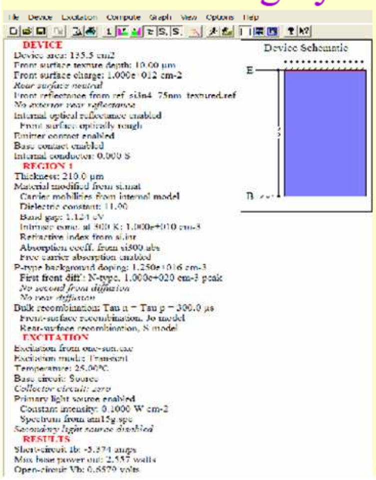

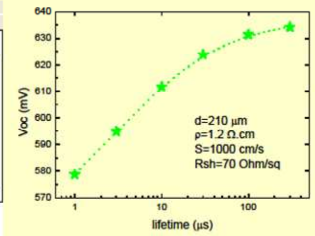

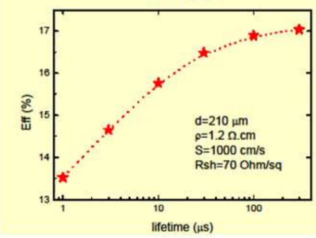

Modeling the solar cell performance (PC1D)

Parameters of solar cells and their impact on performance:

- **carrier lifetime (1-300 μs)**
- **recombination velocity at the rear side (1000-10 cm/s)**
- bulk resistivity of the silicon wafer (1 or 3 Ω.cm)
- sheet resistivity of the n+ layer (50-90 Ω/sq.) (depends on the surface concentration and depth of doped layer)
- recombination velocity at the front side (10^5-10^4 cm/s)
- optical reflectance (surface texturing and ARC coating)
- thickness of the silicon wafer (240-180 μm)

PC1D – external quantum efficiency

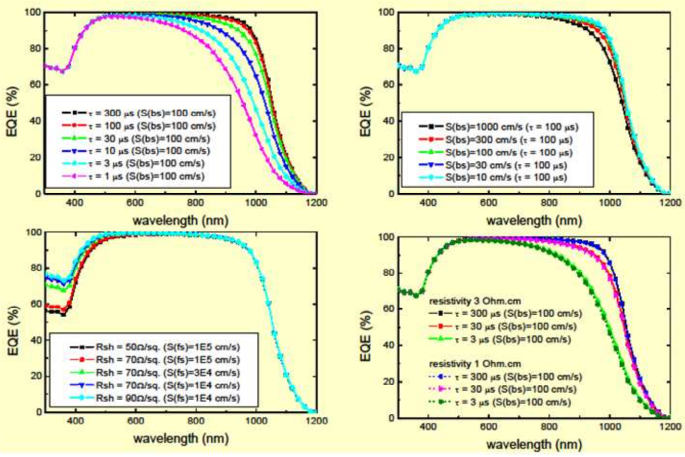

Modeling the solar cell performance (PC1D)

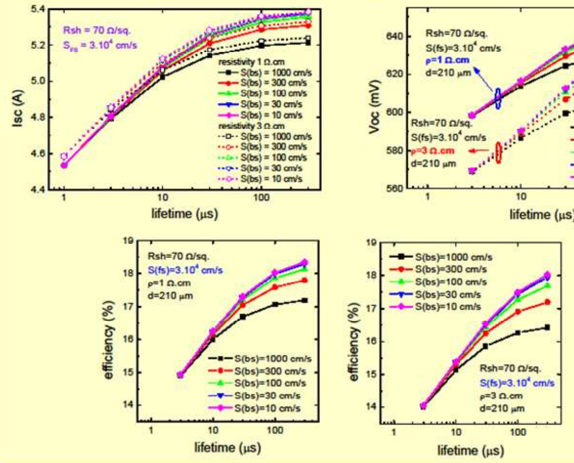

PC1D – influence of wafer thickness

All the calculation until now done with "default" parameters of internal reflectivity

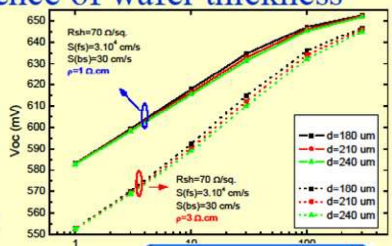

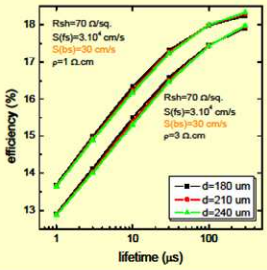

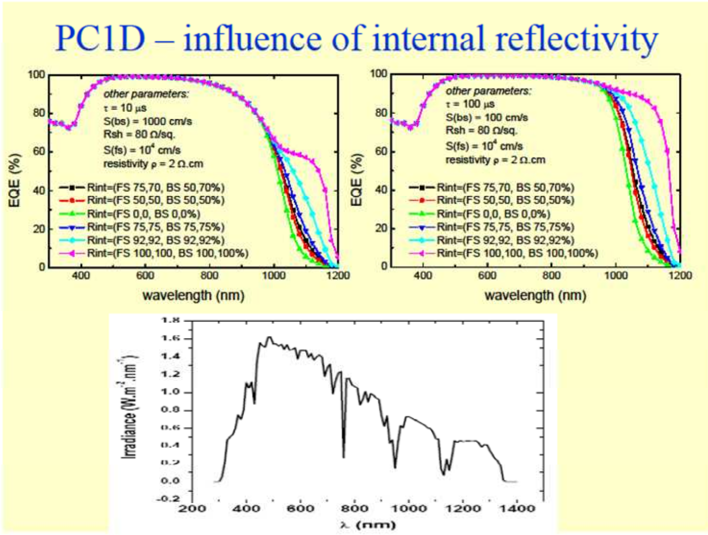
PC1D – influence of internal reflectivity
other parameters:
τ = 10 μs
S(bs) = 1000 cm/s
Rsh = 80 Ω/sq.
S(fs) = 10⁴ cm/s
resistivity ρ = 2 Ω.cm
Rint=(FS 75,70, BS 50,70%)
Rint=(FS 50,50, BS 50,50%)
Rint=(FS 0,0, BS 0,0%)
Rint=(FS 75,75, BS 75,75%)
Rint=(FS 92,92, BS 92,92%)
Rint=(FS 100,100, BS 100,100%)
EQE (%)
wavelength (nm)
other parameters:
τ = 100 μs
S(bs) = 100 cm/s
Rsh = 80 Ω/sq.
S(fs) = 10⁴ cm/s
resistivity ρ = 2 Ω.cm
Rint=(FS 75,70, BS 50,70%)
Rint=(FS 50,50, BS 50,50%)
Rint=(FS 0,0, BS 0,0%)
Rint=(FS 75,75, BS 75,75%)
Rint=(FS 92,92, BS 92,92%)
Rint=(FS 100,100, BS 100,100%)
EQE (%)
wavelength (nm)
Irradiance (W.m⁻².nm⁻¹)
λ (nm)

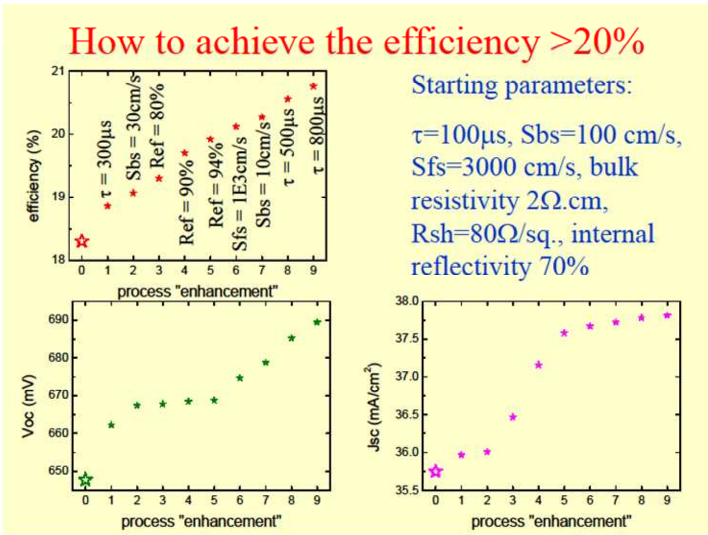
How to achieve the efficiency >20%
Starting parameters:
τ=100μs, Sbs=100 cm/s, Sfs=3000 cm/s, bulk resistivity 2Ω.cm, Rsh=80Ω/sq., internal reflectivity 70%
τ = 300μs
Sbs = 30cm/s
Ref = 80%
Ref = 90%
Ref = 94%
Sfs = 1E3cm/s
Sbs = 10cm/s
τ = 500μs
τ = 800μs
efficiency (%)
process "enhancement"
Voc (mV)
process "enhancement"
Jsc (mA/cm²)
process "enhancement"

The most important parameters and how to achieve and keep their high quality values

1. Carrier lifetime (gettering techniques, clean rooms for the high temperature processes as well as for the etching/cleaning/drying lines)
2. Front surface recombination (structures with selective emitter + double layer ARC)
3. Back surface recombination and internal reflectance (rear surface morphology modification together with dielectric surface passivation and local point contacts - advanced light trapping structure)

Surface morphology modification by APPCE (Atmospheric Pressure Plasma Chemical Etching) – EU project N2P

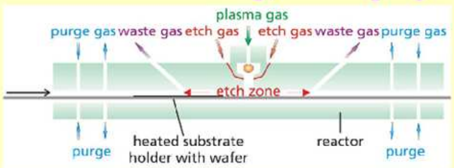

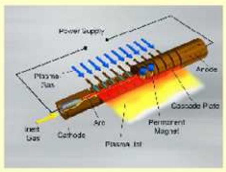

SF_6 (1 slm)

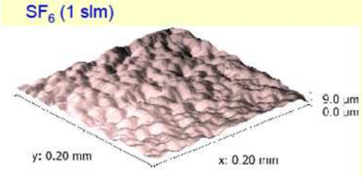

$SF_6 + O_2$ (1+1 slm)

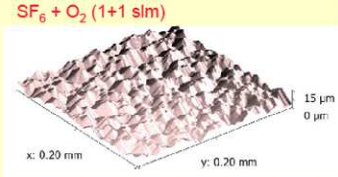

Optimal pyramid angle at the rear surface 135 ° (optical modeling)

Conclusion

• Standard solar cell structure with Al back contact - limitation of the cell performance to the value below 19% (due to limited quality of BSF formation as well as rather low internal reflectivity)

The only way how to surpass the efficiency of 20% for p-type c-Si material:

• Advanced light trapping scheme - the rear side with dielectric passivation (layer with fixed negative charge or BS boron diffusion)

• Selective emitter structure (as a single diffusion process) with double layer ARC (SiO_2 + SiN_x)

Note

PC1D modeling was done taken into account:

- 10 % losses (4-6% for front side metallization shadowing effect and 4% reflectivity of the free glass interface after encapsulation)
- "Constant" reflectivity of the front side (structure of random pyramids with the single layer antireflective coating)

Optical properties of thin NCD films

Zdeněk Remeš, Alexander Kromka
Fyzikální ústav AVČR, v. v. i., Cukrovarnicka 10, Praha 6, remes@fzu.cz

Institute of Physics (FZU) of the Academy of Sciences of the Czech Republic is a public research institute, oriented on the fundamental and applied research in physics. The Department of the Optical Materials has a long-term experience with characterization of the optical and opto-electrical properties of thin films started in 1983 with a M. Vanecek's paper *Density of the gap states in undoped and doped glow discharge a-Si:H*, Solar Energy Materials 8 (1983) 411. Today, the Department of Optical Materials focuses on the technology of preparation and processing of the bulk and thin film materials for optical applications using Bridgman method, MW plasma enhanced chemical vapor deposition, hydrothermal growth, reactive ion etching and plasma grafting. Among the investigated materials we mention for example scintillation crystals and glasses, ZnO nanorods and nanocolumns or nanocrystalline diamond (NCD) layers. These materials and other ones obtained in the framework of external collaborations are characterized by the radioluminescence, photoluminescence, time-resolved photoluminescence with ns resolution, photothermal deflection spectroscopy (PDS), photocurrent spectroscopy and Fourier transform infrared spectroscopy (FTIR). Other characterization methods available are electron paramagnetic resonance (EPR), electron spectroscopy and thermal analysis of properties of solids - conventional Differential Scanning Calorimetry (DSC) and the Temperature-Modulated DSC.

Mgr. Zdenek Remes, PhD. is a permanent contract researcher at the Department of Optical Materials of the Institute of Physics. He is experienced in optical properties of thin films with H-index 16, number of the published papers 61 and citations 589. Z. Remes defended his Ph.D. in 1999 in solid state physics and material science at the Faculty of Mathematics and Physics of the Charles University in Prague. As post-doc he had been working abroad in several internationally reckon laboratories in diamond semiconductor research such as the Institute for materials research (IMO), Hasselt University, Belgium; the Solid State Institute, Technion - Israel Institute of Technology, Haifa and the CEA/Saclay France. He has been responsible recently for several national and international projects, including the cooperation with the Institut Néel - CNRS, Grenoble, France; Slovak Technical University, Bratislava, Slovakia; East China Normal University, Shanghai, P.R. of China, Institute of Semiconductor Physics Siberian Branch of Russian Academy of Sciences, Novosibirsk, Russia and the Institute of Automation and Control Processes of the Far Eastern Branch of Russian Academy of Sciences in Vladivostok.

In this presentation we summarized the selected optical characterization methods available at the Department of the Optical Materials which are suitable for characterization of the thin nanodiamond layers.

We acknowledge the project P108/11/0794 (GACR).

CABIOM cabiom.fzu.cz
Carbon-based Biomaterials and Biointerfaces
Virtual Research Center of the Institute of Physics ASCR, v. v. i.

Optical properties of thin NCD films

Zdeněk Remeš, Alexander Kromka

Fyzikální ústav AVČR,v.v.i., Praha

Optical spectroscopy team

- Mgr. Zdeněk Remeš, PhD.
  - team leader, supervisor, project manager
- Mgr. Halyna Kozak, Ph.D.
  - ATR, GAR FTIR, DLS, SEM, AFM, sample preparation
- Mgr. Jakub Holovský, PhD.
  - FTPS, IR microscopy, PDS
- Ing. Lenka Hoďáková
  - FTIR spectroscopy, T&R spectrocopy, photoluminescence, interference refractometry

Equipment

- Mid IR FTIR Nicolet Nexus 400-4000/cm, N2 purged
  - T&R, ATR, GAR, angle resolved R
- Near IR FTIR Nicolet Nexus 20000-2000/cm
  - FTPS, step scan FTPS
- Photothermal deflection spectroscopy (PDS) 250-3000 nm

Laboratories

- D17: air conditioning
  - Photocurrent spectroscopy (CPM, FTPS)
  - el. measurements
  - FTIR
- D301: UV-NIR, ozone exhaust
  - Photo-thermal spectroscopy (PDS)
  - Steady state PL

Zdeněk Remeš - 2012

New Laboratory of Infrared Spectroscopy

- “Clean room”, air conditioning
- flow box (soft chemistry)
- N2 purged FTIR 400-4000/cm : T&R, ATR, GAR
- IR microscope extended to visible
  - Magnification 10x
  - Space resolution Ø150, 100 and 50 µm

Zdeněk Remeš - 2012

Photothermal deflection spectroscopy

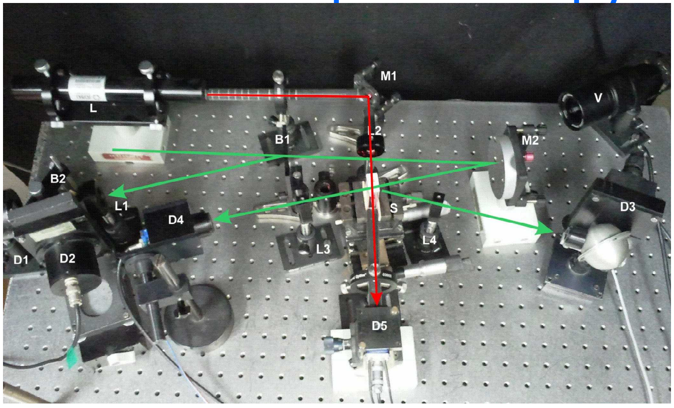

- M1-2: mirrors
- B1-2: beamsplitters
- L: laser
- D1-5: detectors
- L1-4: lens
- V videocamera
- S sample

- 150W Xe or 150W halogen lamp
- Sample in transparent liquid
- Spectral range 250-3000 nm

Zdeněk Remeš - 2012

µ-Spectrometer & microscope

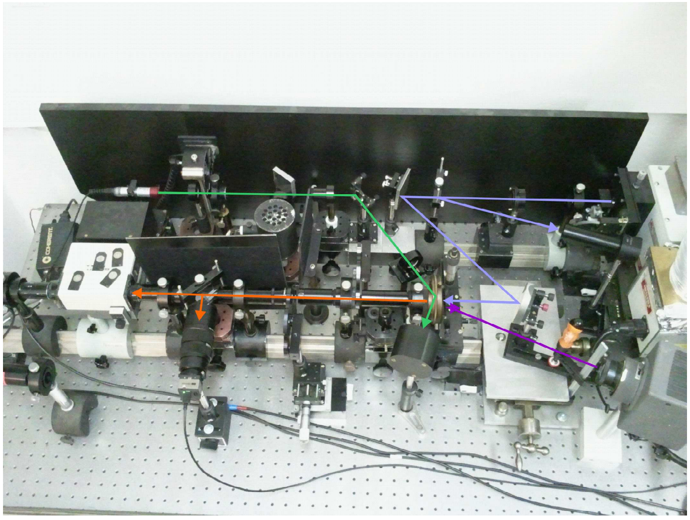

DPC:
•200-1000 nm
•30 W UV bias
•ac 1-50 Hz

Micro-Transmittance:
•300-1100 nm
•Ø20-1000 µm

Photoluminescence:
•SSL 200mW, 532 nm
•400-1600nm
•Res. 2,4,8,16,32 nm
•APL Si, InGaAs
•100-1000 Hz

ac Electrolumin.:
•0-500 V
•0-80 mA
•0-20 Hz, TTL
•400-1600 nm

Thin film optics - Motivation

- We investigate
  - Optical quality = low optical absorption and low scattering in UV
  - Electronic quality = high mobility, long lifetime of photoexcited carriers
  - Color centers
- Achieved by: optimized growth conditions
  post-processing
- Defect characterization by Zdenek Remes:
  - Transmittance & Reflectance spectra (T&R)
  - Photothermal Deflection Spectroscopy (PDS)
  - Dual beam photocurrent Spectroscopy (DBPS)
  - Fourier Transform infrared spectroscopy (FTIR)

Reflectance interferometry

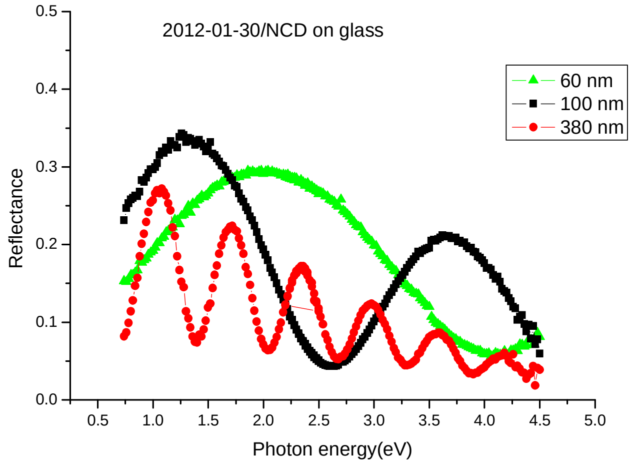

Zdeněk Remeš - 2012

Optical absorptance and scattering spectra

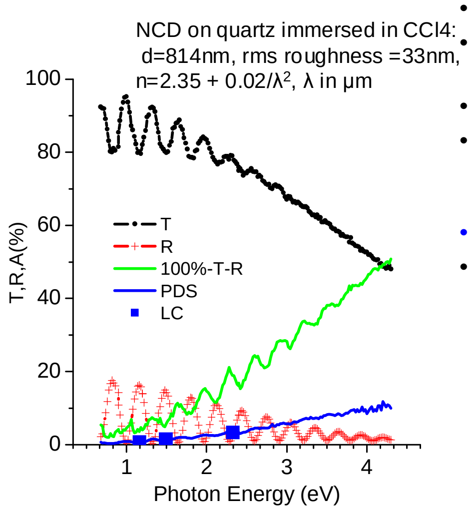

- NCD on glass in transparent liquid
- Multireflections and interferences => film thickness
- Surface scattering => roughness
- Fitting T&R using scalar scattering theory, Exponential Cauchy: $n=n_0 + n_1/\lambda^2$ & $k=k_0\exp(k_1/\lambda)$
- 100%-T-R is scattering not A
- Optical A from PDS normalized by LC

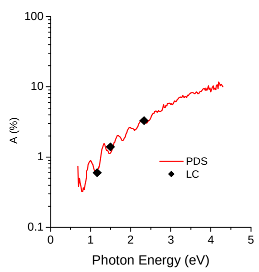

Z. Remes, presented at Diamond 2009 - the 20th European Conference on Diamond, Diamond- Like Materials, Carbon Nanotubes, and Nitrides, 6-10 September 2009 in Athens, Greece

Zdeněk Remeš - 2012

Dual Beam Photocurrent Spectroscopy (DBPS)

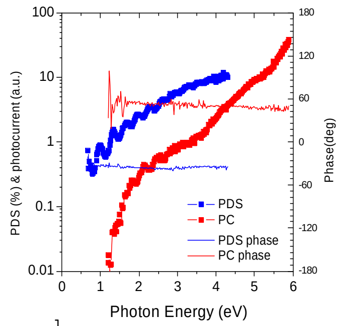

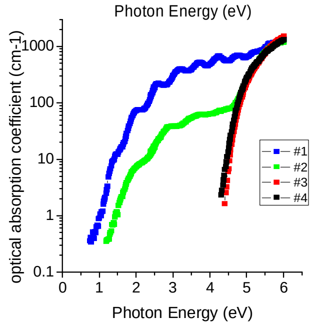

DBPS= continuous UV illumination to keep mobility-lifetime product constant + amplitude modulated photocurrent spectrum in UV-VIS-NIR. Typical intrinsic, oxidized NCD/glass DC ~ 1-10pA (provided by focused 30W D2 lamp), AC ~ 10-1000fA at 500V, 10Hz, 150W Xe lamp

- **Photothermal methods**: total optical absorption dominated by non-diamond content in and between grains and "black spots" => sensitive to the "the worst part of the sample"
- **Photocurrent:** only the absorption processes generating free carriers in the valence or conduction band => sensitive to "the best part of the sample"

- #1: non-optimized NCD/glass
- #2: optimized deposition
- #3: optimized deposition, post-deposition etching of residual non-diamond containation in boiling H_2So_4 + KNO_3
- #4: the same as #3 after anneal at 450ºC => **NCD stable up to 450ºC**
- *However: We see „apparent" opt. absorption, influenced by light scattering*

[1] Z. Remes, DOI:10.1016/j.diamond.2009.02.007
[2] Z. Remes, DOI: 10.1002/pssa.200982211

Zdeněk Remeš - 2012

CONCLUSIONS

- Interference fringes => the thickness of the thin layers
- Optical absorption in thin nanocrystalline layers
  - dominated by grain boundaries
  - Monitored by T&R, PDS
- Photosensitivity of thin nanocrystalline layers
  - Electronic quality
  - localized defect states inside grains
  - monitored by the DBP, CPM, FTPS

Zdeněk Remeš - 2012

Stem cells – open opportunities

Institute of Experimental Medicine AS CR, v.v.i.

Nataliya Romanyuk PhD

February 3, 2012

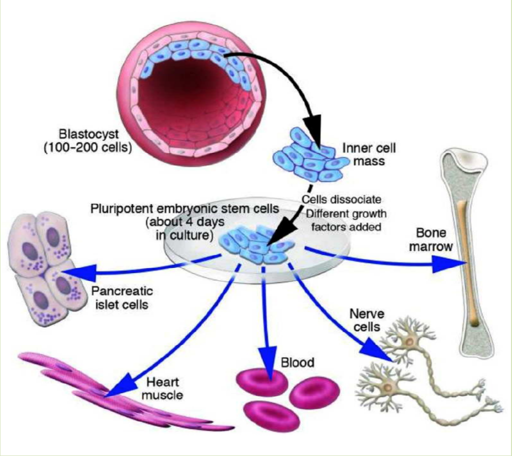

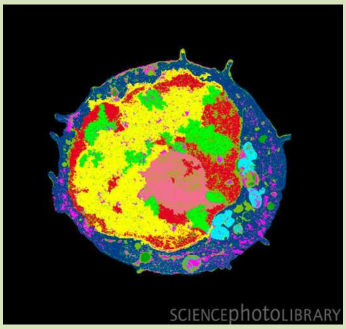

- What stem cells are? Their main features
- What kind of stem cells we know?
- Methods to obtain stem cells
- Stem cells open opportunities for biomedicine and fundamental science
- Progress in stem cell therapy

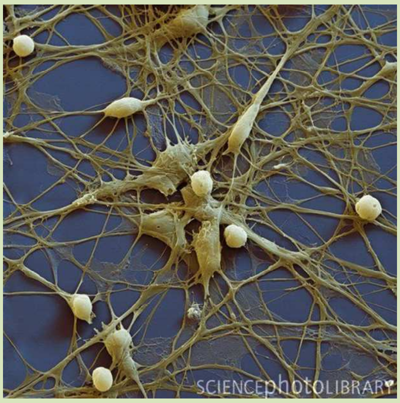

Stem cells are cells found in all multicellular organisms, that can differentiate into diverse specialized cell types (potency) and can self-renew to produce more stem cells (clonality)

Clonality single cell possess the capacity to create more stem cells

Self-renew the ability to go through numerous cycles of cell division while maintaining the undifferentiated state (asymmetric division)

Potency the capacity to differentiate into specialized cell types

Research into stem cells grew out of findings by Ernest A. McCulloch and James E.Till at the University of Toronto in the 1960s

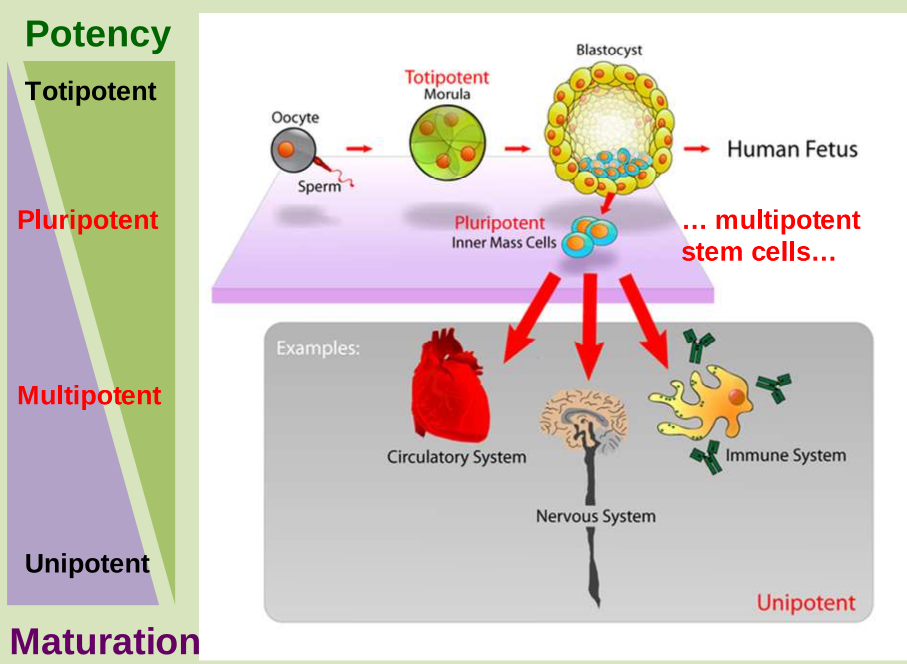

Multipotent stem cells → **Fetal stem cells**

↓

Adult stem cells

from bone marrow, umbilical cord blood, placenta, adipose tissue, olfactory mucosa cells, nervous tissue mammary gland, testicles….

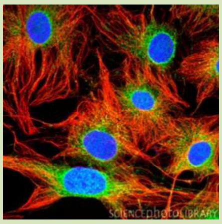

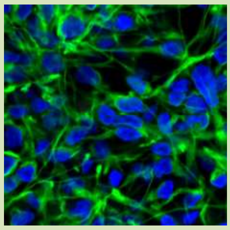

How to make them work???

Multipotent stem cells

Advantages	Disadvantages
Some of them can be easy obtained, but….	…in small number
Safe from tumor formation	Difficult for cultivation, have a very short life time
No ethical issues	Lower proliferative and differentiative potential then pluripotent stem cells have
Possible obtaining and transplantation to the same person (autologous transplantation)	

However, multipotent stem cells are broadly using in research and even in a few clinical trails

Leukemia treatment	Big progress
Wound healing	
Stroke	????
Spinal cord injury	Altogether 65 people took part in this study (35 with complete lesion) Some studies are already running longer then 5 years….

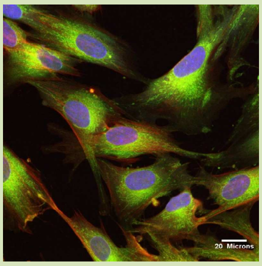

Cells not capable of growing into a whole organism but able to differentiate into any cell type in the body

Pluripotent stem cells

Embryonic stem cells

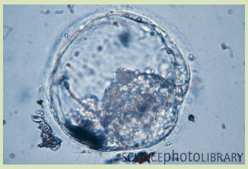

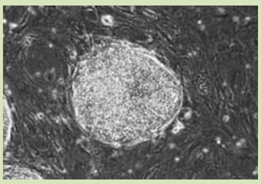

Induced pluripotent stem cells

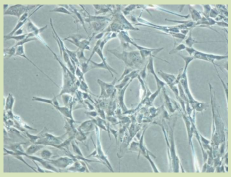

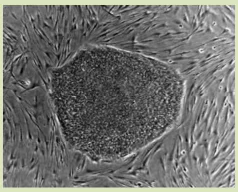

Human Embryonic Stem (hES) Cells
(Thompson et al, 1998)

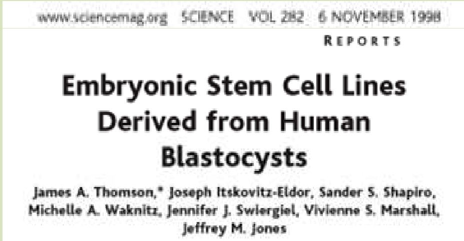
www.sciencemag.org SCIENCE VOL 282 6 NOVEMBER 1998
REPORTS

Embryonic Stem Cell Lines Derived from Human Blastocysts

James A. Thomson,* Joseph Itskovitz-Eldor, Sander S. Shapiro, Michelle A. Waknitz, Jennifer J. Swiergiel, Vivienne S. Marshall, Jeffrey M. Jones

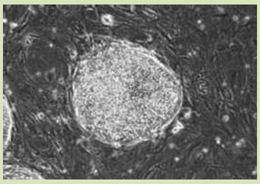

Technology to obtain a human ES cell line

Early embryo – blastocyst
(human 4-5 days, mouse 3.5 days)

- donated for research purposes – written consent
- no monetary compensation

Blastocyst = trophectoderm + ICM (embryoblast)

- Removal of zona pellucida (pronase treatment)
- Isolation of ICM by immunosurgery
- Placing ICM onto a feeder layer of MEFs (CF-1)

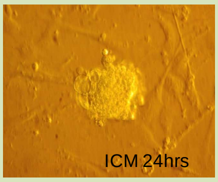

- Culture in appropriate media
  (DMEM/F-12 with KO-SR and FGF-2)
- Hoping for the attachment of the ICM

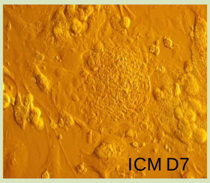

Observation of significant outgrowth
of putative hESCs

The first passage – mechanical disaggregation

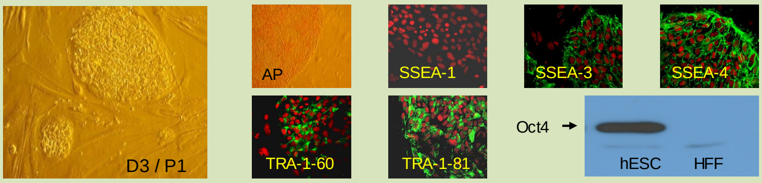

pictures are kindly provide by Dr Ales Hampl

Derivation of hESC is not a 100% successful process

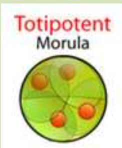

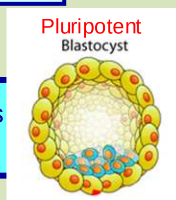

10 morulas 100%	88 blastocysts 100%
	83 isolated ICMs (?) 94%
1 attached morula 10%	57 attached ICMs 69%
No hES cell line 0%	14 hES cell lines 24.6%

International Stem Cell Initiative

(International Stem Cell Forum – Prof. Peter Andrews)

Centre for Stem Cell Biology & UK Stem Cell Bank

- 63 hESC lines
- 17 laboratories
- 11 countries

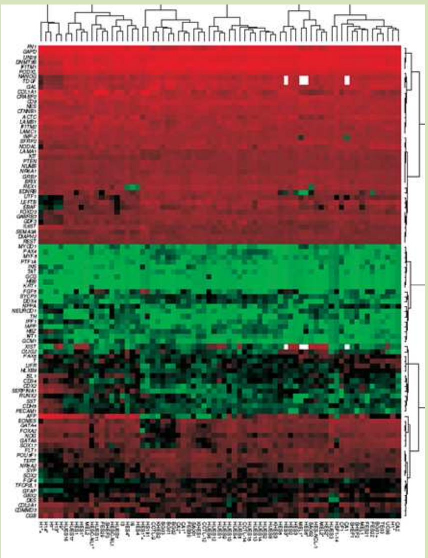

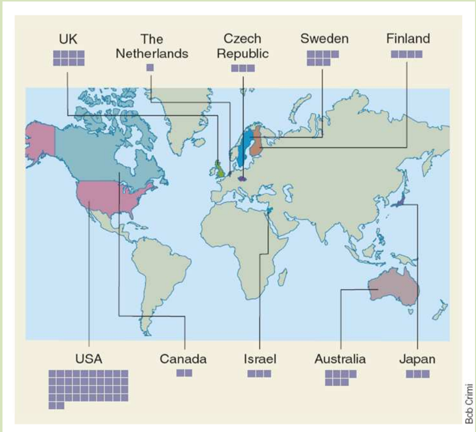

Published
Nature Biotechnology
2007

Legislative

The International Society for Stem Cell Research (ISSCR) provides a survey on regulations regarding the therapeutic use of stem cells worldwide (www.ISSCR.org) and recently approved Guidelines for the Clinical Translation of Stem Cells (December 3, 2008).

In the European Union, the Directive 2004/23/EC of the European Parliament and of The Council (called 'Tissue and Cells Directive', from March 31, 2004) and Commissions Directives (i.e., 2006/17/EC and 2006/86/EC) regulate standards of quality and safety for the donation, procurement, testing, processing, preservation, storage and distribution of human tissues and cells.

In most countries, the derivation and use of human ES cells is controlled by specific guidelines or by law. For instance, in the Czech Republic, 1st legislative act about the use of ES (277/2006 Sb) regulates the import and use of pluripotent human ES cells in basic research.

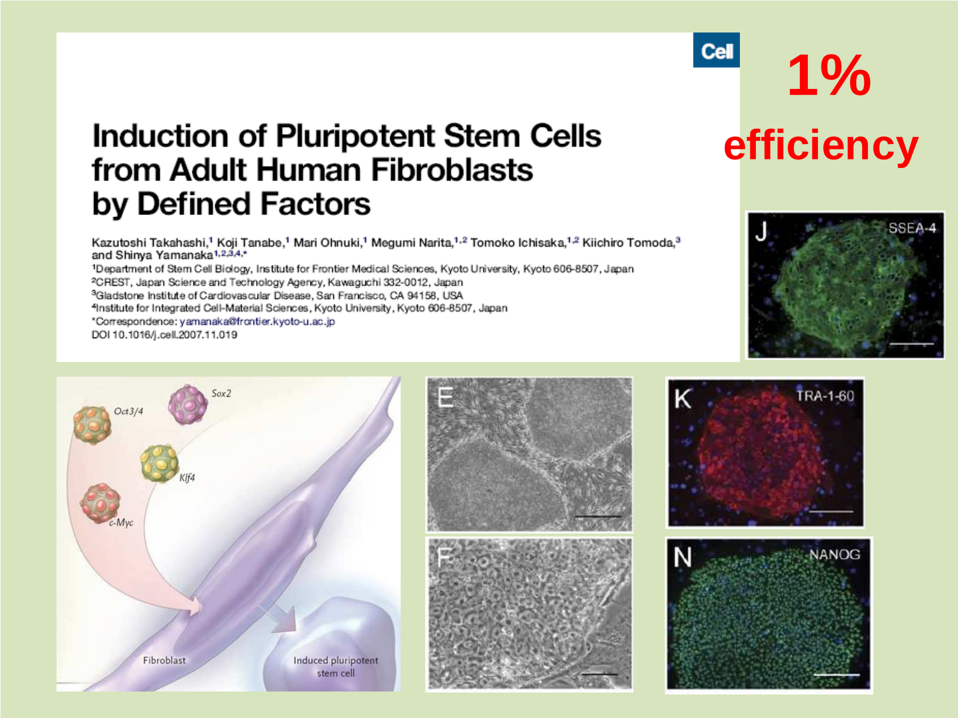

Pluripotent Stem Cells open opportunities

Promise for biomedicine

- Replacement therapy
- Drug development
- Disease modeling
- Toxicity testing

Food for thought

- Mechanism(s) of self-renewal ?
- Mechanism(s) of differentiation arrest – the cancer paradigm ?
- Symmetric/asymmetric division ?
- Cell cycle checkpoint(s) ?
- Mechanisms of differentiation ?

Replacement therapy

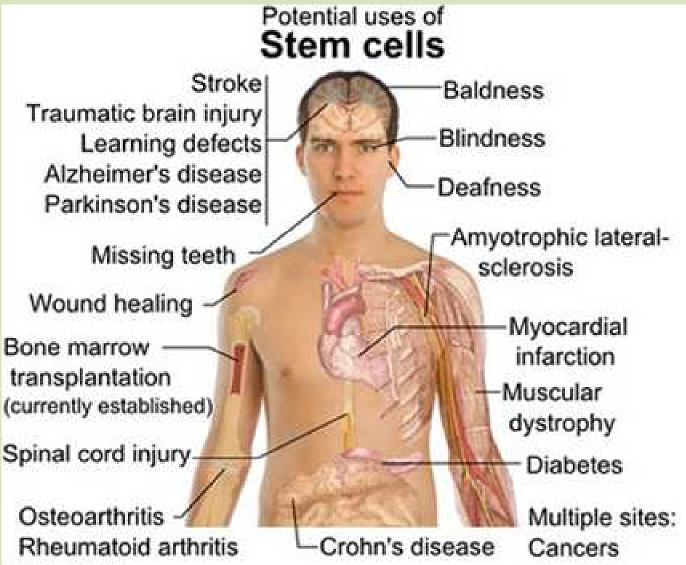

Heart

nature biotechnology

Cardiomyocytes derived from human embryonic stem cells in pro-survival factors enhance function of infarcted rat hearts

Michael A Laflamme[1,2,6], Kent Y Chen[1–3,6], Anna V Naumova[1,4], Veronica Muskheli[1,2], James A Fugate[1,2], Sarah K Dupras[1,2], Hans Reinecke[1,2], Chunhui Xu[5], Mohammad Hassanipour[5], Shailaja Police[5], Chris O'Sullivan[5], Lila Collins[5], Yinhong Chen[5], Elina Minami[1,3], Edward A Gill[3], Shuichi Ueno[1,2], Chun Yuan[1,4], Joseph Gold[5] & Charles E Murry[1,2]

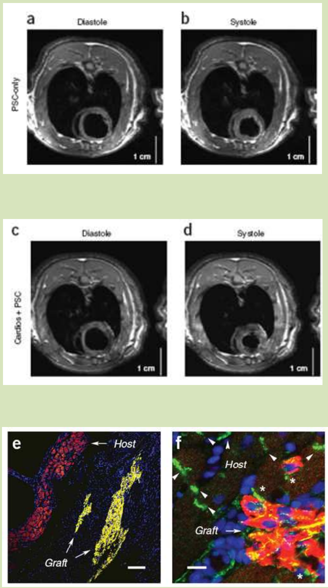

STEM CELLS®

EMBRYONIC STEM CELLS

Generation of Insulin-Producing Islet-Like Clusters from Human Embryonic Stem Cells

JIANJIE JIANG,[a] MELINDA AU,[a] KUANGHUI LU,[a] ALANA ESHPETER,[b] GREGORY KORBUTT,[b] GREG FISK,[a] ANISH S. MAJUMDAR[a]

Pancreas

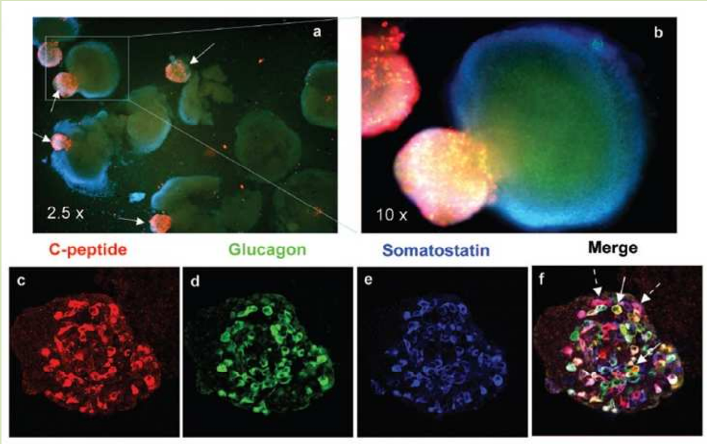

Expression of islet-specific hormones in hESC-derived budding islet-like clusters

STEM CELLS®

EMBRYONIC STEM CELLS

Efficient Differentiation of Functional Hepatocytes from Human Embryonic Stem Cells

SADHANA AGARWAL, KATHERINE L. HOLTON, ROBERT LANZA

Liver

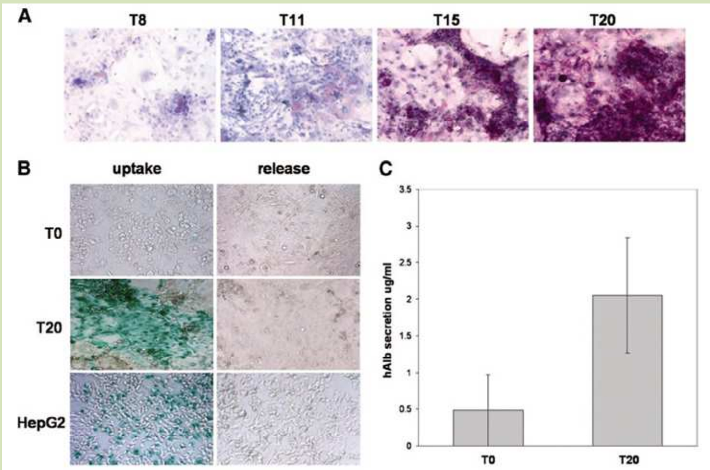

Human embryonic stem cell (hESC)-derived hepatic cells exhibit hepatocyte-like functions

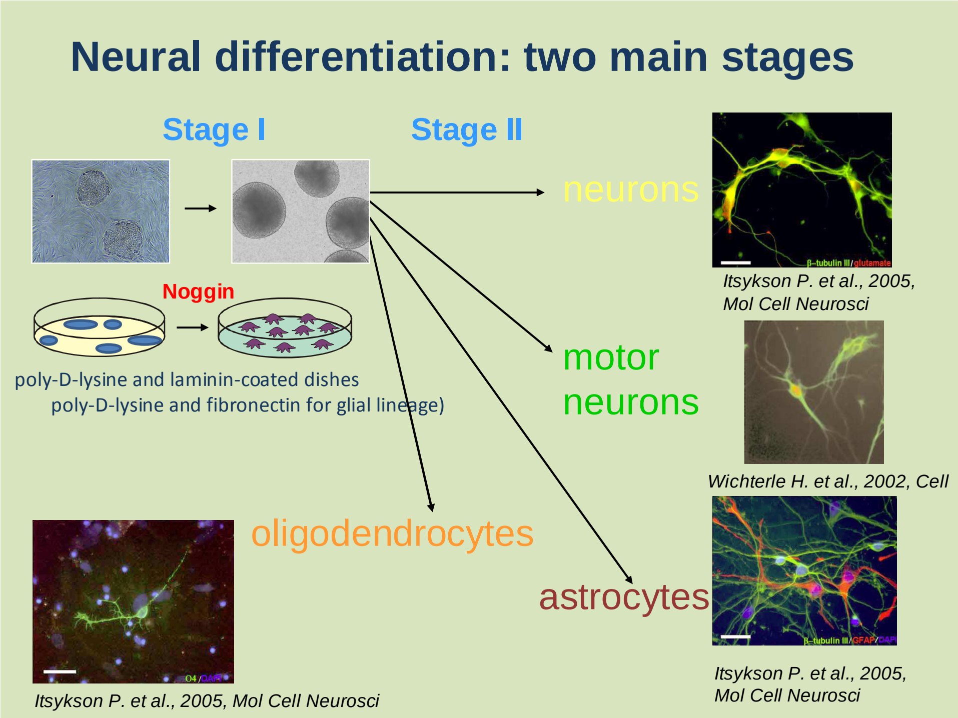
Neural differentiation: two main stages
Stage I
Stage II
Noggin
poly-D-lysine and laminin-coated dishes
poly-D-lysine and fibronectin for glial lineage)
neurons
Itsykson P. et al., 2005, Mol Cell Neurosci
motor neurons
Wichterle H. et al., 2002, Cell
oligodendrocytes
astrocytes
Itsykson P. et al., 2005, Mol Cell Neurosci
Itsykson P. et al., 2005, Mol Cell Neurosci

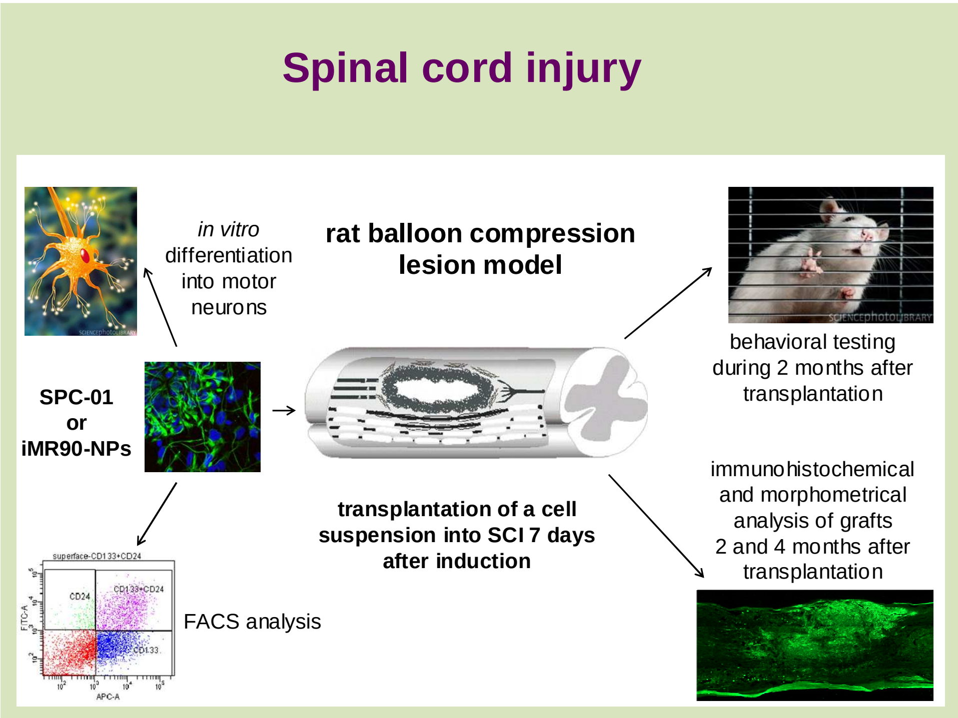
Spinal cord injury
in vitro differentiation into motor neurons
rat balloon compression lesion model
behavioral testing during 2 months after transplantation
SPC-01 or iMR90-NPs
transplantation of a cell suspension into SCI 7 days after induction
immunohistochemical and morphometrical analysis of grafts 2 and 4 months after transplantation
FACS analysis


Thank you for your attention!

Stabilization Principles of III-V Semiconductor Surfaces

O. Romanyuk
Institute of Physics, Academy of Sciences of the Czech Republic, Prague

Outline

III-V semiconductor reconstructions

- Surface reconstruction principles

Surface structure of GaSb

- Temperature effects

Surface structure analysis of GaN

- GaN(000-1) (1x1) structure analysis by LEED I-V curves
- Optical properties by REELS and DFT calculations

Biocompatibility of semiconductors

III-V compound semiconductors

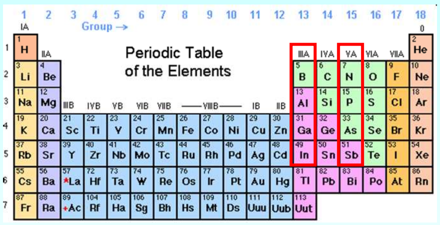

Zinc blende

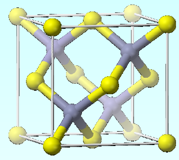

GaP, GaAs, GaSb...

Wurtzite

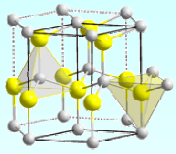

BN, AlN, GaN...

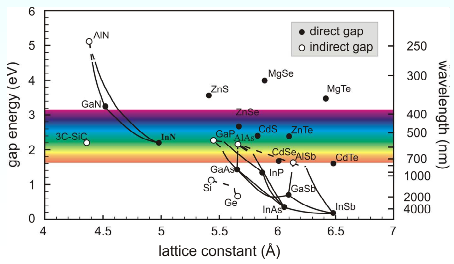

Lattice constants and optical properties vary for different III-Vs

III-V band gaps cover from infrared to unltraviolet wavelength

Varity of applications: LED, lasers, microelectronic devices, etc.

Zinc blende surfaces

[001]

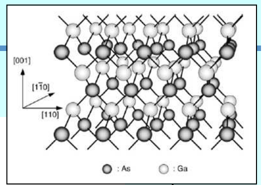

Crystal Faces

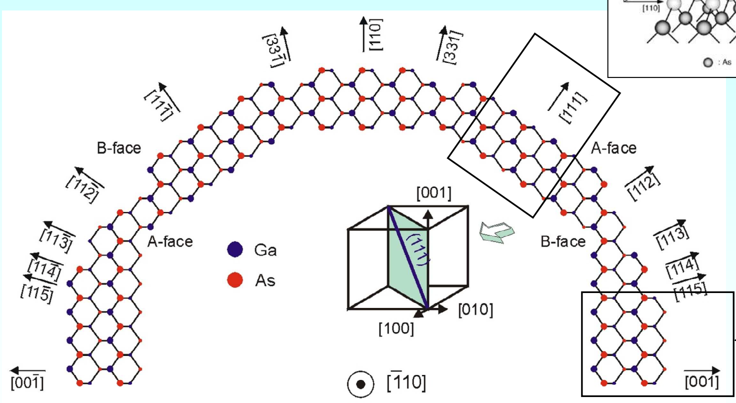

- Dangling bonds appear on truncated bulk crystal
- Surface energy is energy needed to cut bond to make a surface
- Surface energy is reduced by atomic rearrangement on a surface (re-bonding)

➡ Atomic reconstruction has electronic nature

STM images of GaAs surfaces

Scanning tunneling microscope image of GaAs(001)-(2x4) surface

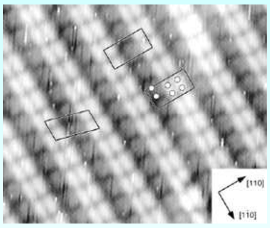

A. Ohtake / Surface Science Reports 63 (2008) 295–327

Structure model of GaAs(001)-(2x4) surface

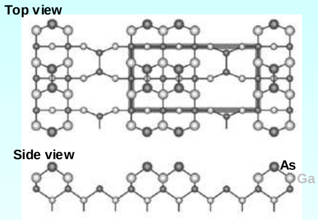

GaAs(001)-c(4x4) surface

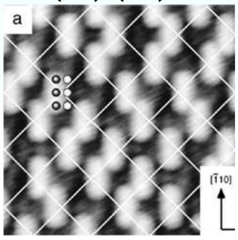

Structure model of GaAs(001)-c(4x4)-α

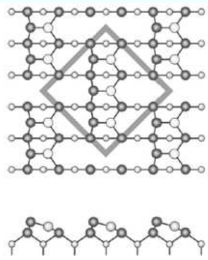

(d) Three Ga-As dimer (α) model.

Principles of surface reconstruction

Minimization of the surface free energy is a driving force of reconstruction

- The surface structure observed will be the lowest free-energy structure kinetically accessible under the preparation conditions.
- III-V surfaces tend to be autocompensated: accumulate no charge on a surface
- III-V surfaces tend to be semiconducting: to occupy VB states and empty CB states

=> Bonds do rehybridizate and on a surface within a few atomic layers.

Surface motifs for (001) face

dangling bonds

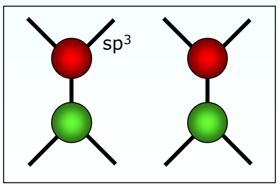

homodimers

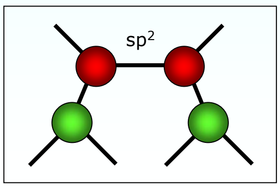

heterodimers

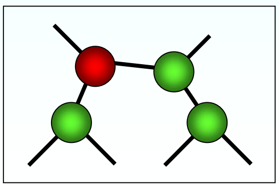

Electron counting model (ECM)

Electronic configuration of GaSb

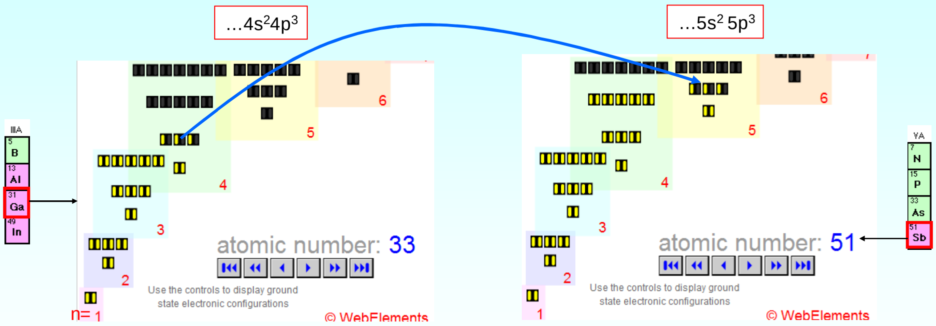

III-V covalent bond forms by sharing valence electrons:

3 electrons (III) and 5 electrons (V)

Electron counting

- There are 4 bonds per atom
- Group III elements – **cations**: 3/4 electrons per bond
- Group V elements – **anions**: 5/4 electrons per bond

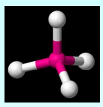

M.D. Pashley, PRB 40 (1989) 10418

ECM states:
Within a surface unit cell
Cation electronic states = anion states

	Partial Charge
Bond III-V	0
Bond III-III	-0.5
Bond V-V	0.5
DB III	0.75
DB V	-0.75

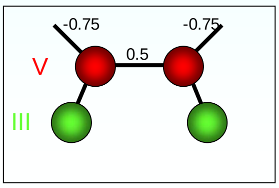

Partial charge counting: GaAs(001)-c(4x4)

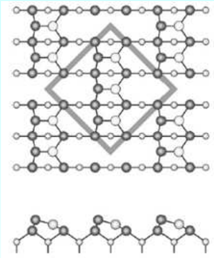
(d) Three Ga-As dimer (α) model

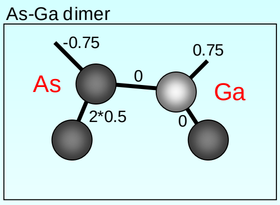

1 e

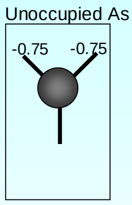

-1.5 e

	Partial Charge
Bond III-V	0
Bond III-III	-0.5
Bond V-V	0.5
DB III	0.75
DB V	-0.75

Structure consist of

3 dimes: 3*1 = 3
2 unocc. As: 2*(-1.5) = – 3

In total, 0 e

Outline

III-V semiconductor reconstructions

- Surface reconstruction principles

Surface structure analysis of GaSb

- Temperature effects

GaSb(111)A reconstructions

A. Proessdorf et. al., PRB 83, (2011) 155317

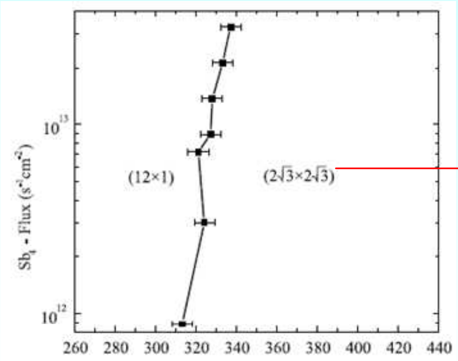

FIG. 5. Surface reconstruction phase-transition diagram for the GaSb(111)*A* surface with Sb_4 flux plotted vs substrate temperature measured by a thermocouple.

GaSb(111)*A* $(2\sqrt{3} \times 2\sqrt{3})$

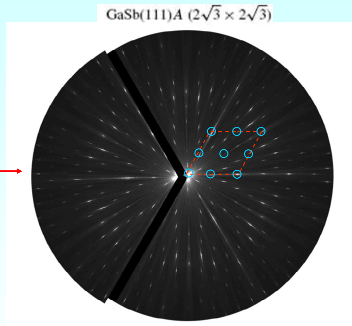

GaSb(111)*A* $(2\sqrt{3} \times 2\sqrt{3}) + (2 \times 2)$ reconstruction

GaSb(111)A structure models

Structure models

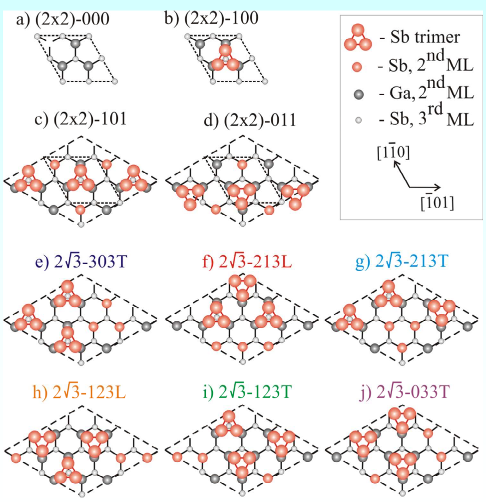

<u>Model building principles:</u>

- 2√3 unit cell size is fixed (from experiment).
- All models obey electron counting model (ECM)
  M.D. Pashley, PRB 40 (1989) 10418.
- Stoichiometry is varied: Sb-trimers, Sb substitution sites, Ga-vacancies.

Computational details

Total energy calculation within DFT

Local density approximation (LDA) for the exchange-correlation energy functional

Norm-conserving pseudopotentials, FHI-LDA

2√3 unit cell is used for all calculations

forces less than 10^{-4} Ha/Bohr

Surface formation energy

$$\Delta\gamma A = E_{tot} - (n_{Sb} - n_{Ga})\Delta\mu_{Sb} - n_{Sb}\mu_{GaSb}^{bulk}$$

$$-H_f < \mu_{Sb} - \mu_{Sb}^{bulk} < 0$$

E_{tot} - total energy of slab
n - number of atoms
μ - the chemical potential
H_f - the heat of formation

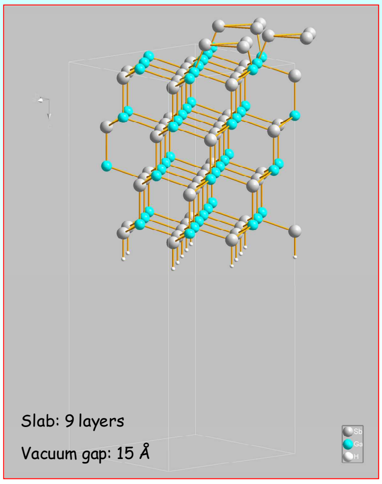

ABINIT code is used
www.abinit.org

Relative surface formation energy

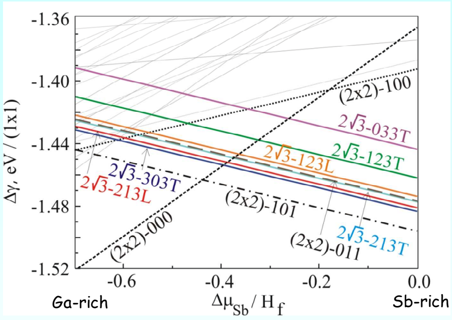

Stable structures

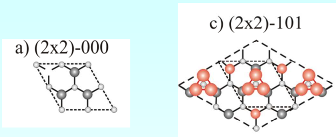

- (2x2) models are stable in ground state

- Energy of the 2√3 structures is higher (>12 meV/1x1)

Why a 2√3 diffraction pattern is observed for GaSb(111)A ?

Phase probability at elevated temperature

Partition function:

$$Z = \sum_i Z_i = \sum_i g_i \exp\left(-\frac{\Delta\gamma_i A}{k_B T}\right)$$

Degeneracy factor

$$g_i = f_i n_i m_i$$
$$f_i = \sigma_{(1\times1)}/\sigma_r$$

Phase concentration:

$$c_i = Z_i/Z, i \in S$$

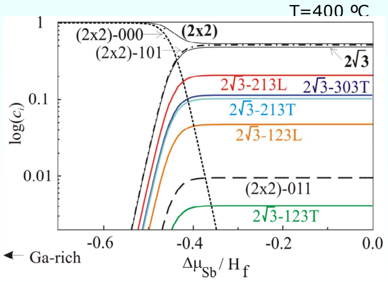

Total 2√3 concentration is about 30%

TABLE I: Symmetry-determined degeneracy factor g_i, two-dimensional space group number No., number of symmetry operations σ_r, and energy differences $\Delta\Gamma = \Delta\gamma_{101} - \Delta\gamma_i$ (meV/(1 × 1)) relative to the energy of the (2 × 2)-101 structure for the different structure models. Model notations refer to notations in Fig. 1.

Model	No. (σ_r)	g_i	$\Delta\Gamma$	Model	No. (σ_r)	g_i	$\Delta\Gamma$
c) (2 × 2)	14 (6)	4	0	f) $2\sqrt{3}$	3 (2)	36	15
d) (2 × 2)	14 (6)	4	19	g) $2\sqrt{3}$	3 (2)	36	18
e) $2\sqrt{3}$	15 (6)	12	12	h) $2\sqrt{3}$	3 (2)	36	22
j) $2\sqrt{3}$	15 (6)	12	52	i) $2\sqrt{3}$	3 (2)	36	34

***g* is higher for larger surface unit cells and with low symmetry**

Romanyuk et. al., PRB 82, (2010) 125315

Phase probability at elevated temperature

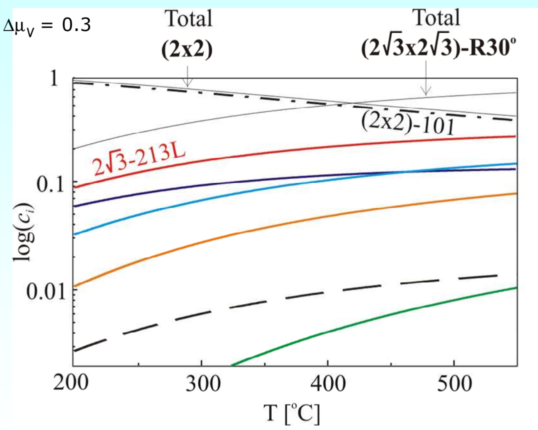

Romanyuk et. al., PRB 82, (2010) 125315

Experimental confirmation

- Temperature dependence of RHEED intensities is measured.
- cooling and heating with step 0.05° / sec at Sb-rich conditions
- 2√3 rod: (1/6, 1/6), (2/6, 2/6), (4/6, 4/6)
- (2x2)+2√3 rod: (3/6, 3/6)

I(2√3) / I(2x2 + 2√3)

(2x2) phase concentration decreases in comparison with 2√3 phase concentration

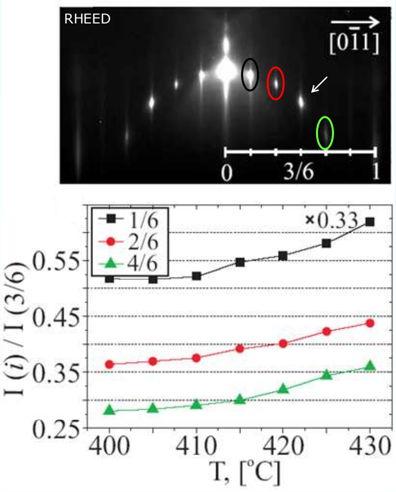

Romanyuk et. al., PRB 82, (2010) 125315

Entropic contributions

- Temperature effects

- GaSb(111)A 2√3 phases are stabilized by configurational entropy at elevated temperatures.
- Size and symmetry of the surface unit cell determine degeneracy factor *g*
- The larger unit cell with a lower symmetry is favored by the configurational entropy.

Outline

III-V semiconductor reconstructions

- Surface reconstruction principles

Surface structure analysis of GaSb

- Temperature effects

Surface structure analysis of GaN

Photoelectron spectroscopy laboratory

ADES 400 – photoelectron spectrometer with hemispherical analyzer

Equipment

- X-ray lamp XR50 (SPECS), XPS
- UV lamp UVL-Hi (VG Microtech), UPS
-electron gun EGG-3101 (Kimball Physics),
-EPES, REELS, LEED
- Ion gun: AG2 (VG Scientific), IQE 12/38 (SPECS)
- mass spectrometer, Prisma (Pfeiffer-Balzers)
- manipulator. x,y,z, polar and azimuth angles
- evaporation cell EFM 3 (Omicron)

GaN samples from Kyma

Wurtzite

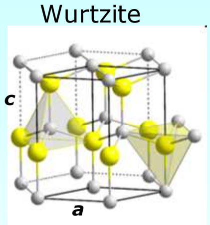

BN, AlN, GaN...

GaN is technologically important material for optoelectronics (LEDs, laser).

In-plane ***a*** and out-of-plane ***c*** lattice constants are different.

There is strong spontaneous polarization field due to differenct lengths of ionic covalent bonds. This decreases afficiency of the devices.

In zincblende crystals, all bond lengths and angles are similar -> total dipol moment vanishes.

Polarization field could be reduced for non-polar and semipolar GaN faces

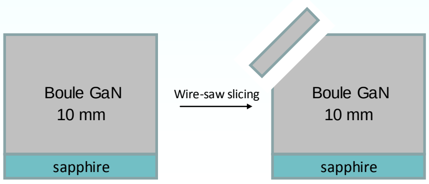

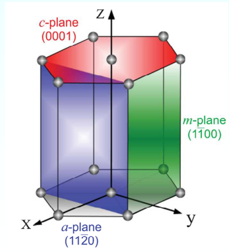

GaN nonpolar and semi-polar surfaces

Collaboration with Kyma Tech. (USA) in 2010-2011

Non-polar facets

Semipolar facets

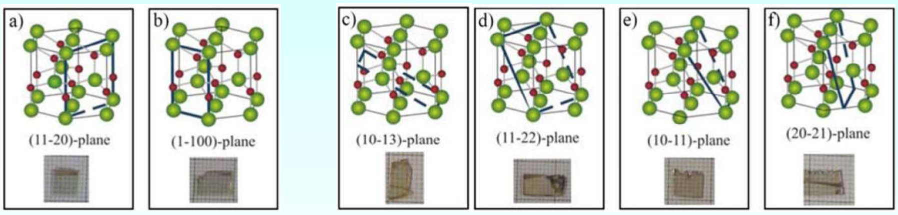

Angle-Resolving Electron Spectrometer (ADES-400)

Surface preparation: etching, ion sputtering, annealing

Surface analysis:
Quantitative LEED, REELS, UPS, XPS, PED

Theoretical support

Ab initio DFT
Band structures, DOS
PED, LEED intensities

Optical response:
dielectric function, optical constants

Quantitative LEED analysis of GaN(000-1)

GaN(000-1) – polar surface

- Crystal was chemically cleaned
- Annealed in NH_3 at 1000 °C, 10^{-7} Torr
- LEED intensity-voltage (I-V) curves were measured from 130 – 500 eV

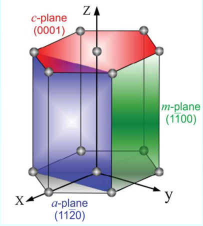

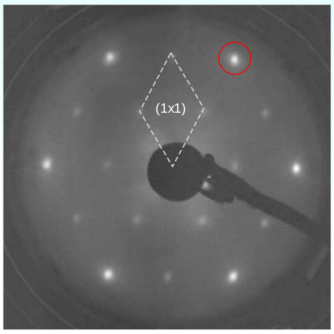

Structure models:

- The bare GaN(0001), (000-1) models
- Adlayer of N (Ga) on top of (0001) or (000-1) surface

Quantitative LEED analysis of GaN(000-1)

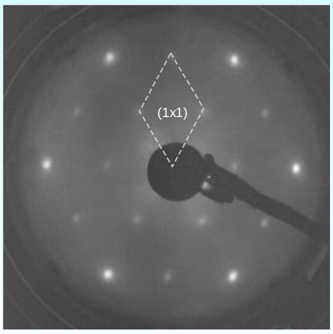

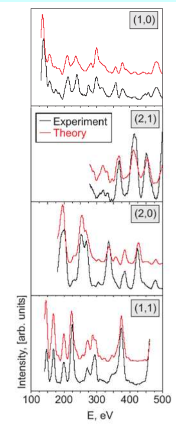

Structure violates ECM

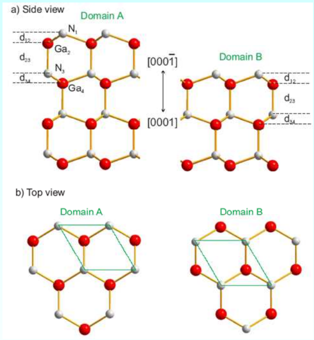

R_P reliability factors

Model	R_P	Model	R_P
$(000\bar{1})$	0.21 ± 0.04	(0001)	0.61 ± 0.10
$(000\bar{1})$-N	0.35 ± 0.06	(0001)-N	0.66 ± 0.11
$(000\bar{1})$-Ga	0.39 ± 0.07	(0001)-Ga	0.81 ± 0.14

Interlayer distances — Vibrational amplitudes

i,j	$d_{i,j}$, Å	Atom	u, Å
1,2	0.52 ± 0.11 (0.37)	N_s	0.20 ± 0.1
2,3	1.96 ± 0.04 (2.04)	Ga_s	0.14 ± 0.05
3,4	0.64 ± 0.03 (0.64)	N_b	0.11 ± 0.06
		Ga_b	0.10 ± 0.07

O. Romanyuk, et.al., Surf.Sci. (2012)

Electronic band structure of GaN(000-1) (1x1)

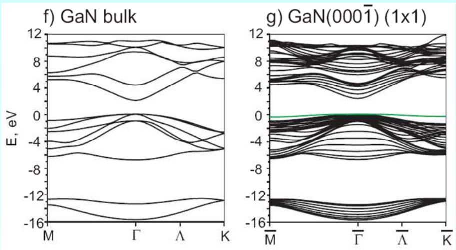

Density of states

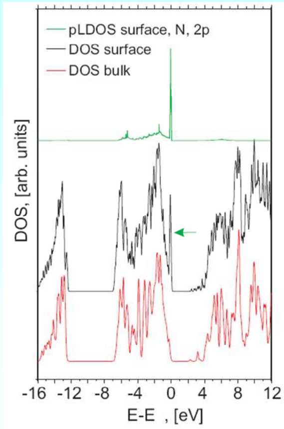

Surface state on a top of valence band is formed by N dangling bond

- DB occupation ¾ electrons / bond
- 2p orbital may be saturated by H
- LEED I-V is not sensitive to detect H
- To fulfill ECM, 2x2 cell is needed (3 H atoms and 1 N dangling bond)

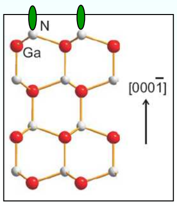

Optical properties measurements

REELS measurements

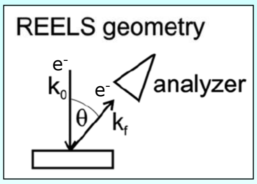

REELS spectra from GaN(000-1) (1x1)

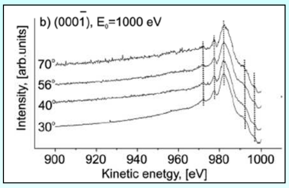

Dielectric function by DFT

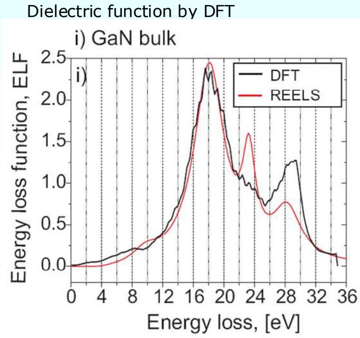

Optical constants by REELS: (000-1), (10-13), disord. GaN

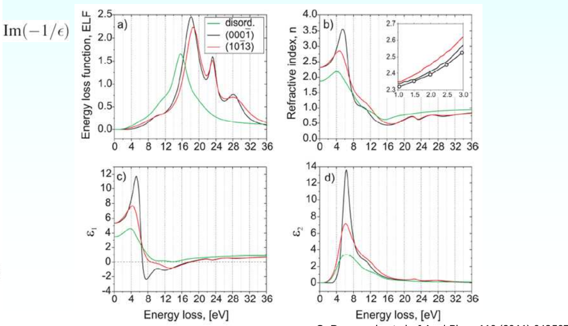

O. Romanyuk, et.al., J.Appl.Phys. 110 (2011) 043507

Outline

III-V semiconductor reconstructions

- Surface reconstruction principles

Surface structure analysis of GaSb

- Temperature effects

Surface structure analysis of GaN

Biocompatibility of semiconductors

Biocompatibility of semiconductors. Literature review

Goals:

- Control over physiological activities in the body by chips
- To find biocompatible materials with a potential to interact with biological systems on molecular scale
- Biocompatible electrodes are required
- Biocompatibility -> long term implants
- To implement signal transmission between microelectronics and biological systems

Analogies with biological systems:

- Electrical circuit in material word -> neural network in biological systems
- Neural cells are electroactive -> potentially could be interacted and governed by chips

Biocompatibility of semiconductors. Literature review

Neuronal transistor in gloved hand

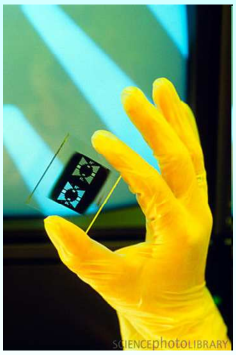

This chip contains the first two-way communication link to be established between a living nerve cell and a silicon chip. The breakthrough, made by German biophysicist **Peter Fromherz (Max Planck Ins. of Biochem.)**, in 1995. No electric current flows across the junction. Instead, the chip induces a charge inside the cell, which makes it "fire".

Neuron silicon chip.

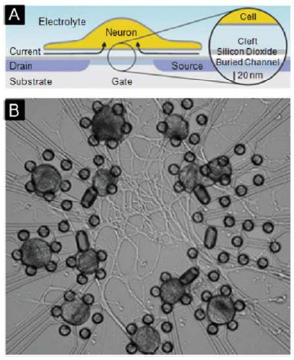

Y. Cui, et.al, Science 2001, 293, 1289

Adv. Mater. **2009**, *21*, 3970–4004

Si wafers Literature review

Si is toxic for biological systems and surfaces need to be biofunctionalized to promote a cell adhesion

Coating the surface with bioactive molecules such as polylysin or laminin, plasma treatment.

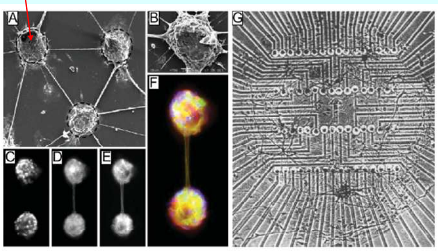

Figure 9. A) A SEM image of an engineered neural network. The dashed circles mark the polylysine islands used to define the network. B) Each of the cell clusters contains hundreds of cells and extends between 1 and 8 bundles. C–F) Multiple staining of two interconnected clusters. C) DAPI, cell nuclei. D) NFM, the bundle connecting them is composed of axons and dendrites. E) MAP2, neurons. F) red, axons; green, dendrites; blue, cell body. The yellow color arises from coincidence of green and red fluorescence (from [336]). G) Neuronal network made from 76 neurons growing on the matrix of standard 64 electrodes. Adapted with permission from [377b]. Copyright 1994, Academic Press.

Adv. Mater. **2009**, *21*, 3970–4004

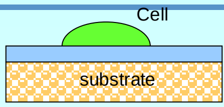

interface

Types of interaction with cells:

- Electrical: current, contacts
- Optical: photostimulation by light

[203] T. C. Pappas, W. M. S. Wickramanyake, E. Jan, M. Motamedi, M. Brodwick, N. A. Kotov, *Nano Lett.* **2007**, *7*, 513.

Light-induced action potentials

↓

GaN

↙ Lasers ↘ LED

GaN wafers
Literature review

ARTICLE IN PRESS

Gallium nitride is biocompatible and non-toxic before and after functionalization with peptides

Scott A. Jewett[a,1], Matthew S. Makowski[a,b,1], Benjamin Andrews[c], Michael J. Manfra[d], Albena Ivanisevic[e,*]

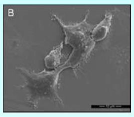

Biomaterials

Assessment of GaN chips for culturing cerebellar granule neurons

Tai-Horng Young*, Chi-Ruei Chen

Biomaterials 27 (2006) 3361–3367

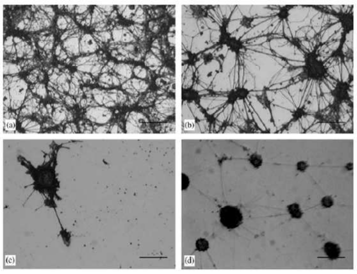

Fig. 3. Photomicrographs of cerebellar granule neurons cultured on (a) n-type GaN, (b) p-type GaN, (c) Si and (d) TCPS after 6 days in culture (scale bar = 100 μm).

Neurons networks were found more dense on GaN that on Si substrates

GaN substrate is more suitable for cell growth than Si

Variety of the GaN samples on a desk

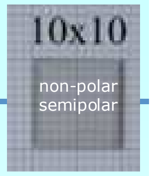

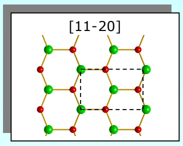

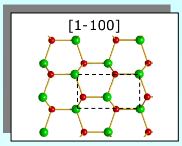

- Surface atomic structure study
- Electronic structure study

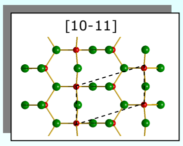

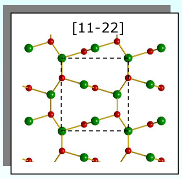

Potential substrates for optoelectronic devices with high efficiency

- Surface functionalization mechanism study on a microscopic level

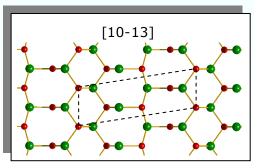

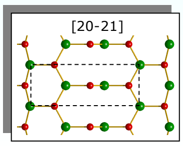

- Absorption O, H, NH_x molecules
- Absorption organic molecules (glycin: $C_2H_5NO_2$) as a part of **biocompatibility** research

Conclusions

- The surface structure observed will be the lowest free-energy structure kinetically accessible under the preparation conditions.
- Surface structure of III-V semiconductors (zincblende) obey ECM: number of anion electronic states have to be equil to the number of cation electronic states.
- Configurational entropy play a crucial role espessially for the phases with a small energy difference but with different unit cell size. The larger unit cell with a lower symmetry is favored by the configurational entropy.
- Polar GaN(000-1) was studied by LEED I-V curves technique and DFT calculations. We determined a surface polarity, atomic structure and optical properties of the GaN surface.
- GaN is perspective semiconductor for biological applications. Non-polar and semipolar surfaces provide variety of structural properties that have to be analyzed in the nearest future.

Acknowledgments

P. Jiříček, J. Zemek

Institute of Physics, ASCR, Prague

F. Grosse, A. Proessdorf, V. Kaganer, W. Braun

Paul-Drude-Institut für Festkörperelektronik, Berlin, Germany

T. Paskova

The North Carolina Univ., USA

Measurement of the magnetic hysteresis and Barkhausen noice at controlable magnetic conditions

Oleksandr Stupakov

Institute of Physics ASCR, Na Slovance 2, Prague, Czech republic

Magnetic measurements

B/M = *f* (H)

Inductive method – $dH/dt \neq 0$

Faraday's law:

$U_{ind} = -n \cdot d\Phi/dt = -nS \cdot dB/dt$

n is number of induction windings,
Φ is magnetic flux,
S is sample cross-section,
B is magnetic induction

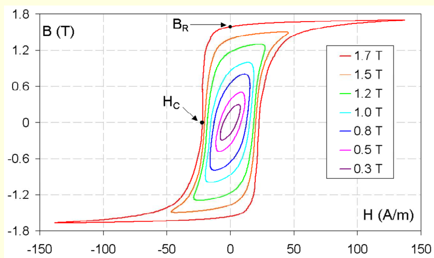

Magnetic field determination

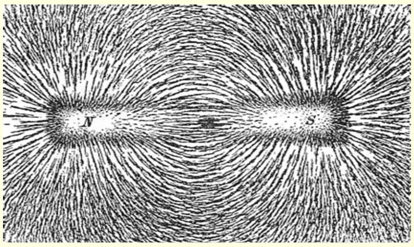

Technical way –

current field method

$$H_i = NI/l_m$$

N is number of magnetizing windings,
I is magnetization current,
l_m is effective magnetic path

- demagnetization factor × M

Electrical steels

are the most important magnetic materials produced today (efficient flux multipliers).

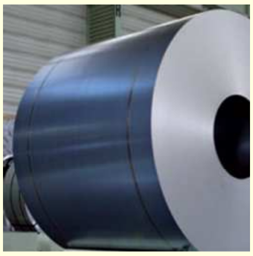

• **Grain oriented (GO) steels -** 3% Si-Fe alloys with grain orientation and very low power loss and high permeability in rolling direction (high anisotropy – transformers).

• **Non-oriented (NO) steels -** have similar magnetic properties in all directions (motors, generators, alternators, ballasts, small transformers)

Electrical steels

- **Norman P. Goss** (1906–77), inventor and researcher from Ohio, USA, in 1935 he patented a heat treatment method to obtain grain-oriented electrical steel ⇒ protected technology
- **Lamination coating** ⇒ to increase electrical resistance between laminations, reducing eddy currents, to provide resistance to corrosion ⇒ introduced stress improves the magnetic properties.
- **Laser scribing, amorphous/nanocrystalline ribbon**
- **50 Hz sinusoidal magnetization, hysteresis loss**

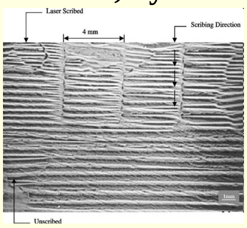

Standard techniques

Single Sheet Tester (SST)

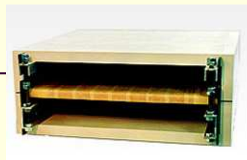

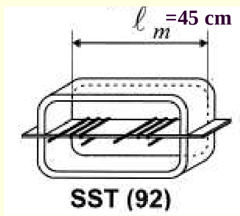

Epstein

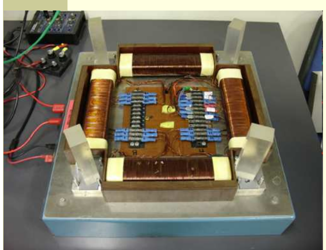

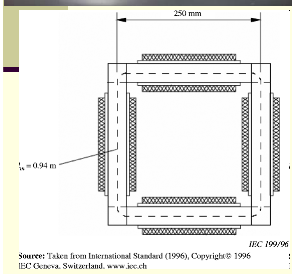

1) Epstein frame: > century old, high accuracy ⇔ expensive, time consuming
2) Single Sheet Tester: EU initiative to simplify the technique ⇔ no exact coincidence but good linear correlation with Epstein data ⇒ different "design" sources of field determination error

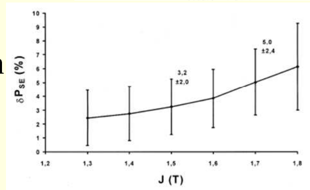

Fig. 3. Mean values of relative differences δP_{SE} of all measurements, averaged for each polarization; with σ_1 bars, numbers at the bars: values $\delta P_{SE} \pm \sigma_1$ at 1.5 T and at 1.7 T

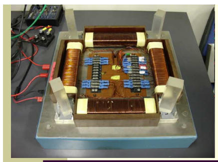

Standard techniques

Cumbersome quasi-closed circuits of both standard instruments are required for high repeatability of the results (measurement error is 2–3%, bad contact can lead to 5-10% error): they keep

• the induction waveform of the sinusoidal shape in accordance with standard requirement and application conditions

• the current field method valid (field is proportional to current)

<u>Problems:</u>

• Different ‘‘design’’ sources of field determination error ⇒ No exact match between Epstein and SST data ⇒ slow replacement of the outdated Epstein with SST in practice.

• Standard procedures cannot be adapted for continuous online testing on a production line.

SST with H-coil

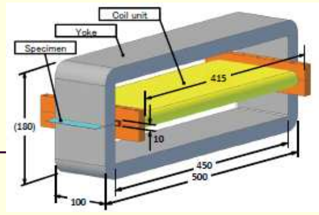

Tangential field sensor (flat H-coil sensor)

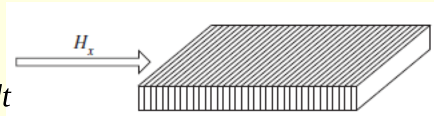

$$U_{ind} = -n \cdot d\Phi/dt = -nS\mu_0 \cdot dH/dt$$

• 0.5x25x25 mm, 400 turns of ∅ 0.05 mm wire ⇒ sensitivity of ~3 μV $(A/m)^{-1}$

• complexity of preparation and calibration

• large size

• accurate integration of a weak induced voltage

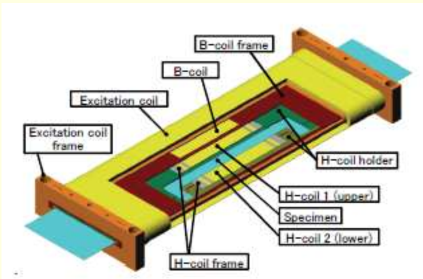

Compensation field method

Rogowski–Chattock potentiometer evaluates a magnitude of the magnetization imperfection ⇒ An analog feedback loop supplies a correction current to additional magnetization coils in order to minimize the potentiometer signal ⇒ It adjusts the magnetization process to the ideal condition of the closed magnetic circuit, when the current field method can be applied

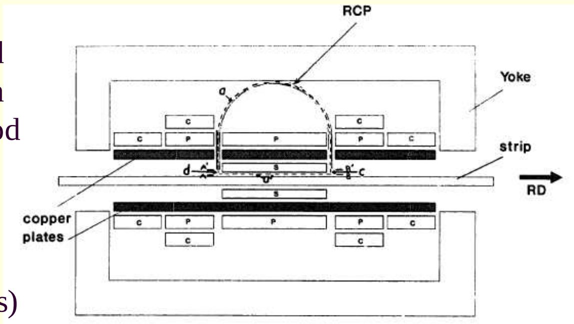

(Czech Technical University, Prof. V.Havlíček, end of 80s)

Portable SST

Rotational SST

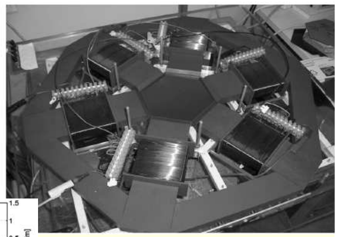

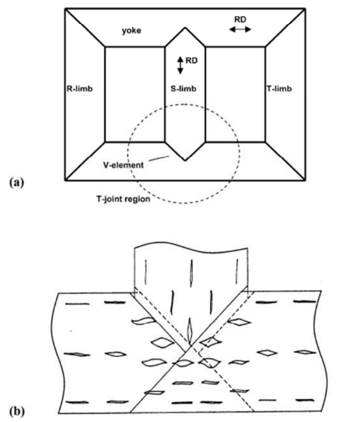

Fig. 2. T-joint which is the core region that is most affected by rotational magnetization. (a) Typical global core geometry. (b) Detail of T-joint region with distribution of induction patterns $B(t)$ as determined on the model core (from [26]).

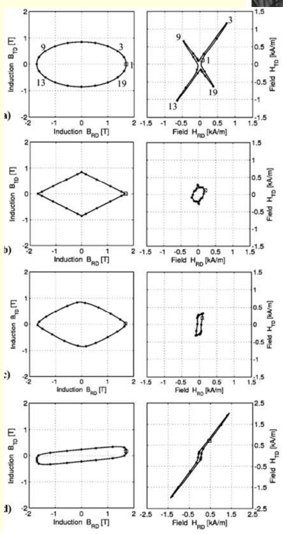

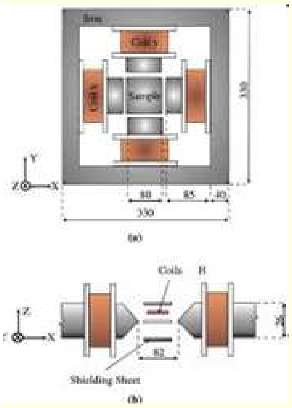

Barkhausen noise (BN)

Discovered by German physicist Heinrich Barkhausen in 1919 ⇒ loudspeaker connected to the induction coil showed acoustic noise ⇒ first experimental verification of ferromagnetic domains postulated theoretically (discrete irreversible changes of magnetic moments)

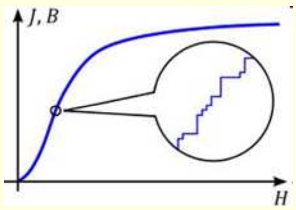

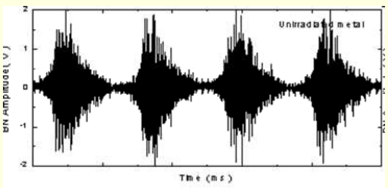

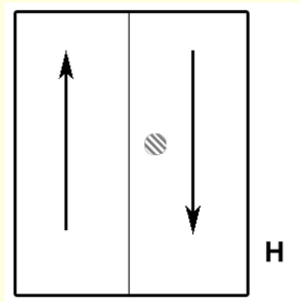

Introduction: drawbacks of BN

- Main problem is high instability of BN technique with respect to experimental conditions / parameters and sensor unit design.
  ↳ this problem is usually solved in a technical way: the measurement system is adapted to a certain industrial task to provide relatively stable results for a specific experimental configuration.
- ↳ There is a lack of general understanding and interpretation of the BN effect ⇒ physical research should be done?

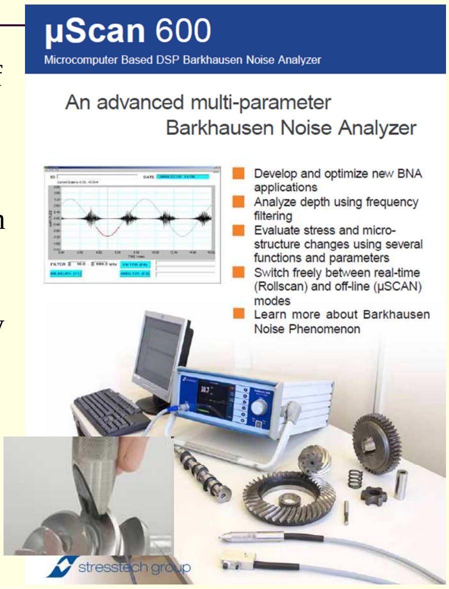

Introduction: nature of BN

- BN is assumed to provide a complex *surface* micro-magnetic response
- and to contain more information than macroscopic hysteresis data
  ↳ the challenge is to read and to interpret the micro-magnetic BN data
- ⇒BN is of stochastic nature so only the average properties are reproducible
- ⇒BN provides qualitatively similar response to magnetic hysteresis measurements, but level of the BN signal is not normalized to any physically based value, such as a magnetic induction.

Hysteresis measurements

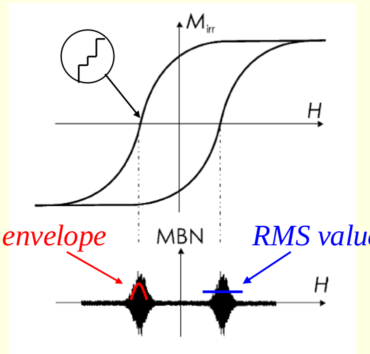

Barkhausen noise measurements

Experiment

- Surface field measurement – extrapolation of tangential field profile *($H_i \sim I$, H_{sur}, H_{ext}; field shielding)*
- Magnetization condition control (induction waveform for hysteresis testing, surface field – BN)
- Three stage control: B_{max} amplitude, H_{max} symmetry and the B(t)/H(t) waveform.
- BN surface pancake coil

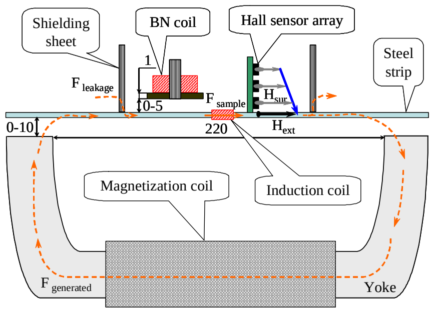

Scheme of measurement setup (shown sizes are in mm).

Digital feedback for B(t) control

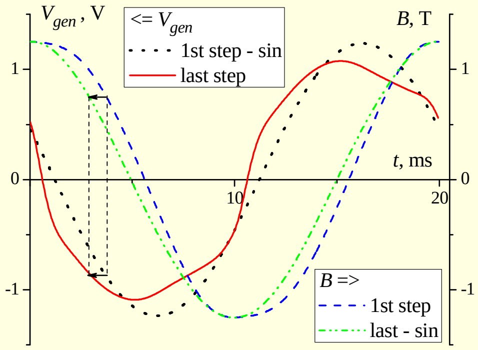

Magnetization voltages V_{gen} (left axis) and measured magnetic inductions B (right axis) at the first and the last iteration steps of the digital feedback algorithm, respectively.Principle of the V_{gen} re-sampling isillustrated by arrows (electrical steel).

Digital feedback for B(t) control

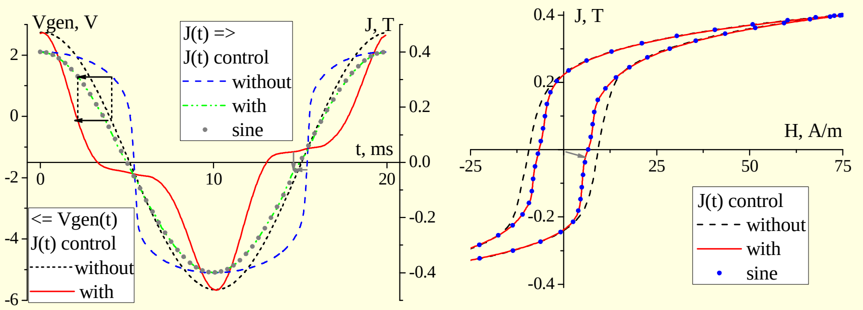

(Left) Same waveforms of $V_{gen}(t)$ (left axis) and magnetization J(t) (right axis) for the measurements of amorphous ribbon in solenoid. (Right) The corresponding hysteresis loops measured with and without the J(t) waveform control.

Stability with air gap

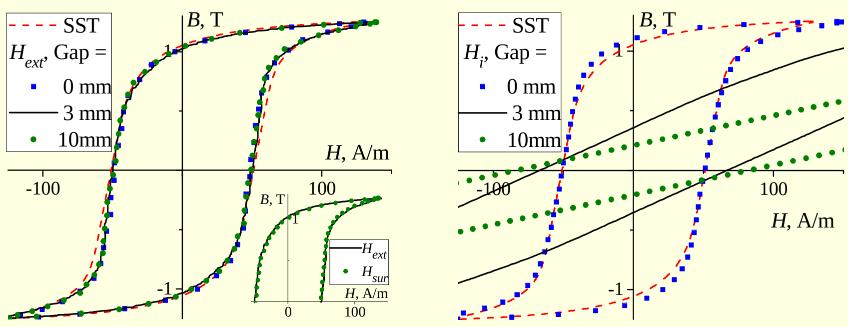

Typical hysteresis loops of a NO steel measured by the standard SST and the single-yoke setup with different air gaps as functions of the extrapolated H_{ext} (left figure) and the current H_i (right figure) fields. The inset shows the $B(H_{ext})$ and $B(H_{sur})$ loops.

Stability with air gap

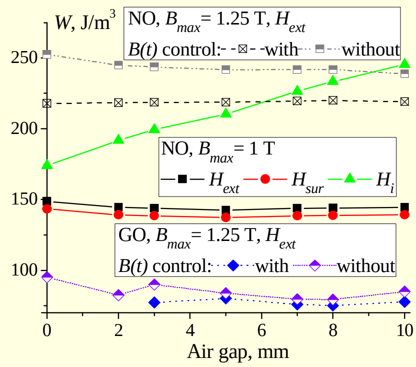

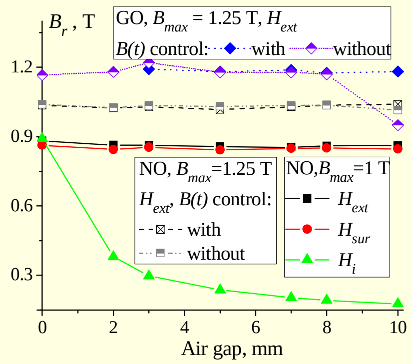

Stability of the hysteresis loss W (left figure) and the remanent induction B_r (right figure) with the air gap for typical NO and GO steels and different experimental conditions.

Correlations with SST

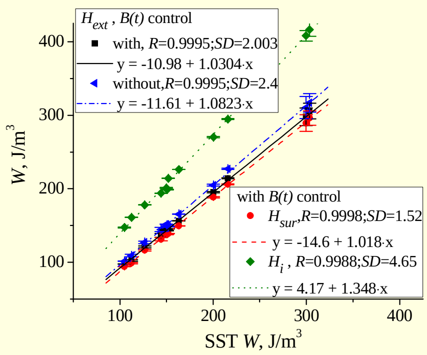

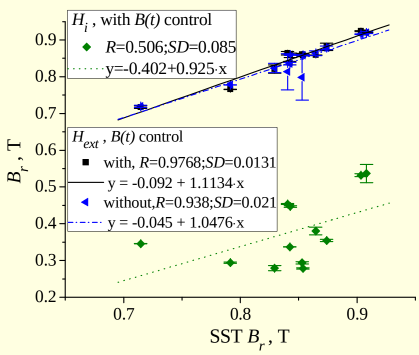

Relations of the hysteresis loss W (left figure) and the remanent induction B_r (right figure) with the correspondent SST parameters for the NO steels and B_{max} = 1 T. The error bars are evaluated as the standard error of two identical tests from the opposite sample sides.

Correlations with SST

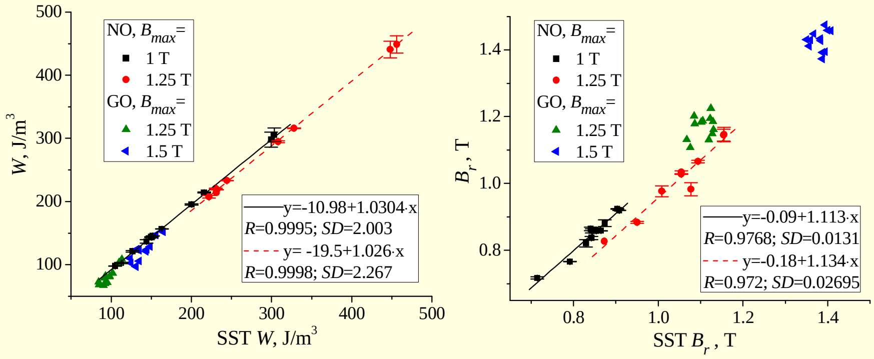

Relations of the hysteresis loss W (left figure) and the remanent induction B_r (right figure) with the corresponding SST parameters for both steel series and induction amplitudes B_{max}. The curves are shown for the H_{ext} field method with the B(t) waveform control.

BN coil lift-off

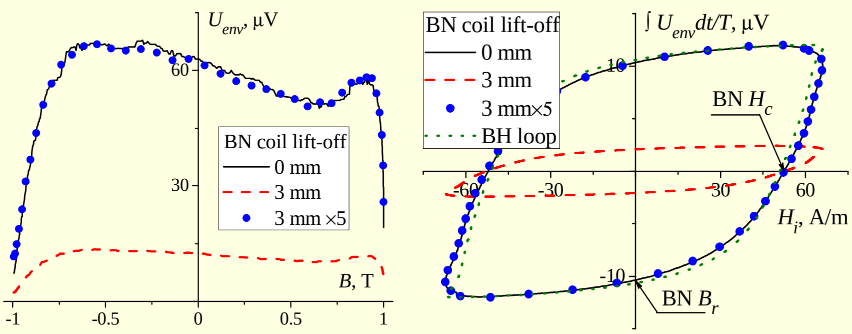

Left: Typical BN envelopes of a NO steel versus the magnetic induction B. The circular symbols present the data for the 3 mm lift-off scaled up to 5 times. Right: The corresponding BN loops (time integrals of the BN envelope) versus H_i. The hysteresis loop with normalized induction axis is also shown for comparison.

BN coil lift-off, yoke gap

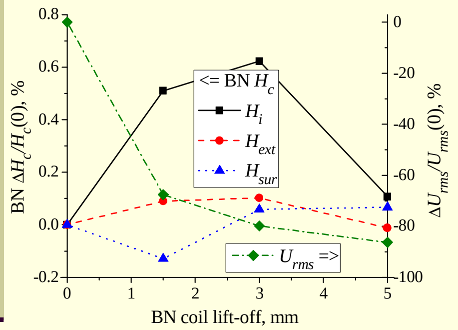

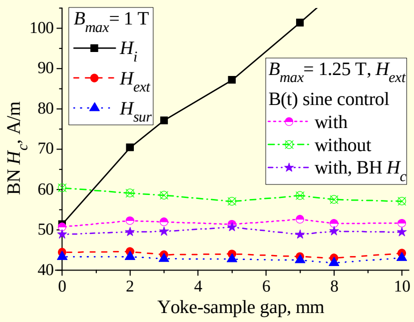

Left: Normalized relative changes of BN H_c (left scale) and BN rms values, U_{rms}, (right scale) with BN coil lift-off. Right: Variations of BN H_c with the gap between the yoke and the sample.

BN H_c ⇔ BH H_c-W correlations

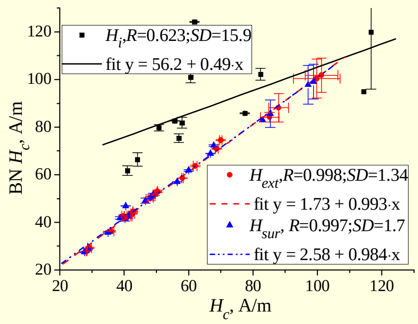

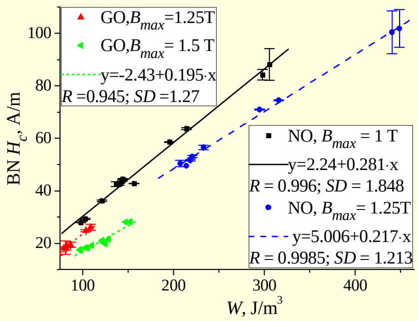

Relations of BN H_c with the hysteresis coercivity H_c (left fig.) and losses W (right fig.) measured in the single yoke configuration. In the left fig. the data for the NO steels and three field methods are shown; in the right fig. the H_{ext} data are shown for the both steels and B_{max}.

BN $H_c \Leftrightarrow$ BH H_c-W correlations

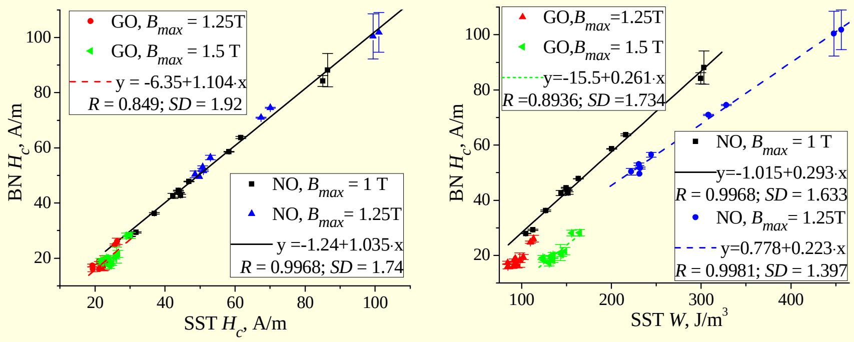

Relations of BN H_c with the SST coercive force H_c (left figure) and the SST hysteresis losses W (right figure). The H_{ext} field data are shown for the NO and the GO steels measured at the different B_{max}.

Conclusions

- The physically based measurements with control of the induction waveform and simultaneous direct determination of the magnetic field provide stable results with an acceptable linear correlation to the standard SST data.
- Simultaneous *local* measurements of surface field and BN signal stabilize the BN coercivity. It shows high stability to variations of the experimental conditions and strong linear correlations to the hysteresis coercive force and losses.
- Practical implementation requires a low-noise field sensor with the sensitive area up to several cm in size.
- The linear correlation with SST data is non perfect: the slopes are close to unit, but the offsets are non-zero and dependent on the tested magnetic parameter and the induction amplitude.

Acknowledgments

Thank You for Your attention

The author appreciates the financial support of the Czech Science Foundation (GACR) under the postdoctoral project no. 102/09/P108.

Contact: stupak@fzu.cz, http://www.fzu.cz/~stupak

PHOTONIC STRUCTURES AND THEIR PREPARATION

M. Varga[1, 2], L. Ondič[1, 3], K. Hruška[1], J. Potměšil[1], J. Libertínová[1], A. Kromka[1], Z. Remeš[1]
[1]*Institute of Physics of the ASCR,v.v.i., Cukrovarnicka 10, Praha 6, 16253, Czech Republic*
[2]*Institute of Electronics and Photonics, FEI STU, Ilkovičova 3, SK-812 19 Bratislava*
[3]*Faculty of Mathematics and Physics, Charles University, Ke Karlovu 3, 121 16 Prague 2, Czech Republic*

Abstract

Photonic crystals are periodically structured electromagnetic media, generally possessing photonic band gaps: ranges of frequency in which light cannot propagate through the structure. This periodicity, which length scale is proportional to the wavelength of light in the band gap, is the electromagnetic analogue of a crystalline atomic lattice, where the latter acts on the electron wavefunction to produce the familiar band gaps of semiconductors, and so on, in solid-state physics [1]. Several examples of organisms and structures possessing photonic crystals and iridescence are visible all around us (Morpho didius, Pavo cristatus, Chrysochroa vittata, Chrysina resplendens, …) [2].

Photonic crystals are attractive optical materials for controlling and manipulating the flow of light. One dimensional photonic crystals are already in widespread use in the form of thin film optics with applications ranging from low and high reflection coatings on lenses and mirrors to color changing paints and inks. Higher dimensional photonic crystals are of great interest for both fundamental and applied research, and the two dimensional ones are beginning to find commercial applications. The first commercial products involving two-dimensionally periodic photonic crystals are already available in the form of photonic crystal fibers, which use a microscale structure to confine light with radically different characteristics compared to conventional optical fiber for applications in nonlinear devices and guiding exotic wavelengths. The three-dimensional counterparts are still far from commercialization but offer additional features possibly leading to new device concepts (e.g. optical computers), when some technological aspects such as manufacturability and principal difficulties such as disorder are under control [3]. In 1996, Thomas Krauss made the first demonstration of a two-dimensional photonic crystal at optical wavelengths (800–900 nm) [4].

Present contribution deals with the preparation of two-dimensional photonic crystal (2D-PhC) on a nanocrystalline diamond film [5]. Diamond is a material with excellent optical properties and therefore its applicability in photonics can be expected [6]. In addition diamond-based materials exhibit an unique combination of physical properties, such as extreme hardness, high acoustic velocity, high breakdown field, high thermal conductivity, and many others [7]. Hence diamond can support high optical power and high electrical current and can serve as a matrix for various light sources, such as quantum dots. The photoluminescence efficiency of the embedded light source can be enhanced by periodical nanopatterning of diamond layer if the PhC dimensions are carefully modeled.

Modeling of the photonic crystals dimensions was done by RSoft DiffractMOD software. The NCD films were grown by microwave plasma-assisted chemical vapor deposition (CVD) using an ellipsoidal cavity resonator (Aixtron P6, GmbH). Before the CVD growth, high quality quartz substrates (UQG, Ultrasil, 10x10x1 mm^3) were cleaned in isopropyl alcohol and dried by a nitrogen gun. Then, they were seeded in a liquid suspension of ultradispersed detonation diamond (UDD) powder with an average size of *ca*. 5-10 nm in diameter (NanoAmando, New Metals and Chemicals Corp. Ltd., Kyobashi) using an ultrasonic treatment procedure for 40 min. The NCD films were grown in hydrogen (99%) and methane (1%) based gas mixture. The CVD process parameters were as follows:

microwave power 2.5 kW, total gas pressure 50 mbar and the substrate temperature 570 °C. 2D-PhC was fabricated as follows: the NCD films were coated with electron sensitive polymer (PMMA, 100-120 nm in thickness). The PMMA polymer was nanopatterned by electron beam lithography (EBL) using "*e*-LiNE system" (Raith GmbH) forming the base matrix with regularly repeated openings ordered into a square lattice with a various lattice constants. Then, Au layer of 70 nm thickness was evaporated and processed by lift-off strategy to form a masking matrix. Plasma etching by using capacitively coupled RF-plasma in a CF_4/O_2 gas mixture (Phantom LT RIE System, Trion Technology) led to formation of geometrically ordered nanopillars (PhC structure) with the surface area of 1x1 mm^2.

The diamond character of films was investigated by Renishaw InVia Reflex Raman spectrometer with the excitation wavelength 442 nm. The surface morphology and grain size of deposited diamond films were investigated by scanning electron microscopy (SEM, e_LiNE writer, Raith GmbH). Atomic force microscopy (AFM) images were taken in tapping mode using silicon tip Multi75Al. The film thickness was evaluated from the interference fringes in the reflectance spectra measured in visible and near infrared region using the IR-Plan Advantage Spectra-Tech microscope (space resolution 100μm) equipped with 20W tungsten halogen lamp as a light source, BWTEK BTC112E TE Cooled CCD array spectrometer (spectral range 400 – 1000 nm) and a commercial software for modeling the optical properties of thin films (FilmWizard).

Photonic properties of the PhC sample were probed by illuminating the PhC along the Γ-X direction with the collimated white light incident at the angle varying from 0 to 25° where 0 is the angle normal to the sample plane. The transmitted light was then collected by an optical fiber. The incident light interacts with the periodicity and in case the phase-matching condition is fulfilled it can couple into the leaky modes of the PhC which is revealed in the transmission spectra by the deep minima at the spectral positions of leaky modes. The photonic band diagrams of leaky modes shown for the S- and P-polarized light were created by converting the angle-resolved transmission spectra into a 2D map of transmission efficiency. Photonic bands can be clearly recognized originating at the Γ-point at different wavelengths which depends on the dimensions of the PhC. The agreement of the experiment with a simulation was verified.

In summary we described the preparation of diamond-based PhC structures and showed that by engineering dimensions of the PhC the spectral position of the resonances can be tuned.

Acknowledgement: This work was supported by the grants P108/11/0794, GAAV (Grant No. KJB100100903), MSMT LH12236 and Purkyne Fellowship. This work was carried out in frame of the LNSM infrastructure.

[1] http://ab-initio.mit.edu/photons/tutorial/photonic-intro.pdf
[2] http://www.viewsfromscience.com/documents/webpages/natural_photonics_p1.html
[3] http://en.wikipedia.org/wiki/Photonic_crystal
[4] T. F. Krauss, R. M. DeLaRue, S. Brand, *Nature 383 (6602)*, (1996), pp. 699–702
[5] L. Ondič, K. Dohnalová, M. Ledinský, A. Kromka, O. Babchenko, B. Rezek, *ACS Nano 5*, (2011), pp. 346-350
[6] I. Aharonovich, A.D. Greentree, S. Prawer, *Nature Photonics* 5, (2011), pp. 397–405
[7] C. E. Nebel, *Nat. Mater. 2*, (2003), pp. 431–432

Photonic structures and their preparation

M. Varga[1, 2], L. Ondič[1, 3], K. Hruška[1], J. Potměšil[1], J. Libertínová[1], A. Kromka[1], Z. Remeš[1]

[1]Institute of Physics of the ASCR,v.v.i., Cukrovarnicka 10, Praha 6, 16253, Czech Republic
[2]Institute of Electronics and Photonics, FEI STU, Ilkovičova 3, SK-812 19 Bratislava
[3]Faculty of Mathematics and Physics, Charles University, Ke Karlovu 3, 121 16 Prague 2, Czech Republic

varga@fzu.cz

Content

1. Introduction
   - photonic structures in nature
   - photonic structures in technology
   - requirements for photonic crystals

2. Experimental part
   - diamond film deposition
   - sample characterization
   - sample preparation - Electron Beam Lithography
     - metal evaporation – masking matrix
     - plasma etching process

3. Results
   - PhC transmission

4. Summary

Photonic structures in nature

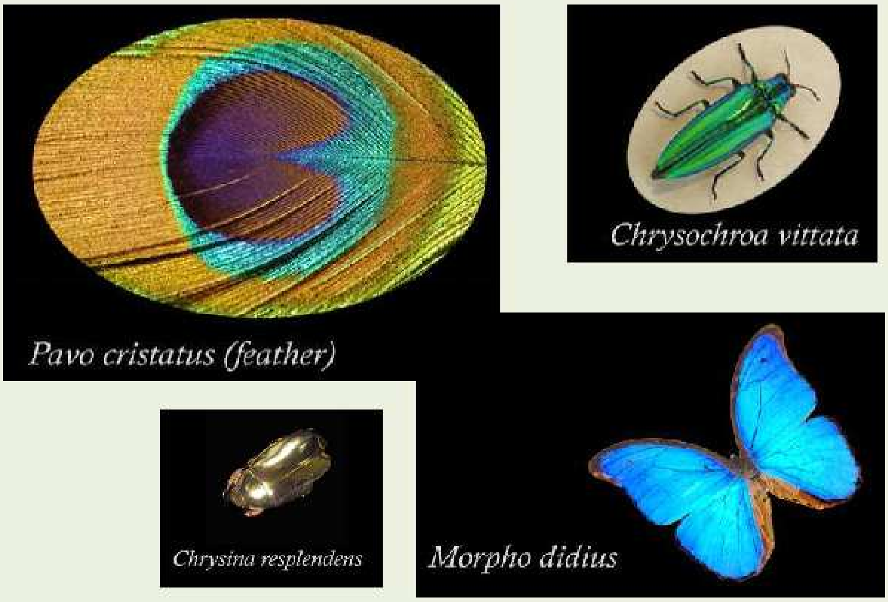

http://www.viewsfromscience.com/documents/webpages/natural_photonics_p1.html

Photonic structures in technology

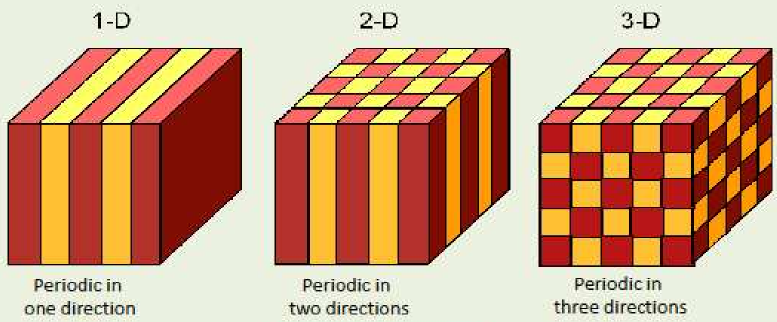

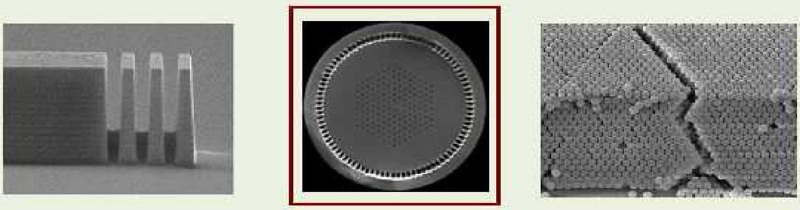

Bragg reflectors

2D photonic crystals
& Ph. Crystal fibres

Silica crystals

Requirements for photonic crystals

SET 1

	A	B	C
h (nm)	137	137	137
d (nm)	206	206	206
a (nm)	343	343	343
wh (nm)	40	60	120

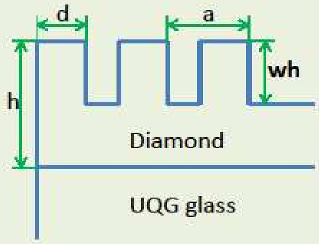

SET 2

	A	B	C
h (nm)	165	165	155
d (nm)	200	200	200
a (nm)	390	330	345
wh (nm)	100	100	55

h – diamond layer thickness
a - lattice constant
d - diameter of nanopillar
wh – nanopillar height

Diamond film deposition

Deposition conditions – AIXTRON P6

Substrate	Time (min)	Pressure (mbar)	H_2 (sccm)	CH_4 (sccm)	Ratio H_2:CH_4 (%)	Power (W)	Temperature (°C)
UQG	80	50	300	3	1	2500	570

Photo image of Aixtron P6

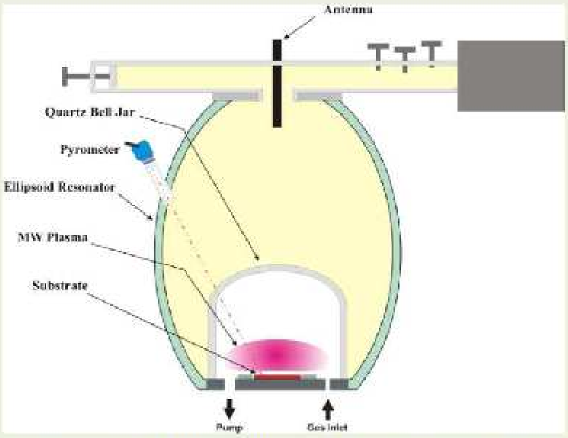

Schematic view of MWCVD ellipsoidal cavity reactor Aixtron P6

Sample characterization

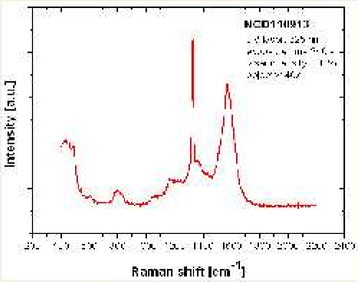

Raman spectra

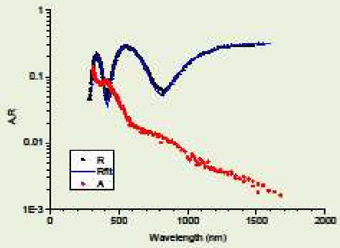

Reflectance and absorptance spectra

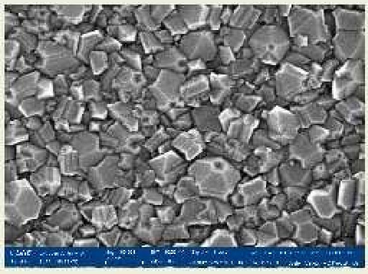

SEM image

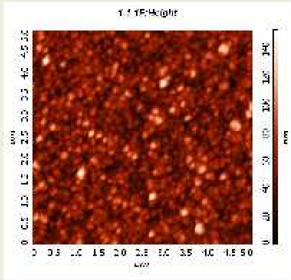

AFM image

Electron Beam Lithography

EBL using *"e-LiNE system" (Raith GmbH)*

- NCD film coated with electron sensitive polymer (PMMA – circa 110 nm in thickness)
- forming the base matrix with regularly repeated openings
- ordering into a square lattice with a lattice constant based on requirements
- EBL processing – not easy to estimate process parameters for achieving required diameters (mainly depends on layer roughness and lattice constant)

SET 1

	A	B	C
Required - d (nm)	206	206	206
EBL (pAs/dot)	0,05	0,06	0,07
EBL - d (nm)	165	200	230

SET 2

	A	B	C
Required - d (nm)	200	200	200
EBL (pAs/dot)	0,1	0,085	0,09
EBL - d (nm)	215	220	210

Electron Beam Lithography examples

SET 1 – sample A

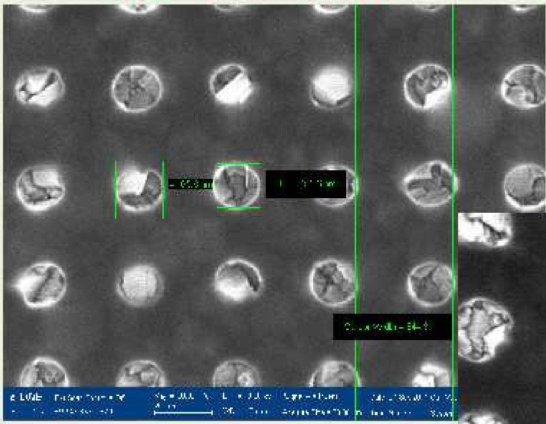

SET 2 – sample A

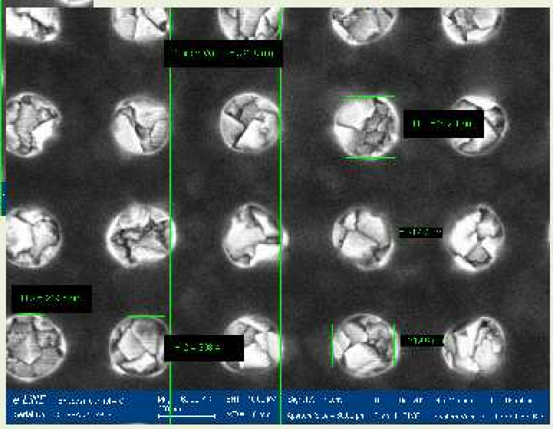

1–4.2.2012 The 3rd Rokytnice scientific and educational workshop 9 2. Experimental part

Masking – metal evaporation – lift off

- gold layer of 70 nm thickness was evaporated and processed by lift-off strategy to form a masking matrix

SET 1

	A	B	C
Required - d (nm)	206	206	206
EBL - d (nm)	165	200	230
Au mask - d (nm)	100	130	130

SET 2

	A	B	C
Required - d (nm)	200	200	200
EBL - d (nm)	215	220	210
Au mask - d (nm)	130	150	130

1–4.2.2012 The 3rd Rokytnice scientific and educational workshop 10 2. Experimental part

Au masking matrix

SET 1 – sample A

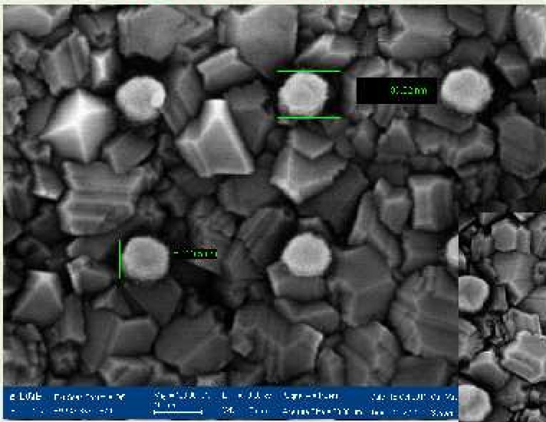

SET 2 – sample A

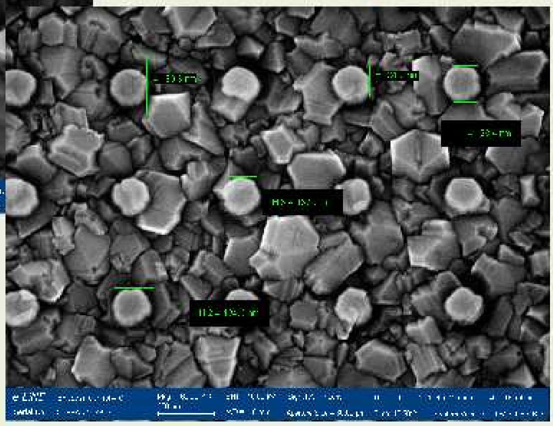

Etching process

- plasma etching by using capacitively coupled RF-plasma in a CF_4/O_2 gas mixture led to formation of geometrically ordered nanopillars
- Phantom LT RIE System, Trion Technology

SET 1

	A	B	C
Required - wh (nm)	40	60	120
Etched - wh (nm)	45	60	120
Required - d (nm)	206	206	206
EBL - d (nm)	165	200	230
Au mask - d (nm)	100	130	130
Etched - d (nm)	150	160	190

SET 2

	A	B	C
Required - wh (nm)	100	100	55
Etched - wh (nm)	100	130	55
Required - d (nm)	200	200	200
EBL - d (nm)	215	220	210
Au mask - d (nm)	130	150	130
Etched - d (nm)	165	175	155

After etching process

SET 1 – sample C with Au

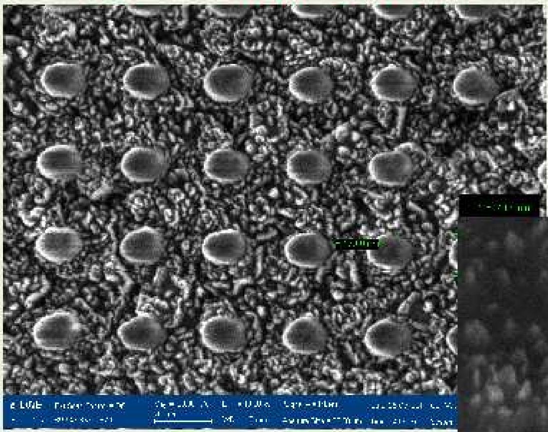

SET 2 – sample A

PhC transmission - SET 1 sample A

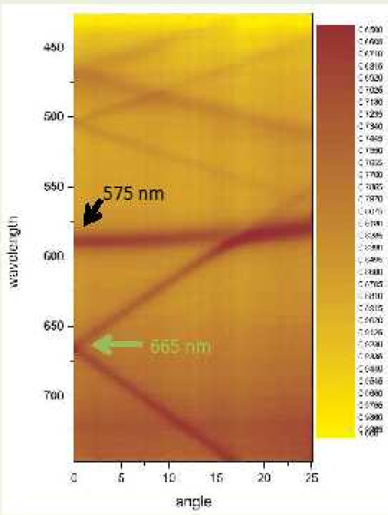

S polarization, GX

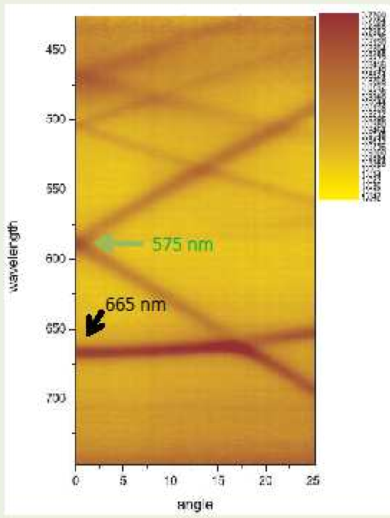

P polarization, GX

PhC transmission - SET 1 sample B

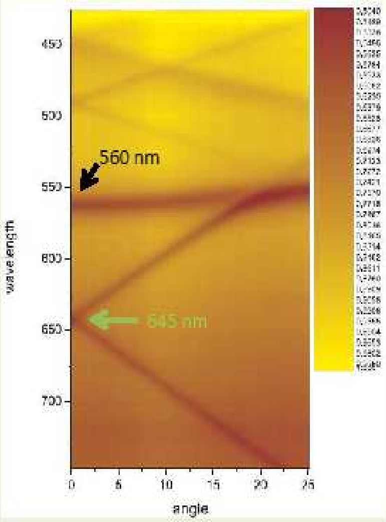

S polarization, GX

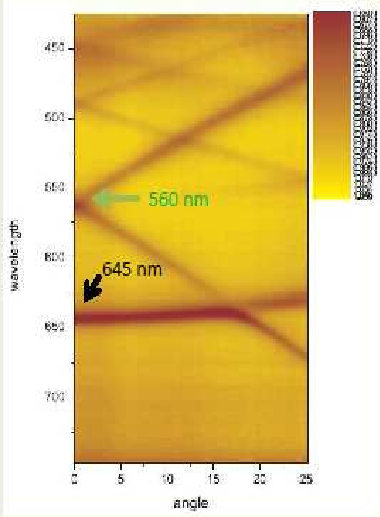

P polarization, GX

PhC transmission - SET 1 sample C

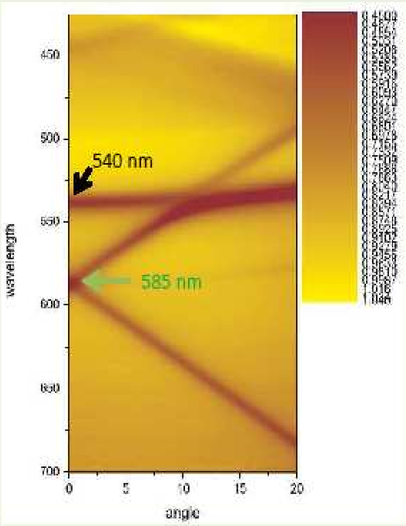

S polarization, GX

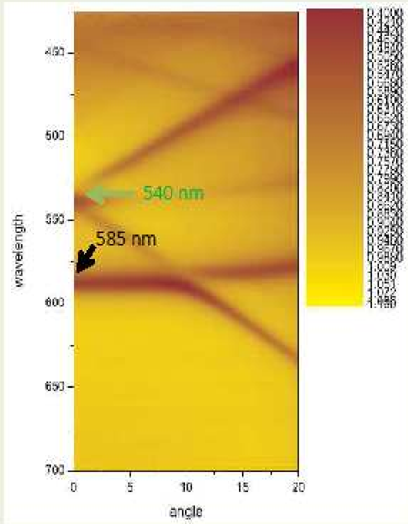

P polarization, GX

Summary

- relatively good optimized diamond growth rate (requirement of film thickness)

- satisfactory diamond quality (film analysis)

- problems with EBL estimation (required diameter)

- metal evaporation and RIE etching – different diameter of the columns

- RIE etching should be improved (roughness)

- after all the samples were fine and work (PhC transmission)

- various diameter and height of diamond columns shift the active light wavelenght

- reflectance measurements show optical losses in diamond

Thermoelectric conversion of heat to electricity - principles, materials, characterization and applications.

Jiří Hejtmánek, Karel Knížek,...

Physical properties & Technology of materials

Characterization & Thermoelectric modules

Institute of Physics of the ASCR, v.v.i.

Department of Magnetics and Superconductors
www.fzu.cz

Physical properties & Technology of materials

Characterization & Thermoelectric modules

OUTLINE

Introduction-motivation

Thermoelectricity
-Thermoelectric conversion of energy – principles & characteristics

Measuring techniques and characterization
- Thermoelectric materials- measuring techniques and analysis
-Characterization of modules

Materials
-Classical semiconductors
- Oxides
-Novel approaches

Thermoelectric Modules
-Principles
-State of art situation

Applications and energy consideration

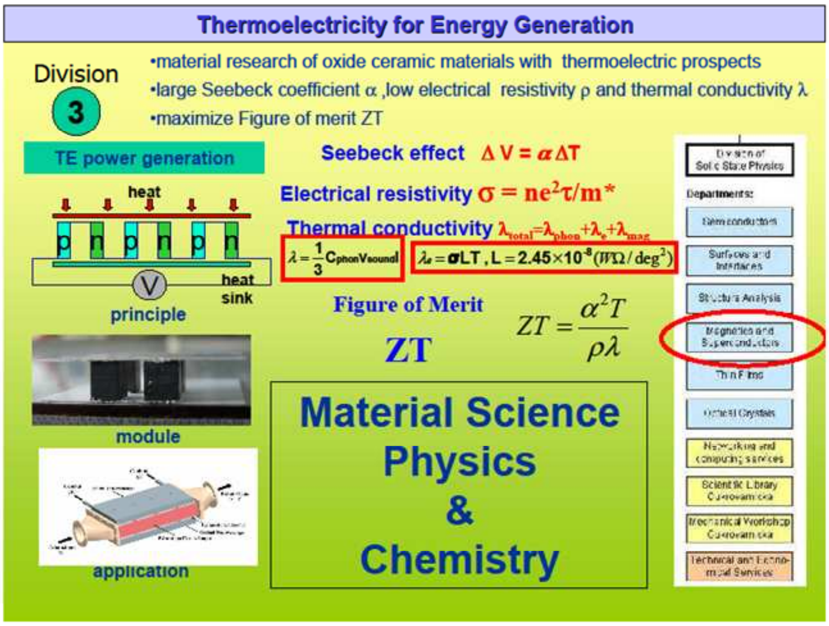

Thermoelectricity for Energy Generation
Division 3
•material research of oxide ceramic materials with thermoelectric prospects
•large Seebeck coefficient α ,low electrical resistivity ρ and thermal conductivity λ
•maximize Figure of merit ZT
TE power generation
heat
p n p n p n
V
heat sink
principle
module
application
Seebeck effect $\Delta V = \alpha \Delta T$
Electrical resistivity $\sigma = ne^2\tau/m^*$
Thermal conductivity $\lambda_{total}=\lambda_{phon}+\lambda_e+\lambda_{mag}$
$\lambda = \frac{1}{3} C_{phon} v_{sound} l$
$\lambda_e = \sigma LT , L = 2.45\times10^{-8} (W\Omega/deg^2)$
Figure of Merit
ZT
$ZT = \frac{\alpha^2 T}{\rho\lambda}$
Material Science
Physics
&
Chemistry
Departments:

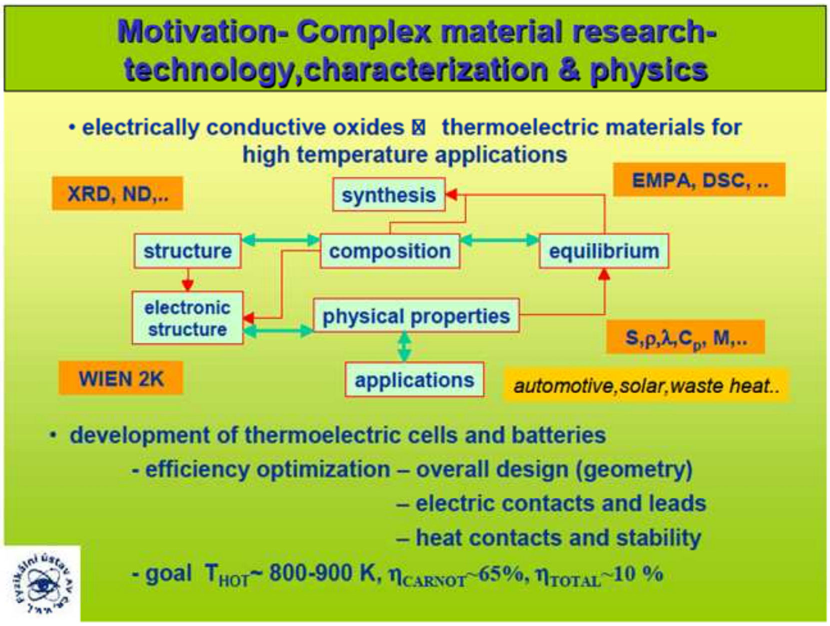

Motivation- Complex material research-
technology,characterization & physics
• electrically conductive oxides ⊠ thermoelectric materials for high temperature applications
XRD, ND,..
EMPA, DSC, ..
synthesis
structure
composition
equilibrium
electronic structure
physical properties
S,ρ,λ,C_p, M,..
WIEN 2K
applications
automotive,solar,waste heat..
• development of thermoelectric cells and batteries
- efficiency optimization – overall design (geometry)
– electric contacts and leads
– heat contacts and stability
- goal T_{HOT}~ 800-900 K, η_{CARNOT}~65%, η_{TOTAL}~10 %

Readiness and Facilities for Technology and Characterization of Thermoelectrics

- transport characterization
- Electrical resistivity (~1200K)
- Seebeck coefficient (~1200K)
- Hall coefficient (~300K)
- Thermal conductivity (~300K)
- Magnetic properties (~800K)
  - magnetization, *ac*- χ
- structure (~1200K)
  - XRD, neutron diffraction
- low temperature C_p (~300K)
- electronic structure

- material synthesis and fabrication
- -ceramic processing, contacts , ..
- -microscopy, analysis , crystal structure….

Thermoelectricity

-Thermoelectric conversion of energy – principles & characteristics

$$ZT = \frac{S^2}{\rho\lambda} T$$

Seebeck Coefficient (S), Temperature (T), El. resistivity (ρ), Thermal Conductivity (λ)

Thermoelectric Effects

- Electrical energy may be reversibly converted into thermal energy and vice versa by three thermoelectric effects.
- Thermoelectric effects, i.e., the Seebeck effect, Peltier effect and Thomson effect are named after the person who first observed or predicted them.
- Chronology.
  - 1821: Seebeck observes compass needle deflect near loop formed by dissimilar conductors.
  - 1835-1838: Peltier discovers Peltier effect and Lenz utilizes it to reversibly freeze water & melt ice.
  - 1838-1850: Very little interest in thermoelectricity during the "era of electromagnetism."
  - 1851: Thomson predicts the existence of the Thomson effect.

Seebeck Effect (Thermopower)

- In 1821, Thomas Seebeck found that an electric current would flow continuously in a closed circuit made up of two dissimilar metals, if the junctions of the metals were maintained at two different temperatures.

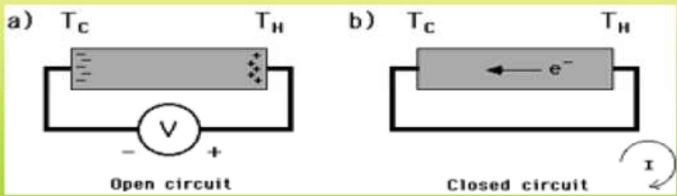

$S = dV / dT$;

S is the Seebeck Coefficient with units of Volts per Kelvin

S is positive when the direction of electric current is same as the direction of thermal current

Peltier Effect

- In 1834, a French watchmaker and part time physicist, Jean Peltier found that an electrical current would produce a temperature gradient at the junction of two dissimilar metals.

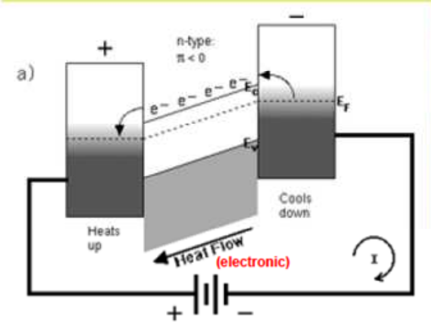

Π < 0 ; Negative Peltier coefficient

High energy electrons move from right to left.

Thermal current and electric current flow in opposite directions.

Explanation of Thermopower in metals

(Band Structure View Point)

Key role of Fermi-Dirac equilibrium distribution for the probability of electron occupation of energy level *E* at temperature *T*

$$f(E) = \frac{1}{1+\exp\left(\frac{E-E_F}{k_B T}\right)}$$

Effect of Temperature

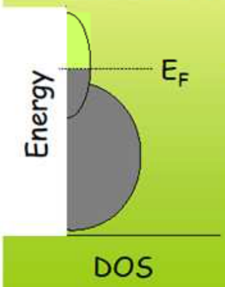

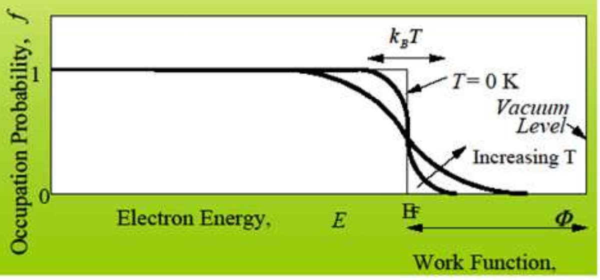

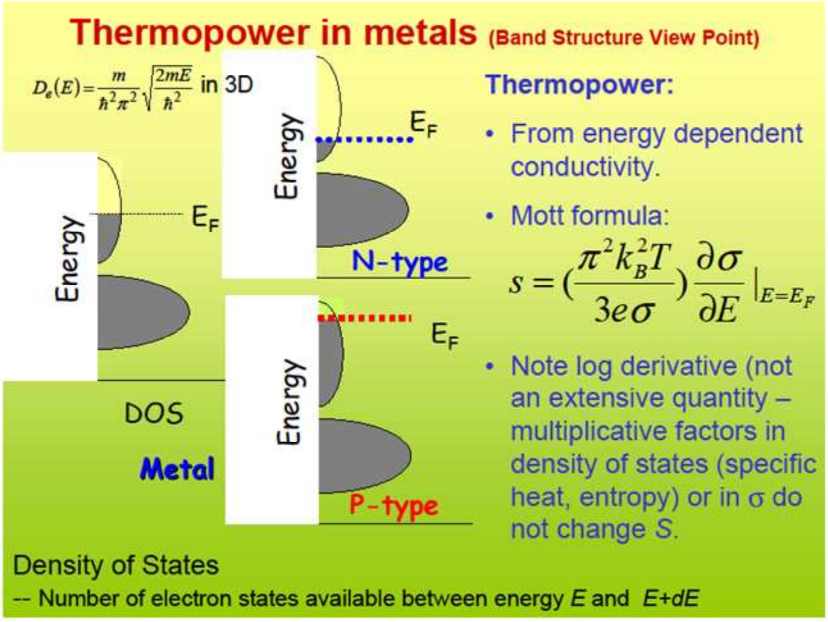
Thermopower in metals (Band Structure View Point)
$D_e(E)=\frac{m}{\hbar^2\pi^2}\sqrt{\frac{2mE}{\hbar^2}}$ in 3D
Energy
E_F
DOS
Metal
N-type
P-type
Thermopower:
• From energy dependent conductivity.
• Mott formula:
$s=(\frac{\pi^2 k_B^2 T}{3e\sigma})\frac{\partial\sigma}{\partial E}|_{E=E_F}$
• Note log derivative (not an extensive quantity – multiplicative factors in density of states (specific heat, entropy) or in σ do not change S.
Density of States
-- Number of electron states available between energy E and $E+dE$

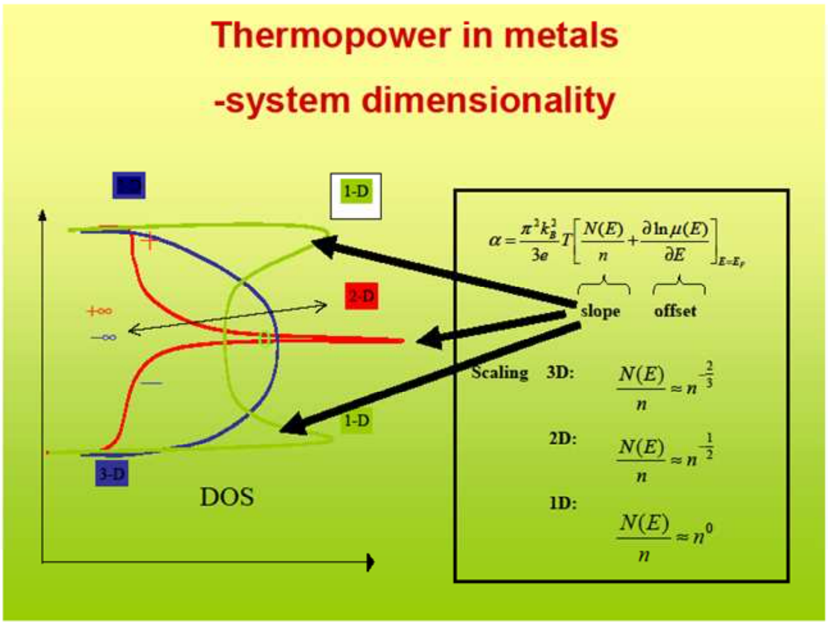
Thermopower in metals
-system dimensionality
1-D
2-D
3-D
+∞
−∞
+
−
DOS
$\alpha=\frac{\pi^2 k_B^2}{3e}T\left[\frac{N(E)}{n}+\frac{\partial\ln\mu(E)}{\partial E}\right]_{E=E_F}$
slope
offset
Scaling 3D: $\frac{N(E)}{n}\approx n^{-\frac{2}{3}}$
2D: $\frac{N(E)}{n}\approx n^{-\frac{1}{2}}$
1D: $\frac{N(E)}{n}\approx n^{0}$

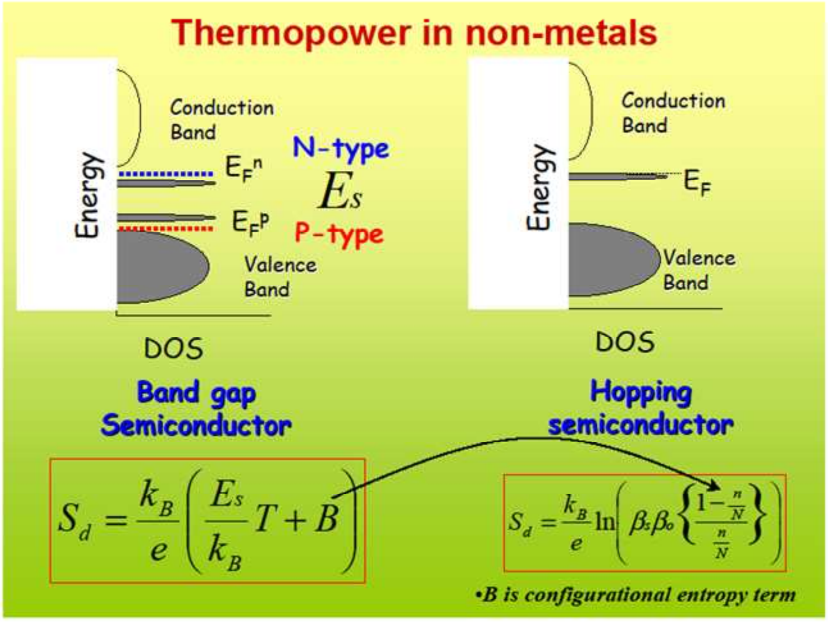

Thermopower in non-metals
Conduction Band
N-type
E_F^n
E_s
E_F^p
P-type
Valence Band
Energy
DOS
Band gap Semiconductor
Conduction Band
E_F
Valence Band
Energy
DOS
Hopping semiconductor
$S_d = \frac{k_B}{e}\left(\frac{E_s}{k_B}T + B\right)$
$S_d = \frac{k_B}{e}\ln\left(\beta_s\beta_o\left\{\frac{1-\frac{n}{N}}{\frac{n}{N}}\right\}\right)$
•B is configurational entropy term

7

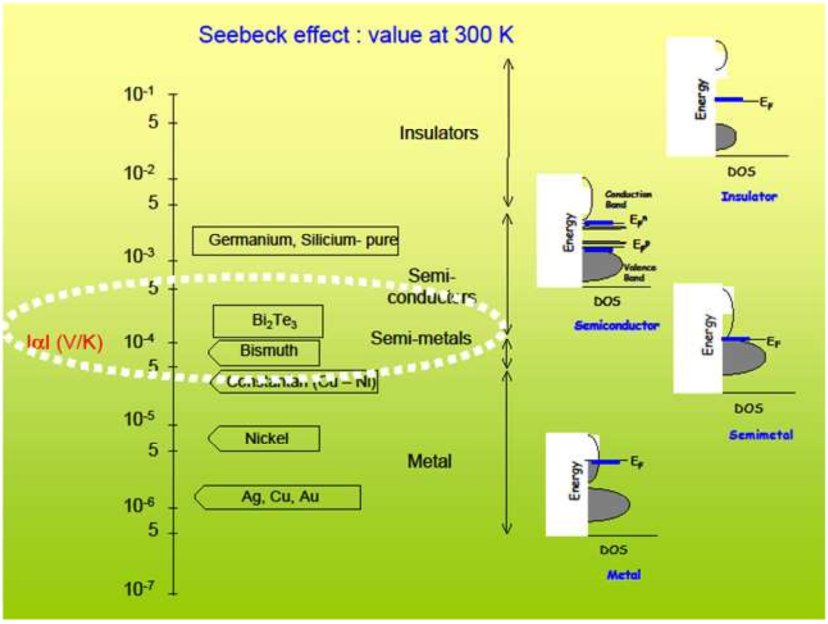

Seebeck effect : value at 300 K
|α| (V/K)
Insulators
Semi-conductors
Semi-metals
Metal
Germanium, Silicium- pure
Bi_2Te_3
Bismuth
Nickel
Ag, Cu, Au
Insulator
Semiconductor
Semimetal
Metal

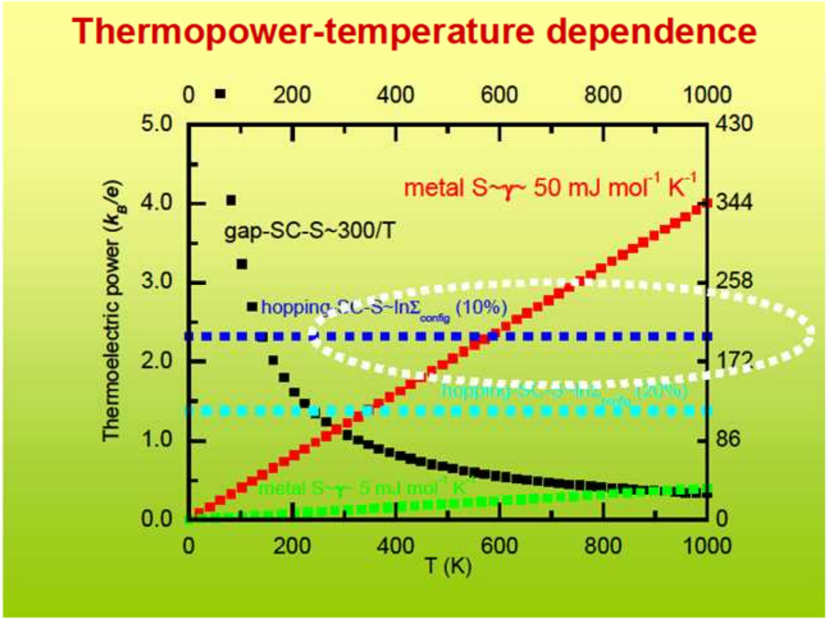
Thermopower-temperature dependence
Thermoelectric power (k_B/e)
T (K)
metal S~γ~ 50 mJ mol^{-1} K^{-1}
gap-SC-S~300/T
hopping-SC-S~lnΣ$_{config}$ (10%)
metal S~γ~ 5 mJ mol^{-1} K
0 200 400 600 800 1000
0.0 1.0 2.0 3.0 4.0 5.0
0 86 172 258 344 430

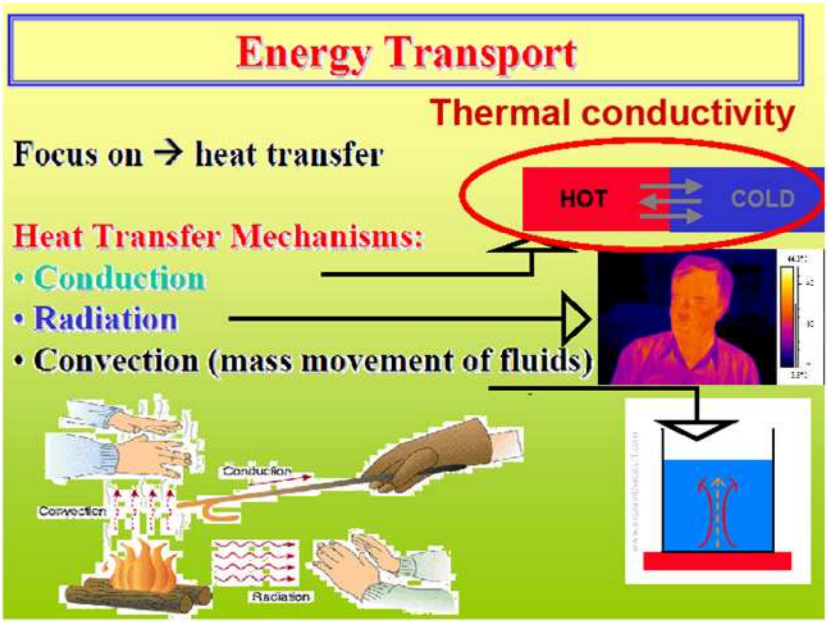
Energy Transport
Thermal conductivity
Focus on → heat transfer
HOT
COLD
Heat Transfer Mechanisms:
• Conduction
• Radiation
• Convection (mass movement of fluids)
Conduction
Convection
Radiation

Thermal Conductivity of Solids

Solids transmit thermal energy by two modes:

- **elastic vibrations of the lattice moving through the crystal in the form of waves**

- **free electrons moving through the lattice also carry energy similar to the case in gases (this is observed in metals)**

$$\lambda_{total} = \boldsymbol{\lambda}_{\mathbf{phon}} + \lambda_e$$

Thermal conductivity: $\lambda = \frac{1}{3} C v \ell$

Specific heat (C), Velocity (v), Mean free path (ℓ)

Thermal Conductivity of Solids

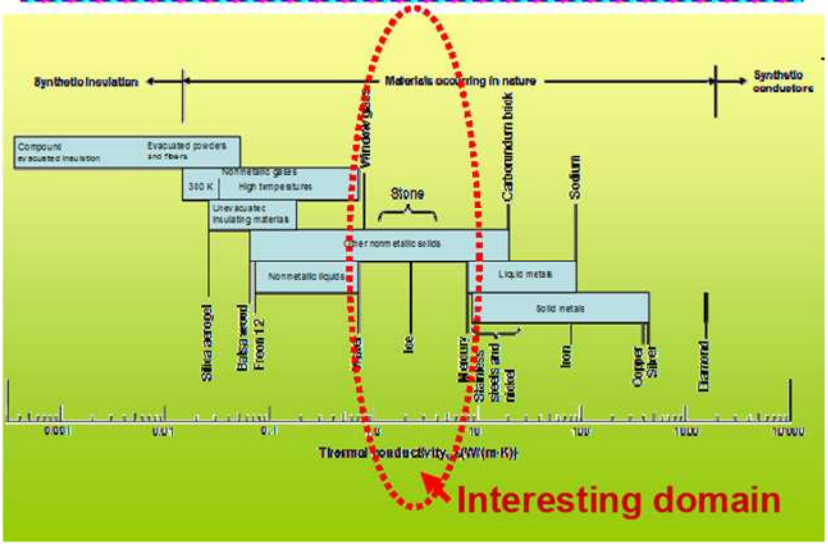

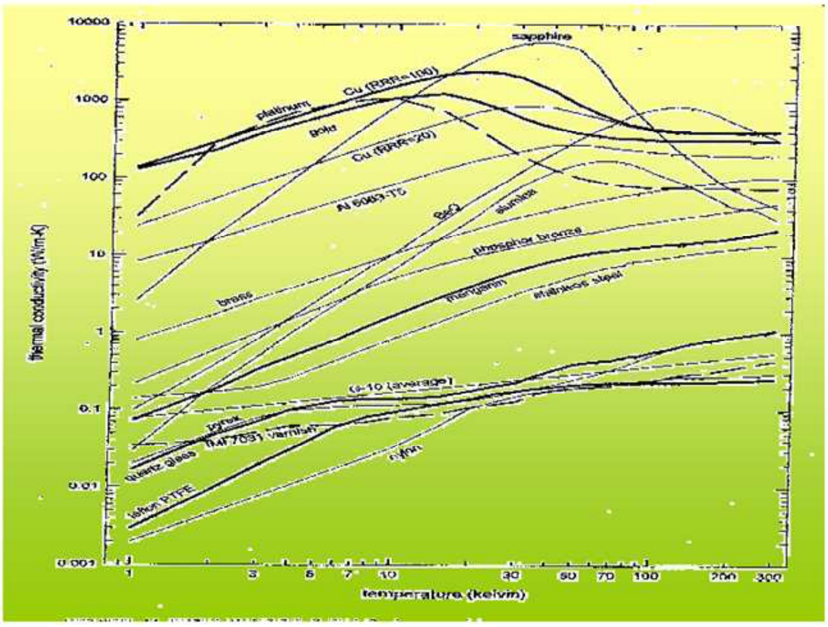
thermal conductivity (W/m-K)
temperature (kelvin)
sapphire
Cu (RRR=100)
platinum
gold
Cu (RRR=20)
Al 6063-T5
BeO
alumina
phosphor bronze
brass
manganin
stainless steel
G-10 (average)
pyrex
GE 7031 varnish
quartz glass
nylon
teflon PTFE

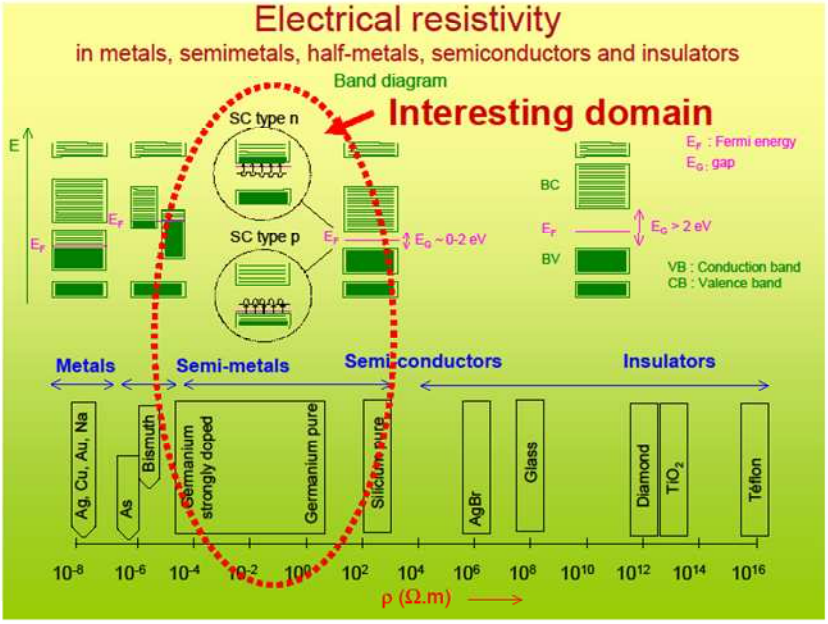
Electrical resistivity
in metals, semimetals, half-metals, semiconductors and insulators
Band diagram
Interesting domain
SC type n
SC type p
E
EF : Fermi energy
EG : gap
BC
BV
EG ~0-2 eV
EG > 2 eV
VB : Conduction band
CB : Valence band
Metals
Semi-metals
Semi-conductors
Insulators
Ag, Cu, Au, Na
As
Bismuth
Germanium strongly doped
Germanium pure
Silicium pure
AgBr
Glass
Diamond
TiO2
Téflon
ρ (Ω.m)

Many thanks for your attention….

Do not hesitate to ask any questions…

END

Ladislav Fekete, FZÚ AVČR

Terahertzová spektroskopia

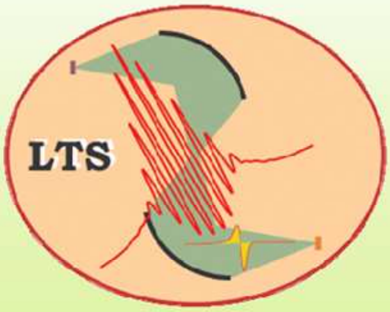

Terahetrz range

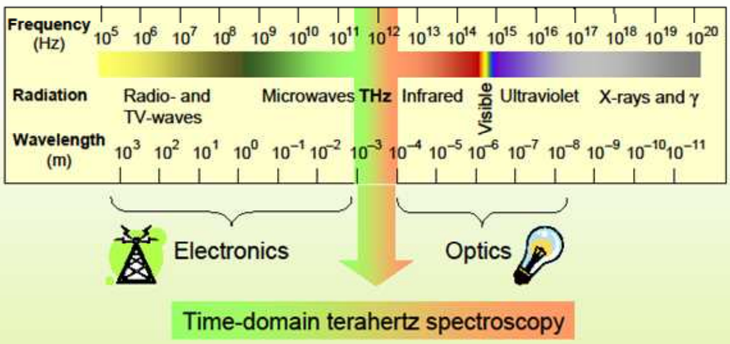

1 THz ↔ 1 ps ↔ 33 cm^{-1} ↔ 0.3 mm ↔ 48 K ↔ 4.1 meV

Possible detection of the electric field AMPLITUDE => complex N, σ, ε

THz pulses I.B

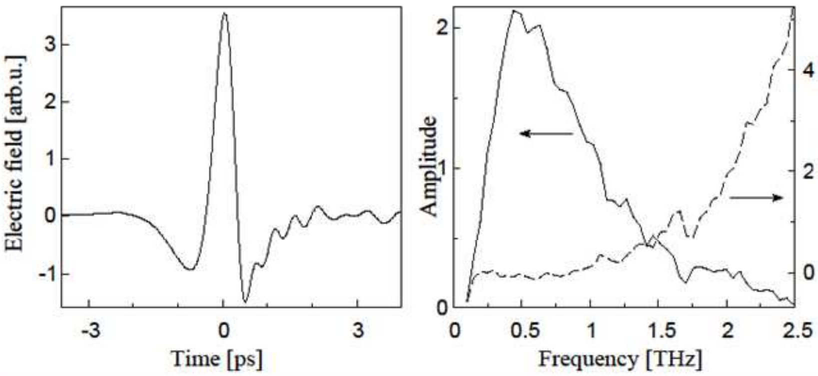

Time evolution of the electric field **FT →** **Spectrum of the THz pulses**

Metódy v THz oblasti: 100 GHz – 3 THz

Metóda	Výkon	Frekvenčná oblasť	Meranie	Fázová citlivosť
Synchrotron, Lineárny urychlovač, FEL	Primerný - 10W Maximálny – 1 MW	0.1 – 30 THz	Pulzné, frekvenčná oblasť, širokopásmová	možná, ale nepoužíva sa
Backward wave oscillator spectroscopy	300 mW - 1mW	0.03 – 1.2 THz 1 – 40 cm^{-1} 200 GHz ladenie	frekvenčná oblasť, CW Monochr.	Interferometricky
Time-domain THz spectroscopy	Primerný - 0,7 μW Maximálny – 2,3 kW	0.1 – 3 THz 3 – 100 cm^{-1} 4GHz rozliš.	časová doména, pulzné žiarenie, širokopásmová	Inherentná
Fourier transform infrared spectroscopy	1 μW	0.7 – 300 THz 20 – 10000 cm^{-1} 4GHz rozliš.	časová doména, kontinuálne žiarenie, širokopásmová	možná, ale nepoužíva sa
QCL	CW: 0,3μW (10K) Pulz.: Max. – 300μW CW: 1,6W (300K)	1-65 THz 200 GHz ladenie	Pulzné, CW, Monochr., frekvenčná oblasť	---

Experimental setup

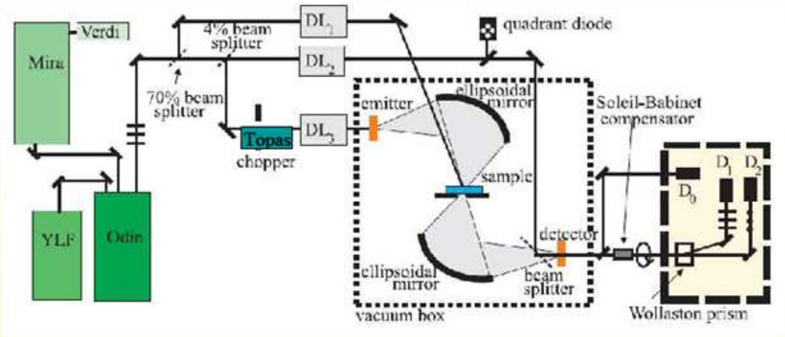

- MIRA: 800 nm, 50 – 80 fs, Spectral bandwidth 15 – 40 nm, Repetition rate 76 MHz, Energy per pulse 8 nJ, Photons per pulse~3.5×10^{10}, Average power 650 mW, Pulse peak power 140 kW
- ODIN: Pump laser 527-DP Nd:YLF 12 W, 800 nm, 40 fs,Spectral bandwidth 15 – 30 nm, Repetition rate 1 kHz, Energy per pulse1 mJ, Photons per pulse~4×10^{15},Average power 1 W, Pulse peak power 25 GW
- TOPAS: travelling-wave optical parametric amplifier of super-fluorescence, Tuning range240 – 3000 nm, Pulse length~50 fs, Energy per pulse1 – 100 μJ (depending on the output wavelength)

Experimental setup

1. **ZnTe Emitor**
2. **THz puls**
3. **Sample**
4. **Optical excitation puls**
5. **Transmited THz puls**
6. **Sampling optical puls**
7. **ZnTe Elektrooptic detektor**
8. **Vacuum box**

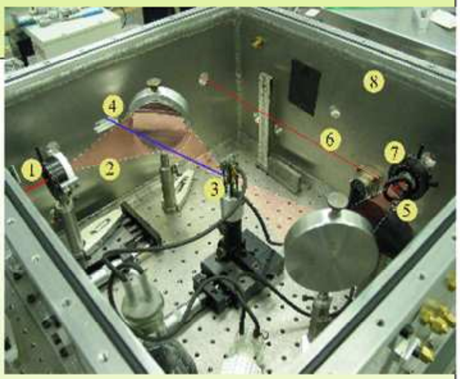

- Cryostat: temperature range 5 – 300 K
- High temperature cell (furnace): temperature range 300 – 1000 K
- Subpicosecond resolution
- 700 ps pump-probe delay maximum range
- Excitatation ranage 240 – 3000 nm

Optical rectification

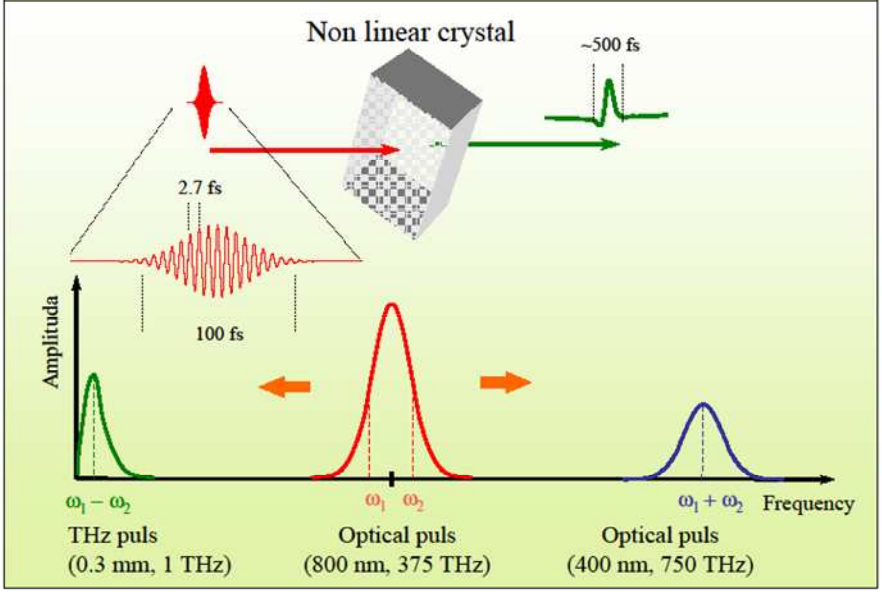

Electrooptic sampling

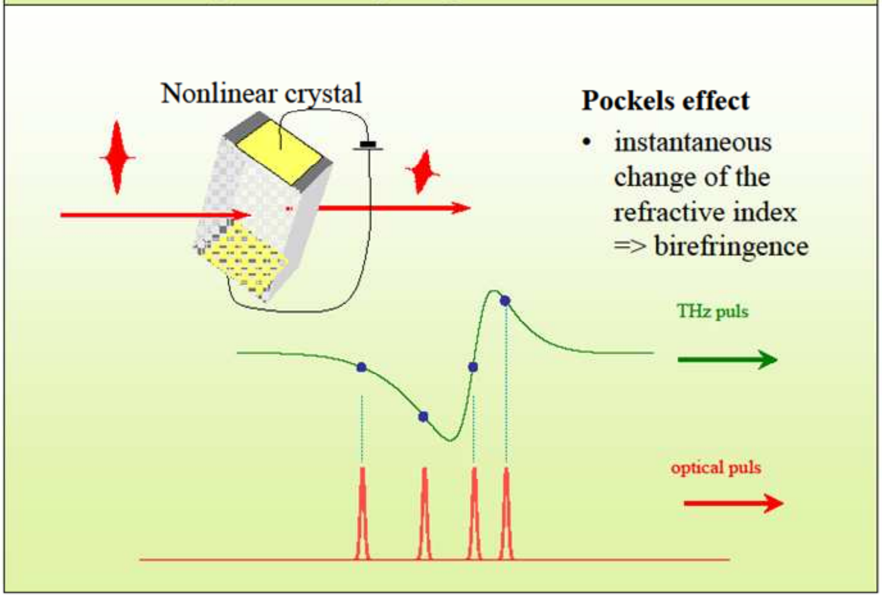

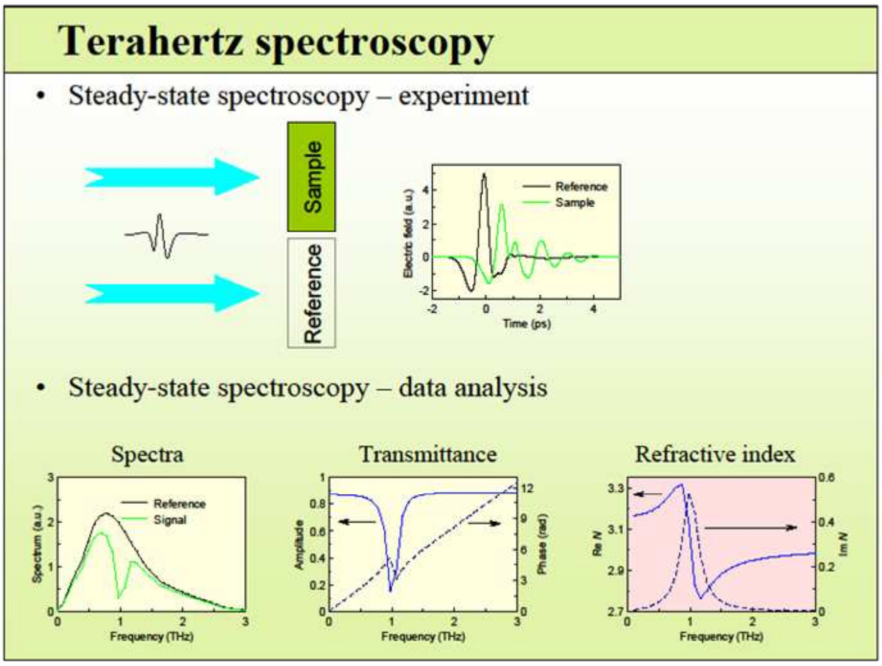
Terahertz spectroscopy
• Steady-state spectroscopy – experiment
Sample
Reference
Reference
Sample
Electric field (a.u.)
Time (ps)
• Steady-state spectroscopy – data analysis
Spectra
Reference
Signal
Spectrum (a.u.)
Frequency (THz)
Transmittance
Amplitude
Phase (rad)
Frequency (THz)
Refractive index
Re N
Im N
Frequency (THz)

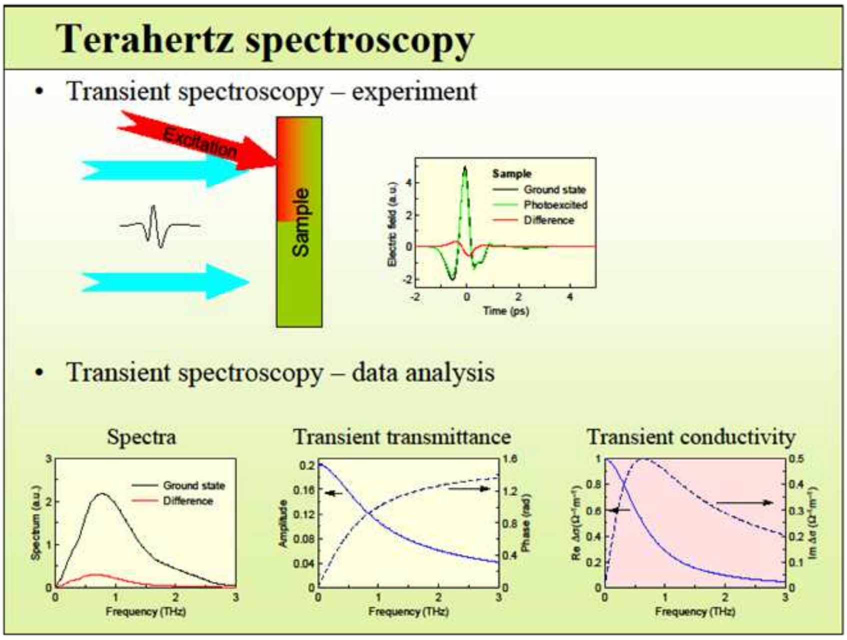
Terahertz spectroscopy
• Transient spectroscopy – experiment
Excitation
Sample
Sample
Ground state
Photoexcited
Difference
Electric field (a.u.)
Time (ps)
• Transient spectroscopy – data analysis
Spectra
Ground state
Difference
Spectrum (a.u.)
Frequency (THz)
Transient transmittance
Amplitude
Phase (rad)
Frequency (THz)
Transient conductivity
Frequency (THz)

Basic terms

Conductivity	Susceptibility
$\hat{\sigma}(\omega)$	$\hat{\chi}(\omega)$
=	=
$ne_0\hat{\mu}(\omega)$	$n\hat{\alpha}(\omega)$
Charge density × mobility	Carrier density × polarizability

Refractive index *N*: describes propagation of electromagnetic waves in matters

$$\hat{N}(\omega) = \sqrt{\hat{\varepsilon}} = \sqrt{1+\hat{\chi}} = \sqrt{1-\hat{\sigma}/(i\omega\varepsilon_0)}$$

Optical-pump THz-probe experiments I.B

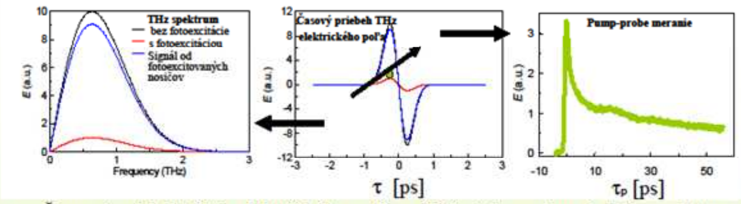

- Časový priebeh THz elektrického poľa –(FT)–> komplexné THz spektrum
- **Neexcitovný (nedopovaný) polovodič – priehľadny**
- **Fotoexcitovaný polovodič – voľne/lokalizované nosiče**
  - komplexná spektrálna odozva – $\Delta N(\omega)$, $\Delta\varepsilon(\omega)$, $\Delta\sigma(\omega)$
  - pokles intenzity – doba života nosičov (τ_p)
  - $\Delta\sigma = -i\,\omega\,\varepsilon_0\,\Delta\varepsilon$ ($\Delta\varepsilon$ -Re = disperzia systému)
    ($\Delta\sigma$ -Re = straty – at 0 = DC vodivosť)
  - Dynamika $\Delta\sigma(\tau_p)$, $\Delta\varepsilon(\tau_p)$,
- **2D data v (ω,ω_p) priestore pre ultrarýchlu (<1ps) dynamiku**

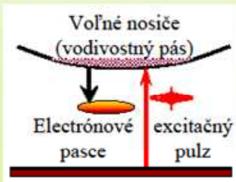

Free carriers
– Drude model

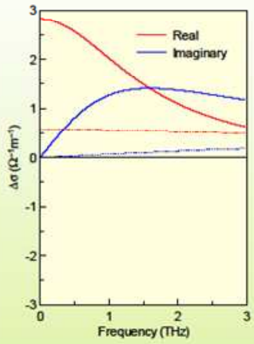

$n = 10^{15}$ cm^{-3}
m = mass of electron
τ = 100 fs (solid lines); 20 fs (dotted lines)

Bound charge carriers
– oscillator model

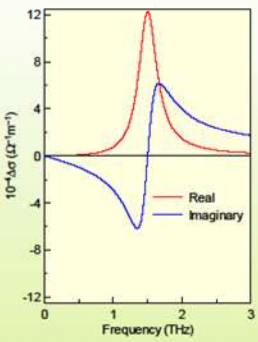

$n = 1.6\times10^{22}$ cm^{-3}
m = mass of proton
$\tau = (500\text{ fs})^{-1}$

Bound charge carriers
– relaxator model

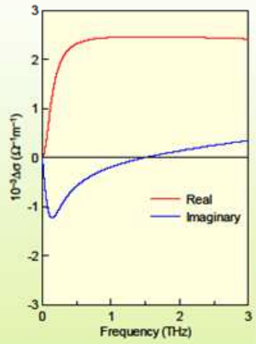

$n = 1.6\times10^{22}$ cm^{-3}
m = mass of proton
$\tau = (10\text{ fs})^{-1}$

Silicon: carriers response

- Si crystal (bulk material)

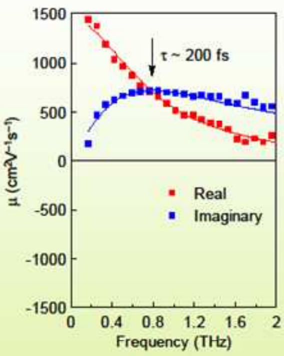

→ Drude behavior
(typical free charge carriers)

- Microcrystalline silicon

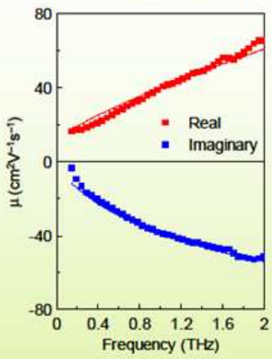

→ localized carriers

THz in astronomy

- Generally, in millimeter and submillimeter region, molecules like OH, O3, HCl, ClO,HOCl, BrO, HNO3, N2O, HCN, CH3CN, volcanic SO, CO, CH3OH, H3O+, charged molecule composed of carbon and fluorine - the CF+ ion, hydrogen and deuterium (H2D+), water molecule and many others have their fingerprints and can be traced. Besides spec-troscopic research of the universe the detected THz radiation is used to study formation of new stars from clumps in molecular clouds or other objects like galaxies at approximately-250 degrees Celsius temperature.

Tarantula Nebula. Herschel telescope: red at 250 µm and green at 100 and 160 µm. The warmest spots appear in blue, 24- and 70- µm from Spitzer.

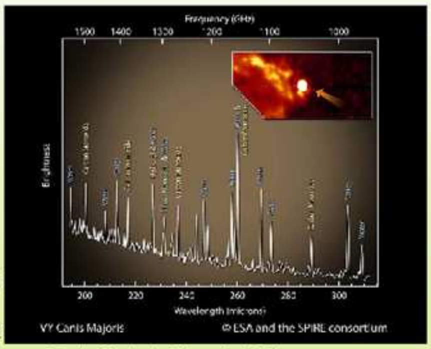

Canis Majoris, Herschel Telescope

THz tomografia a zobrazovanie

- Materiály neabsorbující THz záření
  - plastické hmoty
  - keramiky
  - skla
- Materiály silně absorbující THz záření
  - kovy
  - **voda**
- Vznik kontrastu: rozdíl THz indexů lomu
- Neškodnost THz záření

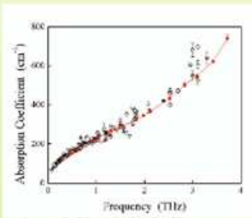

from J. Xu et al., J. Chem. Phys. 24, 036101, 2006

Penetration depth in liquid water:

2 cm @ 2 GHz
160 µm @ 100 GHz
81 µm @ 300 GHz
45 µm @ 1 THz
18 µm @ 3 THz

THz tomografia a zobrazovanie

Spozdenie $= \frac{d}{c}(n-1)$

Poznáme index lomu a absorbciu $n + i\kappa$

Určíme hrúbku d.

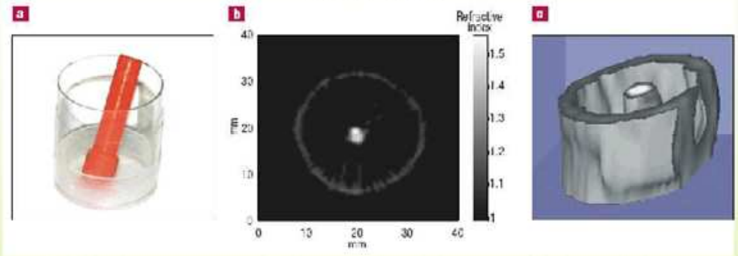

Optický obraz | Terahertzový obraz (rez) | Terahertzový obraz

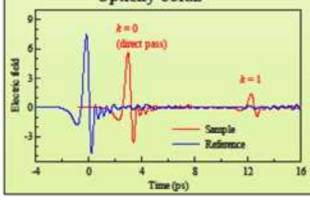

B. Ferguson and X.-C. Zhang, Nature Mat. 1, 26 (2002)

THz tomografia a zobrazovanie

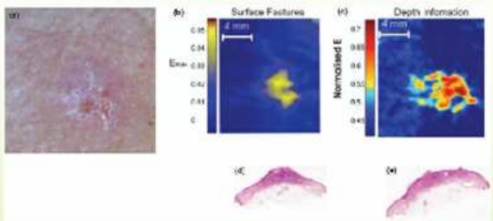

Terahertzový obraz nádoru bazálních buniek

V. P. Wallace et al., British J. Dermatol. **151**, 424 (2004)

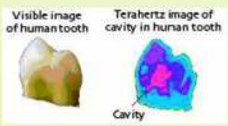

Terahertzový obraz zubného kazu TeraView Ltd.

THz tomografia a zobrazovanie

Trojrozmerné terahertzové zobrazovanie povrchov a vnútra tabliet

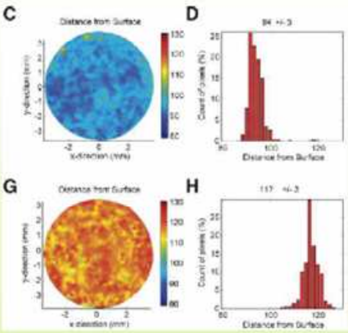

THz tomografia a zobrazovanie

Optický a terahertzový obraz vodoznaku bankoviek

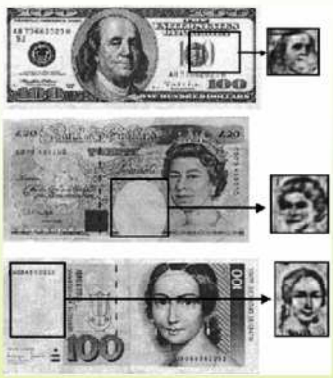

Q. Chen and X.-C. Zhang, Appl. Phys. Lett. 74, 3435 (1999)

Terahertzový a optický obraz polovodičového integrovaného obvodu v pouzdře

B. B. Hu and M. C. Nuss, Opt. Lett. ***20****, 1716 (1995)*

mapa koncentrácie nosičov, silná koncentácia THz poľa AFM hrotom 40 nm (λ/3000) priestorové rozlíšenie na 2.54 THz,

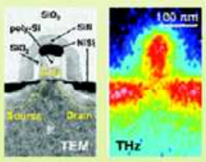

J.A. Hubert, Nano Lett., 2008, 8 (11), pp 3766–3770

THz spektroskopia

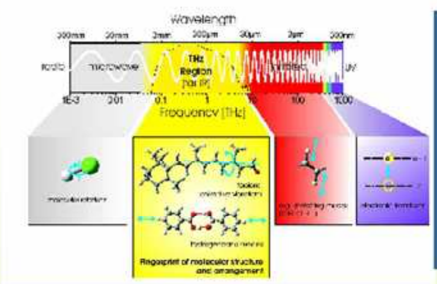

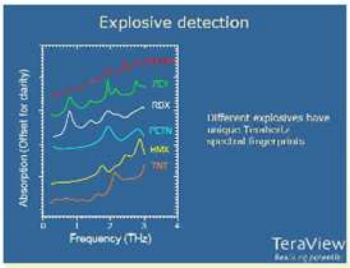

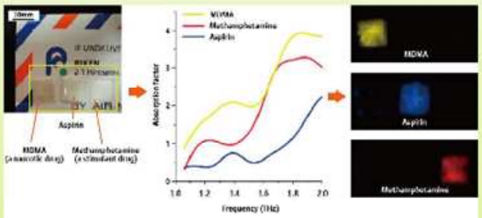

Diskusia VI.

! ? ? ! ?

Ďakujem za pozornosť

? ! ! ! ?